



## City Research Online

### City, University of London Institutional Repository

---

**Citation:** Ingram, P. (2000). The Application of Numerical Models to Natural Stiff Clays. (Unpublished Doctoral thesis, City, University of London)

This is the accepted version of the paper.

This version of the publication may differ from the final published version.

---

**Permanent repository link:** <https://openaccess.city.ac.uk/id/eprint/30797/>

**Link to published version:**

**Copyright:** City Research Online aims to make research outputs of City, University of London available to a wider audience. Copyright and Moral Rights remain with the author(s) and/or copyright holders. URLs from City Research Online may be freely distributed and linked to.

**Reuse:** Copies of full items can be used for personal research or study, educational, or not-for-profit purposes without prior permission or charge. Provided that the authors, title and full bibliographic details are credited, a hyperlink and/or URL is given for the original metadata page and the content is not changed in any way.

The application of numerical models to  
natural stiff clays

by

Peter James Ingram

A dissertation submitted for the  
Degree of Doctor of Philosophy

City University, London  
Department of Civil Engineering  
Geotechnical Engineering Research Centre

May 2000

CONTENTS		
LIST OF TABLES	6	
LIST OF FIGURES	7	
ACKNOWLEDGEMENTS	18	
DECLARATION	19	
ABSTRACT	20	
LIST OF SYMBOLS	21	
CHAPTER 1	INTRODUCTION	24
1.1	BACKGROUND	24
1.2	BASIC ASSUMPTIONS	24
1.3	FRAMEWORK	25
1.3.1	Reconstituted clay	26
1.3.2	Natural clay	27
1.3.3	Initial states	28
1.4	METHODOLOGY	29
1.4.1	Interpretation of data	30
1.4.2	Finite element modelling of triaxial tests	30
1.4.3	Evaluating model input parameters	31
CHAPTER 2	BEHAVIOUR OF STIFF OVERCONSOLIDATED CLAYS	32
2.1	INTRODUCTION	32
2.2	VOLUMETRIC RESPONSE	33
2.3	THE BEHAVIOUR OF STIFF OVERCONSOLIDATED CLAYS IN STRESS SPACE	36
2.4	VERY SMALL STRAIN STIFFNESS	41
2.5	THE INFLUENCE OF CREEP	46
2.6	ANISOTROPY	50
2.7	SUMMARY	52
CHAPTER 3	MODELLING OF STIFF OVERCONSOLIDATED CLAYS	54
3.1	INTRODUCTION	54
3.2	MODELS FOR STIFF CLAYS	56
3.2.1	The 3-SKH model	56
3.2.2	The Brick model	58

3.3	MODELLING FEATURES ASSOCIATED WITH CLAYS IN THE NATURAL STATE	60
3.3.1	Modelling natural soil structure	60
3.3.2	Modelling anisotropy	63
3.3.3	Modelling time effects (creep)	66
3.4	SUMMARY	68
CHAPTER 4	REPRESENTING THE BEHAVIOUR OF NATURAL STIFF CLAYS USING THE 3-SKH MODEL.	70
4.1	INTRODUCTION	70
4.2	MODELLING NATURAL SOIL STRUCTURE	71
4.2.1	Calculation of preconsolidation pressure defining the natural state boundary surface - modelling element tests	72
4.2.2	Calculation of preconsolidation pressure defining the natural state boundary surface - modelling boundary value problems	74
4.3	MODELLING STRUCTURAL ANISOTROPY USING THE 3-SKH MODEL	77
4.4	MODELLING VOLUMETRIC CREEP USING THE 3-SKH MODEL	78
4.5	MODELLING $G'_{MAX}$ USING THE 3-SKH MODEL	79
4.6	SUMMARY	81
CHAPTER 5	MODELLING LABORATORY ELEMENT TESTS ON NATURAL STIFF CLAY	82
5.1	INTRODUCTION	82
5.2	MODELLING THE EFFECT OF NATURAL STRUCTURE BY INCREASING THE SIZE OF THE BOUNDING SURFACE	83
5.2.1	Origin of the Boom clay	84
5.2.2	Calculation of soil parameters	85
5.2.3	Analysis procedure	89
5.2.4	Results for reconstituted tests	90
5.2.5	Results for natural tests	93
5.2.6	Summary	95
5.3	MODELLING VOLUMETRIC CREEP	97
5.3.1	Evaluation of the model for volumetric creep	97
5.3.2	Evaluation of creep model for laboratory tests	98
5.3.3	Evaluation of creep model for geological time periods	101

5.3.4	Summary	102
5.4	MODELLING BEHAVIOUR CHARACTERISED BY DEPOSITIONAL ANISOTROPY	102
5.4.1	Determination of material parameters	103
5.4.2	Modelling Oxford Clay using conventional 3-SKH model	106
5.4.3	Modelling Oxford Clay using cross-anisotropic 3-SKH model	107
5.4.4	Summary	109
5.5	GENERAL REMARKS	110
CHAPTER 6 ANALYSIS OF BOUNDARY VALUE PROBLEMS IN RECONSTITUTED CLAY		111
6.1	INTRODUCTION	111
6.2	MODEL FOUNDATION	112
6.2.1	Selection of model parameters	112
6.2.2	Analysis procedure	113
6.2.3	Results	115
6.2.4	Summary	119
6.3	TUNNEL PROBLEM	119
6.3.1	Selection of parameters	120
6.3.2	Analysis procedure	120
6.3.3	Results	120
6.3.4	Summary	121
6.4	SUMMARY	122
CHAPTER 7 ANALYSIS OF BOUNDARY VALUE PROBLEMS IN NATURAL DEPOSITS		124
7.1	INTRODUCTION	124
7.2	THE INFLUENCE OF DEPOSITIONAL HISTORY ON BOUNDARY VALUE PROBLEMS	125
7.2.1	Modelling the geological history and formation of natural structure	126
7.2.2	Analysis of a tunnel with different geological histories	128
7.2.3	Analysis of a foundation with different geological histories	130
7.2.4	Summary	131
7.3	THE INFLUENCE OF CREEP ON A BOUNDARY VALUE PROBLEM	132
7.4	EXCAVATION IN OXFORD CLAY	133

7.4.1	Introduction	133
7.4.2	Ground conditions	134
7.4.3	Previous analysis of the Elstow excavation	134
7.4.4	Determination of material parameters	136
7.4.5	Geometry of the problem	136
7.4.6	Method of analysis	136
7.4.7	Comparison of results	139
7.4.8	Discussion	146
7.5	SUMMARY	149
CHAPTER 8 SUMMARY AND CONCLUSIONS		151
8.1	CHARACTERISATION OF STIFF CLAYS FOR MODELLING	151
8.1.1	Natural clay structure	151
8.1.2	Anisotropy	153
8.1.3	Ageing effects	153
8.2	METHODOLOGY OF NUMERICAL ANALYSES	153
8.3	IMPLICATIONS OF THE RESULTS OF NUMERICAL MODELLING	154
8.3.1	Modelling stable structure and anisotropy	154
8.3.2	Modelling volumetric creep	158
8.4	LIMITATIONS OF THE CURRENT RESEARCH AND FURTHER WORK	158
8.5	CONCLUSIONS	159
REFERENCES		
APPENDIX		
TABLES		
FIGURES		

## LIST OF TABLES

Table 5.1	Table of initial states and calculated preconsolidation pressures for tests carried out on natural samples of Boom clay based on both the reconstituted and natural normal compression lines
Table 5.2	Table of initial states and calculated preconsolidation pressures for tests carried out on reconstituted Boom clay
Table 5.3	Summary of Boom clay parameters for the 3-SKH model
Table 5.4	Summary of parameters used for the parametric study to determine the parameters defining the behaviour of the kinematic surfaces in the 3-SKH model for Boom clay
Table 5.5	3-SKH model parameters for London clay (Stallebrass and Viggiani, 1994)
Table 5.6	Variations used for the parametric study to determine T, S and $\phi$ for Oxford clay
Table 5.7	3-SKH model parameters for Oxford clay
Table 6.1	Modified Cam Clay parameters for Speswhite kaolin (Morrison 1994)
Table 6.2	3-SKH model Parameters for Speswhite kaolin (Stallebrass 1990) (Viggiani 1992)
Table 6.3	Brick model parameters for Speswhite kaolin (Ingram, 2000)
Table 6.4	Brick Model stepwise curve string data for Speswhite kaolin (Ingram, 2000)
Table 7.1	3-SKH model parameters for Silica sand (after Grant, 1998)
Table 7.2	Stress states prior to geotechnical event for various geological histories defining natural soil structure
Table 7.3	Parameters used for the soil strata underlying the excavation in Oxford clay

## LIST OF FIGURES

- Figure 1.1 Framework for the behaviour of reconstituted clay in volumetric space
- Figure 1.2 Framework for the behaviour of reconstituted clay in stress space
- Figure 1.3 Framework for the behaviour of natural clay in volumetric space
- Figure 1.4 Framework for the behaviour of natural clay in stress space
- Figure 1.5 Description of initial state for a stiff clay
- Figure 2.1 The effects of secondary compression and structure on void ratio during normal compression (after Leroueil and Vaughan, 1990)
- Figure 2.2 A schematic representation of compression of 'structured' and 'destructured' soils in the oedometer test (after Leroueil and Vaughan, 1990)
- Figure 2.3 Scanning electron micrograph of reconstituted Pappadai clay compressed to  $\sigma'_v = 22$  MPa (after Cotecchia, 1996)
- Figure 2.4 Scanning electron micrograph of natural Pappadai clay compressed to  $\sigma'_v = 22$  MPa (after Cotecchia, 1996)
- Figure 2.5 Compression data for reconstituted and minced samples of a structurally complex clay (after Fearon, 1998)
- Figure 2.6 Normalising compression data by the use of void index  $I_v$  to identify the Intrinsic compression line (ICL) (after Burland, 1990)
- Figure 2.7 Normalised reconstituted compression curves, identifying the Intrinsic compression line (ICL) (after Burland, 1990)
- Figure 2.8 The intrinsic compression line (ICL) and the sedimentation compression line (SCL) for normally consolidated clays (after Burland, 1990)
- Figure 2.9 The sensitivity framework, showing sedimentation compression curves for clays of equal sensitivities (after Cotecchia, 1996)
- Figure 2.10 One dimensional compression of Boom clay (after Coop et al., 1995)
- Figure 2.11 One dimensional compression data for reconstituted samples of clay plotted in terms of void index  $I_v$  (after Burland et al, 1996)
- Figure 2.12 Comparison of natural (intact) and reconstituted (intrinsic) Hvorslev surfaces: a) Pietrafitta clay; b) Todi clay; c) Vallericca clay; d) Corinth marl (after Burland et al, 1996)
- Figure 2.13 Isotropic and  $K_0$  compression and swelling data for reconstituted and natural samples of Pappadai clay (after Cotecchia and Chandler, 1997)
- Figure 2.14 Normalised state boundary surfaces for reconstituted and natural samples of Pappadai clay (after Cotecchia and Chandler, 1997)
- Figure 2.15 Normalised state boundary surface for natural Pappadai clay, showing critical state friction lines for reconstituted and natural samples (after Cotecchia and Chandler, 1997)
- Figure 2.16 Initial states for shearing tests carried out on Vallericca clay, medium and high pressure tests (after Amorosi and Rampello, 1998)

- Figure 2.17 Normalised stress paths for medium and high pressure shearing stages (after Amorosi and Rampello, 1998)
- Figure 2.18 Normalised stress paths for Boom clay in triaxial compression and extension (after Coop et al, 1995)
- Figure 2.19 State paths for boulder clay from Chapel cross (after Coop et al, 1995)
- Figure 2.20 State boundary surfaces for natural and reconstituted Vallericca clay, normalised by the equivalent pressure at failure (after Rampello et al, 1993)
- Figure 2.21 Shearing paths of reconstituted and natural samples in the compression plane: (after Rampello et al, 1993)
- Figure 2.22 Schematic of state boundary surfaces for reconstituted and natural samples of clay, showing location of critical states.
- Figure 2.23 Schematic of normalised state boundary surfaces for reconstituted and natural samples of clay, showing location of critical states.
- Figure 2.24 Schematic of normalised state boundary surfaces for reconstituted and destructuring natural samples of clay, showing location of critical states.
- Figure 2.25 An idealisation of the variation of stiffness with strain for soil (after Atkinson and Salfors, 1991)
- Figure 2.26 Triaxial cell incorporating bender elements (after Viggiani and Atkinson, 1995)
- Figure 2.27 Isotropic stress states at which bender element tests were carried out (after Viggiani and Atkinson, 1995)
- Figure 2.28 Variation of  $G_0$  with stress and overconsolidation ratio,  $R_0$ , for reconstituted samples of Speswhite kaolin (after Viggiani and Atkinson, 1995)
- Figure 2.29 Variation of  $G_0$  with stress and overconsolidation ratio,  $R_0$ , for reconstituted samples of Speswhite kaolin (after Viggiani and Atkinson, 1995)
- Figure 2.30 Charts showing the variation of coefficients  $A$ ,  $n$ , and  $m$  for the relationship for  $G_0$  (after Viggiani and Atkinson, 1995)
- Figure 2.31 Variation of normalised  $G_0$  with mean effective stress and overconsolidation ratio,  $R_0$ , for natural and reconstituted samples of London clay (after Viggiani and Atkinson, 1995)
- Figure 2.32 Variation of normalised  $G_0$  with overconsolidation ratio,  $R_0$ , for natural and reconstituted samples of London clay (after Viggiani and Atkinson, 1995)
- Figure 2.33 Variation of normalised stiffness with overconsolidation ratio for reconstituted Speswhite kaolin (after Jovicic, 1997)
- Figure 2.34 Variation of normalised stiffness with overconsolidation ratio for reconstituted Boom clay (after Jovicic, 1997)
- Figure 2.35 Variation of normalised  $G_0$  with mean effective stress and overconsolidation ratio,  $R_0$ , for natural and reconstituted samples of Vallericca clay (after Rampello et al, 1994)

- Figure 2.36 Undrained shear modulus of natural and reconstituted Boom clay (after Coop et al, 1995)
- Figure 2.37 Normalised shear stiffness against yield stress ratio for natural and reconstituted samples of Pappadai clay (after Cotecchia, 1996)
- Figure 2.38 Variation of  $G_0$  with mean effective stress for a) Vallericca clay; b) Bisaccia clay (after D-Onafrio et al, 1998)
- Figure 2.39 Initial shear stiffness,  $G_0$ , normalised by: a) the reconstituted equivalent pressure; b) the appropriate equivalent pressure (after Rampello and Silvestri, 1993)
- Figure 2.40 Schematic diagram in volumetric space showing possible state path for soil subject to creep
- Figure 2.41 The effect of sustained loading on stress-strain and strength behaviour (after Mitchell, 1976)
- Figure 2.42 Definition of instant and delayed compression compared with primary and secondary compression (after Bjerrum, 1967)
- Figure 2.43 Laboratory creep test on Drammen clay (after Bjerrum, 1967)
- Figure 2.44 The effect of cementation in volumetric space (after Bjerrum, 1967)
- Figure 2.45 Drained creep tests on natural samples of London clay (after Bishop, 1966)
- Figure 2.46 Rest periods for London clay following different approach paths (after Richardson, 1988)
- Figure 2.47 Graph of deviator stress against shear strain for constant  $p'$  tests with different rest periods and approach paths (after Richardson, 1988)
- Figure 2.48 Results from recent stress history tests for path OX: a) approach paths; b) stiffness curves for different stress path rotations (after Richardson, 1988)
- Figure 2.49 Stress probes to investigate recent stress history (after Smith et al, 1992)
- Figure 2.50 Stiffness curves following various stress path rotations (after Smith et al, 1992)
- Figure 3.1 The three surface kinematic hardening model in stress space (after Stallebrass, 1990)
- Figure 3.2 The principal of the translation rule for the kinematic surfaces in the 3-SKH model (after Stallebrass, 1990)
- Figure 3.3 Normal compression line and swelling line in  $\ln v : \ln p'$  space (after Al Tabbaa, 1987)
- Figure 3.4 3-SKH model predictions for different stress path rotations (after Stallebrass and Taylor, 1997)
- Figure 3.5 The s-shaped curve of stiffness against strain (after Simpson, 1992)
- Figure 3.6 Recent stress history tests, results for path OX: a) stress paths; b) stiffness curves (after Richardson, 1988)
- Figure 3.7 Strain vectors following different approach paths in stress space (after Stallebrass, 1990)

- Figure 3.8 A man pulling bricks attached to him by strings in strain space (after Simpson, 1992)
- Figure 3.9 The s-shaped curve represented in a stepwise fashion by the brick concept (after Simpson, 1992)
- Figure 3.10 Isotropic normal compression lines for materials with various degrees of bonding (after Gens and Nova, 1993)
- Figure 3.11 Successive yield surfaces for increasing degrees of bonding, with surface a representing the unbonded material (after Gens and Nova, 1993)
- Figure 3.12 The reduction of bonding,  $b$ , with increasing damage (after Gens and Nova, 1993)
- Figure 3.13 Predicted isotropic normal compression lines for materials with various degrees of bonding (after Gens and Nova, 1993)
- Figure 3.14 Measured and computed triaxial shearing test data: a) deviator stress versus axial strain; b) volumetric strain versus axial strain (after Gens and Nova, 1993)
- Figure 3.15 Model for destructuration of clays represented in stress space (after Rouainia and Muir Wood, 1998)
- Figure 3.16 Predictions of one dimensional compression for various amounts of initial structure  $r_0$  (after Rouainia and Muir Wood, 1998)
- Figure 3.17 Comparison of model predictions and experimental data for an undrained triaxial test on Norrköping clay showing: a) stress-strain response; b) stress path (after Rouainia and Muir Wood, 1998)
- Figure 3.18 Characteristic surfaces of the MSS model (after Kavvadas and Amorosi, 1998)
- Figure 3.19 One dimensional compression curves computed by the MSS model for various parameter combinations (after Kavvadas and Amorosi, 1998)
- Figure 3.20 Comparison between experimental results and model predictions for medium pressure drained and undrained tests on anisotropically consolidated Vallericca clay (after Kavvadas and Amorosi, 1998)
- Figure 3.21 Comparison between normalised stress paths of experimental results and model predictions for medium pressure drained and undrained tests on anisotropically consolidated Vallericca clay (after Kavvadas and Amorosi, 1998)
- Figure 3.22 Proposed anisotropic bounding surfaces: a) translated; b) rotated (after Mroz et al., 1979)
- Figure 3.23 Model predictions of  $K_0$  for: a) translated bounding surface; b) rotated bounding surface (after Mroz et al., 1979)
- Figure 3.24 Proposed yield surface compared with experimental results (after Davies and Newson, 1993)
- Figure 3.25 Yield surface for anisotropic model in stress space (after Banerjee and Yousef, 1986)
- Figure 3.26 Yield, failure and loading surfaces for MIT-E3 model (after Whittle, 1993)

- Figure 3.27 Definition of anisotropic parameters for  $G_{\max}$
- Figure 3.28 Stress paths during undrained shearing for the version of the 3-SKH model incorporating anisotropic values of  $G_{\max}$  (after Jovicic, 1997)
- Figure 3.29 Definition of primary and secondary consolidation (after Mesri and Choi, 1985)
- Figure 3.30 Definition of equivalent time (after Burhignoli et al, 1994)
- Figure 3.31 Definition of creep model in stress space (after Burghignoli et al, 1994)
- Figure 4.1 Schematic showing location of reconstituted and natural normal compression lines in  $\ln v : \ln p'$  space for a natural clay with stable fabric and  $S_t > 1$
- Figure 4.2 Schematic showing possible path taken in  $\ln v : \ln p'$  space during deposition of a clay deposit
- Figure 4.3 Schematic showing the relative locations of points defined on the reconstituted and natural normal compression lines by the mean effective stress due to overburden
- Figure 4.4 The inclusion of volumetric creep in the 3-SKH model; a) in stress space; b) in volumetric space
- Figure 5.1 Finite element mesh representing a 'single element' of uniform soil for the analysis of triaxial tests.
- Figure 5.2 One dimensional normal compression lines of natural and reconstituted Boom clay (after Coop et al., 1995)
- Figure 5.3 Variation of stress ratio at failure with mean effective stress for Boom clay (after Coop et al., 1995)
- Figure 5.4 Reconstituted isotropic normal compression data for test *rec1* showing calculated normal compression line
- Figure 5.5 Isotropic swelling stages for tests *rec2* and *boom3* plotted as bulk modulus divided by mean effective stress against mean effective stress normalised by the preconsolidation pressure on the reconstituted normal compression line.
- Figure 5.6 Charts linking the plasticity index with the stiffness coefficients  $A$ ,  $n$ ,  $m$  (after Viggiani and Atkinson, 1995)
- Figure 5.7 Predictions of  $G_{\max}$  against mean effective stress using parameters derived from Agah (1996) and from charts presented by Viggiani and Atkinson (1995)
- Figure 5.8 Predictions of  $G_{\max}$  against overconsolidation ratio using parameters derived from Agah (1996) and from charts presented by Viggiani and Atkinson (1995)
- Figure 5.9 Stress path predictions for test *ruth* for parameter sets 16-20
- Figure 5.10 Shear stiffness predictions for test *ruth* for parameter sets 16-20
- Figure 5.11 Schematic diagram showing the relative positions of the reconstituted and natural normal compression lines in volumetric space.
- Figure 5.12 Drained and undrained stress paths for reconstituted samples of Boom clay

- Figure 5.13 3-SKH model predictions of drained and undrained stress paths for reconstituted samples of Boom clay
- Figure 5.14 Drained and undrained stress paths for reconstituted samples of Boom clay normalised by the current preconsolidation pressure
- Figure 5.15 3-SKH model predictions of drained and undrained stress paths for reconstituted samples of Boom clay normalised by the current preconsolidation pressure
- Figure 5.16 Shear stiffness behaviour for reconstituted samples of Boom clay
- Figure 5.17 3-SKH model predictions of shear stiffness behaviour for reconstituted Boom clay
- Figure 5.18 Graph of stress ratio against axial strain for reconstituted Boom clay
- Figure 5.19 3-SKH model predictions of stress ratio against axial strain for reconstituted Boom clay
- Figure 5.20 Graph of pore water pressure against deviator stress for reconstituted samples of Boom clay
- Figure 5.21 Graph of 3-SKH model predictions of pore water pressure against deviator stress for reconstituted Boom clay
- Figure 5.22 Undrained stress paths for natural samples of Boom clay
- Figure 5.23 3-SKH model predictions of undrained stress paths for natural Boom clay using an initial state boundary surface computed from the reconstituted compression behaviour
- Figure 5.24 3-SKH model predictions of undrained stress paths for natural Boom clay using an initial state boundary surface computed from the natural compression behaviour
- Figure 5.25 Shear stiffness behaviour for natural samples of Boom clay
- Figure 5.26 3-SKH model predictions of shear stiffness behaviour for natural Boom clay using an initial state boundary surface computed from the reconstituted compression behaviour
- Figure 5.27 3-SKH model predictions of shear stiffness behaviour for natural Boom clay using an initial state boundary surface computed from the natural compression behaviour
- Figure 5.28 Graph of stress ratio against axial strain for natural Boom clay
- Figure 5.29 3-SKH model predictions of stress ratio against axial strain for natural Boom clay using an initial state boundary surface computed from the reconstituted compression behaviour
- Figure 5.30 3-SKH model predictions of stress ratio against axial strain for natural Boom clay using an initial state boundary surface computed from the natural compression behaviour
- Figure 5.31 Graph of pore water pressure against normalised deviator stress for reconstituted samples of Boom clay
- Figure 5.32 Graph of 3-SKH model predictions of pore water pressure against deviator stress for natural Boom clay using an initial state boundary surface computed from the reconstituted compression behaviour

- Figure 5.33 Graph of 3-SKH model predictions of pore water pressure against deviator stress for natural Boom clay using an initial state boundary surface computed from the natural compression behaviour
- Figure 5.34 Schematic diagram in volumetric space showing possible state paths for soil subject to ageing effects distinguishing creep and bonding.
- Figure 5.35 Stress probes followed during test to establish the influence of recent stress history (after Stallebrass, 1990)
- Figure 5.36 Schematic diagrams showing the configuration of the surfaces of the 3-SKH model after following paths corresponding to various recent stress histories and being allowed to creep
- Figure 5.37 Graph of shear stiffness against deviator stress for various stress path rotations where no creep has been modelled
- Figure 5.38 Graph of shear stiffness against deviator stress for various stress path rotations where a period of 1 year of creep has been modelled
- Figure 5.39 Graph of shear stiffness against deviator stress for various stress path rotations where a period of 1000 years of creep has been modelled
- Figure 5.40 Graph of shear stiffness against deviator stress for a 90 degree stress path rotation showing predictions for various modelled periods of creep
- Figure 5.41 Graph of deviator stress against percentage shear strain for a 90 degree stress path rotation showing predictions for various modelled periods of creep
- Figure 5.42 Graph of shear stiffness against deviator stress for a 180 degree stress path rotation showing predictions for various modelled periods of creep
- Figure 5.43 Graph of deviator stress against percentage shear strain for a 180 degree stress path rotation showing predictions for various modelled periods of creep
- Figure 5.44 Graph of deviator stress against percentage shear strain for a -90 degree stress path rotation showing predictions for various modelled periods of creep
- Figure 5.45 Graph of deviator stress against percentage shear strain for a 0 degree stress path rotation showing predictions for various modelled periods of creep
- Figure 5.46 Graph showing the effect of creep on shear stiffness during undrained shearing.
- Figure 5.47 Graph showing the effect of creep on stress paths during undrained shear.
- Figure 5.48 The effect of different periods of creep on shear stiffness for a single element simulation of the geological history of a deposit of London clay.
- Figure 5.49 The effect of different periods of creep on stress path direction for a single element simulation of the geological history of a deposit of London clay.

- Figure 5.50 Isotropic normal compression line data for reconstituted Oxford clay (after Atkinson and Cherrill, 1988)
- Figure 5.51 One dimensional normal compression lines for reconstituted and natural samples of Oxford clay
- Figure 5.52 Graph of  $K'/p'$  against  $p'/p'_c$  for three constant  $q$  swelling stages for test t06 on natural Oxford clay
- Figure 5.53 Graph of shear stiffness at various stress levels (after Hird and Pierpoint, 1997)
- Figure 5.54 Stress probes followed during test t06 on natural Oxford clay (after Pierpoint, 1997)
- Figure 5.55 Stiffness curve for Oxford clay constant  $p'$  test T06SHR03 plotted against model predictions for varying values of  $T$ ,  $S$  and  $\phi$ .
- Figure 5.56 Stiffness curve for Oxford clay constant  $p'$  test T06SHR04 plotted against model predictions for varying values of  $T$ ,  $S$  and  $\phi$ .
- Figure 5.57 Stiffness curve for Oxford clay constant  $p'$  test T06SHR06 plotted against model predictions for varying values of  $T$ ,  $S$  and  $\phi$ .
- Figure 5.58 Undrained stress paths for tests on Oxford Clay plotted against model predictions for isotropic parameters
- Figure 5.59 Undrained stress paths for tests on Oxford Clay plotted against model predictions for both isotropic and anisotropic parameters
- Figure 5.60 Stiffness curve for Oxford Clay undrained test 'Y3' plotted against model predictions for both isotropic and anisotropic parameters
- Figure 5.61 Stiffness curve for Oxford Clay undrained test 'Y8' plotted against model predictions for both isotropic and anisotropic parameters
- Figure 5.62 Deviator stress against axial strain for Oxford Clay undrained test 'Y3' plotted against model predictions for both isotropic and anisotropic parameters
- Figure 5.63 Deviator stress against axial strain for Oxford Clay undrained test 'Y8' plotted against model predictions for both isotropic and anisotropic parameters
- Figure 5.64 Stiffness curve for Oxford clay constant  $p'$  test T06SHR03 plotted against model predictions for varying values of  $T$ ,  $S$  and  $\phi$  and for anisotropic model prediction.
- Figure 5.65 Stiffness curve for Oxford clay constant  $p'$  test T06SHR04 plotted against model predictions for varying values of  $T$ ,  $S$  and  $\phi$  and for anisotropic model prediction.
- Figure 5.66 Stiffness curve for Oxford clay constant  $p'$  test T06SHR06 plotted against model predictions for varying values of  $T$ ,  $S$  and  $\phi$  and for anisotropic model prediction.
- Figure 6.1 The change in stress distribution in the clay layer during consolidation, preparation and testing of the centrifuge foundation model (after Stallebrass and Taylor, 1997)

- Figure 6.2 Diagram showing general layout of the centrifuge foundation model (after Stallebrass and Taylor, 1997)
- Figure 6.3 Finite element mesh used for analyses carried out using the CriSP finite element program for the 3-SKH model and Modified Cam clay
- Figure 6.4 Load/time ramps applied during the centrifuge foundation test, showing 3-SKH model and Modified Cam clay simulations.
- Figure 6.5 Finite element mesh used for analyses carried out using the SAFE finite element program for the Brick model
- Figure 6.6 Load-displacement curves comparing measured data with 3-SKH model and Brick model predictions at the centre of the foundation
- Figure 6.7 Comparison of predicted 1<sup>st</sup> load-displacement curves predicted using the 3-SKH model for consolidation and drained/undrained assumptions
- Figure 6.8 Typical strain ranges around geotechnical structures (after Mair, 1993)
- Figure 6.9 Settlement profile at 580N first loading comparing measured data and 3-SKH model and Modified Cam clay predictions
- Figure 6.10 Settlement profile at 660N first loading comparing measured data and 3-SKH model and Modified Cam clay predictions
- Figure 6.11 Settlement profile at 660N re-loading comparing measured data and 3-SKH model and Modified Cam clay predictions
- Figure 6.12 Settlement profile at end of first loading comparing measured data and Brick model prediction
- Figure 6.13 Settlement profile at end of swelling comparing measured data and Brick model prediction
- Figure 6.14  $K_0$  profiles predicted from finite element analyses compared to various methods of estimating  $K_0$  from the literature
- Figure 6.15 The centrifuge tunnel model (after Grant, 1998)
- Figure 6.16 Location of LVDT's at the surface of the centrifuge tunnel model (after Grant, 1998)
- Figure 6.17 Surface settlement plotted against reduction in tunnel support pressure for centrifuge tunnel test
- Figure 6.18 Enlargement of the initial part of the graph of surface settlement plotted against reduction in tunnel support pressure.
- Figure 6.19 Normalised tunnel settlement profiles at ground surface for a 20% volume loss for centrifuge tunnel test
- Figure 7.1 Approximate size and location of the kinematic surfaces of the 3-SKH model prior to the modelling of the geotechnical events for an element of soil at the top of the clay layer
- Figure 7.2  $K_0$  profiles predicted by the finite element analyses prior to reduction of tunnel pressures
- Figure 7.3 The geometry of the tunnel problem
- Figure 7.4 Finite element mesh used for the tunnel problem
- Figure 7.5 Clay/gravel interface settlement profiles at 0.5% volume loss

- Figure 7.6 Percentage reduction in tunnel support pressure against percentage volume loss
- Figure 7.7 Surface settlement above tunnel centreline against percentage reduction in tunnel support pressure
- Figure 7.8 Finite element mesh for the foundation problem
- Figure 7.9 Settlement profiles predicted at the clay/gravel interface for a foundation displacement of 5mm
- Figure 7.10 Change in vertical force applied to foundation against displacement at centreline
- Figure 7.11 Detail of initial portion of change in vertical force applied to foundation against displacement at centreline curve
- Figure 7.12 Settlement troughs at ground surface for 1.5% volume loss.
- Figure 7.13 Normalised settlement profiles at ground surface, showing Gaussian distribution.
- Figure 7.14 Schematic showing location of monitoring sections and soil strata
- Figure 7.15 Prediction of vertical displacement at 1.5m depth for model O.C. (after Pierpoint, 1996)
- Figure 7.16 Prediction of vertical displacement at 11m depth for model O.C. (after Pierpoint, 1996)
- Figure 7.17 Prediction of vertical displacement at 14m depth for model O.C. (after Pierpoint, 1996)
- Figure 7.18 Prediction of horizontal displacement at section L for model O.C. (after Pierpoint, 1996)
- Figure 7.19 Prediction of horizontal displacement with varying  $K_0$  at various distances from the excavation centreline for model O.C. (after Pierpoint, 1996)
- Figure 7.20 Prediction of vertical displacement with varying  $K_0$  at various depths for model O.C. (after Pierpoint, 1996)
- Figure 7.21 Finite element mesh for the Elstow excavation analyses
- Figure 7.22  $K_0$  profiles predicted by the finite element analyses prior to excavation
- Figure 7.23 Predicted unloading curve for the Oxford clay analyses
- Figure 7.24 Amplified displacements (x100) along excavation profile
- Figure 7.25 Displacement vectors for the Elstow excavation analysis Elstow a (magnified by 100)
- Figure 7.26 Displacement vectors for the Elstow excavation analysis Elstow b (magnified by 100)
- Figure 7.27 Displacement vectors for the Elstow excavation analysis Elstow c (magnified by 100)
- Figure 7.28 Displacement vectors for the Elstow excavation analysis Elstow d (magnified by 100)
- Figure 7.29 Displacement vectors for the Elstow excavation analysis Elstow e (magnified by 100)

- Figure 7.30 Observed vectors of displacement around the Elstow excavation (after Pierpoint, 1996)
- Figure 7.31 Settlement profiles at ground surface
- Figure 7.32 Vertical displacement at 1.5m below ground surface
- Figure 7.33 Vertical displacement at 8m below ground surface
- Figure 7.34 Vertical displacement at 11m below ground surface
- Figure 7.35 Vertical displacement at 14m below ground surface
- Figure 7.36 Horizontal displacement at excavation centreline (section F)
- Figure 7.37 Horizontal displacement at section H
- Figure 7.38 Horizontal displacement at section I
- Figure 7.39 Horizontal displacement at section L
- Figure 7.40 Horizontal displacement at section M

## ACKNOWLEDGEMENTS

Firstly, I'd like to thank my supervisor Dr Sarah Stallebrass for providing helpful encouragement and input throughout my time at City University. In particular I'd like to thank her for reading the endless drafts of this work over the last few months and for her time and patience in general. I'd also like to thank Dr Brian Simpson of Arup Geotechnics for his helpful input, particularly whilst I was wrestling with numerical analyses at Arup's.

The Geotechnical Engineering research group at City University have provided a friendly environment in which to carry out this research. The academic staff have been instrumental in creating this atmosphere of collaboration and support. Thanks to Prof. Neil Taylor for his encouragement and for arranging my support for the past few months, Prof. John Atkinson for his always well focused assistance, and to Dr. Matthew Coop for his useful comments and data.

I would also like to thank all the researchers who have been at City during my stay who have helped to make this a memorable time. Particular thanks must go to Dr. Ruth Fearon, Dr. Richard Grant, Ulrich Klotz, Beatrice Baudet and Andy McNamara for their friendship, and to anyone else who kept up the supply of cakes and good humour.

I was supported throughout the first three years of this work by an EPSRC grant, and a CASE award provided by Ove Arup and Partners and I gratefully acknowledge these.

I must also thank Dr N. Pierpoint for the useful data that he supplied.

Finally thanks are due to my mother and father for encouraging me all this time, and particularly to Samantha for putting up with me for the last three and a half years and supporting me in everything I have done.

## DECLARATION

I grant powers of discretion to the University Librarian to allow this dissertation to be copied in whole or in part without further reference to me. This permission covers only single copies made for study purposes, subject to normal conditions of acknowledgement.

## ABSTRACT

This dissertation describes a series of methods and approaches to the modelling of features of the stress-strain behaviour of natural stiff clays. A review of experimental work on these clays has shown that natural structure, anisotropy and creep are major causes of these features. Nevertheless, work by several authors (Burland, 1990, Cotecchia, 1996) has demonstrated that the behaviour of natural stiff clays fits reasonably well into the Critical State framework developed for reconstituted clays, in particular, those clays with a stable natural structure, which are the focus of much of the work in this dissertation.

The methods that have been developed to model the effects of natural structure, anisotropy and creep are extensions to a constitutive model developed from tests on reconstituted clay. They have been evaluated by modelling both laboratory tests, where conditions are well defined, and field problems, where conditions are more complex.

A series of laboratory tests carried out on samples of reconstituted and natural Boom clay were modelled to investigate the influence of assuming a natural state boundary surface on predictions for the natural clay. Tests on natural samples of Oxford clay were modelled to investigate the application of the model to a clay which has a response characterised by depositional anisotropy. Analyses were carried out using a version of the constitutive model adapted to allow periods of volumetric creep to test whether the consequences of modelling creep by increasing the size of the state boundary surface at constant stress were consistent with observations.

The methods were also used in the analysis of field problems. A series of analyses were undertaken to investigate the importance of allowing for the effects of natural structure and anisotropy on predicted ground movements around a tunnel, a foundation and an open excavation. These analyses also investigate the effect of assuming different scenarios for the formation of natural structure during the geological history of the deposit. Analyses were also carried out to investigate the consequences of allowing periods of creep on the predicted displacements around a tunnel.

The work showed that the methods used to model the features of natural stiff clays affected predictions in a manner consistent with observations, for the analyses of laboratory element tests. Analyses of field problems showed that using these methods significantly affects predictions of ground movements, but that the application of the methods depends on a detailed understanding of the processes undergone during the geological history of the clay, which are in practice often unclear.

## LIST OF SYMBOLS

$A$	Dimensionless constant (in expression for $G'_o$ )
$C_\alpha$	Coefficient of secondary compression
$G'_{ec}$	Elastic shear stiffness in 3-SKH model
$G'_{hh}$	Shear modulus in the horizontal plane for a cross-anisotropic soil
$G'_{max}$	Very small strain shear stiffness
$G'_o$	Very small strain shear stiffness
$G'_{onc}$	Very small strain shear stiffness for normally consolidated sample
$G'_u$	Undrained shear stiffness
$G'_{vh}$	Shear modulus in the horizontal plane for a cross-anisotropic soil
$G'_{vv}$	Shear modulus in the horizontal plane for a cross-anisotropic soil
$I_v$	Void index
$K'$	Bulk modulus
$K_o$	Coefficient of earth pressure at rest
$M$	Slope of critical state line projected in $q':p'$ plane
$N$	Specific volume of normally consolidated soil at $p' = 1\text{kPa}$
$N^*$	Specific volume of normally consolidated reconstituted soil at $p'=1\text{kPa}$ in $\ln v:\ln p'$ space
$N_n^*$	Specific volume of normally consolidated natural soil at $p'=1\text{kPa}$ in $\ln v:\ln p'$ space
$R_o$	Degree of overconsolidation
$S$	Ratio between the radii of history and yield surfaces (3-SKH model)
$S_t$	Sensitivity
$T$	Ratio between the radii of history and bounding surfaces (3-SKH model)
$e$	Void ratio
$e^*_{100}$	Void ratio at $\sigma'_v = 100$ for a reconstituted soil on the NCL
$e^*_{1000}$	Void ratio at $\sigma'_v = 1000$ for a reconstituted soil on the NCL
$h$	Hardening function for 3-SKH model
$m$	Dimensionless constant (in expression for $G'_o$ )
$n$	Dimensionless constant (in expression for $G'_o$ )
$2p'_o$	$p'$ at the intersection of the current swelling line with the NCL

$p'$	Current mean effective stress
$p'_a$	Coordinate of the centre of history surface (3-SKH model)
$p'_b$	Coordinate of the centre of yield surface (3-SKH model)
$p'_c$	Preconsolidation pressure
$p'_c$	Preconsolidation pressure for reconstituted clay
$p'_{cc}$	Apparent preconsolidation pressure after volumetric creep
$p'_{cn}$	Preconsolidation pressure for natural clay
$p'_e$	Equivalent pressure on the normal compression line
$p'_e$	Equivalent pressure on the reconstituted normal compression line
$p'_{en}$	Equivalent pressure on the natural normal compression line
$p'_m$	Previous maximum mean effective stress
$p'_r$	Reference pressure (=1kPa)
$p_{yn}$	Yield stress of natural sample
$q'$	Current deviator stress
$q'_a$	Coordinate of the centre of history surface (3-SKH model)
$q'_b$	Coordinate of the centre of yield surface (3-SKH model)
$s'$	Mean effective stress in plane strain
$s_u$	Undrained shear strength of reconstituted soil
$s_{un}$	Undrained shear strength of natural soil
$t$	Deviator stress in plane strain
$v$	Specific volume
$\alpha^2$	Ratio of horizontal to vertical shear stiffness
$\beta_\phi$	Effect of overconsolidation ratio on frictional resistance (Brick model)
$\beta_\gamma$	Effect of overconsolidation ratio on stiffness (Brick model)
$\epsilon_a$	Axial strain
$\epsilon_e$	Equivalent strain for geotechnical structure
$\epsilon_s^p$	Plastic shear strain
$\epsilon_r$	Radial strain
$\epsilon_s$	Shear strain
$\epsilon_v$	Volumetric strain
$\epsilon_v^p$	Plastic volumetric strain
$\epsilon_x$	Horizontal strain in plane strain

$\varepsilon_y$	Vertical strain in plane strain
$\phi'$	Friction angle
$\gamma$	Volumetric strain in plane strain
$\Gamma^*$	Specific volume of reconstituted soil on critical state line at $p'=1\text{kPa}$ in $\ln v:\ln p'$ space
$\kappa$	Slope of swelling line in $v:\ln p'$ space
$\kappa^*$	Gradient of swelling line in $\ln v:\ln p'$ space
$\lambda$	Slope of the normal compression line in $v:\ln p'$ space
$\lambda^*$	Gradient of normal compression line in $\ln v:\ln p'$ space
$\mu$	Drucker-Prager modification factor (Brick model)
$\nu$	Poisson's ratio
$\theta$	Angle of stress path rotation
$\sigma'_h$	Horizontal effective stress
$\sigma'_v$	Vertical effective stress
$\sigma'_{ve}$	Equivalent vertical stress on the reconstituted NCL
$\sigma'_{ven}$	Equivalent vertical stress on the natural NCL
$\sigma'_{vmax}$	Maximum previous vertical stress
$\sigma'_x$	Horizontal effective stress in plane strain
$\sigma'_y$	Vertical effective stress in plane strain
$\upsilon$	Shear strain in plane strain
$\psi$	Secondary compression index in terms of natural strains

## CHAPTER 1 INTRODUCTION

### 1.1 BACKGROUND

Over the past ten to fifteen years a number of constitutive models simulating the behaviour of stiff overconsolidated soils have been developed from the results of high quality laboratory testing at small strains (for example, Stallebrass, 1990, Puzrin and Burland, 1998). The majority of these models have been created to simulate the behaviour of reconstituted soil samples, thus they may lack the ability to model some of the phenomena associated solely with soils in their natural state in the ground. This may contribute to their inability to predict the precise patterns of behaviour observed in the field (Addenbrooke et al., 1997). Several workers have identified aspects of behaviour that are particularly important when modelling the response of natural samples of soil (Leroueil and Vaughan, 1990, Cotecchia and Chandler, 1997), including the effects of fabric, bonding and creep. In natural deposits the response of the soil is likely to be affected by more than one of these effects occurring simultaneously. The general aim of the work contained within this dissertation is to improve confidence in the prediction of ground movements for boundary value problems in the field. More precisely, the main aim is to identify the aspects of natural clay behaviour not accounted for in the existing constitutive models for stiff clays which may be used in design, and to find practical solutions for including them in analyses.

### 1.2 BASIC ASSUMPTIONS

The work within this dissertation is intended to be a guide to improving the method of accounting for the behaviour of natural stiff clays for the solution of field problems. The aim is to develop practical methods, that can be incorporated into analyses, which have a tangible effect on predictions. Emphasis is therefore placed on aspects of the behaviour of natural stiff clays that can be measured and characterised in a reasonably straightforward manner.

Clays can be examined at both the macro and micro level by laboratory testing and imaging techniques. Cotecchia (1996) stated that at the macro level, natural and reconstituted clays behave similarly, and that at the micro level it is impossible to distinguish features leading to changes in behaviour. Scanning electron micrographs are at present not generally specified in site investigation schedules, and at present do not yield input parameters for design. The practical nature of this project therefore leads to the examination of clay in terms of macro mechanics i.e. looking at the effect of structure in clays rather than the physical pattern of the structure at a microscopic scale.

Natural and reconstituted clays are assumed to fall within the framework of critical state soil mechanics. Although natural clays are affected by factors not directly accounted for in many critical state models it is assumed that a change in position, size or shape of the state boundary surface is sufficient to represent the overall behaviour. The validity of this assumption is discussed in more detail in Sections 2.2 and 2.3.

Due to the nature of soil sampling and testing it is at present not possible to obtain a truly undisturbed sample of clay. Future advances in testing and sampling may reduce this problem or remove it entirely, but currently sample disturbance is an issue. The structure of an 'intact' sample may have changed from the structure in the ground e.g. by the breaking of inter-particle bonds due to straining caused by swelling of a sample, or may not be truly representative of the overall soil mass due to inhomogeneities. The structure of a sample of soil carefully sampled and stored is however likely to be more representative of the in-situ clay than a reconstituted sample. The term 'natural' is therefore used in preference to 'intact' within this dissertation to describe clay that has been sampled and tested without intentional remoulding.

### 1.3 FRAMEWORK

Much of the modelling of clay in the following chapters was carried out using the 3-SKH model (Stallebrass, 1990), and therefore the behaviour of stiff clays will be examined in a framework relevant to this model. The 3-SKH model (Section 3.2.1) is an elasto-plastic kinematic hardening model formulated as an extension of Modified Cam clay (Roscoe and Burland, 1968). Results will be compared with the behaviour

predicted by the model, so as noted earlier it will be assumed that they can be analysed within the framework of critical state soil mechanics. The approach to modelling natural clays will compare the behaviours of natural and reconstituted clays in order to try to quantify additional aspects of behaviour seen in the natural clays. The sensitivity framework introduced by Cotecchia (1996), an extension of work by Mitchell (1976) and Burland (1990) can be used to quantify the effect of structure in natural clays. The following sections outline the approach to the description and characterisation of the behaviour of reconstituted and natural clay that will be used in this dissertation.

### 1.3.1 Reconstituted Clay

The state of a reconstituted soil can be characterised with respect to the normal compression line (or critical state line) and the current and previous mean stress. Natural soils are more complex and are discussed in Section 1.3.2.

The normal compression line for a reconstituted clay is assumed to follow a straight line in volumetric space of the form:

$$\ln v = \ln N^* - \lambda^* \ln p' \quad (1.1)$$

which can be seen in Figure 1.1. The reconstituted clay is assumed to reach a critical state which is defined in the volumetric space shown in Figure 1.1 by:

$$\ln v = \ln \Gamma^* - \lambda^* \ln p' \quad (1.2)$$

Figure 1.2 shows the state boundary surface, which is defined in the model as:

$$q^2 + M^2 p'^2 = M^2 p' p'_c \quad (1.3)$$

where critical state is defined as the intersection of this surface with the line:

$$q = Mp' \quad (1.4)$$

which is controlled by the coefficient of friction,  $M$ .

Cotecchia (1996) described reconstituted clay as structured, where the structure was simply different to the structure of a natural sample of the same clay. Reconstituted clays are likely to have a more stable and uniform structure than their natural counterparts, and as such may form a useful basis for comparison as suggested by Burland (1990).

### 1.3.2 Natural Clay

The compression line of a natural clay will often plot to the right of the normal compression line for a reconstituted sample of the same clay, Figure 1.3. This can be ascribed to a number of influences such as layering, development of bonds etc. but can be encompassed by the term 'natural structure'. The normal compression line for natural clays can often only be reached by compression of the sample to much higher pressures than required for the reconstituted clay. The normal compression line for the natural clay may run parallel to the intrinsic normal compression line indicating the development of a stable natural structure, or may converge with the intrinsic normal compression line, indicating a meta-stable structure caused by yielding and the degradation of structural bonds etc. The analyses in this work deal mostly with the former type of compression behaviour, as it is the simplest case; Section 2.2 discusses whether this is reasonable. The sensitivity framework described by Cotecchia (1996) is used as a measure of the additional structure caused by the depositional process, rather than a measure of the stability of the structure.

In stress space, figure 1.4, the state boundary surface for a natural clay is likely to occupy a larger area than the state boundary surface for a reconstituted sample of the same clay.

Natural clays are often referred to as 'structured' as opposed to 'unstructured' reconstituted clays. Cotecchia (1996) pointed out this misnomer stating that natural clays simply had a different structure to reconstituted clays referred to herein as natural structure. Processes undergone leading to structural changes in a natural clay are numerous, and Cotecchia (1996) identified structure due to depositional and post-

depositional processes. Natural clay structure in the context of modelling however, may be better grouped into processes leading to a change in size of the state boundary surface, and processes which move the soil state to a new elastic wall. The former group encompasses most depositional and post-depositional processes such as interparticle bonding, where structure formed during either period leads to an 'enhanced' structure compared to the reconstituted structure (Sections 2.2 and 2.3). As already mentioned, this structure can be related to the reconstituted structure by the sensitivity framework (Cotecchia, 1996). The latter group would include ageing effects such as creep (Section 2.5).

### 1.3.3 Initial states

Traditionally, overconsolidation ratio is calculated from:

$$\sigma'_{vmax} / \sigma'_v \quad (1.5)$$

where  $\sigma'_{vmax}$  is the maximum previous vertical stress, and  $\sigma'_v$  is the current vertical stress. This is not particularly helpful if a soils state is not solely determined by the previous maximum vertical stress, and is not the most convenient description for relating to critical state models which are defined in terms of a normal compression line for isotropic compression.

In a conventional Cam clay type model with elastic deformations within the state boundary surface, the position of the current state boundary surface at the start of a finite element analysis can be described by the highest mean effective stress reached during isotropic normal compression,  $p'_m$  (Figure 1.5). This allows a measure of the degree of overconsolidation,  $R_0$ , to be calculated from

$$R_0 = p'_m/p' \quad (1.6)$$

where  $p'$  is the current mean effective stress. This is not strictly true however for overconsolidated clays even if reconstituted in the laboratory, as the size of the current state boundary surface may be affected by plastic straining within the state boundary

surface and may therefore no longer correspond to  $p'_m$ . The intersection of the state boundary surface with the current elastic wall can be defined by the preconsolidation pressure,  $p'_c$  ( $p'_{cn}$  for a natural soil) which may change due to effects other than the maximum stress during deposition. For an overconsolidated clay

$$R_0 = p'_c/p' \text{ (or } R_0 = p'_{cn}/p') \quad (1.7)$$

may therefore be more appropriate.

For a natural clay, (figure 1.5) the preconsolidation pressure may be

$$p'_{cn} = p'_m + f(?) \quad (1.8)$$

as the processes undergone in the ground may increase the size of the state boundary surface in relation to the surface defined by deposition alone. Note that  $p'_c$  is only equal to  $p'_m$  (maximum stress achieved during isotropic compression) when a reconstituted soil is at an isotropically normally compressed state. For all comparisons carried out in the following chapters,  $p'_c$  or  $p'_{cn}$  will be used in preference to  $p'_m$  for describing soil state.

#### 1.4 Methodology

In order to fulfil the stated aim of this work, i.e. to improve predictions for field problems, it is necessary to be able to assess model predictions against some reference behaviour. The method proposed for achieving this is; firstly, to review the available laboratory data to characterise important aspects of natural stiff clay behaviour for modelling. Secondly, to use methods developed from consideration of the data to model laboratory tests to assess improvements in predictions. Lastly, to use the improved methods to model boundary value problems to investigate their significance for subsequent predictions.

#### 1.4.1 Interpretation of Data

Two main types of comparisons between predicted and measured data are carried out in sections of the dissertation reviewing numerical analyses undertaken to evaluate the modelling procedures.

- 1) Comparisons of model predictions with laboratory element data
- 2) Comparisons of model predictions with boundary value / field problems

Comparisons of predictions with laboratory test data will concentrate on the behaviour far from failure, in particular the prediction of stiffness and the use of data from undrained stress paths to characterise the anisotropy of the soil following Graham and Houlsby (1983) and Stallebrass (1990).

For comparisons with overconsolidated stress paths wet of critical, post peak behaviour will be ignored as localisation phenomena govern the response of these tests as failure is approached (Atkinson and Richardson, 1987). Clay samples tested at these overconsolidated states do not reach uniform critical states although the interpretation of test data often assumes that they do. Model predictions do reach critical state uniformly and are therefore likely to predict failure at a different location in stress space.

Comparisons of analyses with boundary value and field problems will concentrate on the magnitude and pattern of deformations. Consideration will also be given to the influence of the initial state, as the 3-SKH model computes a  $K_0$  profile which results from the stress history of the soil.

#### 1.4.2 Finite Element Modelling of Triaxial Tests

A number of finite element triaxial simulations are carried out in this work. The simulations are generally carried out for two purposes:

- a) To model behaviour of element (triaxial) tests for comparison with laboratory data.

- b) To evaluate model parameters by comparison with triaxial data.

The finite element triaxial simulations are referred to in the text as ‘single element’ analyses although strictly speaking they consist of two triangular axisymmetric elements of unit length. The term single element is used in reference to the uniform stress conditions that are applied to simulate triaxial paths, i.e. they behave as a single element of uniform soil. Single element predictions are a convenient way of evaluating finite element output using relatively little computing time.

### 1.4.3 Evaluating Model Input Parameters

Wherever possible, measured parameters will be used for the modelling of clays in the following chapters. The need to massage ‘measured’ parameters to fit data is indicative of deficiencies in the soil model itself, and is not helpful in trying to evaluate predictions from a given model. All of the parameters for the soil model used principally in this work can be measured by having the necessary data, and where possible parameters will be measured and not fine tuned. Due to the specific tests required to evaluate some of the model parameters, measured values may not be available if the testing program was not designed to yield parameters for the specific model, where this is the case parameters may be obtained parametrically. Where it is necessary to conduct a parametric study to gain model parameters, a typical set of data will be modelled using single element predictions to fix them. Model parameters evaluated in this way will then be used unchanged to make any subsequent predictions of other data sets from the same clay.

## CHAPTER 2      BEHAVIOUR OF STIFF OVERCONSOLIDATED CLAYS

### 2.1      INTRODUCTION

The work in this chapter has been broken down into several key areas where behaviour of a natural clay may differ from the behaviour of the same clay reconstituted. The review concentrates on aspects of clay behaviour which are well supported by laboratory data and can conceptually be fitted within the most general critical state framework as outlined in Chapter 1.

The effects investigated in this review are essentially the products of the geological processes that have taken place to bring a deposit of clay to its current state.

Recent laboratory work investigating the presence of natural structure in clays at the macro level has been carried out by several authors (e.g. Burland, 1990, Leroueil and Vaughan, 1990). The relationship between the reconstituted and natural structure of the clay is generally evaluated by comparing test data plotted both in volumetric and stress space. Evaluating natural structure within this framework is convenient if it is proposed to simulate the behaviour within critical state models. Consequently, the majority of the review of natural structure within this chapter is carried out within this framework.

In addition, the very small strain stiffness behaviour of natural clays is examined. The review is particularly aimed at establishing whether there is an additional effect of structure on clay stiffness other than that which can be accounted for by state.

Little data comparing the stress-strain response of reconstituted and natural soils at small to medium strains exists and therefore this range of behaviour will be dealt with in terms of anisotropic characteristics of stiff clays, which have a large effect on the behaviour at these strains.

The response of a natural clay to loading is likely to be anisotropic due to the one-dimensional nature of deposition and the stress paths followed. The various types of anisotropy are identified and methods for measuring anisotropy are investigated.

Time effects may also be important in determining the stress-strain response of clay to further loading. Volumetric creep, or the change in volume with time at constant load, for clay is examined to see whether it may be significant for stiff clay.

This chapter highlights the above features of the behaviour of stiff natural clays and assembles evidence from the literature relating these features to the behaviour expected for a reconstituted stiff clay. In order to successfully model these clays, it is necessary to have a clear understanding of how their behaviour differs from or is similar to a reference reconstituted material. Particular attention has been given to research which compares the behaviour of natural and reconstituted stiff clays within the same framework. This enables the identification of aspects of behaviour which our current models are likely to already be able to replicate and the areas where they are currently lacking.

## 2.2 VOLUMETRIC RESPONSE

Leroueil and Vaughan (1990) identified the main features of the loading curve for a natural soil in  $e:\log\sigma'_v$  space, that correspond to different stages in the development of depositional structure as a soil is deposited and subsequently loaded (Figure 2.1). After deposition to a vertical effective stress of  $\sigma'_{vi}$  and a void ratio  $e_i$ , there is secondary compression at a constant vertical effective stress such that the void ratio decreases to  $e_o$ . This could be assumed to give rise to an apparent increase in preconsolidation stress from  $\sigma'_{vi}$  to  $\sigma'_{vb}$ . Yield is observed at a vertical effective stress of  $\sigma'_p$  owing to the development of interparticle bonding and other structural effects. They called the area below the normal compression line the permissible space for all structural states, and the space enveloped by the normal compression line and the enhanced yield curve of the structured soil, the structure permitted space, Figure 2.2. Cotecchia (1996) however showed that reconstituted samples were not destructured as thought by Leroueil and Vaughan but simply possessed a different structure to the natural clay. Scanning electron micrographs presented by Cotecchia and reproduced in Figures 2.3 and 2.4 show the microstructure of reconstituted and intact Pappadai clay. The structure of the reconstituted clay, whilst more uniform in nature still shows structural features

consistent with an anisotropic fabric although the structure is more open due to the lower stresses involved. Further evidence of the existence of structure in reconstituted clays was presented by Fearon (1998) who tested a structurally complex clay from within a landslide. Two methods of preparation were used for comparison with intact samples, reconstitution as described by Burland (1990), and mincing, which further destroyed the structure of the sample. Figure 2.5 shows the normal compression lines for these two 'reconstituted' samples which are very different, emphasising the care that should be taken when applying this term. Fearon (1998) suggested that the term "structure permitted space" coined by Leroueil and Vaughan (1990) should be replaced by "natural structure permitted space".

Burland (1990) termed the properties of reconstituted clays intrinsic properties due to their independence from the natural state. He defined a reconstituted clay as being a sample that has been mixed at a water content greater than or equal to the liquid limit, and preferably consolidated in a consolidometer. Burland used the void index  $I_v$  to normalise the volumetric state of the clay with respect to composition. The void index is defined as follows:

$$I_v = \frac{e - e_{100}^*}{e_{100}^* - e_{1000}^*} \quad (2.1)$$

Where  $e_{100}^*$  and  $e_{1000}^*$  are the intrinsic void ratios corresponding to  $\sigma'_v = 100\text{kPa}$  and  $\sigma'_v = 1000\text{kPa}$  respectively as seen in Figure 2.6. This normalisation resulted in a unique line representing one-dimensional compression data for a variety of reconstituted clays in  $I_v:\log\sigma'_v$  space, Figure 2.7, which he called the intrinsic compression line ICL. Burland then re-plotted in-situ natural soil data from Skempton (1970) and from new tests in  $I_v:\log\sigma'_v$  space. These data plotted to the right of the ICL, in a 'moderately narrow band'. A regression line was fitted through the data defining a unique sedimentation compression curve approximately parallel to the ICL, Figure 2.8. Burland termed this line the sedimentary compression line SCL. After re-analysis of these data Cotecchia (1996) found that the ratio of the yield stress of the natural clays and the equivalent stress on the ICL of the reconstituted samples at the same water content was analogous to the sensitivity of the clay,  $S_t$ , where:

$$S_t = s_{un}/s_u \quad (2.2)$$

and  $s_u$  and  $s_{un}$  are the undrained strengths of the reconstituted and natural samples respectively. Cotecchia recognised that the soils used in the construction of the SCL plotted by Burland (1990) corresponded to clays of medium sensitivity (4 - 9). Cotecchia (1996) went on to plot a series of sedimentary compression curves (SCC) corresponding to the yield stresses of clays of different sensitivities, Figure 2.9, and noted that Burland's sedimentary compression line could be seen as a SCC for soils of sensitivity of 5 - 6. These data also showed that clays of low sensitivity plot nearer to the ICL than clays of higher sensitivity. Cotecchia and Chandler (1998) showed that sensitivity could also be written in terms of mean effective stress as:

$$St = p'_{yn}/p'_e \quad (2.3)$$

where  $p'_{yn}$  and  $p'_e$  are the yield stress of the natural sample and equivalent pressure on the reconstituted normal compression line in terms of mean effective stress.

Leroueil and Vaughan (1990) showed in schematic form, Figure 2.1, that post-yield the normal compression line for the natural clay converged with the intrinsic normal compression line at high stresses. For soft clays this is often the case, and could be attributed to interparticle bonds breaking down such that the structure of the natural sample becomes similar to the structure in the reconstituted sample. Tests on stiff clays carried out by several authors show compression behaviour of clays that does not collapse to the intrinsic compression curve even at high stresses. Coop et al. (1995) and Rampello and Silvestri (1993) both present data from tests on stiff clays which show intact normal compression lines that run parallel to the intrinsic curve. Figure 2.10 shows the results for one-dimensional compression of natural and reconstituted samples of Boom clay (see Section 5.2) showing no steep convergence of the compression curves. The sensitivity of this clay as defined by Cotecchia in terms of yield stress is approximately 1.5 from these results. Rampello and Silvestri (1993) also showed that the normal compression line of natural Vallericca clay was separate from but parallel to the normal compression line for the reconstituted clay. Coop and Cotecchia (1995) attributed the non-convergence of the natural normal compression line for Sibari clay to the reconstituted normal compression line, to the clay having a distinctly different

macroscopic fabric due to its deposition. The same distinction between natural structure being caused by depositional fabric or bonding was made by Coop et al. (1995) comparing tests on Boom clay and Calcarenite. For modelling, it may be convenient to separate the macroscopic effects of natural structure into fabric (parallel natural and reconstituted normal compression lines) and bonding (natural normal compression line converges to reconstituted), although clearly the behaviour may be characterised by a combination of these effects.

### 2.3 THE BEHAVIOUR OF STIFF OVERCONSOLIDATED CLAYS IN STRESS SPACE

Section 2.2 outlined the volumetric response expected for a natural clay compared to a reconstituted sample of the same soil. The normal compression line of the natural clay generally plots on, or to the right of the intrinsic normal compression line, and its position can be characterised by sensitivity. The critical state model relates volume, mean effective stress and deviator stress together in a framework that can be seen in Figures 1.1 and 1.2. It follows from this that, if a clay falls within the critical state framework, a natural normal compression line plotting to the right of the intrinsic normal compression line in volumetric space will define a larger state boundary surface in stress space, Figure 1.4. So, for natural clays with sensitivity greater than 1, and corresponding to the critical state model, the state boundary surface will be larger than the reconstituted state boundary surface. This leads to several issues. Firstly, although the natural state boundary surface may be larger than the reconstituted state boundary surface, is it similar in shape for a given clay? Secondly, is the difference in size of the state boundary surface purely attributable to the higher volume for the same mean effective stress that the natural clay is able to sustain. Lastly, where does critical state lie compared to the reconstituted critical state.

Burland et al. (1996) presented data from a series of tests on four stiff clays. Figure 2.11 shows the one-dimensional compression data for the four clays normalised in the manner proposed by Burland (1990). All the natural clays plot above the intrinsic compression line indicating sensitivities of greater than 1. It would be expected that all four natural samples of clay would define a state boundary surface that is larger than the corresponding state boundary surface for the reconstituted samples of the same

materials. Corinth marl is the most sensitive of the clays, lying just to the right of the sedimentary compression line implying a sensitivity of 5-6 (Cotecchia, 1996), with the others having a lower sensitivity. Figure 2.12 shows the Hvorslev surfaces for the four clays plotted in plane strain stress space, normalised by the equivalent vertical stress on the intrinsic one dimensional normal compression line denoted as  $\sigma'_{ve}$ . All four clays exhibit natural Hvorslev failure lines that exist in states outside the intrinsic failure surfaces, as expected. The shapes of the Hvorslev surfaces appear similar for all the clays, indicating that, as observed by other authors (Cotecchia, 1996, Coop et al., 1995) the state boundary surfaces of the natural and intact samples of the same clay are of similar shape. It is impossible to say whether the difference in size of the state boundary surfaces of the reconstituted and natural samples of clay can be explained purely by the difference in the position of the normal compression lines of the clays. It is worth noting however, that the difference in size of the Hvorslev surfaces for the Corinth Marl, the most sensitive clay, appears to be greatest which certainly provides evidence of the link between sensitivity in compression and shearing.

Cotecchia and Chandler (1997) present data for reconstituted and natural samples of Pappadai clay, a stiff structured Italian marine clay. The normal compression lines for the natural and reconstituted samples are shown in Figure 2.13. The compression lines are similar in gradient with  $\lambda$  for the remoulded clay being 2.04 and  $\lambda$  for the natural clay being 2.54. The normal compression line for the natural clay plots well to the right of the reconstituted normal compression line, with sensitivity,  $S_t$ , of around 2.5. Stress paths and yield points from a series of tests on both remoulded and natural samples of Pappadai clay are shown in Figure 2.14 plotted in stress space, normalised by the equivalent pressure on the intrinsic normal compression line (denoted as  $p'_e$ ). The data for the natural clay define a state boundary surface that is substantially larger than the state boundary surface for the remoulded clay. The shapes of the state boundary surfaces drawn on the graph by Cotecchia and Chandler (1997) are similar for both the reconstituted and natural samples of clay, and could reasonably be represented by a Modified Cam clay state boundary surface. The authors plot a critical state for the natural clay, falling within the state boundary surface for the stress paths. This could point to possible destructuration of the clay during shearing leading to the collapse of the bounding surface toward the state boundary surface for the reconstituted soil. The authors also defined different critical state friction coefficients for the reconstituted and

natural samples. Lines representing these coefficients are plotted in Figure 2.15, and it is clear that the intercept of the line for reconstituted soil,  $M=1.08$  with the natural state boundary surface would be a reasonable representation of both natural and reconstituted behaviour if the emphasis was on modelling pre-failure deformations, before strain softening leading to failure.

Evidence of degradation of structure for a natural sample of stiff clay was also reported by Amorosi and Rampello (1998) relating to tests on Vallericca clay. A series of triaxial tests were carried out on natural samples of clay at medium and high pressures as shown in Figure 2.16. Normalised shearing stages from both high and medium pressure tests are shown in Figure 2.17. The tests sheared from high pressures define a state boundary surface well within the state boundary surface for the medium pressure tests which shows that destructuration of the natural structure took place during compression to the initial state for the high pressure tests. For the medium pressure tests on the wet side of critical which arrive at critical state uninterrupted by the premature formation of shear planes, the stress paths head towards a critical state consistent with the results for the high pressure tests. This evidence points to significant destructuration in both volumetric compression and shearing for the Vallericca clay. For the purposes of modelling a clay like Vallericca clay, where there is evidence of destructuration, it may be necessary to allow for this within the formulation of our models, especially when modelling behaviour in the laboratory. Whilst destructuration certainly occurs in some stiff clays, it would not seem to be as marked as for soft clays, so the use of a standard critical state model without collapsing boundary surfaces to represent the destructuration may be appropriate for field problems, where movements are relatively small and far from failure. Data from tests on stiff clays where destructuration does not occur are now reviewed to investigate whether there is a difference in the size or shape of the state boundary surface unaccountable for by normalisation with respect to the volumetric behaviour. This would indicate whether the presence of natural structure affects volumetric and shear behaviour in different ways.

A series of tests on reconstituted and natural clays was carried out by Coop et al. (1995) to investigate the influence of structure on clay behaviour. Figure 2.10 shows one-dimensional compression data for reconstituted Boom clay, which defined a sensitivity of 1.55 for this clay. Figure 2.18 shows stress paths for the natural and

reconstituted Boom clay normalised with respect to equivalent pressure. In this case, the values of equivalent pressure used to normalise the data were calculated from the appropriate normal compression lines for the reconstituted and natural clay. Normalising the shearing stages in this way should remove the component of structure causing the normal compression line for the natural clay to exist at higher specific volumes than the intrinsic normal compression line. Any effect of structure evident in the stress paths, i.e. the state boundary surfaces not being coincident could be considered additional to this volume effect. The stress paths for the natural and reconstituted samples all lie close to a single state boundary surface, indicating that any additional effect of structure on shear behaviour may be small. The evidence that there may be a small additional effect of natural clay structure on the shear response is provided by the stress paths of the natural samples which all plot outside the reconstituted data, but apparently within the same normalised state boundary surface, although all the natural tests are dry of critical and limited data from tests on reconstituted soil dry of critical make it difficult to be conclusive. It is possible that the difference in the micro structure of reconstituted and natural samples of Boom clay may result in some additional shearing resistance of the natural clay leading to a slightly different shape of state boundary surface. The different gradient of the natural and reconstituted stress paths dry of critical can be explained by considering the test procedures used, and is related to the previous stress path. Reconstituted samples were simply swelled to the state from which they were sheared, whereas the natural samples were first swelled during the sampling process, and then re-compressed to the desired mean effective stress. These different recent stress histories, would affect the subsequent stress paths in the way observed (Stallebrass, 1990), which will be dealt with further in Section 5.2. Coop et al. (1995) also present data from a series of tests on reconstituted and natural samples of a boulder clay from Chapelcross in Scotland. The maximum stress used in the triaxial tests for these samples was insufficient to identify a natural normal compression line, so shearing data was normalised with respect to the normal compression line for the reconstituted soil by the equivalent pressure  $p'_e$ . Figure 2.19 shows the normalised shearing data from the natural and reconstituted tests, which seem to define a single state boundary surface. This indicates that the natural normal compression line may be the same as for the reconstituted soil i.e.  $S_t = 1$  which was attributed to heavy remoulding of the clay by glacial movements. The authors also

point out the possibility that stress relief during sampling erased the structure of the natural samples.

Rampello et al. (1993) performed a series of tests on reconstituted and natural Vallericca clay to determine whether there is any additional effect of natural clay microstructure after normalising to account for the different positions of the natural and reconstituted normal compression lines for this clay. Figure 2.20a shows the natural and reconstituted data plotted, normalised with respect to the equivalent pressure on the intrinsic compression line. The state boundary surface for the natural stress paths is larger than for the reconstituted stress paths, as expected for this sensitive clay. Figure 2.20b shows the same data with the natural tests this time normalised by the equivalent pressure on the natural normal compression line. The peak states for the natural samples of Vallericca clay still plot outside the peak states for the reconstituted samples, although the difference is greatly reduced. As for Boom clay (Coop et al., 1995) most of the effect of structure on the state boundary surface in stress space, is removed by normalising with respect to the relevant normal compression line. Again some additional resistance to deviatoric stress seems to remain after normalisation pointing to some possible extra effect of microstructure on shearing.

The location of the critical state for natural soil samples should also be considered, to test the applicability of our current critical state models to stiff natural clays. Cotecchia (1996) plotted failure points for the Pappadai clay which identified a critical state line located between the reconstituted normal compression line and the normal compression line for the natural clay. In volumetric space therefore, it is possible for stable stiff clays to have different critical states to their reconstituted counterparts. Similar data was also plotted for Vallericca clay (Rampello et al., 1993) and is shown in Figure 2.21. For the critical state model, this would lead to a critical state point in stress space lying to the right of the critical state point for the reconstituted material, Figure 2.22. It is unclear from the literature whether the critical state friction angle for a natural stiff clay is the same as for a reconstituted sample, but for the case where they are equal, the critical states for the natural and reconstituted samples may become coincident when the data are normalised with respect to the appropriate normal compression line (Figure 2.23). Stiff clays are often heavily overconsolidated in the natural state, so element tests are conducted dry of critical where behaviour in the  $p':q$  plane is characterised by

peak states and the formation of shear planes preventing a critical state being easily identified. Tests on natural and reconstituted Boom clay (Coop et al., 1995) which is not heavily overconsolidated in the natural state indicate a critical state friction angle which is consistent for both the natural and reconstituted clay. The standard critical state model should therefore be appropriate for describing this clay. Clays demonstrating significant destructuration, in particular soft clays, generally tend towards a critical state defined by the reconstituted behaviour. Clays behaving in this manner identify separate critical state points in stress space when normalised by the equivalent pressure on the appropriate normal compression line for the natural or reconstituted clay (Figure 2.24). Destructuration in shear and compression are clearly linked, and the critical states for natural destructured clay normalised with respect to a  $p'_e$  which does not account for the erasure of natural structure in compression should not correspond to the normalised reconstituted critical state. Conceptually, normalising to an equivalent pressure based on a destructuring natural normal compression line should cause the critical states to be coincident, although in practice this may be difficult to measure. It is clear, that for this form of behaviour, the use of a model able to predict destructuration would be of benefit in predicting the correct response.

The assumption that natural and reconstituted samples of the same clay share the same value of critical state friction angle, but fail at a different location in stress and volumetric space due to the larger bounding surface for the natural clay would seem a reasonable approach for modelling in the absence of evidence to the contrary for a particular clay. This allows the use of a standard critical state model without destructuration. This approach is clearly only acceptable for clays with a stable natural structure. In addition, it would seem reasonable to assume that the state boundary surface for the natural clay is the same shape as for the reconstituted clay.

#### 2.4 VERY SMALL STRAIN STIFFNESS

It is now well established that the stiffness of fine grained soils follows a non-linear pattern of the type idealised by Atkinson and Salfors (1991) which is shown in Figure 2.25. The figure shows a constant shear stiffness at very small strains representing a maximum value,  $G'_{max}$ , shown as  $G'_0$  in the figure. Atkinson and Salfors identified the

limit of very small strains as being generally around 0.001%. Many authors have presented similar curves based on laboratory tests. This section will concentrate on the factors affecting the elastic stiffness  $G'_{\max}$  for reconstituted and natural soils. The elastic stiffness can be measured both in situ and in the laboratory using various dynamic methods which relate shear wave velocity to stiffness. The relative ease of use of this method and the reproducibility of results make it an ideal base for the determination of soil parameters for use in numerical analysis.

Atkinson and Salfors (1991) stated that the very small strain stiffness of a soil was related to its current stress and overconsolidation ratio. The implication of this for soil modelling is that it is not enough simply to assume a constant maximum stiffness regardless of these factors. Viggiani and Atkinson (1995) described a series of tests on reconstituted clay conducted in a stress path triaxial cell to examine the influence of current stress and overconsolidation ratio on  $G'_{\max}$ . This work recognised that if stiffness is dependant on state, then that state could be uniquely defined by  $p'$  and  $R_0$  for a clay and therefore there was no need for the more complex formulae used by other workers in the field which include volume. The very small strain stiffness measurements were made by bender elements incorporated into the triaxial apparatus in an arrangement shown in Figure 2.26. Samples of Speswhite kaolin, powdered slate dust, London clay and "North Field" clay were tested. Stiffness measurements were taken at a variety of overconsolidation ratios and values of mean effective stress, Figure 2.27, enabling comparisons to be made between stiffness and state. Figure 2.28 shows data for a typical test on Speswhite kaolin. The figure shows  $G'_{\max}$  (denoted as  $G'_0$ ) plotted against mean effective stress  $p'$  on a logarithmic scale, both axes have been normalised by the reference pressure  $p_r$  (taken as 1 kPa). The measurements made at overconsolidated states plot above those for the normally consolidated measurements, which coincide closely with the straight line given by the equation:

$$\frac{G'_0}{p_r} = A \left( \frac{p'}{p_r} \right)^n \quad (2.4)$$

where  $A$  and  $n$  are non-dimensional soil parameters. The points in Figure 2.28 representing the measurements at overconsolidated states fall close to lines parallel to the line for the normally consolidated states. Figure 2.29 shows the same data plotted

as  $G'_0/G'_{0nc}$  against the logarithm of overconsolidation ratio, where  $G'_{0nc}$  is the value of  $G'_{max}$  for a normally consolidated sample at the same mean effective stress. The authors showed that a straight line given by:

$$\frac{G'_0}{p_r} = A \left( \frac{p'}{p_r} \right)^n R_0^m \quad (2.5)$$

where  $m$  is another non-dimensional soil parameter, fits these data reasonably well. Data from other tests on Speswhite kaolin, and tests on other soils all corresponded to the same relationship, but for the other soils the values of  $A$ ,  $n$ , and  $m$  changed. Figure 2.30 shows the parameters obtained from the tests, along with data from other authors plotted against plasticity index. The charts show that the parameter  $A$  is highly dependent on soil plasticity but that the parameter  $m$  is relatively insensitive to soil plasticity. Equation 2.5 used in conjunction with the charts presented would seem to be a reasonable way of estimating values of  $G'_{max}$  for use in numerical analysis, the practicality of doing this will be investigated later.

Viggiani and Atkinson (1995) also carried out an investigation into the effect of natural structure on the applicability of Equation 2.5. by taking a series of bender element measurements for a sample of undisturbed London clay. Figure 2.31 shows the data for the natural and reconstituted measurements plotted as  $G'_0/p_r R_0^m$  against  $p'/p_r$  this should lead to the data falling on a straight line as Equation 2.5 can be rewritten as

$$\frac{G'_0}{p_r R_0^m} = A \left( \frac{p'}{p_r} \right)^n \quad (2.6)$$

The overconsolidation ratios for the data points were calculated with respect to the appropriate normal compression line for the natural and reconstituted samples. The data presented fall on a straight line, demonstrating that  $G'_{max}$  for both reconstituted and natural samples of clay is dependent on current state and overconsolidation ratio, and not on any additional component of structure or fabric. Plotting the same data as  $G'_0/G'_{0nc}$  against  $R_0$ , figure 2.32, which enabled the exponent  $m$  to be evaluated, also shows the data plotting as a straight line except perhaps at larger values of overconsolidation ratio. Jovicic (1997) carried out two series of tests on reconstituted

clays to investigate the applicability of Equation 2.6 for stiffnesses at high values of overconsolidation ratio. The first series were carried out on a sample of Speswhite kaolin subjected to overconsolidation ratios of up to 90. Figure 2.33 shows the values of  $G'_{\max}/G'_{\max\text{nc}}$  for the tests plotted against  $R_0$  both on logarithmic axes. Also shown on the graph is the best fit line from Viggiani and Atkinson (1995) for Speswhite kaolin. At overconsolidation ratios of greater than about 10 the formula proposed by Viggiani and Atkinson no longer holds, with stiffness apparently becoming independent of overconsolidation ratio at high values of  $R_0$ . The second series of measurements taken by Agah (1996) and reported by Jovicic (1997) are for Boom clay and are plotted in the same manner in figure 2.34. For the Boom clay, the relationship holds for relatively high overconsolidation ratios. Jovicic speculated that the difference was due to the different plasticity of the clays. It is clear, as stated by Jovicic that this is an area that needs investigating further in order that a better overall picture may be built up, and at present some care must be taken in the use of Equation 2.5.

There is at present relatively little data comparing  $G'_{\max}$  measurements for samples of natural and reconstituted stiff clays of the same type assessed within the framework proposed by Viggiani and Atkinson (1995). Data are presented here from various authors who have analysed tests in this manner. Rampello et al. (1994) present evidence to support Viggiani and Atkinson's findings. Values of  $G'_{\max}$  for intact and reconstituted samples of Vallericca clay were measured at a variety of values of overconsolidation ratio and mean effective stress. Figure 2.35 shows the data for Vallericca clay plotted within the same framework as the data presented by Viggiani and Atkinson (1995). It can again be seen that the data for the reconstituted and intact samples plot together and as such would seem to be independent of any additional component of natural structure not accounted for by the difference in volumetric state. Small strain stiffness data presented by Coop et al. (1995) for Boom clay, Figure 2.36, and by Cotecchia (1996) for Pappadai clay, figure 2.37, also provide additional evidence that the effect of structure on the magnitude of  $G'_{\max}$  measured in natural clays compared to the same clay reconstituted can be explained by the difference in volumetric state .

D'Onafrio et al. (1998) report noticeable increased initial stiffnesses in natural samples of Vallericca and Bisaccia clay. The structure of the Bisaccia clay was characterised by

interparticle bonding, whereas no evidence of cementing was obtained for the Vallerica clay. Figure 2.38 shows initial stiffness plotted against mean effective stress for both clays, along with lines computed from the equation:

$$\frac{G_0}{p'_r} = S \left( \frac{p'}{p'_r} \right)^n \left( \frac{p'_e}{p'} \right)^c \quad (2.7)$$

which is similar to Equation 2.5. The tests on natural samples of Vallericca clay fall reasonably close to a line which is normalised to take account of the increased overconsolidation ratio due to the natural normal compression line being located to the right of the reconstituted line. This indicates that there is little additional effect of structure apart from the effect of the difference in state for the Vallericca clay, which is in agreement with the work by Rampello et al. (1994) for this clay. The intact tests for the Bisaccia clay fall above the line predicted by Equation 2.7. The authors conclude that this indicates that for this clay, there is some additional effect of structure on stiffness. The results are inconclusive however, as in this case the stiffnesses calculated from Equation 2.7 for the natural samples use  $p'_e$  from the normal compression line for the reconstituted tests. Using a value of  $p'_{en}$  calculated from a natural normal compression line somewhere to the right of the reconstituted normal compression line might well account for some if not all of this difference.

Rampello and Silvestri (1993) presented data from 3 sets of tests on Pietrafitta clay, a stiff clay of lacustrine origin. Stiffness measurements were taken on reconstituted samples, plus two natural samples which were stored separately. One of the intact samples “natural 1992” was thought to have undergone swelling during storage removing the effect of cemented interparticle bonds. Figure 2.39 shows the initial stiffnesses of the tests plotted against mean effective stress, both normalised by the equivalent pressure,  $p'_e$  for the appropriate normal compression line. The samples labelled “natural (1990)”, which were thought to more closely resemble the natural structure than the swelled “natural (1992)” samples still show higher values of initial stiffness, despite the difference in state having been accounted for. The increased stiffnesses measured for the “natural (1990)” samples were attributed to interparticle cementing evident in this clay from SEM analysis.

The equation proposed by Viggiani and Atkinson (1995) is able to characterise  $G'_{max}$  for both reconstituted and natural stiff clays if the correct  $R_0$ , relative to the appropriate state boundary surface is used. There may however be problems with using the relationship at high overconsolidation ratios. More test data are needed to increase confidence in this relationship.

Several authors e.g. Jovicic (1997), Pierpoint (1996) and Pennington et al. (1997) have measured anisotropic values of  $G'_{max}$  by polarising waves across the sample in both horizontal and vertical directions using bender elements incorporated in a standard triaxial cell. These measurements highlight the anisotropy of the soil due to its depositional and strain history, and will be dealt with in Section 2.6.

## 2.5 THE INFLUENCE OF CREEP

It has been observed that when soil remains at a constant effective stress for a period of time it is likely to demonstrate a stiffer response to further loading (Richardson, 1988). There are many phenomena associated with this observed time related change in behaviour of soils. The main causes are thought to be bonding of a variety of physical and chemical forms, and secondary compression or creep. Schmertmann (1981) attributed creep to the dispersion of clay particles during periods of rest into more stable structures. He also stated that it was unlikely that laboratory ageing times were sufficiently long to cause strength increases from bond formation between particles, and suggested that these were only likely to take place over geological time. It is therefore likely that the observed effects of ageing a sample in the laboratory are due primarily to creep. Therefore, this section which deals with time effects that are also possible in reconstituted soils will tackle the effects of creep, and for simplicity, volumetric creep.

Volumetric creep, which was described by Bjerrum (1967) as “a delayed compression representing the reduction in volume at unchanged effective stresses”, has been shown to account for some of the additional stiffness associated with rest periods at constant effective stress in tests such as those by Bishop (1966), Som (1968) and Bjerrum (1967).

Creep can be represented in volumetric space as shown in the plot of specific volume against mean effective stress in Figure 2.40. The soil undergoes a change in specific volume at a constant value of effective stress over time. The apparent increase in preconsolidation pressure due to volumetric creep was termed quasi-preconsolidation pressure by Leonards and Ramiah (1960). Mitchell (1976) stated that “deformation under sustained stress ordinarily produces an increase in stiffness to the action of subsequent stress increase” as shown in the schematic diagram, Figure 2.41. These two observations seem consistent with the dependence of small strain stiffness on overconsolidation ratio (Section 2.4) which, after creep straining will equal the ratio of quasi-preconsolidation pressure to the original preconsolidation pressure before creep deformations commenced, i.e. higher than the overconsolidation ratio before creep.

It is generally accepted that creep deformations follow a logarithmic relationship of the form

$$\Delta v = C_{\alpha} \ln(\Delta t/t_0) \quad (2.8)$$

where  $\Delta v$  is the change in specific volume due to creep,  $C_{\alpha}$  is the secondary compression index,  $\Delta t$  is the time at a constant effective stress, and  $t_0$  is a reference time, which denotes the onset of creep (often the end of primary consolidation).

Bjerrum (1967) discussed the effect of rest periods on soft Norwegian clays, where large amounts of secondary compression occur, in his Rankine lecture. He divided the compression caused by the application of loading into instant and delayed components (Figure 2.42) rather than the more conventional primary and secondary compression arguing that creep straining occurs during both primary and secondary compression. He noted that the reduction in water content during delayed compression led to a more stable structure with an increased number of contact points between soil particles. This leads to the development of what he termed a reserve resistance against further compression, such that for additional loading the clay would behave as if overconsolidated. The effect was demonstrated by tests on Drammen clay (Figure 2.43) where a sample was consolidated and held at a constant pressure for thirty days. Further loading allowed a load of 1.25 times the original preconsolidation pressure to

be applied before the loading resumed its course along the normal compression line. Bjerrum also discussed other possible ageing processes for the Norwegian clays, in particular particle bonding. This additional structure was thought in principle to be brittle, with the current state returning to the normal compression line after the degradation of the bonds, Figure 2.44. It should be noted that these effects would seem to act in addition to creep resulting from delayed compression, such that their effects could be considered additive.

Bishop (1966) conducted a series of creep tests on undisturbed block samples of London clay in a specially built apparatus. He noted the difficulty of maintaining a sustained constant load on a sample over a long period of time without leaks in the apparatus or other technical problems occurring. The tests consisted of a series of samples being set up in the cell, and loaded to various stress levels which corresponded to a percentage of their measured drained peak strength Figure 2.45. The samples were then held at these stresses and any movements observed. The samples show a rate of strain increasing approximately linearly with log time, with strain rate increasing as failure is neared. This type of situation where creep in soils leads to failure may be important where soil is loaded to near its peak strength. The modifications to the soil model proposed in Section 4.4 do not allow creep of this type to be simulated.

Richardson (1988) presented data from a series of stress path tests on reconstituted London clay to investigate the influence of what were termed threshold effects. The definition of threshold effects followed that of Atkinson (1973), in grouping the effects of recent stress history and rest periods together. Stallebrass (1990) demonstrated that recent stress history is not simply a threshold effect, so this definition is not strictly accurate. The aim of these tests was to establish whether time and stress path effects are additive or independent. Figure 2.46 shows consolidation data from a series of stages from tests comprising a number of different stress probes where rest periods were allowed at the same stress state, but following stress paths which approached from different directions. The direction of the stress path is defined by the angle  $\theta$  as shown in Figure 5.35. Primary consolidation takes place over approximately the same period for all the tests, although the magnitude of volumetric straining is dependent on the approach path. Secondary compression continues at a rate which was shown to correspond to the relationship,

$$\varepsilon_v = C_\alpha \ln (\Delta t/t_0) \quad (2.9)$$

which yielded a value of  $C_\alpha = 0.000665\%$  for all samples with  $t_0$  set equal to 1 minute. This formulation is based on the assumption that creep straining only occurs after primary consolidation, contrary to the theory proposed by Bjerrum.

Constant  $p'$  paths were followed after varying rest periods for samples with approach paths of  $0^\circ$ ,  $90^\circ$  and  $180^\circ$ . Rest periods of 3, 48, and 246 hours were allowed, for the tests with  $90^\circ$  approach paths. Figure 2.47 shows deviator stress plotted against shear strain for these tests. Stiffness was seen to increase with the duration of the rest period, with the author noting that the sample stiffness had almost doubled after 246 hours. Samples subjected to paths of  $0^\circ$  and  $180^\circ$  also showed similar gains in stiffness over similar rest periods. The similarity between the gains in stiffness for the different approach paths would appear to indicate that time and stress path effects are additive, causing a cumulative effect on stiffness. Unfortunately, it is difficult to reconcile these results with the stiffness relationship proposed by Viggiani and Atkinson (1995) for small strain stiffness. If this relationship is applied to the increase in preconsolidation pressure implied by the secondary compression index calculated over the relatively short time periods involved in these tests, very small gains in stiffness would be expected. However, Richardson was unable to measure very small strain stiffness in these tests. The difference in stiffness calculated from the small strain measurements may actually be the difference in secant stiffness which represents the cumulative effect of a small but constant increase in tangent stiffness.

Jamiolkowski et al. (1979) noted the dependence of the secondary compression index on vertical effective preconsolidation pressure. High preconsolidation pressures combined with the stiff clays to be modelled in this work ensure that the creep rates associated with these stiff clays are very small, such as those measured by Richardson.

Ageing phenomena which are measured in the laboratory are most likely to be caused by creep. Volumetric creep can be simply represented by a logarithmic function relating volumetric strain to time. The consequences of volumetric creep are an

increase in stiffness and an apparent increase in preconsolidation pressure. The effect of creep is less marked in stiff overconsolidated clays compared to soft clays.

## 2.6 ANISOTROPY

The behaviour of natural stiff clays in the small to medium strain range will be reviewed in the context of anisotropic response. Three main forms of anisotropy can be identified, structural anisotropy, stress induced anisotropy and recent stress history. Structural anisotropy will occur mostly in natural deposits, as it develops due to the deposition of a clay strata, although it can be simulated in the laboratory for reconstituted samples by compression to high stresses in a consolidometer Jovicic (1997). Stress induced anisotropy and recent stress history occur in both reconstituted and natural clays and are a consequence of the current state of the soil and the stress or strain changes leading to the current state. The stress-strain response of stiff soils at small to medium strains may be strongly affected by any of the three types of anisotropy outlined above.

Structural or depositional anisotropy is the anisotropy caused by the one dimensional deposition of a deposit of clay over geological time. Most natural stiff clays were deposited in this manner, and display axisymmetric properties, that is, the vertical response to stress or strain changes is different to the response in the horizontal plane. This form of behaviour is known as cross anisotropy and can be described relatively easily for inclusion in constitutive models. Tests designed to identify the extent of structural anisotropy should be carried out at an isotropic stress state to isolate this effect from stress induced anisotropy (Jovicic, 1997) although this may not ensure that there is no effect of recent stress history induced by the path followed prior to testing. However, dynamic tests which essentially create stress path reversals should fully isolate the structural anisotropy. Several authors (e.g. Jovicic, 1997, Pierpoint, 1996, Pennington et al., 1997) have measured anisotropic values of  $G'_{\max}$  in dynamic tests. These measurements can be made in a conventional triaxial cell incorporating bender elements (Figure 2.26) by orientating the sample or including bender elements orientated horizontally across the sample. Anisotropic values of  $G_{\max}$  should reflect the structural anisotropy of the clay, and may be useful as parameters for constitutive

modelling of clays where the behaviour is thought to be strongly affected by this type of behaviour.

Stress induced anisotropy is simply the component of anisotropy caused by the current anisotropic stress state and is independent of the previous stress or strain history of the soil.

Recent stress history, defined by Atkinson et al. (1990) as either a sudden change in the direction of the stress path or a period of time at a constant stress state, causes the stress-strain response of soils at small strains to exhibit anisotropic characteristics. Atkinson et al. (1990) described a series of laboratory stress path tests carried out by Richardson (1988) to investigate the effect on stiffness of samples loaded from the same initial state approached by different stress paths. Typical stress paths are illustrated in Figure 2.48 showing samples brought to the same state O, along different approach paths in  $p'$ ,  $q'$  stress space, and subsequently loaded along path OA. The samples were held at the same state O for equal periods of time, so the different stiffnesses measured could be attributed to stress path rotation only. Figure 2.48a shows a series of constant  $p'$  and constant  $q'$  stress paths, and Figure 2.48b shows the corresponding tangent stiffness curves. It can be seen that the initial stiffness for  $\theta = 180^\circ$  is much higher than for  $\theta = 0^\circ$ , with  $\theta = \pm 90^\circ$  falling in between. Similar tests were also carried out by Stallebrass (1990) in order to develop a constitutive model based on this form of anisotropy.

The effect of stress path rotation was also noted by Smith et al. (1992) in a series of laboratory stress path triaxial tests on natural Bothkennar clay. The samples were consolidated to the in situ stress and a series of stress paths as shown in Figure 2.49 were followed. Normalised stiffness curves showed different small strain stiffnesses depending on the path taken (Figure 2.50). These paths however did not show the effect of stress path rotation as clearly as Richardson (1988) or Stallebrass (1990), as loading took place along different paths. Therefore the effect of recent stress history could not be isolated, as the path taken could also affect the stiffness.

The stress-strain behaviour of a natural clay is likely to be influenced by all three of these factors to a greater or lesser extent. It may be necessary to determine the relative

importance of the three types of anisotropy on the behaviour of a given natural clay to enable satisfactory modelling of its behaviour.

## 2.7 SUMMARY

This chapter has highlighted areas where the behaviour of natural stiff clays differs from the behaviour of reconstituted samples of the same clay. Despite the differences, the pattern of behaviour of the natural samples has been shown to fit reasonably well into the Critical State framework developed for reconstituted clays. Differences between natural and reconstituted samples are generally related to either the processes undergone during formation of a deposit, or the higher stresses experienced by the deposit. The review has shown how the effects of natural structure can be seen in terms of the clays macro and micro behaviour. The natural structure can be accounted for by analysis of the macro behaviour in terms of sensitivity, which represents the difference between the natural and reconstituted structure in volumetric space. This measure of sensitivity also seems to account for most of the effect of the structure of natural samples in stress space indicating that the effect of natural structure in shear and compression is linked, although for some stiff clays there still seems to be an additional effect of structure in shear loading which is not accounted for by the changes in volume measured by sensitivity,  $S_t$ . Some stiff clays destructure, whilst others have a more stable natural structure which is evident from near parallel natural and reconstituted normal compression lines.

Due to the high level of overconsolidation of many natural stiff clays, the identification of the critical state friction angle can be difficult, as clays sheared wet of critical tend to localise. For stable natural clays at least, it seems reasonable to assume, in the absence of evidence to the contrary, that the natural and reconstituted values are equal. In volumetric space, the location of the critical state line for a natural stiff clay is not likely to coincide with the critical state line for the reconstituted clay, except for the case where  $S_t = 1$ , or if significant destructuration occurs. Where natural structure can be identified as stable, it is reasonable to assume that the critical state point in stress space normalised with respect to the equivalent pressure on the appropriate normal compression line will coincide with critical state for the reconstituted sample.

The relationship proposed by Viggiani and Atkinson (1995) relating  $G'_{\max}$  to current mean effective stress and overconsolidation ratio appears also to be valid for natural clays. There is evidence that the high overconsolidation ratios at which many natural clays exist in the ground may render this relationship less accurate. For natural clays with high overconsolidation ratios it may therefore not be appropriate to extrapolate a relationship derived for a reconstituted sample of the same clay without a separate measurement of the stiffness of the natural sample to confirm the relationship.

Processes undergone by the natural clay post deposition have also been investigated experimentally. Volumetric creep can be measured in the laboratory over long periods although creep rates for stiff clays are very low compared to those for soft clays. Volumetric creep is however, conceptually easy to incorporate into critical state models, and has been measured over a relatively short duration in the laboratory for some stiff clays. The volume change associated with creep in stiff clays may not be as dramatic as for soft clays, but does have some effect on the subsequent stress-strain response. This effect may not solely be linked to the increase in overconsolidation ratio.

Anisotropy caused by both depositional and post depositional processes is clearly an important feature of the behaviour of natural stiff clays. Three main types of anisotropy can be identified from the literature, structural anisotropy, stress induced anisotropy and recent stress history. All three can be isolated by careful laboratory testing, and their effects measured. A knowledge of the relative importance of the particular types of anisotropy to a given clay is likely to be important for the correct determination of the subsequent stress-strain response.

## CHAPTER 3      MODELLING OF STIFF OVERCONSOLIDATED CLAYS

### 3.1      INTRODUCTION

The literature review in Chapter 2 highlighted aspects of the behaviour of natural stiff clays where additional care is needed when applying soil models formulated from tests on reconstituted clays. The key areas which will be considered in the present research were identified as:

- i)      In volumetric space the normal compression line for the natural clay may exist at a higher specific volume than the normal compression line for a reconstituted sample of the same clay. The structure causing this difference can be attributed to a combination of fabric and bonding (Mitchell, 1976, Cotecchia, 1996). The position of the natural normal compression line can be related to the normal compression line for the reconstituted sample by sensitivity, defined as  $S_t = p'_{yn}/p'_e$  (after Cotecchia and Chandler, 1998). Normalising by sensitivity to allow for the effects of natural structure seen in volumetric space, accounts for most, if not all of the effect of structure on soil response in deviatoric stress space.
- ii)     Natural clay structure can be erased by loading, both in shear and volumetric compression, particularly where the structure is characterised by interparticle bonding. Destructuration in stiff clays is not as dramatic as for soft clays, and the stresses required are much higher. For the analysis of geotechnical events, far from failure, destructuration is unlikely to dominate the overall response.
- iii)    The stiffness relationship proposed by Viggiani and Atkinson (1995) is valid for natural clays, as long as the difference in position of the relevant normal compression line is accounted for. Care should be taken however at high overconsolidation ratios, as the fit can be less accurate.
- iv)    Natural clays exhibit significant anisotropy, which can be characterised as either structural, stress induced, or recent stress history anisotropy. Structural

anisotropy is less important for reconstituted clays, but can be reproduced in the laboratory as shown by Jovicic (1997).

- v) When modelling natural deposits, it may be necessary to account for other processes during their formation which may cause 'ageing', such as volumetric creep.

The first section of this chapter outlines two constitutive models that were developed from tests on reconstituted clays. The majority of finite element modelling in the following chapters is carried out using the 3-SKH model (Stallebrass, 1990). The model uses kinematic surfaces to predict the effect of recent stress history observed in tests by Richardson (1988) and Stallebrass (1990). Consequently, the model is also able to predict stress induced anisotropy if stress changes induced during deposition are modelled in order to generate the correct response to further loading. The stiffness relationship proposed by Viggiani and Atkinson (1995) has already been incorporated into the formulation of the model, which has been implemented into a version of the CriSP finite element program (Britto and Gunn, 1987) SSCRISP which was developed by Stallebrass (1992). The model was validated against tests on reconstituted clays and has been used to model a series of centrifuge tests (Stallebrass et al., 1996, Stallebrass and Taylor, 1997, Grant et al., 1997, Grant et al., 1998), making significantly improved predictions of the distribution of movements compared to conventional critical state models. The model is described in more detail in Section 3.2.1.

Also described below is the Brick model (Simpson, 1990) which was formulated to model the same observations as the 3-SKH model but using a different approach to simulate the effect of recent stress history. This model is also able to predict stress induced anisotropy, and calculates  $G'_{\max}$  based on the state and overconsolidation ratio of the soil but not using the equation given by Viggiani and Atkinson (1995). The Brick model is used for comparison for some of the analyses in the following chapters. These models represent two of the most thoroughly evaluated models resulting from the advances in understanding of the stress/strain response of overconsolidated soils made in the past few years.

The second section of this chapter highlights methods used by other authors in the literature to model soil behaviour specific to natural stiff clays. Techniques used to model natural structure, anisotropy and ageing processes are discussed with a view to incorporating some aspects of these into the current formulation of the 3-SKH model. It is not the intention of this work to produce a new model or even a substantially modified model, but rather, to improve the method of application of the current model to stiff natural clays. For this work a simple approach will be used where possible to highlight areas where it is possible to make significant gains in the quality of predictions with this model.

## 3.2 MODELS FOR STIFF CLAYS

### 3.2.1 The 3-SKH model

The Three-Surface Kinematic Hardening model (Stallebrass 1990) is an extension of the standard Modified Cam clay model that incorporates two kinematic surfaces within the state boundary surface to account for the small strain behaviour of overconsolidated clays observed in laboratory tests. The 3-SKH model replicates the observed behaviour as elasto-plastic deformations controlled by the two kinematic surfaces. Figure 3.1 shows the three surfaces plotted in  $p':q$  space. The inner surface, from now on referred to as the yield surface, defines the region of purely elastic behaviour, which is believed to exist for very small strains. The boundary of the yield surface denotes the onset of elasto-plastic behaviour. As loading continues, the stress state drags the yield surface towards the history surface, which defines the extent of the influence of recent stress history. Plastic deformations dependant purely on state begin as the state boundary surface is reached, in the same way as other Cam clay based models. The translation rule which controls the movement of the surfaces ensures that they do not intersect by causing the centres of the surfaces to move in the direction of the line joining their conjugate points, see Figure 3.2.

In its original form, the model is defined by a total of eight soil parameters, five of which are the standard Modified Cam clay parameters. All eight parameters may be obtained from the results of relatively simple laboratory tests. The most recent version

which incorporates the Viggiani and Atkinson (1995) equation for  $G'_{max}$  requires the 3 coefficients used in this equation to be defined.

The three surfaces are defined mathematically in triaxial stress space as follows:

The yield surface is given by:

$$(p'-p'_b)^2 + \frac{(q-q_b)^2}{M^2} = T^2 S^2 p'_o \quad (3.1)$$

Where  $p'_b$  and  $q_b$  are the coordinates of the centre of the yield surface,  $T$  is the ratio between the radii of the history and bounding surfaces and  $S$  is the ratio between the radii of the history and yield surfaces.

The history surface is given by:

$$(p'-p'_a)^2 + \frac{(q-q_a)^2}{M^2} = T^2 p'_o{}^2 \quad (3.2)$$

Where  $p'_a$  and  $q_a$  are the co-ordinates of the centre of the history surface.

The bounding surface is defined by the standard Modified Cam Clay yield locus.

The normal compression line is defined in  $\ln v : \ln p'$  space following the work by Butterfield (1979) with a constant slope of  $\lambda^*$ . The slope of the 'elastic wall' is  $\kappa^*$  which corresponds to the initial slope of the unloading curve in  $\ln v : \ln p'$  space where deformation is elastic, Figure 3.3. As in Modified Cam clay the critical state line is defined in  $p', q$  space as  $q = Mp'$ , where  $M$  is the coefficient of friction.

An extension of the Modified Cam clay hardening rule links the expansion and contraction of all three surfaces to changes in plastic volumetric strain. Predictions of stiffness for different stress paths made using this model can be seen in Figure 3.4. As the change in stress path becomes more abrupt, the initial stiffness of the new stress path increases, with a complete reversal giving rise to the highest initial stiffness. The

model also predicts a variation in shear and volumetric strains during shearing or compression, which leads to a pattern of strain paths which are characteristic of observed recent stress histories. For undrained tests the effects are seen most clearly in the anisotropic shape of the effective stress paths. This prediction replicates the main characteristics of the behaviour seen in stress path triaxial tests by Richardson (1988) and Stallebrass (1990). The model can predict effects of both the stress induced anisotropy created by the formulation of a deposit, and the recent stress history caused by further stress changes.

### 3.2.2 The Brick Model

In his Rankine lecture, Simpson (1992) presented a novel approach to modelling soils, “bricks on strings”. The model was based around an analogue representing the s-shaped relationship between stiffness and log strain as shown in Figure 3.5.

The model was inspired by a series of stress path triaxial tests conducted by Richardson (1988), to investigate the effects of recent stress history. Richardson consolidated specimens to point A in Figure 3.6a, and then studied the decay of stiffness as the sample was loaded along the constant  $p'$  path OX. The specimens were taken to the starting point O along different paths, AOX, (AO)COX, (AO)BOX, (AO)DOX. The results showed that the more abrupt the change in direction of stress path, the higher the stiffness, with stiffness highest after a full reversal of stress path direction, (Figure 3.6b).

Stallebrass (1990) demonstrated from similar tests on Speswhite kaolin that even after an abrupt change in stress path the soil generally initially continued straining in the same direction that it had during the previous stress path. This was demonstrated by plotting strain vectors, as seen in Figure 3.7.

After studying these tests Simpson (1992) proposed the physical analogue of a man pulling a series of bricks inside a room to model the observed soil behaviour. The man and the bricks are shown in Figure 3.8, negotiating several changes of direction. In Figure 3.8a the bricks can be seen lined up behind the man, as they are pulled in one

continuous direction. Figure 3.8b represents a reversal of direction, where the soil initially behaves elastically as the strings are slack, with elasto-plastic behaviour as some of the strings are tight and others slack, followed by predominantly plastic behaviour when all strings are tight as in 3.8a. If the man turns through 90° then the bricks initially continue in the same direction, then gradually align as in 3.8d.

Simpson used the room to represent strain space with the man representing a point within that space. The brick analogue represents the s-shaped curve in a stepwise fashion as shown in Figure 3.9. The length of each step is a strain represented by the length of each string, and the height of the step is the proportion of material represented by the bricks. The area under the curve is equivalent to  $\sin\phi'$ . Failure is reached when the s-shaped curve meets the strain axis.

Simpson formulated the model in plane strain using volumetric strain and shear strain as axes where:

$$\gamma = ((\varepsilon_x - \varepsilon_y)^2 + \gamma_{xy}^2)^{0.5} \quad (3.3)$$

$$v = \varepsilon_x + \varepsilon_y \quad (3.4)$$

To represent results in stress space the stress invariants  $s'$  and  $t$  were used instead of the more familiar  $p'$  and  $q$  where:

$$s' = (\sigma'_x + \sigma'_y)/2 \quad (3.5)$$

$$t = (\sigma'_x - \sigma'_y)/2 \quad (3.6)$$

A complete model was developed using some of the assumptions of the critical state model, together with the brick concept.

The most recent version of the Brick model uses seven soil parameters, as well as a series of data representing the s-shaped curve. These parameters are relatively straightforward to derive, and have been obtained for several clays including London clay (Simpson, 1992) and Speswhite kaolin (Ingram, 2000).

### 3.3 MODELLING FEATURES ASSOCIATED WITH CLAYS IN THE NATURAL STATE

This section reviews models described in the literature which have been formulated to model aspects of behaviour associated with natural clays. The majority of the models are extensions to critical state models formulated to cope with certain specific features of soil behaviour. Models simulating the three main areas identified in Chapter 2 are investigated, that is, natural structure, anisotropy, and creep. The aim of this work is to identify methods that may be used to incorporate these features into the present 3-SKH model in a simple manner.

#### 3.3.1 Modelling natural soil structure

In Chapter 2 recent work on the behaviour of natural clays was examined, for example, Burland (1990) and Leroueil and Vaughan (1990). It is clear from this work that the effect of natural structure should be considered when modelling stiff clays. This section examines recently proposed models designed to include this effect in their predictions. The majority of work in this area has centred on developing models that simulate the effect of a decay of structure modelling for example the degradation of cementation or bonds due to loading. Whilst several authors (Cotecchia and Chandler, 1997, Amorosi and Rampello, 1998) have reported element tests showing the degradation of natural structure in shear and compression tests on stiff clays it would certainly not seem to occur for all stiff clays. This is in contrast to soft clays where the degradation of natural structure is likely to be an important factor in determining the overall response of an engineering problem and the use of a destructuration model could be critical in predicting the correct mechanisms. Additionally, for these clays where destructuration is more significant and can easily be identified from near normally consolidated states it should be easier for these models to be calibrated. In stiff clays however, where movements are smaller and where clays often show no significant destructuration use of a more conventional critical state type model may be more appropriate. The review of models below is not intended to be exhaustive, but to show possible methods of incorporating natural soil structure into a constitutive model as a background to the methods used in this dissertation and outlined in Chapter 4.

Several authors have produced models replicating the effect of erasure of natural clay structure. Gens and Nova (1993) extended the model presented by Nova (1988) to represent the degradation of structural bonds which used a single bounding surface with elastic behaviour within. The effect of bonding is modelled by assuming that the bounding surface enlarges due to a particular degree of bonding relative to the unbonded material. This increase in the size of the bounding surface is represented in volumetric space in Figure 3.10 by different isotropic normal compression lines. Figure 3.11 shows the unbonded bounding surface (denoted A) with successive surfaces for larger degrees of bonding. The surfaces are enlarged such that the preconsolidation pressure increases and the intercept of the state boundary with the deviatoric axis becomes cohesive. It was assumed that the changes in size of the bounding surface would be controlled by both conventional plastic hardening and bond degradation. Degradation was assumed to be related to a measure of damage that decayed with plastic straining such that the bonded material reduces to the unbonded behaviour, Figure 3.12. The model was used to simulate an isotropic compression test, Figure 3.13, predicting natural structure converging to the unbonded material during compression. Predictions of shearing, Figure 3.14, showed similarities with experimental results for a soft limestone which are the graphs on the left of the figure.

A similar approach was used by Chazallon and Hicher (1995) after consideration of soil microstructure. Forces applied to a material were assumed to be resisted by the frictional forces between grains and the strength of bonds. The frictional component was simulated using an elasto-plastic model, with an elastic model used to simulate damage to the interparticle bonds. The model proposed by Vatsala et al. (1998) was based on a comparable method, with separate constitutive laws for bond and frictional components. The standard behaviour was modelled using Modified Cam clay, with the yield surface for bonding being defined by another expression.

A method of incorporating natural structure within a constitutive model by the addition of a 'structure surface' was presented by Rouainia and Muir Wood (1998). The model was an extension to the 'Bubble' model developed by Al Tabbaa and Muir Wood (1989) for reconstituted soils. The model incorporates an additional surface to the two in the standard 'bubble' model, a structure locus that collapses toward the bounding surface for the reconstituted soil which is termed the reference locus. Figure 3.15 shows the three surfaces in stress space with the sizes of the reference and structure loci

related by a scalar variable,  $r$ . The variable  $r$ , represents the degradation of the material which accounts for the damage caused to the soil structure by both shear and volumetric straining. An additional parameter  $A$ , represents the relative effect of shear and volumetric strains on the natural structure. Note that for this model, the size of the inner kinematic surface is related to the reference locus, not the current structure locus. Model predictions for one dimensional compression plotted in Figure 3.16 show that the compression curves where natural structure is modelled ( $r_0=2,3$ ) plot to the right of the reconstituted compression curve ( $r_0=1$ ) and collapse toward it as compression continues. Predictions of the undrained shearing response of the same clay, Figure 3.17, are significantly improved compared to predictions with no natural structure modelled. In particular, the model predicts the strain softening seen in the experimental data, which is not predicted by the standard 'bubble' model. No predictions have been reported for stiff clays.

A destructuring model was also developed by Kavvadas and Amorosi (1998) and used to model laboratory tests on natural samples of stiff Vallericca clay. The model is similar to the 'bubble' model proposed by Rouainia and Muir Wood (1998) in that it has an inner yield surface enveloped by an outer bounding surface. The bounding surface, called the bond strength envelope (BSE) can be seen in Figure 3.18 along with the internal plastic yield envelope (PYE). The bond strength envelope represents the natural structure of the clay, and its size is related to the natural normal compression line of the clay. Degradation of natural structure is controlled by both volumetric and shear components of plastic strain controlled by an exponential damage law. Destructuration during one-dimensional compression can be seen in Figure 3.19. An evaluation of the model against tests carried out by Amorosi (1996) on natural Vallericca clay which demonstrated a degradation of structure for this clay in both shear and volumetric compression was carried out with the model. Figure 3.20 shows laboratory data plotted against predicted data for drained and undrained tests. The predicted data replicates the strain softening seen in the laboratory data for the undrained tests, and the overall prediction is good. Normalised stress paths for drained and undrained anisotropically normally consolidated tests are shown in Figure 3.21 for both model predictions and laboratory data. The predicted curves again predict the strain softening associated with the degradation of structure for this clay. The common feature of these models is an increased size of the bounding surface or state boundary surface. In some cases there is a cohesion intercept with the deviator stress axis.

None of the models for destructuration discussed above appear to have been used to model boundary value problems. For multi-surface models like the 3-SKH model, the position of the surfaces prior to a geotechnical event is defined by the history of deposition. In conventional analyses, the preconsolidation pressure required for the definition of an initial state is often calculated from knowledge of previous maximum overburden (e.g. Powrie and Li, 1991, Simpson, 1992, Powrie et al., 1999). Clearly, the preconsolidation pressure defining the state of clays exhibiting natural structure is not purely related to overburden, but to the accumulation of fabric and bonding which will have changed the size of the state boundary surface and hence the position of the normal compression line. For stiff clays, where destructuration may be less of an issue than for soft clays, it was decided to concentrate on simulating the presence of the depositional structure, rather than its erasure. The analyses in this dissertation will therefore concentrate on the application of the recent work on characterising natural structure (Burland, 1990, Cotecchia, 1996, Cotecchia and Chandler, 1997) to modelling stiff clays where the additional structure can be described by assuming that it is caused by fabric only. In other words, if it is assumed that the natural normal compression line is parallel to the reconstituted normal compression line, and does not destructure towards it.

### 3.3.2 Modelling Anisotropy

There are several methods that have been used in the literature to model the structural anisotropy of clays using a critical state model. The methods reviewed in this section can be roughly divided into two main types, rotational hardening/translating bounding surface models, and models incorporating anisotropic elastic parameters.

Rotational hardening models allow the bounding surface to rotate to represent the current anisotropic stress state. Whereas translating bounding surface models model similar phenomena by translating the origin of the boundary surface. Mroz et al. (1979) presented a two surface kinematic hardening model with a rotating/translating boundary surface which can be seen in Figure 3.22. They stated that the change in position of the boundary surface represented the 'textural' anisotropy developed during deposition. Analyses using both translated and rotated surfaces were carried out, Figure

3.23, and compared with in-situ  $K_0$  measurements, good agreement was found for the translated surface. Conventional Modified Cam clay is unable to predict  $K_{0nc}$  values measured in the laboratory. Davies and Newson (1993) developed a model with a rotated yield locus orientated about the  $K_0$  consolidation line, Figure 3.24. The model required only one extra parameter, the gradient of the  $K_0$  consolidation line. The model has a separate plastic potential such that flow is non-associated, and a rotational hardening law. The rotational hardening law increases the angle of orientation of the surface for increases in deviatoric stress, with the angle decreasing for a reduction of deviatoric stress. Similar approaches were proposed by Banerjee and Yousef (1986), Figure 3.25, and Whittle (1993), Figure 3.26.

Translated boundary surfaces were proposed by Kavvadas and Amorosi (1998) for their destructuration model. Figure 3.19 shows the proposed model in stress space with the boundary surface (bond strength envelope) offset both horizontally and vertically from an isotropic state. Rouainia and Muir Wood (1998) use a similar method to simulate structural anisotropy, Figure 3.16, for their model for structured clays. It is not clear from either paper how the initial position of the boundary surface is determined, or how structural anisotropy develops/decays.

A problem with these types of formulation is that the location of critical state can be dependent on the path taken to reach it. The uniqueness of the critical state coefficient is a fundamental concept of critical state soil mechanics and hence it should be independent of the stress path taken to failure. Wheeler (1997) took steps to address this issue by formulating a rotating yield surface model which forces the surface to rotate so that the orientation of the yield curve at critical state is independent of the initial anisotropy and the stress path taken to achieve critical state.

Most critical state models incorporate a region where behaviour is elastic, and therefore the inclusion of anisotropic elastic parameters within the formulation of a constitutive model is an obvious approach to modelling anisotropy. Graham and Houlsby (1983) described a simplified form of elastic cross anisotropy. Figure 3.27 shows an element of clay labelled with the three characteristic stiffness parameters. For cross anisotropy stiffness is assumed equal in both horizontal planes. The authors identified the parameter  $\alpha^2$  which is a measure of the ratio of horizontal to vertical stiffness, i.e.

$$\alpha^2 = G'_{hh}/G'_{vh} \quad (3.7)$$

Jovicic (1997) developed a version of the 3-SKH model incorporating cross anisotropic values of  $G'_{max}$ . The anisotropy is modelled by the incorporation of the parameter  $\alpha^2$  as defined by Graham and Housby (1983). Figure 3.28 shows undrained stress paths calculated by the 3-SKH model for both anisotropic and isotropic parameters. The anisotropy has a small effect on the direction of the predicted undrained stress path, and the author attributed this to the effect of the recent stress history causing the current stress point to have already traversed the elastic yield surface reducing the effect of the elastic anisotropy. The model has yet to be applied to a clay for which structural anisotropy is known to dominate the stress strain response.

Anisotropic elasticity was applied to the modelling of stiff Oxford clay by Hird and Pierpoint (1996). The model incorporated non-linear elastic stiffness curves derived from stress path tests, which varied in compression and extension. Stress path reversals were modelled by resetting the stiffness behaviour, modelling in a crude way some recent stress history effect. Model predictions of deformations around an excavation in Oxford clay were noticeably improved by the modelling of anisotropy compared to the isotropic predictions using this model. Addenbrooke et al. (1997) used a similar approach to model ground movements around single and twin tunnels in London clay. The elastic anisotropy was not found to significantly influence results at a value consistent with measurements for London clay.

Both rotational hardening and translating surface models for anisotropy are interesting approaches to modelling the structural anisotropy of stiff overconsolidated clays. In order to evaluate the ability of a model to fully represent the structural anisotropy formed during deposition of a clay, the behaviour predicted by the model for a soil sheared at an isotropic state following anisotropic consolidation must be considered. Both a translated and a rotated state boundary surface model are likely to produce an anisotropic stress-strain response due to the position of the current isotropic stress point in relation to an anisotropic boundary surface. These models will not predict  $G'_{max}$  anisotropy, which is a measurable feature of many overconsolidated stiff clays unless explicitly allowed for in the definition of elastic shear stiffness in the model. Models

incorporating anisotropy in this way may also predict a non unique critical state, however Wheeler (1997) presented a method to remedy this problem. Formulations, where stiffness is anisotropic in the elastic region, with failure associated with a critical state defined on an isotropic boundary surface remove the problem of a non-unique critical state. The anisotropy of shear stiffness measured by authors including Jovicic (1997) and Pierpoint (1996) is included in these formulations. Models of this type can predict shear stiffness anisotropy at an isotropic state, representing a response characterised solely by structural anisotropy. It is not clear what aspects of anisotropy observed in stiff clays are not predicted by a model which can predict recent stress history effects and the anisotropy of  $G'_{\max}$  within a fixed isotropic state boundary surface as no comparisons have been carried out.

The true anisotropic response of a clay is likely to be affected by a combination of the three main forms of anisotropy identified in Chapter 2. Careful lab testing can isolate the effects of each type of anisotropy, so a model explicitly accounting for each effect is likely to be more flexible. The behaviour of different clays is characterised by different dependencies on the various modes of anisotropic behaviour, which affect the response in different ways. The extended version of the 3-SKH model implemented by Jovicic (1997) will therefore be used to represent structural anisotropy for a stiff clay, the standard version already accounting for recent stress history and stress induced anisotropy to some degree. Comparisons made using this version of the model so far have been for clays where recent stress history and stress induced anisotropy seem to dominate the subsequent stress strain response. The model will therefore be used to predict behaviour of a clay where the structural anisotropy is thought to dominate the response.

### 3.3.3 Modelling time effects (creep)

There are three main types of model for creep in the literature, simple empirical relationships, such as in equation 2.9, elastic-visco-plastic models based on the concept of 'overstress', and elastic-visco-plastic models incorporating time dependent potentials (Burghignoli et al., 1994). The following is intended to provide examples of the variety of models currently available.

Mesri and Choi (1985) used creep equations along with the more traditional concepts of soil mechanics to derive a model of the form of the first group identified above. An expression for one-dimensional consolidation was re-written such that the change in void ratio was the sum of the primary and secondary compression components, following Bjerrum (1967), Figure 3.29. The equation was used in a multi-layer program to calculate settlements for foundations and embankments.

Borja and Kavazanjian (1985) developed a model consistent with the second group outlined above, in order to describe the stress-strain-time behaviour of clays. Time dependent creep straining was implemented into a modified Cam clay type model using bounding surface plasticity. Creep straining was assumed to follow the pattern postulated by Bjerrum (1967), where strains relating to compression are divided into immediate and time dependent or delayed strains. The size of the yield surface was assumed to be a function of both time independent strain hardening and time itself, resulting in an increase in overconsolidation with time. The relationship between creep strains and time was implemented numerically into a consolidation formulation such that the additional influence of creep could be simulated for a variety of creep tests.

Yin and Graham (1989) presented another model of the second type based on the concept of establishing 'equivalent times' during time dependent straining. The formulation allows the development of creep strains both during the entire period of straining, and after the end of primary consolidation only, by the appropriate choice of  $t_0$ . The model can be used to simulate a variety of different creep tests.

An example of the third type of creep model was proposed by Burghignoli et al. (1994), who outlined an elastic-visco-plastic model for deformations due to creep. The model was based on the assumption that the inelastic components of straining can be divided into a time independent plastic component and a time dependent viscous component. Following Yin and Graham (1989) they employed the concept of 'equivalent time' which is the time taken to achieve the current specific volume from a normally consolidated state, Figure 3.30, to relate a reduction in creep rate to an increase in overconsolidation ratio, for stress paths within the Modified Cam clay state boundary surface. The model relates a viscous potential to the yield surface, Figure 3.31, which controls the rate of creep deformations.

The models available to predict deformations due to secondary compression vary in their complexity from simple equations to replicate the basic processes involved, to complex constitutive relationships that allow the modelling of a variety of creep and rate effects. However, the complex creep models are still incorporated into relatively simple stress-strain models such as Modified Cam clay. Burghignoli et al. (1994) stated that it was likely that the way forward was to represent creep deformations using kinematic hardening models, with an elastic inner nucleus representing the threshold of viscous phenomena. In Section 4.4 a method of incorporating volumetric creep into a constitutive model incorporating kinematic surfaces to model the stress-strain behaviour is outlined. The intention was to investigate the effects of incorporating an empirical relationship relating time to an increase in preconsolidation pressure after the dissipation of pore pressures into a more complex model for the stress-strain behaviour.

### 3.4 SUMMARY

Work described in this chapter has focused on methods for modelling the aspects of behaviour important to natural stiff clays identified in Chapter 2. Two models have been presented, developed from tests on reconstituted clays that already replicate some of the necessary aspects of behaviour. Both calculate the initial elastic shear stiffness from equations incorporating mean effective stress and overconsolidation ratio, and are capable of representing recent stress history and stress induced anisotropy. One of the models, the 3-SKH model (Stallebrass, 1990) is to be used as the basis for further analyses to try to improve the quality of predictions for natural stiff clays, particularly for boundary value problems.

Models presented in the literature for natural clay structure were reviewed, mostly these are designed to take account of destructuration caused by the degradation of bonds. Little work seems to have been done to date on the application of these models to geotechnical events. The development of structure and how to model this was identified as an area for further investigation, and in the following chapters the consequences of various assumptions about how structure develops will be investigated. It was decided to restrict modelling in the following chapters to clays where the natural normal compression line lies parallel to the reconstituted normal compression line, i.e. modelling fabric dominated natural soil structure. It is possible to

relate the size of the kinematic surfaces in a model to the size of either the reconstituted or natural state boundary surface. In the model proposed by Rouainia and Muir Wood (1998) the former approach was adopted.

The 3-SKH model can already model recent stress history and stress induced anisotropy, so a suitable method of representing structural anisotropy within the current formulation was researched. Rotational and translational methods of incorporating anisotropy can lead to a non-unique critical state, and do not isolate structural anisotropy. A version of the 3-SKH model was presented which incorporates anisotropic elasticity (Jovicic, 1997). This formulation ensures a unique critical state, and isolates structural anisotropy. One measurable parameter defines the initial structural anisotropy, but it is not clear whether this approach can significantly affect predictions if structural anisotropy dominates the behaviour.

A variety of creep models have been reviewed, varying in complexity. In order to investigate the effect of volumetric creep, a simple model for creep will be combined with a complex model for the stress-strain behaviour of soil. This will be undertaken by increasing the size of the boundary surface for the 3-SKH model over time at constant stress. The increase in size of the surface will be predicted using an empirical relationship related to the accumulation of volumetric strain over time.

Chapter 4 outlines the precise methods employed to investigate the proposed ways of incorporating additional features of the behaviour of natural clays not already accounted for in the basic formulation and application of the 3-SKH model.

## CHAPTER 4 REPRESENTING THE BEHAVIOUR OF NATURAL STIFF CLAYS USING THE 3-SKH MODEL.

### 4.1 INTRODUCTION

The literature review in Chapter 2 highlighted areas of behaviour important for the full description of the behaviour of natural stiff clays. The features of behaviour identified in Chapter 2 will be used to develop methods of improving the application of the 3-SKH model to these clays. The main areas where work on developing new techniques will focus are:

- a) Accounting for the additional natural structure exhibited by natural stiff clays when compared with a reconstituted sample of the same clay.
- b) Accounting for the effect of anisotropy caused by depositional processes, that is the structural anisotropy of the clay.
- c) investigating the effect of volume change at constant stress associated with volumetric creep.

Chapter 3 reviewed the methods used to incorporate these features into soil models of varying complexity. This chapter describes the methods adopted to represent these forms of behaviour within the 3-SKH model. The method of calculating  $G'_{\max}$  currently employed in the 3-SKH model is also assessed. Consideration is given to the relationship proposed by Viggiani and Atkinson (1995) for  $G'_{\max}$  which is not specific to natural clays. Analyses are carried out in Chapter 5 using the modifications and procedures proposed here in order to investigate the consequences of modelling these features of soil behaviour on the prediction of the response of natural stiff clays in element tests. Further analyses are carried out in Chapter 7 to assess the effect of these changes on predictions of boundary value problems.

The methods were incorporated into SSCRISP (Stallebrass, 1992) and all significant changes to the program code can be seen in Appendix A. Changes made to the program to incorporate natural structure and creep affected the subroutine VARTRI, which

calculates the configuration of the kinematic surfaces. All changes to the code were verified by comparison with hand calculations. Changes made to incorporate the anisotropy of  $G'_{\max}$  are detailed in Jovicic (1997).

The underlying philosophy behind the methods and modifications presented in this chapter was to develop simple methods using straightforwardly measurable soil parameters. The methods used were simple so that they could be incorporated into the analysis of boundary value problems to investigate their applicability to geotechnical events and not only laboratory test data.

## 4.2 MODELLING NATURAL SOIL STRUCTURE

In order to represent the effect of structure exhibited by natural samples of a stiff clay, it was decided that it was most important that the size of the state boundary surface should be correct for the natural clay. Allowing for natural clay structure in this way ensures that subsequent behaviour is related to the correct degree of overconsolidation i.e. the state of the soil is defined correctly within the critical state framework. Note that normalising real data by the correct state boundary surface indicates that almost all of the effect of stable natural structure is caused by the change in state therefore if the model for the reconstituted soil is correct, increasing the state boundary surface should have the same effect. In the 3-SKH model the size of the state boundary surface and the value of  $p'_c$  define the size of the boundary surface which is the intersection of the state boundary surface and the current elastic wall. This in turn determines the size of the kinematic surfaces and hence the value of  $p'_c$  affects the detail of the small strain response of the soil as well as the degree of overconsolidation which will have more impact as the soil approaches failure and the state of the soil with respect to the critical state point becomes important. A method was adopted which enabled the state boundary surface of the model to be calculated from the position of the natural normal compression line, which was related to the normal compression line for the reconstituted soil by the sensitivity,  $S_t$ . Using this approach with the standard hardening relationship for the 3-SKH model does not allow for the destructuration caused by the breakage of interparticle bonds that characterises some natural clays. Nevertheless, many natural stiff clays define normal compression lines that remain parallel to the line

for the reconstituted clay, where the structure is of a stable fabric type as discussed in Section 2.2. This approach is only valid for those stiff clays which do not exhibit significant collapse of natural structure. Analyses carried out in the following chapters will be for these types of stiff clay only. The first part of this section outlines the method used to calculate the preconsolidation pressure that will define the natural state boundary surface for the analysis of laboratory tests. The second part of this section shows how these methods can be adapted and applied to computations for boundary value problems.

#### 4.2.1 Calculation of Preconsolidation Pressure Defining the Natural State Boundary Surface - Modelling Element Tests

Figure 4.1 shows a schematic of the normal compression lines defined by tests on reconstituted and natural samples of the same clay in  $\ln v : \ln p'$  space. The sensitivity,  $S_t$ , of the natural clay can be defined by the following (Cotecchia and Chandler, 1998).

$$S_t = p'_{en}/p'_e \quad (4.1)$$

The reconstituted normal compression line in Figure 4.1 is given by:

$$\ln v = \ln N^* - \lambda^* \ln p' \quad (4.2)$$

so it follows that the equation of the natural normal compression line can be written as:

$$\ln v = \ln N^* - \lambda^* \ln p' + \lambda^* \ln S_t \quad (4.3)$$

assuming that the lines remain parallel. The general equation for a swelling line is:

$$\ln v = \ln v_{\kappa} - \kappa^* \ln p' \quad (4.4)$$

so for the normal compression and swelling lines in figure 4.1 we can write:

$$\ln v_{cn} = \ln N^* - \lambda^* \ln p'_{cn} + \lambda^* \ln S_t \quad (4.5)$$

$$\ln v_{cn} = \ln v_{\kappa} - \kappa^* \ln p'_{cn} \quad (4.6)$$

$$\ln v_1 = \ln v_{\kappa} - \kappa^* \ln p'_1 \quad (4.7)$$

which reduce to give:

$$p'_{cn} = \exp \left[ \frac{\ln N^* - \ln v_1 + \lambda^* \ln S_t - \kappa^* \ln p'_1}{(\lambda^* - \kappa^*)} \right] \quad (4.8)$$

where  $p'_{cn}$  is the preconsolidation pressure on the natural normal compression line defined by the sensitivity of the soil, for a sample with a known specific volume and mean effective stress. This allows an appropriate value of the preconsolidation pressure defining the current state boundary surface for a natural sample of a clay at a known state, to be calculated from the reconstituted normal compression line if the sensitivity of the clay is known. It is obvious that  $p'_{cn}$  could be calculated directly from the equation of the natural normal compression line in a similar manner, without knowledge of the sensitivity. This method however, has some advantages. Defining the natural preconsolidation pressure in this way clearly relates natural behaviour to reconstituted. The sensitivity of the soil can be measured/inferred in a number of ways (Cotecchia and Chandler, 1998), so it may not be necessary to conduct high pressure compression tests to define the natural normal compression line directly if using this method. For the purposes of the current work, it is useful to be able to compare predictions made assuming that a clay exhibits natural structure, with predictions made assuming that the behaviour is analogous to the reconstituted response.

As noted in Chapter 1 all analyses using the 3-SKH model are carried out using the finite element program CriSP (Britto and Gunn, 1987) in particular the version 'SSCRISP' modified by Stallebrass (1992) to incorporate the model. No modifications are necessary to the code to incorporate the above method, as  $p'_c$  is already included in the input to define the current state.

#### 4.2.2 Calculation of Preconsolidation Pressure Defining the Natural State Boundary Surface - Modelling Boundary Value Problems

The application of this approach to the analysis of boundary value problems offers some complications not present in its application to element tests. In element tests re-consolidation stages that occur before shearing clearly define the recent stress history of the soil and natural structure has been acquired at any time before these stages. It is therefore only necessary to define an appropriate value of  $p'_c$  at the start of the simulation before modelling the re-consolidation stages which determine the recent stress history of the sample. In the field the recent stress history is often part of the geological history and hence influenced by when the soil developed its natural structure, that is either during deposition or post-deposition. The 3-SKH model requires that the recent stress history of a geotechnical problem is modelled so that the kinematic surfaces can align correctly with the current stress state, in a boundary value problem this may be the recent depositional history. This requires the modeller to consider when is the most reasonable stage to assume that the clay has developed natural structure. Little is known about the evolution of natural clay structure nor are current soil models able to predict this evolution as a deposit is formed over geological time. Some judgement is therefore required to determine when the clay behaviour should be affected by a change from its reconstituted to its natural normal compression line increasing sensitivity,  $S_t$ . Several methods are proposed for simulating the natural structure for a boundary value problem below and these will be used in the analyses in Chapter 7.

As noted above, the complex processes involved in deposition and erosion of materials make it difficult to determine the onset of the formation of structure in the field, so that it can be modelled correctly. If we consider the simple example of a formation deposited along a normal compression line represented in  $\ln v: \ln p'$  space by the line A-B in Figure 4.2, the point B is fixed by the maximum overburden experienced by the clay. After deposition, erosion of the open surface takes place, swelling the clay along the line B-C. The formation of additional structure may have occurred at any time after deposition such that under recompression the clay will yield on a natural normal compression line to the right of the line A-B. It is also possible that the clay may have developed structure during deposition, causing it to compress along a line within the

envelope of the two normal compression lines, or possibly directly along the outer. It is likely that for many stiff clays a combination of these depositional and post depositional effects combine to form the overall natural structure. Theoretically it is possible to reduce the range of possible histories if the specific volume and mean effective stress of the sample are known and the maximum overburden is fixed. In practice, this is difficult particularly as the history is often uncertain. In addition, it is likely that a number of processes such as creep, causing changes in volume at constant stress are occurring during and post deposition and during erosion. For the modeller there are three simple assumptions that can be made about the formation of the natural structure, and these are investigated below. It is almost invariable that the time scale for the formation of structure must be assumed as it is very unlikely that it is possible to actually know what happened in the field.

The first, and most obvious approach is that structure was formed during deposition of the clay. Figure 4.3 shows reconstituted and natural normal compression lines for an assumed deposit in  $\ln v: \ln p'$  space. The soil could be assumed to compress down either line up to the value of mean effective stress defined by the overburden, shown as  $p'_m$  in the figure. For the 3-SKH model which is formulated in  $\ln v: \ln p'$  space as shown, specific volume does not appear in the constitutive equations. This means that whichever normal compression line the clay is compressed down because  $p'_m$  is the same in both cases, the subsequent behaviour will always be the same since although the state boundary surfaces are different, the current bounding surfaces are the same. For models formulated such that specific volume forms part of the constitutive equations, representing the formation of structure in this way will affect the stress/strain response. For the purpose of comparison with predictions assuming natural structure in the clay an analysis assuming that the clay follows the reconstituted normal compression line will be carried out. For the 3-SKH model these results would also represent the assumption of structure forming purely during deposition.

The second possibility is to assume that the clay forms post depositional structure directly after deposition and prior to erosion of the top surface. This can simply be represented in the model by an increase in the preconsolidation pressure calculated for a given overburden stress. The apparent increase in preconsolidation pressure can be calculated from the ratio of the previous maximum pressure - i.e. the overburden, to the

yield stress on the natural normal compression line, which is conveniently represented by sensitivity (Cotecchia, 1996). This is different to the previous option because the size of the bounding surface is not uniquely defined by the overburden stress. The size of the inner kinematic surfaces is also increased.

The third option for the inclusion of additional natural structure post deposition is to increase the size of the bounding surface at an overconsolidated state which in the simple case might correspond to the period after the erosion of the upper layers of soil. The size of the new enlarged state boundary surface is again defined by a preconsolidation pressure increased by the ratio of soil sensitivity,  $S_t$ . In the finite element analyses this can be achieved by increasing the preconsolidation pressure during a single increment in a similar way to that used for the creep model (Section 4.4), only in this case the amount by which the preconsolidation pressure increases corresponds to the sensitivity,  $S_t$ . This approach also causes an increase in the size of the kinematic surfaces in the 3-SKH model in common with the simple representation of volumetric creep outlined in Section 4.4. The centres of the surfaces do not move and hence the current stress point is then within the surfaces. The result of creating a natural structure in this way is to ensure that the initial part of the subsequent stress strain behaviour is elastic, and could conceptually model the accumulation of bonds and other forms of structure. effectively reducing the recent stress history effect. The changes made to the subroutine VARTRI (Stallebrass, 1992) are shown in Appendix A.

For all three methods it is necessary to calculate the correct preconsolidation pressure for the natural clay. For the finite element program used to carry out the boundary value analyses described in Chapter 7, specific volume is not one of the main parameters defining state. Hence an alternative to equation 4.8 must be used in order to obtain the appropriate value of preconsolidation pressure. The increase in preconsolidation pressure from a value based purely on stress history (in many cases the overburden) to the corresponding value on the natural normal compression line can be calculated by modifying Equation 4.8. By substituting for the specific volume in Equation 4.8, it is possible to obtain the expression:

$$p'_{cn} = \exp \left[ \frac{(\lambda - \kappa) \ln p'_c + \lambda \ln S_t}{(\lambda - \kappa)} \right] \quad (4.9)$$

where  $p'_c$  is the point on the isotropic axis where the elastic wall meets the reconstituted state boundary surface. This is usually calculated from the stress history of the clay only. This allows the increase in preconsolidation pressure due to natural structure to be estimated from knowledge of the preconsolidation pressure calculated from the overburden. This is the parameter used in the model to describe the state of the soil.

#### 4.3 MODELLING STRUCTURAL ANISOTROPY USING THE 3-SKH MODEL

Whilst there are several methods of incorporating structural anisotropy within a critical state model, as discussed in Section 3.3.2, it was decided to experiment further with the formulation proposed by Jovicic (1997) incorporating a cross anisotropic description of  $G'_{max}$ . This formulation was used for several reasons. Firstly, incorporating anisotropy in this way eliminates the problem of non-uniqueness of critical state which can be a feature of rotational or translational hardening models. Secondly, this model has already been implemented in a version of the 3-SKH model where elastic shear stiffness is constant, so modification to follow the stiffness relationship proposed by Viggiani and Atkinson (1995) is all that is necessary to make this version compatible with the current isotropic version. This method of incorporating anisotropy separates the structural anisotropy from recent stress history and stress induced anisotropy which are already accounted for in the formulation of the 3-SKH model. Anisotropy of  $G'_{max}$  is a measurable phenomenon which characterises structural anisotropy, as long as it is measured at an isotropic state to remove the influence of stress induced anisotropy, it is therefore potentially a convenient parameter to use to characterise the behaviour of the soil. Formulating the model in this way allows for the relative effect of the different phenomena governing anisotropic response to be accounted for explicitly. Lastly, to date this method has only been used to model the behaviour of clays where the recent stress history effect dominates the response (Jovicic, 1997). Whilst only having a small effect on the behaviour of these clays as shown in Figure 3.31, work presented in Section 5.4 on Oxford clay demonstrates that this method of incorporating structural anisotropy can significantly enhance the quality of predictions for this clay.

#### 4.4 MODELLING VOLUMETRIC CREEP USING THE 3-SKH MODEL

Richardson (1988) envisaged creep as, “the state of a soil falling below a state boundary surface as the surface continues to expand with passing time”, and this is in essence how creep behaviour has been incorporated into the model. The primary objective was to model creep rates for boundary value problems in stiff clay over time periods associated with the formation of a deposit. This is a preliminary evaluation of the effect of allowing volume change with constant effective stress within a kinematic hardening model hence the use of a complex formulation was rejected. A creep equation has been used as follows:

$$\varepsilon_v = \psi \ln (\Delta t/t_0) \quad (4.10)$$

which is of the form proposed by Borja and Kavazanjian (1985) and describes the accumulation of plastic volumetric strains,  $\varepsilon_v$ , with passing time. This formulation requires a new parameter,  $\psi$ , the secondary compression index, to be included in the description of the soil model. The secondary compression index has been denoted  $\psi$  instead of the more common  $C_\alpha$ , because it has been calculated with respect to the natural strains that are used in the formulation of the model. The reference time,  $t_0$ , is used to make the equation non-dimensional. In this formulation  $t_0$  is held constant and equal to one minute. This implies that the volume change during creep is dependant only on  $\psi$ , which is independent of the time to the end of primary consolidation. This is consistent with the simplified approach adopted, and the fact that pore pressure consolidation is not modelled in any of the analyses presented here. The duration of creep straining,  $\Delta t$ , is a variable defined in the input for the analyses in units of minutes. Plastic volumetric strain computed by equation 4.10, is added in a single increment, which moves the state to a new swelling line or elastic wall, as shown in the  $v:p'$  plot in Figure 4.4b. This requires only a relatively minor change to the finite element program SSCRISP used for these analyses to allow the surfaces to expand whilst the stress state remains constant (Appendix A). This enlarges the bounding surface which is a projection of the state boundary surface on an elastic wall, such that the preconsolidation pressure increases from  $p'_{ci}$  to  $p'_{cc}$ . This process is described by the hardening rule for the model, which follows the Cam clay models in linking plastic volumetric strain to a hardening parameter  $p'_c$ . As the bounding surface expands, the

inner surfaces also increase in size about their centres. The consequences of implementing creep in this way are twofold, firstly, the state of the soil is now within the inner yield surface, therefore the initial stiffness of the soil will once again correspond to the elastic maximum value, but the effect of recent stress history is still preserved although in a modified state. Secondly, since the elastic shear stiffness is related to overconsolidation ratio in the model (Viggiani and Atkinson, 1995), the elastic initial shear stiffness is increased. An evaluation of the effects of modelling creep in this way is carried out in Chapter 5.

#### 4.5 MODELLING $G'_{MAX}$ USING THE 3-SKH MODEL

The application of the relationship proposed by Viggiani and Atkinson (1995) is not specific to natural clays, as it can also be used to predict the behaviour of reconstituted clays. Some additional considerations may be necessary to apply this formula to natural clays, and these are explored below.

It is clear from the literature reviewed in Section 2.4 that the equation proposed by Viggiani and Atkinson (1995)

$$\frac{G_0}{p_r} = A \left( \frac{p'}{p_r} \right)^n R_0^m \quad (4.11)$$

holds for a number of clays, certainly to overconsolidation ratios of up to around 10. For overconsolidation ratios of greater than 10 it is not clear whether the relationship is still valid, although this would seem from Jovicic (1997) to depend on the individual clay concerned. Normalised stiffness measurements for natural and reconstituted clays are coincident for a number of clays when the data are normalised to the relevant bounding surface, leading to the conclusion that stiffness in clays is not affected by structure except from the effect on  $R_0$ . There are some exceptions to this however, and it is not clear from the literature whether the coincidence of the normalised measurements may be related to large straining during sampling erasing structural effects. The relationship proposed by Viggiani and Atkinson (1995) has already been implemented into the 3-SKH model which allows the model to predict a variation in

elastic shear stiffness with current stress and overconsolidation characterised by  $R_0$ . For the natural clay,  $R_0$  can be defined as:

$$R_0 = (p'_{cn}/p') \quad (4.12)$$

where  $p'_{cn}$  is the preconsolidation pressure on the natural normal compression line, and  $p'$  is the current mean effective stress. The selection of the coefficients  $A$ ,  $n$  and  $m$ , to define the stiffness relationship for natural clays requires some care, especially where the clay is heavily overconsolidated. The following approaches are possible

- a) Use of the parameters derived from dynamic tests on reconstituted samples of a clay. This may be especially useful for clays where the high stresses needed to reach the normal compression line in the laboratory may make estimates of overconsolidation ratio,  $R_0$  difficult.
- b) Estimating the coefficients from the charts presented by Viggiani and Atkinson (1995), which link  $A$ ,  $n$  and  $m$  to plasticity index, may be a reasonable approach for clays where insufficient or no dynamic stiffness measurements have been made. Care should be taken when following this approach, and careful validation against static laboratory measurements of stiffness, or any available dynamic data must be considered.

A comparison between coefficients estimated from dynamic tests following a) and coefficients estimated from the plasticity charts following b) is made in Section 5.2.2, which shows that values computed for  $G'_{max}$  can vary quite significantly between the two methods.

It is also theoretically possible to use the equation proposed by Viggiani and Atkinson (1995) to estimate  $R_0$  for a natural sample given a set of dynamic measurements of  $G'_{max}$ . This technique could potentially be useful in determining the position of the natural normal compression line for a clay where no high pressure compression test data are available. Given a measurement of  $G'_{max}$  at a known state and the stiffness relationship given in equation 4.11 with coefficients derived from tests on reconstituted samples of the same soil it is theoretically possible to find  $R_0$ . Unfortunately, the values

of the coefficient  $m$  are relatively low such that  $G'_{max}$  has a relatively low dependence on overconsolidation ratio. Consequently, large errors in the determination of preconsolidation pressure could occur using this method. This approach was tried for the purpose of estimating natural preconsolidation pressures for the Boom clay (Section 5.2.2) but was thought to be unreliable.

#### 4.6 SUMMARY

The above chapter has described a toolkit of minor modifications and novel approaches to the application of the 3-SKH model designed to improve the way in which it represents the behaviour of natural stiff clays. The underlying idea behind the work was to model additional features of behaviour associated with stiff natural clays in a simple manner so that they could be straightforwardly incorporated into finite element analysis with no fundamental changes to the existing model. It is clear, particularly from the section presenting methods of incorporating natural soil structure by increasing the size of the bounding surface, that the application of models for natural soils requires careful thought, as the evolution of the features affecting the behaviour is not easy to model. The following chapters will investigate the use of these methods to represent the behaviour of stiff natural clays. Application of the methods to both laboratory element tests and boundary value problems will be considered to assess whether these additions significantly improve predictions.

## CHAPTER 5    MODELLING LABORATORY ELEMENT TESTS ON NATURAL STIFF CLAY

### 5.1    INTRODUCTION

The analyses carried out within this chapter are designed to test the significance of adopting the modelling techniques outlined in Chapter 4 when simulating laboratory element tests. All the analyses in this chapter are modelled as a uniform element of soil using the 3-SKH model implemented in a version of the finite element program CriSP (Britto and Gunn, 1987). The uniform element of soil, referred to herein as a 'single element' can be seen in Figure 5.1 and is in fact two axisymmetric triangular cubic strain elements with boundary conditions such that all stresses and strains within are equal. This formulation allows triaxial tests to be modelled by the application of the correct combination of stresses or strains at the boundary. A deficiency of modelling triaxial tests in this way is the inability to model the localisation phenomena particularly associated with overconsolidated clays (Atkinson and Richardson, 1987). Comparisons with test data will therefore be restricted to the ability of the model to predict the observed patterns of behaviour before localisation dominates the response.

The simulation of the behaviour of three stiff natural clays is described within this chapter, which highlights the different approaches that are necessary to model their response. The first section of this chapter focuses on Boom clay, which is a lightly overconsolidated stiff clay. The 3-SKH model is used to model a series of tests which were presented by Coop et al. (1995) on both reconstituted and natural samples. These tests were chosen because the normal compression lines for both the natural and reconstituted Boom clay had been identified from high pressure oedometer tests and were shown to be near parallel, indicating a stable, fabric dominated structure. The parameters for these analyses were calculated from the reconstituted data, and used to model both the reconstituted and the natural clays. The natural clays were modelled twice, first assuming that the state boundary surface was characterised by a preconsolidation pressure based on the reconstituted normal compression line, and secondly assuming that the state boundary surface was consistent with a preconsolidation pressure based on the natural normal compression line which was related to the reconstituted by sensitivity (Cotecchia, 1996).

The second series of analyses investigate the method for incorporating volumetric creep within the 3-SKH model as outlined in Section 4.4. The aim of the analyses which are carried out for both Speswhite kaolin and London clay was to investigate whether the inclusion of this mode of behaviour had a significant effect on the predicted response at element level.

The third series of analyses investigate the use of the 3-SKH model to simulate the behaviour of Oxford clay. The 3-SKH model is used to analyse a series of tests on natural samples of Oxford clay which were presented by Pierpoint (1996). The natural Oxford clay is of medium sensitivity, in contrast with the low sensitivity Boom clay, and has behaviour characterised by depositional anisotropy.

## 5.2 MODELLING THE EFFECT OF NATURAL STRUCTURE BY INCREASING THE SIZE OF THE STATE BOUNDARY SURFACE

The aim of this section is to assess the improvement in model predictions of the behaviour of natural samples in triaxial tests, if parameters derived solely from reconstituted tests are used, and only the size of the state boundary surface defined by a higher preconsolidation pressure for the natural samples is changed. This assessment will be carried out by comparing model predictions and test data for a series of tests on both natural and reconstituted Boom clay which were reported by Coop et al. (1995). First, a set of parameters was calculated from tests on reconstituted Boom clay (Coop et al., 1995), Section 5.2.2 and a series of shearing stages modelled to compare measured and predicted results for the reconstituted clay (Section 5.2.4). Several undrained shearing tests on natural samples were then modelled, using the approach described in Section 4.2 to reproduce the probable stress history and consequent size of the state boundary surface for these samples.

One of the main problems in carrying out the analyses was that the 3-SKH model requires that the previous stress history of the soil is known so that the kinematic surfaces are correctly aligned to simulate the effect of the preceding load path on the subsequent shearing behaviour of the sample. For the tests on reconstituted soil this is straightforward as the stress history is simply defined by the stresses applied in the triaxial cell. The behaviour of the natural samples of Boom clay was also to be

modelled, and it is more difficult to simulate the stress history of these tests, as the geological history is described by a natural preconsolidation pressure that has not been measured directly and may not be defined purely by the previous maximum stresses applied to the soil, but is likely to be defined with respect to the natural normal compression line. The natural normal compression line for one dimensional compression was measured in a high pressure oedometer Figure 5.2 for this clay (Coop et al., 1995). The natural normal compression line for Boom clay lies to the right of the reconstituted normal compression line, as is the case for many natural clays. The normal compression line for the natural tests is parallel to the reconstituted normal compression line, but does not collapse onto it as has been seen for some soils (Coop et al., 1995). From the oedometer tests the sensitivity,  $S_t$ , of the Boom clay is calculated as 1.55, and because the compression curves are parallel there is greater certainty when calculating a natural preconsolidation pressure. It is possible to model the experimental procedure that was carried out to set up the sample in the triaxial cell as this is known, but the preconsolidation pressure must be estimated. A procedure for estimating the preconsolidation pressure based on the sensitivity framework proposed by Cotecchia (1996) is outlined in Section 4.2. The natural clay tests were also modelled assuming that the state boundary surface was defined by the reconstituted normal compression line. These analyses were designed to highlight the pitfalls involved in assuming that natural clays behave in a manner conforming to their reconstituted volumetric behaviour.

### 5.2.1 Origin of the Boom clay

The tests modelled in this section were carried out by Coop et al. (1995) and were on samples excavated from the experimental test drift at Mol in north west Belgium. The Boom clay deposit at Mol is 70m thick, and overlain with approximately 190m of sands and gravels. Boom clay is similar to London clay in terms of sensitivity and plasticity index although it is rather less overconsolidated, having an overconsolidation ratio of around 2.6. The triaxial tests are part of a series of tests carried out by Coop et al. (1995) examining the differences between reconstituted and natural samples and are outlined in tables 5.1 and 5.2. The tables show the states of the samples prior to shearing along with the consolidation history followed in the laboratory. The reconstituted samples were formed by reconsolidation of the clay from a slurry. The

natural samples were taken as block samples from the tunnel face at a depth of 223m. A series of normally consolidated and overconsolidated drained and undrained shearing paths were followed in the tests on the reconstituted clay. The block samples were allowed to swell to a mean effective stress of 600kPa before being reconsolidated to their approximate in-situ stress and then they were all sheared undrained. Conventional and high pressure triaxial tests were carried out, and Coop et al. (1995) note that the critical state friction angle, along with the coefficient of earth pressure at a normally consolidated state  $K_{onc}$  seem to decrease at the higher pressures Figure 5.3, although a constant value has been used to model the tests as the 3-SKH model only allows this. Coop et al. (1995) normalised the shearing stages of the tests by both the equivalent pressure,  $p'_e$  and the coefficient of friction,  $M$  to take account of this variation.

### 5.2.2 Calculation of soil parameters

A summary of the parameters derived for Boom clay for use with the 3-SKH model is given in Table 5.3. The sections below outline the procedure used to obtain the parameters. The procedures involved are similar to those described in Viggiani and Stallebrass (1994)

#### i) Definition of isotropic normal compression line

The isotropic normal compression line for the reconstituted clay is defined by the parameters  $\lambda^*$  and  $N^*$ . These parameters were calculated from the isotropic compression data for the reconstituted test *rec1* as seen in Figure 5.4. A best fit line of the form:

$$\ln v = \ln N^* - \lambda^* \ln p' \quad (5.1)$$

was plotted through the data, such that  $N^* = 3.605$  and  $\lambda^* = 0.0984$ .

ii) Elastic volumetric deformation

Elastic deformations during swelling in the model are described by the bulk modulus  $K'$ , where:

$$K' = p'/\kappa^* \quad (5.2)$$

and  $\kappa^*$  is the gradient of an elastic wall in the 3-SKH model. This enables  $\kappa^*$  to be estimated from the results of isotropic swelling stages following isotropic compression. Figure 5.5, shows a plot of  $K'/p'$ , against  $p'/p'_c$  for two reconstituted tests *rec2* and *boom3*. Estimation of  $\kappa^*$  is difficult, as the soil only behaves elastically at very small strains which could not be resolved accurately in these tests. A value of  $K'/p'$  of 250 is an upper bound to most of the data and given the problems of measuring volumetric deformations at small strains is probably a lower bound to the value of  $K'/p'$  for elastic deformations. However, without any more accurate measurements this is a reasonable estimate, which gives  $\kappa^* = 0.004$ .

iii) Elastic shear deformation

The elastic shear deformation in the model is described by the relationship proposed by Viggiani and Atkinson (1995) to define  $G'_{max}$ . The coefficients  $n$  and  $m$  relating the elastic stiffness of the soil, which is defined in the model as  $G'_{ec}$  to state and overconsolidation ratio respectively, and the constant  $A$ , were calculated by Agah (1996) from a series of bender element tests on normally consolidated and overconsolidated reconstituted Boom clay. Values obtained experimentally by Agah were  $A = 180$ ,  $n = 0.97$ , and  $m = 0.2$ . These were calculated by the method proposed by Viggiani and Atkinson (1995) and outlined in Section 2.4.

Viggiani and Atkinson (1995) presented three charts relating these coefficients to the plasticity index of the soil for a selection of clays, Figure 5.6. Coop et al. (1995) estimated the plasticity index for Boom clay to be 47, by averaging data in the literature. Assuming this value of plasticity index allows the stiffness parameters calculated by Agah (1996) to be superimposed onto the charts and the data fall near to the points already plotted. If the trend lines suggested by Viggiani and Atkinson (1995)

are used to estimate stiffness coefficients for Boom clay, values of  $A = 440$ ,  $n = 0.84$ , and  $m = 0.26$  are obtained. Figure 5.7 shows maximum stiffnesses calculated using the two sets of coefficients for a range of normally consolidated mean effective stresses. It can be seen that the calculated stiffnesses agree well for a  $p'$  of 1000 kPa, but diverge such that for a mean effective stress of 100 kPa the coefficients obtained from the charts predict a maximum stiffness 34% higher than those calculated by Agah (1996). Figure 5.8 shows calculated maximum stiffness plotted against overconsolidation ratio for a mean effective stress of 1000 kPa the predictions again diverge, with the results for the coefficients estimated from the charts predicting higher stiffnesses with increasing overconsolidation ratio. For this case the maximum stiffnesses are 19% higher than those predicted using the coefficients obtained by Agah (1996).

The coefficients used in the analyses were those calculated by Agah (1996), as these were directly measured for a sample of Boom clay. Using coefficients scaled from the charts presented by Viggiani and Atkinson (1995) would be an option if bender element data for a specific soil was not available. Stiffness coefficients derived from the charts could also be used in conjunction with limited measurements of stiffness where for example stiffnesses have only been measured at a single overconsolidation ratio. It is clear that adding more sets of data obtained using the framework suggested by Viggiani and Atkinson (1995) to these charts would improve the confidence with which parameters could be estimated.

#### iv) Critical state friction coefficient

The critical state friction coefficient,  $M$ , was calculated from the average of the stress ratios at failure in the conventional pressure tests on reconstituted Boom clay, where the sample had been sheared to failure. Coop et al. (1995) noted that the critical state friction coefficient and  $K_0$  states for Boom clay reduce with increasing mean effective stress, such that the ratio  $K_0/M$  is approximately constant. For consistency with the formulation of the model  $M$  is assumed to be constant at 1.03.

v) Parameters defining the behaviour of the kinematic surfaces

The ratios  $T$  and  $S$ , which describe the size of the two kinematic surfaces in relation to the bounding surface can be determined experimentally by following a particular pattern of isotropic compression and swelling stages as outlined in Stallebrass (1990). Although the tests on Boom clay do not contain the necessary stress paths, it is possible to determine these values by performing a parametric study as in Viggiani and Stallebrass (1994). This study has also been used to evaluate the hardening modulus,  $\varphi$ . Table 5.4 summarises the variations in the parameters used in the parametric study, which was carried out by simulating the behaviour of the shearing stage of test *ruth*. In the test *ruth* isotropic compression and swelling stages were followed before the sample was sheared undrained from an overconsolidated state dry of critical. Figure 5.9 shows model predictions of undrained stress paths for five of the parametric analyses. The anisotropy created by the recent stress history simulated by the model as it follows the stress changes imposed in the laboratory causes the model predictions to deviate from the laboratory data after a change in deviator stress of approximately 15 kPa. The analysis bcp20 deviated least from the laboratory data due to the value of  $\varphi$  being set at the lowest value of 1.6. reduction of  $\varphi$  below this threshold produced stiffness curves that were unrealistic. A graph of stiffness against deviator stress for the same parametric analyses is plotted with laboratory data in Figure 5.10. Predictions of small strain stiffness for all the analyses are a good representation of the data, confirming the applicability of the elastic shear stiffness coefficients derived by Agah (1996), which were used in these analyses, to this test. The laboratory data shows considerable scatter, but analysis bcp20 again lies closest to the test data. Accordingly the values of the parameters controlling the kinematic surfaces,  $T$ ,  $S$  and  $\varphi$  were chosen to be those used for analysis bcp20. Therefore for all further analyses of Boom clay in this chapter,  $T = 0.2$ ,  $S = 0.04$ ,  $\varphi = 1.6$ .

vi) Calculation of preconsolidation pressure for natural samples

In general, the difference between the preconsolidation pressure of a natural sample and a reconstituted sample at the same mean effective stress and voids ratio can either be estimated by comparison of their respective normal compression lines or by recompressing the sample to a sufficiently high stress to reach the natural normal

compression line. In this case the samples were not recompressed to the natural normal compression line and hence the former method was used. Figure 5.11 shows in schematic form, the isotropic reconstituted and natural normal compression lines for Boom clay, which have been derived from oedometer data. The sensitivity,  $S_t$ , of the natural clay was calculated to be 1.55 (Coop et al., 1995), where sensitivity is described as the ratio between points on the natural and reconstituted normal compression lines at constant specific volume. This can be calculated by the following equation, from the data in Figure 5.2.

$$S_t = \sigma_{v'_{en}} / \sigma_{v'_e} \quad (5.3)$$

Which is an equivalent method of calculating sensitivity for one-dimensional compression. The preconsolidation pressure for the natural samples was then calculated from the sensitivity of the natural clay in the manner described in Section 4.2.1.

The preconsolidation pressure based on the reconstituted compression line was also calculated for the natural samples. This was to allow the natural tests to be modelled assuming that the compression history of the soil was the same as for the reconstituted tests. The intention of doing this was to highlight the effect of assuming reconstituted compression behaviour for a natural sample. This is the type of approach that might be used if no natural clay compression or sensitivity data was available, and leads to an under-prediction of preconsolidation pressure with associated consequences for subsequent predictions.

The initial specific volume, and mean effective stress of the samples along with the calculated preconsolidation pressures for the natural samples modelled are given in Table 5.1.

### 5.2.3 Analysis procedure

A series of simulations using the finite element program SSCRISP (Stallebrass, 1992) to model the triaxial tests as a 'single element' were carried out for a selection of reconstituted and natural Boom clay tests. These were modelled using 2 finite elements

representing a single element with uniform stresses as noted in Section 5.1. Summaries of the tests modelled are given in Tables 5.1 and 5.2. All stages of the tests were modelled to ensure that the configuration of the kinematic surfaces within the 3-SKH model was appropriate for the stress history applied to the sample before the loading stage used for comparison. As noted previously, the stress changes applied to the reconstituted samples were well defined. Stages of the test were modelled as either drained or undrained, depending on the particular test, using an incremental solution approach. This solution procedure requires a large number of increments to ensure accuracy. The number of increments is increased until further increases have no effect on the output. The finite element simulations were stress controlled, except near to failure, where displacements were applied. The natural samples were modelled using preconsolidation pressures calculated from the normal compression lines for both reconstituted and natural soil to investigate the consequences of assuming reconstituted behaviour for natural soils. The same set of model parameters was used for all the simulations. As described in Section 5.2.2 the parameters calculated were the best estimates possible using a standard derivation and no subsequent fine tuning of parameters has been carried out.

#### 5.2.4 Results for reconstituted tests

Five reconstituted triaxial tests were modelled and these are summarised in Table 5.2. Figure 5.12 shows stress paths for the five tests modelled which include test *ruth* which was used to determine the parameters controlling the kinematic surfaces of the 3-SKH model in Section 5.2.2. The additional overconsolidated undrained test modelled, *boomrc*, follows a similar pattern of behaviour to test *ruth*. The normally consolidated undrained test *booml* defines a critical state rather lower than much of the Boom clay data presented by Coop et al. (1995), but provides an opportunity for a comparison of a model prediction from a normally consolidated state. Model predictions of stress paths are presented in Figure 5.13 which in general represent the pattern of the laboratory data well. The model prediction of test *boomrc* shows the same initial anisotropic stress path as for test *ruth* as they share similar recent stress histories. In this case, the deviation from the laboratory path pushes the current stress point wet of critical leading to a significantly different state path compared to the test data. The prediction for normally consolidated test *booml* follows the Modified Cam Clay state boundary

surface to fail at critical state. In reality it is difficult to be sure that a sample is truly normally consolidated at the start of shearing, so a prediction for the same test but at an overconsolidation ratio,  $R_0 = 1.05$  has also been presented. The effect of this is to move the current stress point inside the state boundary surface leading to a shallower path to failure as seen in the laboratory test. The same data are plotted as stress paths normalised by the current preconsolidation pressure  $p'_c$  for the laboratory data in Figure 5.14 and the model predictions in Figure 5.15. Model predictions of current preconsolidation pressure,  $p'_c$ , for the two overconsolidated undrained tests are lower at the start of shearing compared to the current preconsolidation pressures calculated from the specific volumes of the samples in the laboratory tests. For the constant  $p'$  compression and extension tests, current preconsolidation pressure is overestimated for the model predictions. Model predictions of current preconsolidation pressure evolve as the stress history of the triaxial test is modelled and are not fixed at the start of shearing. Predicting a lower  $p'_c$  than expected will be caused by greater plastic volumetric strains being computed during the swelling stages prior to shearing the samples. For test *boomrc* in particular, underprediction of overconsolidation ratio leads to shearing occurring the wrong side of critical state as the surfaces align with the current state.

Drained and undrained shear stiffnesses for all the tests are plotted against deviator stress for the laboratory data in Figure 5.16 and for the model predictions in Figure 5.17. The stiffnesses calculated for the laboratory data have been smoothed using a least squares method (Stallebrass, 1990). The prediction starting at a normally consolidated state for test *boom1* significantly overestimates stiffness compared with other predictions over the entire stress range of the test. The prediction from an overconsolidated state for *boom1* over-predicts stiffness up to a deviator stress of 50 kPa but offers a reasonable prediction of the laboratory data thereafter. The prediction for test *boomrc* underestimates initial stiffness and decays more rapidly compared to the test data. The pattern and magnitudes of the predictions of the other tests resemble the data more closely. A comparison between data and predictions at larger strains can be obtained by plotting stress-strain curves. A graph of stress ratio,  $q/p'$ , against axial strain,  $\epsilon_a$ , for the test data in Figure 5.18 can be compared to model predictions in Figure 5.19. Results from the finite element analyses show a similar pattern to the laboratory data except for *boom1* for which the test data shows failure at a lower stress

ratio, as expected from the stress path data. For the overconsolidated tests *ruth* and *boomrc*, the model over-predicts the strains associated with failure. Failure strain is also over-predicted for the constant  $p'$  extension test *boom11*. Representing the data in this way again shows the over-prediction of stiffness made for the normally consolidated test, with, a more reasonable prediction made by the lightly overconsolidated analysis although the stress ratio at failure is over-predicted as might be expected. Figures 5.20 and 5.21 show test data and model predictions for the generation of excess pore pressure against deviator stress for the undrained tests. Again, the general pattern of the data is reproduced by the model predictions, but the laboratory data show the generation of positive pore pressures, i.e. a compressive response, for all three tests, whereas model predictions for *ruth* and *boomrc* show the development of negative excess pore pressures at some stage during shearing. The positive pore pressures generated in the samples are a little surprising as these samples are at states dry of critical, and indicate that there is an effect of some form of anisotropy, possibly a more dramatic effect of recent stress history than predicted by the model. Model predictions of positive excess pore pressures at large strains for the test occur because the state moves wet of critical during shearing.

The results from the predictions of the reconstituted tests allow an appraisal of model predictions for a stiff clay, with some of the uncertainties associated with clays in the natural state removed. The previous loading of the sample is known with a high degree of confidence which ensures that the modeller can recreate the correct history for the analysis. For all the reconstituted paths except *boomrc*, the model has predicted the general direction of the stress path followed by the clay with some success. Localisation phenomena (Atkinson and Richardson, 1987) often prevent triaxial samples reaching a true uniform critical state in both reconstituted and natural overconsolidated tests, so it is unsurprising that the model generally over-predicts strains associated with failure. For the single element predictions the soil remains a continuum so that all of the soil is undergoing the same strain. In the tests local strains may be very high, but global strains are lower. It is therefore important to have some data from tests wet of critical in order to evaluate the friction angle  $M$ , as the dry side tests often do not reach true critical state. The predictions of initial stiffness made by the model are based on the bender element data by Agah (1996), and are in generally good agreement with the laboratory data despite the difficulty in measuring stiffnesses

reliably at these low strain levels. The decay of stiffness for a variety of paths fits the data reasonably, with the normally consolidated test being an exception. Patterns of behaviour exhibited by the laboratory tests are, in general, reproduced by the model in a satisfactory way.

#### 5.2.5 Results for natural tests

Four undrained triaxial shearing tests on natural samples of the same clay were also modelled using the 3-SKH model. All the tests on natural samples were at overconsolidated states, and followed typical patterns of behaviour for tests on the dry side of critical. The same values were used for the model parameters as those derived for the reconstituted data, with the exception of  $N_n^*$  which defines the position of the normal compression line for the natural clay which lies to the right of the line for the reconstituted clay. This normal compression line describes the increased preconsolidation pressure associated with the larger state boundary surface of the natural clay which was calculated in the manner described in Section 4.2.1. The tests were also modelled assuming that their behaviour was related to a reconstituted state boundary surface for comparison. The stress history for the natural samples was different to the reconstituted clay as it was dependent on the depositional history of the clay over geological time which resulted in the clay having a sensitivity of around 1.5, and a state that was lightly overconsolidated ( $R_o = 2.6$ ). The parallel nature of the natural and reconstituted normal compression lines indicates that the structure of this soil is mostly related to its fabric, Figure 5.2, rather than any high degree of bonding. During sampling, the soil was swelled to around 600 kPa due to the inability of the clay to sustain suctions. The soil samples were then reconsolidated isotropically in the triaxial cell to the required mean effective stress at the start of shearing (see Table 5.1). There is therefore more uncertainty about the stress history of the natural samples although the final loading before shearing is well defined. The different stress history imposed prior to the shearing stages for the natural samples leads to a different shape of stress path compared to that of the reconstituted clay which can be seen in Figure 5.22 which shows the stress paths for the natural tests. Model predictions of the stress paths followed during the tests on natural samples made using the reconstituted state boundary surface, can be seen in Figure 5.23. Model predictions for all tests follow paths that are initiated from a state lying wet of critical due to the underestimation of

overconsolidation ratio associated with assuming a reconstituted state boundary surface. In addition, the recent stress history of the tests is incorrectly modelled which leads to a poor prediction of the anisotropic stress paths of these tests. Figure 5.24 shows model predictions made using the natural state boundary surface. Here the model predictions for *boomi*, *boomo* and *boomq* compute anisotropic stress paths which follow the general trend of the data significantly better than for the reconstituted state boundary surface predictions. The prediction for *boomn* follows the data less closely, but is a more reasonable prediction than the analysis using the reconstituted state boundary surface as if localisation had not occurred in the natural sample it would be more likely to be moving towards a critical state point which was identified in the prediction using the natural state boundary surface. A graph of shear stiffness against the change in deviator stress for the four sets of laboratory data is shown in Figure 5.25. Predictions of the magnitude of initial stiffness are hard to evaluate as the test data are not accurate at these strains so comparisons of stiffness will be restricted to the data at larger strains. Predictions of shear stiffness made using the reconstituted state boundary surface as a reference can be seen in Figure 5.26. As previously stated, it is not possible to accurately assess the initial stiffness predictions, but it is not hard to reconcile the predicted magnitudes with the laboratory data. After a change in deviatoric stress of approximately 500 kPa, predicted stiffnesses for tests *boomi* and *boomn* compare closely to the laboratory data, whereas predictions for tests *boomo* and *boomq* are approximately 50% too low. The pattern of the data is produced apart from *boomo* which exhibits greater stiffness than *boomi* in the laboratory data, but lower in the computed results. The same graph for the predictions made assuming the natural state boundary surface can be seen in Figure 5.27. Here the general pattern is reproduced with the exception of the computed stiffness for *boomi* which decays too slowly, reducing to a level between 30% and 50% higher than the laboratory data. The prediction of stiffness made by the reconstituted analysis represents the laboratory data better, as the analysis predicts a value of deviator stress at failure which is closer to that observed in the laboratory. However, this is based on an incorrect stress path which has contributed to the better prediction from the ‘reconstituted’ analysis. Assuming that the natural state boundary surface is the correct reference on which to base predictions, as the predicted stress path follows the laboratory data more closely, it would be necessary to reduce the critical state friction coefficient for extension to ensure that test *boomi* reached critical state at a more realistic deviator stress. If  $M$  were reduced, it is likely that the fit of the ‘natural’ prediction would be improved. Not enough laboratory

evidence exists to determine a separate value of  $M$  in extension for this clay. In addition, the current version of the model does not allow different coefficients of friction to be specified for extension and compression. As for the predictions made using the reconstituted state boundary surface, it is impossible to evaluate the predictions of initial stiffness, but again it is not hard to reconcile the predictions with the laboratory data, which are up to 15% higher due to the increased degree of overconsolidation. The laboratory data is plotted as a graph of stress ratio against axial strain in Figure 5.28. The laboratory tests on natural samples fail at around the stress ratio of 1.03 used for the model predictions, but on average measured stress ratios for the natural tests are slightly lower at around 0.9. 3-SKH model predictions made using the reconstituted and natural state boundary surfaces as a reference can be seen in Figures 5.29 and 5.30 respectively. Both sets of predictions tend towards failure at higher axial strains than were observed in the test, although this is not as marked as for the reconstituted tests in the previous section. The predictions made using the natural state boundary surface in general represent the laboratory data better at stress ratios approaching 1. Figure 5.31 shows the change in pore pressure plotted against deviator stress for all the tests. Figure 5.32 and 5.33 contain the predicted response by the model for the reconstituted and natural state boundary surface analyses. Comparison of the figures shows that whilst not predicting the precise shape of the pore pressure response curves, which are related to the stress paths, the general pattern of behaviour has been reproduced better by the natural analyses. In particular, pore pressures in extension and compression paths show a change from compressive to dilative behaviour as failure is approached, unlike the analyses using the reconstituted state boundary surface, due to the state relative to the critical state point being correct.

#### 5.2.6 Summary

The analyses carried out in this section represent a simple way of modelling the natural behaviour of a stiff clay. A series of tests on reconstituted samples were carried out, enabling a set of parameters to be obtained for this soil. Compression data was available for the natural samples, so that a preconsolidation pressure defining the state boundary surface for the natural tests could be calculated using the procedure in Section 4.2.1 and consequently a new value for  $N^*$ . In the absence of evidence to the contrary, all other parameters were kept the same as for the reconstituted clay.

Evidence from several authors (Rampello et al., 1994, Coop et al., 1995, Cotecchia, 1996) suggests that the stiffness relationship proposed by Viggiani and Atkinson (1995) is valid for both reconstituted and natural samples, using the same exponents, if the difference in state is accounted for. Testing this relationship was a primary aim of these analyses, but unfortunately no clear conclusions can be drawn. For most of the natural samples, the stiffnesses measured in the laboratory were not accurate in the very small strain range, so there were no measurements to compare to the calculated values of  $G'_{max}$ . Inspection of the data from the natural samples indicates that the calculated values of  $G'_{max}$  for most of the tests seem to fit in with the general trend of the data. Initial stiffness predictions for the reconstituted tests, where the test data allowed better comparisons generally corresponded to the data well.

Model predictions of stress path for the natural clay, using the natural state boundary surface follow anisotropic paths which are closer to the laboratory data than the predictions made using the reconstituted state boundary surface. The quality of the natural predictions is comparable to the predictions for the reconstituted clay. The ability of the model to produce anisotropic paths similar to those observed for these tests would seem to indicate that much of the anisotropy of the stress paths of the Boom clay is attributable to stress induced anisotropy and recent stress history, which are accounted for in the model. Referencing the behaviour of the triaxial tests to the correct state boundary surface using the model is therefore critical in ensuring that correct history is modelled and that the state at the start of shearing falls on the correct side of the critical state point to get the correct response as failure is approached.

Magnitudes of axial strain at failure are generally over-predicted by the model, but this is unsurprising as localisation phenomena (Atkinson and Richardson, 1987) often prevent triaxial samples reaching a true uniform critical state in both reconstituted and natural overconsolidated tests. For the single element predictions the soil remains a continuum so that all of the soil is undergoing the same strain. In the tests locally strains may be very high, but globally, strains are lower.

In general the predictions of both reconstituted and natural tests using the appropriate reconstituted or natural state boundary surface as a reference reproduce the main

patterns of observed behaviour. Whilst it is not possible to predict precisely the exact response of every test, it is possible to make reasonable predictions for a range of behaviour. Allowing for a state which is likely to be more representative for the natural tests by relating the computations to a state boundary surface characterised by the sensitivity of the soil as defined by Cotecchia and Chandler (1998) creates predictions which are comparable in accuracy to predictions for the reconstituted tests where the stress history is more clearly defined. Predictions for the natural clay using the natural state boundary surface are in general significantly improved when compared to predictions made not allowing for the sensitivity of the natural soil.

### 5.3 MODELLING VOLUMETRIC CREEP

This section examines the influence of volumetric creep during the geological history of the soil on the subsequent stress-strain response. Volumetric creep has been implemented into the existing soil model using a simple approach, to examine whether it has a major effect on subsequent predictions of ground movements compared to other features of the behaviour of natural soils. It has been assumed that the soil will not undergo any bonding during the period of creep, and will return to the normal compression line on further loading, rather than yielding to the right of it  $p'_{cb}$  in Figure 5.34.

A description of the method used to incorporate simple volumetric creep into the 3-SKH model is contained in Section 4.4.

#### 5.3.1 Evaluation of the model for volumetric creep

In order to evaluate the effect of incorporating volumetric creep into the 3-SKH model several 'single element' finite element analyses, modelling a uniform element of soil, were undertaken. These analyses were intended to examine the consequences of including creep during periods of 'rest' at constant stress state for simple cases, before the model was used for more complex boundary value problems. The time periods for which creep was allowed represented both laboratory and geological time scales.

### 5.3.2 Evaluation of creep model for laboratory tests

The first analyses, were of a sample of Speswhite kaolin and were loosely based on one of a series of tests by Stallebrass (1990) to examine the effects of recent stress history on laboratory samples. The stress path followed enables a variety of histories to be examined in a single test. No measurement of creep was made in the laboratory tests as this was not the intention of the tests and they are used here simply for convenience. The parameters used for Speswhite kaolin were the same as those outlined in Section 6.2.1. Little data exists for the creep rate of Speswhite kaolin so the secondary compression index measured by Richardson (1988) for London clay was used in these analyses which were intended only to test the significance of allowing for volumetric creep. The sample was isotropically compressed to 720kPa, and swelled back to 300kPa, the soil was then subjected to a series of stress probes which can be seen in diagrammatic form in Figure 5.35. The stress probes allow the stress-strain response of the soil to be measured along the same drained constant  $p'$  stress path but following different approach paths. The effect of creep on the constant  $p'$  path followed in the test was modelled by repeating the test with periods of 1 year and 1000 years of creep inserted before each of the constant  $p'$  stages i.e. at stress state A in Figure 5.35. The period of creep of 1 year was thought to represent the sort of time period achievable in the laboratory using careful testing. The period of 1000 years was used to investigate the logarithmic nature of the creep relationship by allowing creep for a further three log cycles.

Figure 5.36 shows a schematic representation of the configuration of the three surfaces defining the 3-SKH model before each of the constant  $p'$  excursions. The dotted lines show the original configuration of the surfaces, with the solid lines representing the surfaces after a period of creep has been modelled. Figure 5.37 shows shear stiffness data for the four constant  $p'$  paths after each of the four different recent stress histories with no creep allowed. The data are plotted as tangent shear stiffness against deviator stress, following Stallebrass (1990) and the predictions follow the expected pattern as outlined in Section 3.2.1. Figures 5.38 and 5.39 show the same graph plotted for shearing following periods of 1 and 1000 years creep. It can be seen that for all the stress paths except the 90 degree rotation the pattern of behaviour is very similar to the series of tests where there was no creep, but in all cases the initial stiffness is now

equal to  $G'_{ec}$ , the elastic shear modulus computed by the model. For the 90 degree rotation tests the initial stiffness increases slightly as the value of  $G'_{ec}$  is dependent on  $R_0$  (Section 4.5), but the decay of stiffness is more rapid. This can be seen more clearly in Figure 5.40 which again shows plots of shear stiffness against deviator stress this time comparing the results for the three analyses for a 90 degree rotation on the same graph. The stiffness curves predicted following simulation of a period of creep, form a plateau at around 20-30 MPa and are almost indistinguishable from the stiffness curve predicted after no creep from there on. The slower decay in stiffness when there is no creep occurs because at the start of shearing the stress state lies on both the kinematic surfaces and these surfaces are configured such that they have to translate during shearing to become aligned with the new stress path direction. The graph of deviator stress against shear strain shown in Figure 5.41 for the same analyses shows however that the variation of tangent stiffness observed leads to a general increase in secant stiffness over a range of strains up to 2%. The graph of shear stiffness against deviator stress for the 180 degree stress path, Figure 5.42 shows stiffnesses for the analyses where creep has been allowed which are greater both initially and throughout the stress range of the test. The consequences of this on the stress-strain response can be seen in Figure 5.43 where deviator stress against shear strain is plotted, at  $q = 140$  kPa the secant stiffness has increased by almost a factor of 3 after 1000 years of creep. Both the -90 and 0 degree stress paths show the same type of overall increase in stiffness as the 180 degree path, and this can be seen in Figures 5.44 and 5.45. All paths show some increase in initial stiffness as expected, with the analyses allowing 1000 years of creep predicting initial stiffnesses around 2% higher than for the analyses allowing 1 year of creep. All paths show an increase in overall secant stiffness associated with periods of creep, with the highest stiffnesses recorded for the longest creep duration, although for the 90 degree stress path rotation a faster decay of tangent stiffness was experienced by the analyses where creep was allowed. The effect of recent stress history is still evident in the predicted stiffness curves where creep was allowed, and this is in agreement with the conclusions drawn by Richardson (1988) that the effects of time and recent stress history are additive.

The second analysis carried out modelled a sample one dimensionally compressed to 400kPa, and swelled back to 200kPa, the soil was then sheared undrained after periods of zero and one thousand years creep. This was not modelling a particular test as very

limited data is available in the literature, but was designed to be representative of a typical undrained triaxial test. The parameters used for this analysis were the same as those used for the first analysis and can be seen in Table 6.2. Figure 5.46 shows the stiffness curves during undrained shearing for these analyses. It can be seen that for the analysis where one thousand years of creep has been allowed before shearing, the initial elastic stiffness is higher than for the sample with no creep, as expected. As for the 90 degree stress path rotation in the previous section, the rate of decay of stiffness at small strains is greater for the test including creep leading to lower stiffnesses over the strain range 0.005 - 0.1%. The shear stiffness is once again higher for the analysis where creep was allowed at larger strains. This is again due to the way in which the surfaces translate, as noted in the previous section. This difference in the way the surfaces translate can also be seen in the shape of the stress paths in Figure 5.47. At small changes in stress,  $\Delta q'$  less than 50 kPa, the shape of the paths, representing the anisotropy created by the recent stress history, varies significantly when there is no creep as the stress point translates around the edge of the kinematic surface, but is approximately constant when creep has taken place as the stress point now moves through the surface. There is not sufficient detailed evidence to establish whether all these features are observed in laboratory tests, but the model does again predict an overall increase in secant stiffness.

The two analyses above show that incorporating volumetric creep into the 3-SKH model in this simple way can reproduce the main characteristics of the behaviour exhibited by clays allowed to creep in the laboratory. The model is able to predict an increase in initial shear stiffness associated with the increase in apparent overconsolidation ratio, but this is small compared to the increases which might be associated with soft clays, as the value of the secondary compression index used was small. Detailed analysis of the effect of creep on the stress strain behaviour of stiff clays is not possible, as data in the literature are limited, but model predictions generally produced an overall increase in secant stiffness. Richardson (1988) presented evidence that time effects and recent stress history effects are additive (Section 2.5) and this is predicted by the model for the recent stress history tests carried out by Stallebrass (1990).

### 5.3.3 Evaluation of creep model for geological time periods

The second series of analyses investigate the effects of creep during the geological history of a deposit, and were used as a guide for the inclusion of creep in the analysis of the boundary value problem in Section 7.3. The parameters used in the model were those derived for London clay by Stallebrass and Viggiani (1994) for the 3-SKH model and can be seen in Table 5.5. The creep rate  $\psi$  necessary for the application of equation 4.10 was calculated by Richardson (1988) assuming a  $t_0$  of one minute from a series of stress path tests on London clay.

These analyses, simulate an element of soil undergoing a series of stress paths representing the geological stress history which may have been followed by the London clay. After deposition in a normally consolidated state where  $K_0 = 1 - \sin\phi'$ , the soil was swelled back due to erosion of 200 metres of overburden and subsequently reloaded by the deposition of 5 metres of terrace gravel. After the deposition of the terrace gravel, the clay was allowed to creep for 0.5 million years. Two other finite element analyses were carried out, allowing periods of 1 million and 5 million years of creep before the deposition of the terrace gravel in addition to the creep allowed after deposition. These analyses were carried out to investigate whether creep at the end of the erosion stage would have an effect on the behaviour of the soil in addition to the second period of creep after deposition of the Terrace gravels. Figure 5.48 shows the effect of no creep at end of swelling, in addition to one million and five million years of creep, on the predicted stiffness curves from undrained shearing after re-deposition. It can be seen that the additional creep stage has an effect on stiffness throughout shearing, as well as increasing the initial stiffness due to the increase in  $G'_{ec}$ . The creep stage also affects the behaviour of the soil element in stress space (Figure 5.49). In these analyses the preconsolidation pressure  $p'_c$  varied substantially from 1644 kPa for the analysis with creep at the end of re-deposition only, to 2006 kPa for the analysis with 5 million years of additional creep after swelling. It can be seen from both figures that there is no significant change in behaviour resulting from increasing the period allowed for creep from one million to five million years. This might be expected because of the exponential relationship between volume change and time characterising creep such that  $p'_c$  only increased by 24 kPa during the additional 4 million years.

#### 5.3.4 Summary

The method used to incorporate simple volumetric creep into analyses carried out using the 3-SKH model is able to predict key parts of the expected behaviour. Where creep has been simulated, the model predicts an increase in initial stiffness, which is associated with an increase in apparent preconsolidation pressure caused by enlargement of the state boundary surface in the model. The model also predicts an overall increase in secant stiffness. The model predicts time and recent stress history effects which could be considered additive, which is in agreement with the findings of Richardson (1988). Creep can be simulated over both short and geological time periods although for the secondary compression index used, changes in stiffness are relatively small even over geological time periods. It is difficult to evaluate the detailed features of the predictions made due to the scarcity of data for stiff clays, but this work does show that the main features associated with creep can be simulated with only small changes to the application of the 3-SKH model. The effect of allowing creep is noticeable in the simulation of element tests, but it is not clear whether the modifications to the predicted behaviour will have a significant effect on the results of boundary value predictions. In Section 7.3, the proposed method of incorporating creep will therefore be used in the analysis of a simple field problem.

#### 5.4 MODELLING BEHAVIOUR CHARACTERISED BY DEPOSITIONAL ANISOTROPY

This section concentrates on the prediction of the behaviour of Oxford clay. The Oxford clay is a stiff clay of medium sensitivity,  $S_t = 5.7$  with a structure characterised by depositional anisotropy. The behaviour of the Oxford clay is not strongly affected by recent stress history (Pierpoint, 1996), the prediction of which spurred the initial development of the 3-SKH model. The nature of this clay is different to the Boom clay (Section 5.2) which was less sensitive and seemed to be strongly affected by stress induced anisotropy. The aim of this work was to investigate whether the behaviour of this clay could be accommodated within the framework of the 3-SKH model. As part of the finite element analyses carried out for the Elstow investigation in Chapter 7 it was also necessary to define a set of input parameters for the 3-SKH model to characterise this clay.

#### 5.4.1 Determination of material parameters

##### i) Definition of isotropic normal compression line

Atkinson and Cherrill (1988) carried out a series of tests on clays which included tests on reconstituted Oxford clay. Data for isotropic normal compression can be seen plotted as  $\ln v: \ln p'$  in Figure 5.50. The normal compression line obtained from Atkinson and Cherrill, re-plotted as a one dimensional curve using an assumed  $K_{onc}$  of  $1 - \sin \phi'$  where  $\phi' = 22.6$  (Pierpoint, 1996) is plotted against data from high pressure oedometer tests on natural Oxford clay from the Elstow site investigation (Pierpoint, 1996) in Figure 5.51. Also shown on the graph is a one-dimensional normal compression line parallel to the normal compression line for the reconstituted clay and described by a sensitivity of 5.7. The assumed natural normal compression line fits the test data well, and lies on a line parallel to the reconstituted data at higher stresses. The pressures available in the oedometer do not show whether the compression curve for the natural sample would fall toward the reconstituted curve upon further loading, but due to the heavily layered fabric of the Oxford clay, it is reasonable to assume that the structure is relatively stable. From these data the values of  $\lambda = 0.1265$  and  $S_t = 5.7$  were obtained for the natural Oxford clay. The value of  $N^*$  for the reconstituted Oxford clay was  $N^* = 3.962$ . For a natural clay which is of sensitivity greater than 1:

$$N_n^* = N^* + \lambda \ln S_t \quad (5.4)$$

this gives  $N_n^* = 4.182$ .

##### ii) Elastic volumetric deformation

As described in Section 5.2.2,  $\kappa$  can be estimated from the results of isotropic swelling stages following isotropic compression. Figure 5.52, shows a plot of  $K'/p'$ , against  $p'/p'_{cn}$ . As for the Boom clay, the value taken for  $K'/p'$  corresponds to an approximate upper bound to the majority of the data due to the problem of obtaining accurate measurements at very small strains. A value of  $K'/p'$  of 300 was taken, which gives  $\kappa = 0.0033$  for Oxford clay.

iii) Elastic shear deformation

The coefficients describing the relationship between  $G'_{ec}$ , current mean effective stress and overconsolidation ratio to be used in the equation presented by Viggiani and Atkinson (1995) were calculated from the charts presented by Viggiani and Atkinson (1995) and from data presented in Hird and Pierpoint (1997). Hird and Pierpoint (1997) present static and dynamic shear stiffness measurements from tests on Oxford clay. The static measurements were made during a series of constant  $p'$  shearing stages, and were found to correspond to the relationship  $G' \propto p'^{0.67}$ , Figure 5.53. The dynamic measurements of  $G'_0$  recorded values of  $G'_0 \approx 75$  MPa at  $p' = 278$  kPa. The value of  $n = 0.67$  suggested by Hird and Pierpoint (1997) was adopted for these analyses, with the other coefficients in the stiffness relationship being scaled from the charts given in Viggiani and Atkinson (1995). Scaled values for the other coefficients corresponded to a plasticity index of 31 measured in the Elstow site investigation, such that  $A = 980$ , and  $m = 0.235$ . Using this combination of parameters yields a value of  $G'_0 \approx 80$  MPa for  $p' = 278$  kPa, at an overconsolidation ratio calculated from the approximate location of the stress point with respect to the natural normal compression line.

iv) Parameters defining the behaviour of the kinematic surfaces

The values of the parameters  $\phi$ ,  $T$  and  $S$  were determined from the results of a parametric study based on the stress path tests performed as part of the Elstow investigation (Pierpoint, 1996). The tests were carried out on block samples from the Elstow site and from the Kempston pit of the London Brick Company, half a mile away and consisted of a series of drained constant  $q$  and  $p'$  probes of the type carried out by Stallebrass (1990) to investigate the effects of recent stress history. Test T06, which was carried out on a vertically orientated unweathered sample from the Kempston site was chosen for numerical simulation as a full set of stress path probes had been carried out without premature stopping of the test. The 3-SKH model requires the full stress history of the test to be modelled, so the analysis simulated the one-dimensional swelling of the sample from a state with a preconsolidation pressure calculated from the intercept of the current elastic wall with the natural state boundary surface, using the method outlined in Section 4.2.1. The analysis then simulated the series of stress probes followed during the test which can be seen in Figure 5.54. A wide range of

values of the parameters  $T$ ,  $S$  and  $\phi$  were used to identify the best fit between predictions and observations of stiffness along several paths of the test. These values are summarised in Table 5.6. Figure 5.55 shows model predictions alongside experimental data for a constant  $p'$  shearing stage from test T06. The parameters which were chosen to represent the Oxford clay were used in the prediction p3 which corresponds to values of  $T = 0.03$ ,  $S = 0.05$  and  $\phi = 3.0$ . The values for  $T$  and  $S$  for the Oxford clay are small in comparison with the values obtained for the Boom clay (Section 5.2.2) and for London clay (Viggiani and Stallebrass, 1994), in particular the value of  $T$ , but were necessary to predict the correct decay of stiffness over a relatively small change in stress compared to the natural preconsolidation pressure. The curves corresponding to the parameter sets p1 and p2 show the effect of increasing the values of  $T$  and  $S$ , which is to extend the elastic region of stiffness, leading to too rapid a decay of stiffness over the medium strain range. The finite element analysis p4 has the same values of  $T$  and  $S$  as p3, but with a reduced value of  $\phi$  this has the effect of increasing the stiffness at medium to large strains, such that the predictions are too stiff. Prediction of initial stiffness, which is controlled by the equation proposed by Viggiani and Atkinson (1990) represents the very small strain data well.

Figure 5.56 shows another constant  $p'$  path from test T06, compared to predictions from the same analyses as for the previous path. The initial stiffness predicted for this path is 100% too high, with too rapid a decay of stiffness for all paths. Nevertheless, finite element analysis p3 is still the best representation of the data over a wide change in stress.

Data from a constant  $q$  swelling path together with predictions from the numerical analyses results can be seen in Figure 5.57. The initial bulk modulus is controlled by the value of  $\kappa$  and the current mean effective stress and is therefore the same for all the analyses. Consistent with previous comparisons, analyses p1 and p2 over-predict the extent of the elastic region, with the subsequent decay over the medium strain range too rapid. This leads to the bulk modulus at larger strains being under-predicted for these tests. Analysis p4 over-predicts stiffness over a wide range of stress with too little decay after the initial small strain region.

The data presented in Figures 5.53 to 5.57 show that the combination of values used for the parameters are a reasonable choice for representing the behaviour of Oxford clay. This more extensive evaluation of the parameters chosen was carried out because the values of  $T$  and  $S$  are much smaller than used for other stiff clays that have been modelled using the 3-SKH model, with  $T = 0.03$  and  $S = 0.05$ , and the value of  $\varphi$  was larger than normal at 3.

#### 5.4.2 Modelling Oxford clay using conventional 3-SKH model

In deriving the parameters for Oxford clay, most attention was paid to modelling the stiffness relationship. In order to examine the effect of the parameter choices on the anisotropic stress strain response predicted by the model, two undrained triaxial tests were also simulated. The undrained tests were carried out as part of the Elstow site investigation, and consisted of tests on vertically and horizontally orientated block and tube sampled specimens. Test Y3 was performed on a tube sampled specimen, with test Y8 being carried out on a sample trimmed from a block. The tests were saturated at a confining stress of 100kPa and then consolidated isotropically to the required stress at the start of shearing. The tests were modelled numerically by starting the analysis at the stress to which the samples were saturated to in the laboratory, with a preconsolidation pressure calculated from the intercept of the current elastic wall with the natural state boundary surface in the manner described in Section 4.2.1. The analysis then followed an isotropic compression path to the required stress, followed by undrained shearing to failure. An alternative method of simulating the stress history was also investigated. In this approach the analyses started from a  $K_0$  state before saturation in the cell, but it was found that this had no influence on the predicted response to undrained shearing. Figure 5.58 shows the undrained stress paths followed during the laboratory tests along with the model predictions. The laboratory data follow strongly anisotropic stress paths, with  $p'$  reducing. These are similar in type to the paths seen for the overconsolidated Boom clay (Section 5.2), where the direction of path was reasonably well described by the anisotropy created by the recent stress history simulated by the model. In this case, the model predicts little anisotropy due to recent stress history because of the small size of the inner surfaces, and follows a conventional undrained path. Failure for the model predictions is well to the right of the laboratory data due to

the large size of the bounding surface described by the natural preconsolidation pressure. Localisation phenomena are not predicted by the model so a failure occurring at higher mean effective stress than for the real data is as expected.

#### 5.4.3 Modelling Oxford clay using cross-anisotropic 3-SKH model

Pierpoint (1996) modelled Oxford clay using a non-linear cross-anisotropic model, and noted the significant structural anisotropy of the clay. It was therefore decided to re-analyse the tests using a version of the 3-SKH model modified by Jovicic (1997) to incorporate cross-anisotropic values of  $G'_{ec}$ . The model is described in Section 4.3, where it was shown to have a small effect on the anisotropy of the undrained stress paths of a clay where recent stress history effects are important. Recent stress history is less important for the Oxford clay as demonstrated by the small inner surfaces determined for the 3-SKH model in Section 5.2.2, so in this case modelling anisotropy in this manner may be more appropriate.

The undrained tests were modelled in the same way as before, but with the structural anisotropy represented by  $\alpha^2 = 2$  which is reasonable for Oxford clay, where  $\alpha^2$  is a measure of the ratio of horizontal to vertical stiffness (Graham and Houlsby, 1985). The predictions obtained from both the conventional and elastic anisotropic versions of the model and the laboratory data can be seen in Figure 5.59. The initial portions of the stress path curves predicted by the anisotropic  $G'_{ec}$  analyses now closely follow the direction of the laboratory data. In contrast to predictions made by Jovicic (1997), the 3-SKH model formulation incorporating an anisotropic  $G'_{ec}$  has a marked effect on the direction of the undrained stress path. The reason for this relates to the small size of the inner surfaces and the large size of the bounding surface. The constitutive relationship for plastic strain increments for the 3-SKH model taken from Stallebrass (1990) is given by the equation:

$$\begin{bmatrix} \delta \epsilon_v^p \\ \delta \epsilon_s^p \end{bmatrix} = \frac{1}{h} \begin{bmatrix} (p'-p'_b)^2 & (p'-p'_b) \frac{(q'-q'_b)}{M^2} \\ (p'-p'_b) \frac{(q'-q'_b)}{M^2} & \left( \frac{(q'-q'_b)}{M^2} \right)^2 \end{bmatrix} \begin{bmatrix} \delta p' \\ \delta q' \end{bmatrix} \quad (5.5)$$

Equation 5.5 implies that the magnitude of plastic straining depends on the ratio of  $1/h$ , such that if  $h$  is large, the plastic component of strain will be small. At stress states inside the state boundary surface the variable  $h$ , is strongly dependent on the ratios  $T$  and  $S$ , (see Stallebrass, 1990) and hence the size of the surfaces. For the small  $T$  defined for Oxford clay,  $h$  is some orders of magnitude higher than for the Boom clay, which reduces the plastic strain component considerably. With the plastic component of strain reduced in proportion, the elastic strain component dominates. The dominance of the elastic strain component means that the elastic anisotropy implemented in the cross-anisotropic version of the 3-SKH model has a marked effect on predicted behaviour.

Figures 5.60 and 5.61 show graphs of undrained stiffness against deviator stress for the two undrained tests. Plotted alongside the laboratory data are model predictions for both the standard isotropic and the anisotropic version of the 3-SKH model. Predictions of initial stiffness for test Y3 for both versions are close to the test data, with predictions for test Y8 being approximately half the observed values. For both tests however, the region of high stiffness predicted by both versions of the model far exceeds that described by the laboratory data, with the anisotropic analyses predicting a reduction in stiffness before the isotropic analyses. Stiffness at larger strains is still over-predicted by both versions of the model but significantly more so by the analyses with an isotropic  $G'_{ec}$ . Graphs of deviator stress against axial strain are shown in Figures 5.62 and 5.63 for the same data. Predictions of deviator stress associated with particular values of axial strain are higher than for the laboratory data after strains of less than 0.05% for both tests. Anisotropic elastic predictions are again significantly closer than isotropic elastic predictions but are still around a factor of 3 or 4 out at 1% strain. Predictions for these tests could be significantly improved by reducing the size of the state boundary surface by selecting a lower preconsolidation pressure for the tests. It is likely that a large factor in the over-prediction of stiffness decay and under-

prediction of axial strain for a given deviator stress is the much higher deviator stresses that are computed for the predicted data.

Figures 5.64 to 5.66 show the stiffness predictions for the constant  $p'$  and constant  $q$  tests modelled in the parametric study to determine values of  $T$ ,  $S$  and  $\phi$  for Oxford clay plotted along with predictions made using the anisotropic version of the 3-SKH model using the same parameters as p3. Predictions for the isotropic and anisotropic versions of the model plot close together, with the anisotropic version predicting slightly lower stiffnesses over a range of stress. Anisotropic predictions for these tests are closer to the test data than the predictions made using the standard isotropic version for the same parameters.

#### 5.4.4 Summary

The results of this study are interesting since Pierpoint (1996) stated, after examination of the test data used for this work, that the recent stress history effects seen by Atkinson et al. (1990) were minimal, with similar stiffnesses being recorded for various path rotations at the same strain levels. The values of the parameters controlling the extent of the effect of recent stress history were chosen in the same way as for other clays for which this effect is more evident and the small size of the ratios obtained imply little effect of recent stress history. The kinematic surfaces are relatively small and are traversed by a small change in stress during predictions producing little effect of recent stress history. The 3-SKH model was developed to predict this effect, and does predict reasonably the stress and recent stress history anisotropy exhibited by a variety of clays including Boom clay, Section 4.2. It is encouraging that the formulation seems flexible enough to be applied to a clay where the effect of recent stress history is minimal. These analyses of Oxford clay reinforce the idea that the parameters describing the inner surfaces are material properties (Stallebrass and Taylor, 1997) and if rigorously evaluated will determine whether recent stress history effects are important for a particular clay. It may be fortuitous that in this case where the behaviour of the clay was characterised by structural anisotropy with little effect of recent stress history, that the dominance of elastic straining predicted by the model created conditions where the anisotropic elastic version of the model had a large influence on the response.

Jovicic (1997) stated that the influence of the elastic stiffness parameters on the calculated soil deformation is critically dependent on the previous stress path. In addition it would seem that the influence of the elastic stiffness parameters on predicted response is also strongly dependent on the importance of recent stress history to the anisotropic behaviour. For the Oxford clay which has a natural structure characterised by depositional anisotropy and not strongly affected by recent stress history, modelling anisotropy in the manner described above produces a noticeable improvement in the prediction of the stress-strain-volume characteristics of undrained stress paths.

## 5.5 GENERAL REMARKS

Finite element analyses have been carried out in this chapter to predict several aspects of natural stiff clay behaviour in laboratory tests. The predictions for Boom clay, Oxford clay and creep tests were all made by accounting for observed behaviour in a straightforward manner. Predictions made for the three investigations were generally improved by accounting for this behaviour, and the consequences of changes in analysis procedure were consistent with observations.

For laboratory tests, where the recent stress history and state of the samples are well defined, it is conceptually simple to account for natural clay behaviour in the ways described in this chapter. For field problems however, conditions are less well defined. Analyses carried out in Chapter 7 will investigate the effects of modelling natural clay behaviour for boundary value problems.

## CHAPTER 6 ANALYSIS OF BOUNDARY VALUE PROBLEMS IN RECONSTITUTED CLAY

### 6.1 INTRODUCTION

Presented in this chapter are two finite element analyses of boundary value problems in reconstituted clay carried out in the Accutronic 661 geotechnical centrifuge at City University. In order to be able to measure the effectiveness of applying constitutive models to field problems where many uncertainties are likely to exist, it is useful to be able to evaluate predictions of problems with less variation in history and material properties. Centrifuge tests are ideal for evaluating constitutive models, as it is possible to carefully control the precise geological and loading history of a problem. A detailed description of the issues involved in centrifuge testing can be found in Taylor (1995).

Two sets of analyses have been carried out to model real events in reconstituted clay. The first set of analyses were of a centrifuge test, modelling the simple problem of a circular foundation loaded in cycles and were similar to analyses carried out by Stallebrass and Taylor (1997). In addition to the 3-SKH model two other constitutive models, Modified Cam clay (Roscoe and Burland, 1968), and the Brick model (Simpson, 1992), were used to show the relative quality of the model predictions. The models were partially chosen due to their accessibility as Modified Cam clay and the 3-SKH model are already implemented in a version of CriSP (Britto and Gunn 1987), and the Brick model is available in the SAFE finite element program used by Arup Geotechnics. Detailed descriptions of the 3-SKH model and the Brick model can be found in Chapter 3 and in Stallebrass (1990) and Simpson (1992). The modelled foundation test is a complex problem, and is perhaps not well suited to finite element analysis due to the high stresses at the edges of the foundation and the punching failure mechanism. Nevertheless, the analysis provides a useful frame of reference.

The second set of finite element analyses modelled a centrifuge plane strain tunnel test, where internal tunnel pressures were reduced to simulate the excavation of the tunnel and the resulting movements observed. These analyses were carried out using the 3-SKH model only and were intended to act as a reference measure of the quality of computed movements around tunnels that can be obtained using the 3-SKH model to

simulate a well controlled and monitored event in reconstituted soil. A tunnel problem was to be used as the basis for some analyses of field problems in Chapter 7.

## 6.2 Model foundation

The model foundation test simulated is one of a series of tests carried out by Stallebrass & Taylor (1997) on the Accutronic 661 geotechnical centrifuge at City University. The soil sample was prepared in a consolidometer by first compressing to a maximum vertical effective stress of 850kPa, and then swelling back to a vertical effective stress of 100kPa. Figure 6.1 shows the effective stress and pore pressure distributions at various stages of the sample preparation and testing. The rigid circular foundation was of 60mm diameter, and supported an initial load of 373N due to the weight of the loading arrangement. Figure 6.2 shows the arrangement of pore pressure transducers, displacement transducers and the load cell. After sample preparation, the model was placed on the centrifuge, accelerated to 100g and the pore pressures allowed to come into equilibrium. The equilibrium water table in the model was 52mm below the surface. Pore water evaporation was prevented by a layer of liquid paraffin on the surface of the soil and the water level was controlled by a standpipe connected to the base sand layer. The foundation was loaded at a rate of 2.4kPa/s in several cycles. It is important to know in detail all stages of the test, as the analyses using the 3-SKH model and the Brick model begin from the first stage of setting up the sample.

### 6.2.1 Selection of model parameters

The values of the Modified Cam clay parameters were those obtained by Morrison (1994), from a series of laboratory tests to determine parameters for back analysis of centrifuge tests. Values for the horizontal and vertical permeability of Speswhite kaolin were obtained from Al Tabbaa (1987). The parameters used are given in table 6.1.

The parameters required for the 3-SKH model were again obtained from data from Morrison (1994), or were obtained by a parametric study using single element simulations of stress path triaxial data (Stallebrass, 1990). The elastic stiffness  $G'_{ec}$  was

obtained from data produced by Viggiani (1992). The soil parameters for the 3-SKH model can be seen in table 6.2.

Brick model parameters required were obtained from data from Viggiani (1992), Simpson, (1997) and using a parametric study (Ingram, 2000). A full set of Brick model parameters for Speswhite kaolin are given in Tables 6.3 and 6.4.

### 6.2.2 Analysis procedure

#### a) CriSP analyses

The Modified Cam clay and 3-SKH model analyses were carried out using a version of the SSCRISP (Stallebrass, 1992) with triangular cubic strain consolidation elements offering pore pressure degrees of freedom. The mesh is shown in Figure 6.3 and contained 299 elements with 174 nodes. The mesh was constrained by the following boundary conditions.

	Displacement	Pore pressure
Top	Free	Impermeable
Left	Horizontal	Impermeable
Right	Horizontal	Impermeable
Bottom	Horizontal / Vertical	Zero excess

The test was modelled in axisymmetry, with the following main stages.

1. The swelling of the soil in the consolidometer
2. The placing of the foundation and increase in gravity to 100g
3. Equalisation of pore pressures in the centrifuge
4. Replacing the foundation with nodal loads
5. Loading stages

The soil was swelled from a vertical effective stress of 850kPa by removing a surcharge over a long period of time to simulate drained conditions. Some of the surcharge was left on to ensure the soil stayed at a vertical effective stress of 100kPa

(stage 1). The initial  $K_o$  was assumed to be equal to  $1 - \sin\phi$ .  $K_o$  was subsequently controlled by the soil model. The foundation was placed by adding elements with a mass equalling the initial load applied by the loading system and removing the remaining surcharge, gravity was increased to 100g (stage 2). The soil was then consolidated for the time allowed in the test to allow pore pressures to come into equilibrium (stage 3). The foundation elements were replaced by equivalent nodal forces, since the test foundation was smooth, and therefore horizontal fixity of these nodes was not desirable (stage 4). To ensure that the base of the rigid foundation remained level, the soil was loaded by applying equal displacements across its base. Loads were back calculated to give the change in overall load on the foundation. The correct rate of loading was simple to model for the Modified Cam clay model, as the loading cycles took place well within the state boundary surface causing a linear response of load to time. Since the 3-SKH model is highly non-linear within the state boundary surface it was more difficult to ensure that the rate of loading closely fitted the time ramps from the test. An approximation to the correct rate was achieved by using a log time step relationship for each loading increment. The load ramps as modelled are shown in Figure 6.4.

A further 3-SKH analysis was run for comparison with the SAFE analyses described below to examine the consequences of performing a drained-undrained analysis. The stages of the test were similar to the stages used for the Brick analysis, with adaptations made to allow for the differences in input data in the CriSP program. The main difference between the drained-undrained analysis and the consolidation analysis was that in the drained-undrained analysis the surcharge remaining after the swelling stage was not removed until after the equivalent nodal loads were applied. This was to try to replicate an observed stress path reversal just prior to loading seen in the consolidation analysis.

#### b) SAFE analyses

The Brick model analysis was carried out using a version of the model implemented in the Arup Geotechnics' SAFE program. The mesh was reconstructed for use in SAFE, as it needed to be built up of quadrilateral elements, Figure 6.5. The mesh contained 270 elements and 306 nodes, displacement boundary conditions were as before. As

loading under conditions of coupled consolidation was not available in SAFE at the time these analyses were carried out, the problem was modelled drained-undrained in the following stages.

- 1 Deposition from a slurry and swelling in the consolidometer (drained)
- 2 Increase gravity and place foundation (drained)
- 3 Remove surcharge and drain to correct pore pressure distribution (drained)
- 4 Loading and unloading cycles (undrained)

The Brick model, as implemented in SAFE requires that the soil is consolidated from a slurry so that the  $K_0$  profile is determined by the model from the start (stage 1). The foundation was placed in the same way as for the previous runs, but the remaining surcharge after swelling was left on in an effort to reproduce the subsequent swelling as observed in the consolidation analyses (stage 2). SAFE allows direct specification of pore pressures at any stage in the analysis, and therefore it was possible to drain to the correct pore pressure at the appropriate stage of the test. The remaining surcharge was removed prior to loading, to model the swelling exhibited in the consolidation analysis at this stage of the test (stage 3). Loading and unloading was again displacement controlled. The foundation was loaded so the displacement was the same as that in the centrifuge test, rather than the loads being correct as in the Modified Cam clay and 3-SKH analyses, since for Brick it was impossible to reach these loads for the set of parameters used. All stages of this analysis were drained, except the loading stages which were modelled undrained (stage 4). As time was not a factor for this type of analysis, it was not necessary to model the linearity of the load-time ramps.

### 6.2.3 Results

The results of the finite element analyses are compared with the measured data in this chapter as a measure of the performance of the models. Three main issues are considered; comparison of the load-displacement response, comparison of the settlement profiles, and the underlying soil behaviour.

a) Load-displacement response

Figure 6.6 shows load-displacement cycles for all the different analyses, starting at the load applied by the loading pin.

It can be seen that the results from the Modified Cam clay analysis give a good prediction for the settlement of the foundation at the end of first loading, although up to this point displacement is overestimated, and the load-displacement curve is linear. Swelling on unloading is substantially over-predicted, due to the mostly elastic response. A small amount of hysteresis is evident in the response. On re-loading the load-displacement curve continues primarily elastically and therefore starts to under-predict displacements.

The 3-SKH (consolidation) model qualitatively represents the data well. Response to first loading does not appear to be initially stiff enough and the reduction in equivalent stiffness for the foundation is not rapid enough as loading continues. The swelling behaviour exhibits hysteresis, and compares well with the test data. Upon re-loading the model again under-predicts initial stiffness, with decay of stiffness not sufficiently rapid as loading progresses.

The Brick model again represents the essential characteristics of the data, although it predicts a lower bearing capacity than the other models and this prevented the required loads being reached for each loading stage. It was therefore decided to define the end of a loading stage as the point where the computed settlements were equal to those measured in the centrifuge test instead of using the loads. Whilst showing an initial high stiffness, the Brick model then predicts a decrease in stiffness, and hence load bearing capacity, too rapidly, resulting in a reduced bearing capacity. The unload-reload curve would be expected to exhibit hysteresis, but data were only obtained at the end of the unloading and at the start of reloading so this is not shown in the figure. The Brick model seems to represent the main characteristics of the test results qualitatively, although the predicted bearing capacity is in error by 20-30%.

The drained-undrained 3-SKH analysis was performed to investigate the effects of the assumptions used for the Brick model analysis on load bearing capacity. Loading in this manner produced a slightly higher load capacity for the same settlement than the

consolidation analysis. This is likely to be due to the larger swelling excursion just prior to loading. The load displacement curves for the consolidation and drained-undrained runs of 3-SKH model are compared in Figure 6.7.

Equivalent strains (Atkinson, 2000) can be used to compare the accuracy of predictions for different geotechnical problems. An equivalent strain for the foundation test could be calculated from:

$$\varepsilon_e = \delta/B \quad (6.1)$$

where  $\delta$  is the foundation displacement and  $B$  is the diameter of the foundation. For an equivalent strain of 0.1%, which corresponds to the strains which would be expected around typical geotechnical structures (Mair, 1993), Figure 6.8 the foundation displacement computed from Equation 6.1 is 0.6mm. At a displacement of 0.6mm, the computed loads differ from the measured results by the following percentages; Modified Cam clay - 8%, 3-SKH model - 11%, Brick model - 9%. Model predictions are obviously closer, or further away, at other points in the loading cycle, which highlights the difficulties which can be associated with comparisons at a single reference point. Nevertheless, this provides a useful reference measure of the accuracy of predictions.

#### b) Settlement profiles

It is also interesting to look at the settlement profiles for various stages along the load path. Computed results for Modified Cam clay and the 3-SKH model can be seen in Figures 6.9 to 6.11. Figure 6.9 shows the predicted settlement profiles at a foundation load of 580N during first loading. Figure 6.10 shows predicted settlements at a foundation load of 660N during unloading and Figure 6.11 shows predicted settlement profiles for a foundation load of 660N during re-loading. Modified Cam clay predicts heave at approximately 70mm from the edge of the foundation, as opposed to directly next to the foundation, as seen in the test data, and is also unable to reproduce the form of the test data.

The 3-SKH model predicts heave at a position that is in agreement with the test data. The magnitude of heave for first loading and unloading is under-predicted, but this is not surprising, as the settlement of the foundation is less than for the real data. On re-loading at a load of 660N, where the load displacement curve for 3-SKH is relatively near the test data, the magnitude of heave is better predicted, lying very close to the measured values.

Brick model predictions of the settlement profiles can be seen in Figures 6.12 and 6.13. Comparisons of computed data are made at the end of 1<sup>st</sup> loading (Figure 6.12) and at the end of unloading (Figure 6.13). The Brick model also produces heave at a realistic distance from the foundation, but clearly the magnitudes of movement are inconsistent with the loads applied. At equivalent values of foundation settlement the model over-predicts the maximum heave by between 40% and 60%. This may be due to the difference in drainage conditions near the foundation.

c) Underlying soil behaviour

The large difference between the load-displacement curves for the Brick model and the 3-SKH model can perhaps partly be explained by the  $K_o$  profiles computed by following the recent stress history just prior to loading of the foundation. These can be seen in Figure 6.14. The  $K_o$  profile with depth for the 3-SKH model falls slightly below the prediction of Al Tabbaa (1987), but is higher than the prediction for Mayne and Kulhawy (1982). Brick model predictions of  $K_o$  are lower than the predictions by both Al Tabbaa (1987) and Mayne and Kulhawy (1982). The importance of this is that loading commences from a different position in  $p':q'$  space. The lower  $K_o$  value for the Brick predictions results in loading starting from a higher value of  $q'$ , and a lower value of  $p'$  compared to the 3-SKH model. Thus less load is required to bring the foundation to failure, particularly because in the Brick model failure occurs on a Drucker Prager failure surface and does not have to reach a conventional critical state soil mechanics state boundary surface to achieve failure.

#### 6.2.4 Summary

The Brick and 3-SKH models qualitatively predict the deformation characteristics better than Modified Cam clay where response is linear. Stress paths and values of  $K_0$  are important factors determining the behaviour of the model during the load cycles. All of the model predictions of load displacement response were within 11% of the measured data for an equivalent strain of 0.1%.

### 6.3 TUNNEL PROBLEM

A finite element analysis of a tunnel in reconstituted clay was carried out to identify the accuracy with which ground movements induced by excavation of the tunnel can be predicted when the number of unknown quantities is minimised. The analysis was carried out using the 3-SKH model, as this model was to be used to model the more complex in-situ problems detailed in Chapter 7. As one of the boundary value problems in natural deposits was to be the Heathrow express trial tunnel, this simple tunnel analysis is a useful frame of reference.

The tunnel problem analysed here is one of many tests carried out by Grant (1998) using the centrifuge at City University. Figure 6.15 shows the centrifuge model, which consists of a tunnel excavated in Speswhite kaolin in this case at a depth above tunnel crown of  $3D$  where  $D$  is the diameter of the tunnel. The model was consolidated to a vertical effective stress of 500 kPa in the consolidometer, and then swelled back to  $\sigma'_v = 250$  kPa. The model was then removed from the consolidometer, the tunnel was excavated, and a rubber membrane inserted into the void in order that a support pressure could be applied. The model was then placed on the swing, and re-consolidated to equilibrium conditions at 100g over a period of 17.5 hours. Tunnel support pressure was steadily increased to balance the in-situ stresses up to a final value of 304.4 kPa. Tunnel support pressure was then reduced at a rate of 100 kPa per minute. Movements at ground surface were measured using a series of lvdt's at points along the surface as shown in Figure 6.15.

### 6.3.1 Selection of parameters

The parameters used for the 3-SKH model to analyse the tunnel problem were the same as those used for the foundation analysis for Speswhite kaolin, and are detailed in Section 6.2.1.

### 6.3.2 Analysis procedure

The problem was modelled using the 3-SKH model implemented into a version of CriSP (Britto and Gunn, 1987), in plane strain using consolidation elements. The soil was swelled from a vertical effective stress of 500kPa by removing a surcharge over a long period of time to simulate drained conditions, starting at an assumed normally consolidated  $K_0$  of  $1 - \sin\phi'$ . Some of the surcharge was left on to ensure the soil stayed at a vertical effective stress of 250kPa (stage 1) as in the test. The gravitational field was increased to 100g and the remaining surcharge removed (stage 2). The tunnel elements were removed, and replaced with a support pressure equal to 304.4 kPa acting around the circumference of the excavation (stage 3). The pore pressures were then allowed to dissipate for the time allowed in the test of 17.5 hours (stage 4). Tunnel pressures were then reduced at a rate of 100 kPa per minute (stage 5).

### 6.3.3 Results

Figure 6.16 shows the observed “load-settlement” curves for the centrifuge test alongside the movements predicted by the 3-SKH model during the reduction of tunnel pressure. The “load-settlement” behaviour is characterised by the settlement at ground surface at the centreline of the tunnel as a continuous measure against reduction in tunnel support pressure. The figure shows reasonable agreement between the measured and computed results up to a reduction in tunnel support pressure of approximately 200 kPa. After this point, the results diverge from the finite element analysis predicting ultimate settlements 50% less than those observed. This indicates an overall stiffer response to loading for the latter part of the curve for the computed results. Figure 6.17 shows an enlargement of the load-settlement comparison for the range where the

agreement of the results in magnitude is good. As also seen in the foundation example in Section 6.2, the response of the soil to unloading of the tunnel is initially not stiff enough, with settlement over-predicted by the finite element analysis.

Figure 6.18 shows normalised surface settlement profiles at 20% volume loss for both the measured and predicted results. The predicted trough shows the right profile, but is somewhat wider than the measured data. Grant (1998) found that model predictions of centrifuge tunnels using the 3-SKH model were generally too wide.

In order to compare the accuracy of prediction with the accuracy obtained for the foundation model test equivalent strains (Atkinson, 2000) can again be used. An equivalent strain for the tunnel test could be calculated from:

$$\varepsilon_e = \delta/c \quad (6.2)$$

where  $\delta$  is the settlement at ground surface and  $c$  is the depth of cover. For an equivalent strain of 0.1%, which corresponds to the strains which would be expected around typical geotechnical structures (Mair, 1993), Figure 6.8 the surface settlement computed from Equation 6.1 is 0.15mm. At a displacement of 0.15mm, the tunnel support pressure computed by the 3-SKH model is 10% higher than the measured data.

#### 6.3.4 Summary

As for the foundation problem, the 3-SKH model is able to predict the general pattern of movements and behaviour well. In common with the foundation problem, predicted load settlement response is initially not stiff enough, becoming too stiff as loading progresses. Model predictions for the level of strain which might be expected in the field are within 10% of the test data.

## 6.4 SUMMARY

The 3-SKH model, Modified Cam clay and the Brick model have been used to model the behaviour of a stiff clay for real loading events simulated in the centrifuge. Centrifuge tests and their corresponding data represent the clearest picture possible of the stress changes and associated movements around geotechnical structures. The clay used for the tests was reconstituted and followed a known history, and the parameters used had been carefully evaluated. The 3-SKH model and the Brick model predicted behaviour which qualitatively represented the measured data from the foundation problem, whilst Modified Cam clay was unable to predict the non-linear response. Despite being developed to model the same response, and producing similar patterns of behaviour, the Brick and 3-SKH model predicted rather different magnitudes of movement for parameters derived from the same tests.

The 3-SKH model was able to predict a range of behaviour for the foundation and the tunnel problem. Despite the few unknowns in terms of history and measurements etc. the model was still unable to predict the precise magnitudes of movements. Centrifuge tests are an excellent method of evaluating models, as differences in predicted and measured response are related to fewer uncertainties than for the back-analysis of geotechnical problems in the field. In general, the following comments can be made about the analyses in this chapter:

The  $K_0$  profile computed by the model can have a large effect on subsequent predicted behaviour, and may in part explain the discrepancy between Brick model and 3-SKH model predictions in the case of the foundation.

In order to model the complex non-linear loading paths around geotechnical structures well it is important to have non-linear behaviour within the state boundary surface.

Both the 3-SKH model and the Brick model are able to predict the general pattern of movements around these simple, well-characterised problems, although not as local to the structure as measured. Movements however, are less well predicted, but within an order of magnitude of observations.

For the well controlled and well monitored boundary value problems analysed in this chapter, model predictions of overall “load-displacement” behaviour were within 11% of the measured data at strains representative of movements in the field, for all the soil models.

The analyses carried out in this chapter provide a useful frame of reference for comparing the boundary value analyses on natural clays in Chapter 7.

## CHAPTER 7 ANALYSIS OF BOUNDARY VALUE PROBLEMS IN NATURAL DEPOSITS

### 7.1 INTRODUCTION

The finite element analyses of a single uniform element of stiff clay carried out in Chapter 5, demonstrated the effect of modelling different depositional histories on the subsequent predicted response to shearing, and in a separate investigation, the consequences of including a description of simple volumetric creep within the model. The ability of the model to predict the behaviour of the Oxford clay which has a structure characterised by depositional anisotropy, using a cross-anisotropic version of the 3-SKH model, was also investigated.

Several tests on natural samples of Boom clay (Coop et al. 1995) were modelled using the 3-SKH model with values for the model parameters obtained from reconstituted tests. The stiffness relationship presented by Viggiani and Atkinson (1994) was assumed to apply to both the reconstituted and natural samples as long as the definition of  $R_0$  (a measure of overconsolidation ratio) was calculated from the appropriate normal compression line. The tests on natural samples were modelled in two ways, firstly by assuming that the depositional history consisted of compression along the normal compression line defined by the reconstituted state boundary surface, and secondly by assuming that the behaviour was defined by a natural state boundary surface that was not necessarily followed during deposition, but would define any further compression. The relative positions of the two normal compression lines were represented by sensitivity as defined by Cotecchia (1996). The results of the analyses showed that significant improvements in prediction of the pre-failure stress-strain response were possible where the state boundary surface obtained for the natural clay was used to define the depositional history. Predictions of stiffness were difficult to evaluate, as the measurements taken during the triaxial tests were not of sufficient accuracy at very small strains, but the general pattern was close to the test data.

Volumetric creep was modelled for an element under uniform stress conditions by the inclusion in the model of a simple creep law which allowed the accumulation of plastic volumetric strains at constant stress over time thus changing the size of the bounding

surface at the current state and consequently also the size of the kinematic surfaces. The predictions for shearing paths were found to predict some of the aspects of behaviour that can be attributed to volumetric creep.

The Oxford clay was modelled using a cross-anisotropic version of the model implemented by Jovicic (1997) using a state boundary surface consistent with that observed in tests on natural samples. The predictions of undrained stress paths made using this version of the model were significantly better than predictions made using the standard isotropic formulation. The noticeable effect of assuming cross-anisotropy of small strain stiffness in this case was attributed to the particular behaviour of this clay which is not dominated by recent stress history.

The analyses described within this chapter aim to demonstrate the consequences of applying the concepts developed in Chapter 4 and used for the analysis of uniform elements in Chapter 5 to engineering problems. The first set of analyses will investigate the consequences of using a state boundary surface defined by a natural soil for a tunnel problem and a shallow foundation problem, both with the same depositional histories. The second set of analyses will investigate the effects of allowing periods of volumetric creep within a boundary value problem analysis, in this case a tunnel. The third set of analyses back analyse an excavation in Oxford clay (Pierpoint, 1996) which was chosen as careful monitoring was carried out during its construction. This problem was used to investigate whether improved predictions compared to field measurements can be made using the methods developed.

## 7.2 THE INFLUENCE OF DEPOSITIONAL HISTORY ON BOUNDARY VALUE PROBLEMS

Two simple boundary value problems were modelled to investigate the consequences of assuming a state boundary surface defined by the natural normal compression line to describe the depositional history of the deposit, compared to a state boundary surface defined by the reconstituted normal compression line. For the element predictions carried out in Chapter 5, it was not important when the natural soil structure developed as the recent stress history of the soil sample is defined by the path followed in the triaxial test and not the depositional history of the soil. For the modelling of boundary

value problems where the recent stress history is defined by the depositional and post-depositional history of the soil, the assumption of when the natural structure developed may affect model predictions. The series of analyses therefore additionally investigated the effect of allowing the structure of the natural clay to develop at two different points within the depositional history. The two problems were that of a tunnel, whose dimensions were loosely based on the Heathrow express trial tunnel, and a strip footing.

### 7.2.1 Modelling the geological history and formation of natural structure

The stiff clay strata modelled in the analyses was London clay, overlain by Terrace gravels. The basic geological stress history for both the boundary value problems was as follows.

Deposition of the London clay to a level of overburden 195 metres above the current ground level, followed by the erosion of 200 metres of clay and finally the deposition of 5 metres of Terrace gravels. The water table was assumed to lie at 1.4 metres below current ground surface.

The analyses were carried out using the SSCRISP program modified to allow for the development of natural structure post-deposition in a similar way to the method used to simulate volumetric creep described in Section 4.4. To simulate the geological history, elements representing the London clay were swelled under drained conditions to represent erosion of 200 metres of the clay layer. The parameters used in the model were those derived for London clay by Stallebrass and Viggiani (1994), which can be seen in Table 5.5. The re-deposition of the Terrace Gravels was simulated by building a layer of sand elements modelled using the 3-SKH model with properties similar to those used by Grant (1998) for silica sand (Table 7.1). This is not an accurate model of the behaviour of the gravel layer, however it does ensure that the clay layer is reloaded by a layer of drained soil, which at low stress levels has a non-linear stress-strain response. Grant (1998) found that for centrifuge tests of a tunnel in clay, the presence of a stiffer upper layer, results in settlement profiles in the lower layer that are wider compared to those at the same depth in a single-soil profile. Four separate analyses were carried out for each of the two problems. The geological history was first

modelled with a state boundary surface based on the normal compression line for the reconstituted soil (History A). As noted in Section 4.2.2 this analysis also represents the soil behaviour if it is assumed that the soil is swelled from a normally consolidated state on the natural normal compression line, although the soil state in terms of specific volume is different. The preconsolidation pressures in the soil were defined by the intersection between the Modified Cam Clay state boundary surface and the elastic wall corresponding to the maximum vertical and horizontal stresses applied to the soil during one-dimensional compression. The horizontal stress was calculated by assuming  $K_0 = 1 - \sin\phi'$  (Jaky, 1944). The second analysis assumed that the clay started at the same state, but this time overconsolidated by an amount defined by a sensitivity of 1.5 estimated for the London clay i.e. that the natural clay structure was formed post-deposition (History B). The preconsolidation pressures defined at the start of this analysis were calculated by:

$$p'_{cn} = \exp\left[\frac{(\lambda - \kappa) \ln p'_c + \lambda \ln S_t}{(\lambda - \kappa)}\right] \quad (7.1)$$

where  $p'_c$  is obtained as described above. The third type of geological history investigated was characterised by the development of post-erosion structure which was simulated in a manner similar to that used to model creep and outlined in Section 4.4. After the swelling due to erosion and the deposition of the Terrace gravels, the increase in preconsolidation pressure due to the formation of a natural structure consistent with a given sensitivity, in this case 1.5, was calculated by the program and added so that the bounding surface increased in size. As with the method used to model creep, this had the additional effect of increasing the size of the inner surfaces about their centres. This approach to simulating the development of natural structure reduces the effect of recent stress history without eliminating it entirely. The third method was used to perform two analyses. For the first analysis (History C) a sensitivity,  $S_t$ , of 1.5 was again used to characterise the natural structure, the analysis was then repeated with a sensitivity,  $S_t$ , of 5 (History D) to investigate the effect of varying this parameter. Table 7.2 gives the stress state for each history and Figure 7.1 shows the approximate size and location of the kinematic surfaces of the 3-SKH model prior to the modelling of the geotechnical events for an element of soil at the top of the clay layer. The  $K_0$  profiles after the different depositional histories can be seen in Figure 7.2 which shows that the predicted

values of  $K_0$  are the same for histories A, C, and D but differ for History B. This is as expected, as the analysis using History B is the only one in which the effect of structure is introduced before simulating the stress history of the soil. The soil is therefore swelled from a state, which although at the same stress as for the other histories is overconsolidated by an amount related to a sensitivity,  $St = 1.5$ .

These four histories associated with the formation of natural structure were used to analyse the two boundary value problems which are described in more detail below.

### 7.2.2 Analysis of a tunnel with different geological histories

The geometry and approximate geological history of the Heathrow Express trial tunnel (Deane and Bassett, 1995) were used as the basis for this series of finite element analyses. The geometry used is shown in Figure 7.3 and the soil profile is as defined in Section 7.2.1. The tunnel crown is at a depth of 16 metres and for simplicity, no distinction was made between the three construction methods used for this tunnel. Excavation was simulated undrained by removing the tunnel elements, replacing them with nodal forces, and reducing these forces by 50%. The mesh used for these analyses can be seen in Figure 7.4, which also shows the lateral and vertical fixities. The analyses assumed plane strain conditions and the mesh, which consisted of 448 linear strain triangles, was symmetric about a vertical axis through the centreline of the tunnel. The geological histories were modelled drained, with the tunnel excavation modelled undrained. As noted above, four analyses were carried out, investigating the four different histories. The simulation of the tunnel excavation was the same in all of the analyses.

Results for the analyses can be seen plotted as settlement troughs at the interface between the London clay and the Terrace gravel in Figure 7.5 for a volume loss of 0.5%. Profiles of settlement at the ground surface are not presented but are similar in form and show the same pattern of results. Stallebrass et al. (1996) reporting a series of similar analyses of tunnels, investigating the effects of recent stress history, stated that the main effect of increasing the overburden stress and consequently  $p'_c$  is that the computed settlement trough becomes shallower and wider. For these analyses, this is

not strictly true, as the analysis with History C, where the soil has higher preconsolidation pressures than the analysis with the reconstituted History A, predicts a deeper trough at the same volume loss. The initial  $K_0$  for analyses A and C are the same (Figure 7.2) so the deeper trough must be a consequence of the method of simulating the development of natural structure, which moves the stress state within the yield surface. The analysis with History D where the soil behaviour is characterised by significantly higher preconsolidation pressures than the other analyses does predict a wider shallower trough despite structure having been simulated in the same way as for History C. In this case, the effect of the higher preconsolidation and hence the larger state boundary surface clearly dominates the behaviour, whereas for History C, the effect of recent stress history dominates. The analysis with History B predicts a settlement profile different in form to the others, with the maximum settlement occurring not at the centreline, but at a distance of approximately 1.5 metres away. The soil in the analyses with History B has the same sizes of state boundary surfaces as the soil in the analysis with History C, and similar stress paths to the analysis with History A, which both predict troughs with maximum displacement at the centreline. It seems likely that this is a consequence of both the initial  $K_0$  and the position of the stress point in relation to the location of the kinematic surfaces resulting from a combination of recent stress history and adding the effect of natural structure before erosion. For History B, the position of the current stress point is, compared to the other histories likely to lead to a larger difference between the stiffness response in compression and extension, Figure 7.1.

Figure 7.6 shows the variation of percentage volume loss with reduction in tunnel support pressure which could be considered to be a measure of the overall stiffness of the soil. For 0.5% volume loss for which settlement troughs were plotted in the previous figure, History A required a reduction in tunnel support pressure of 16%, History B 19%, History C 23% and History D 50%. Of particular note is the fact that History C leads to a stiffer overall response than History A, yet predicts a deeper settlement trough for the same volume loss, i.e. this method of simulating the history predicts more localised deformation. History C also leads to a stiffer response than History B which predicts a different form of settlement trough despite having the same state boundary surfaces. The less stiff response of History B is likely to relate to a combination of the difference in initial  $K_0$  and position of kinematic surfaces. The predicted response for the analysis with History D requires a larger reduction in tunnel

support pressure to reach the same volume loss, as the significantly larger state boundary surfaces and hence larger values of  $R_0$  dominate the response creating higher overall stiffnesses. A slightly modified pattern of predicted behaviour can be seen in Figure 7.7 which shows percentage reduction in tunnel support pressure plotted against centreline settlement. The pattern of the data is changed, as History B appears to result in a stiffer response. This result can be explained by the different surface settlement profile predicted following History B, where maximum settlement is not at the centreline but a small distance away.

Changing the history to account for natural structure in these simple ways leads to significant differences in the overall stiffness and distribution of movements for the tunnel problem.

### 7.2.3 Analysis of a foundation with different geological histories

A rigid strip foundation, founded at a depth of 5m below ground level was also modelled using the same depositional histories and ground profile as for the tunnel analyses. The analyses were again modelled in plane strain and the mesh was symmetric about a vertical axis through the centreline of the foundation. The strip footing was loaded undrained by applying equal displacements of 5mm along a 5 metre wide section of the mesh. The displacements were applied to the top of the clay layer and the mesh which contains 447 linear strain triangles can be seen in Figure 7.8 along with the location of the nodes at which the displacement was applied.

Settlement profiles for the four analyses can be seen in Figure 7.9 for the maximum displacement of 5mm applied during the analyses. Histories A, B, and C reproduce the form of settlement profile predicted by Stallebrass and Taylor (1997) in a series of analyses of a similar rigid strip foundation. History D produces a wider trough with more far field movement and is consistent with a stiffer and possibly less non-linear overall response resulting from a combination of the larger state boundary surfaces, and consequently larger kinematic surfaces. The larger surfaces ensure that the clay remains globally stiffer over a larger range of stress. Histories A, B and C produce orientations of the surfaces which are more similar and are affected by the recent stress history in a similar way, producing similar profiles. The analyses with Histories B and

C have the same preconsolidation pressure and size of kinematic surfaces, but History B predicts values of  $K_0$  before loading which are approximately 33% higher than for the other analyses. The effect of recent stress history is slightly reduced in History C, as the current stress point moves within the surfaces as they increase in size due to the simulation of the formation of natural soil structure. For these histories, at the small stress changes modelled, the similar configuration of the surfaces dominates the behaviour producing similar settlement profiles. It is worth noting that the settlement profile for History C is slightly less localised than for History B and this is likely to be a consequence of the current stress point being within the kinematic surfaces at the start of foundation loading producing a slightly stiffer response overall. The similarity in the response of the analyses with Histories B and C can be seen clearly in Figure 7.10 which shows load - settlement curves for the four histories. The load settlement response of the analyses with Histories B and C are almost indistinguishable and displace less for a given load than the results for the analysis with History A. The detail of the initial portion of the load settlement curve shown in Figure 7.11 shows the initial stiffer response of the analysis with History C, consistent with the current stress state being located within the yield surface rather than on its edge as in History B. This is in agreement with the work carried out by Stallebrass and Taylor (1997) who showed that for similar analyses of a rigid strip foundation the recent stress history rather than the initial  $K_0$  had the principal effect on behaviour at small stress changes. The difference in history created by the relatively small changes in initial positions of the surfaces does not have a large overall effect on movements, although some effect is evident from the settlement profiles. The analysis with History D (Figure 7.1) predicts a stiffer load-displacement response than for the other analyses which, in common with the settlement profile predictions is consistent with the higher preconsolidation pressures and hence larger surfaces predicted for this analysis.

#### 7.2.4 Summary

It is clear from the analyses in Chapter 5 that there is a significant effect on predicted response of natural clays if the effect of natural structure is modelled as an increase in sensitivity and hence size of state boundary surface. The analyses in this section show that the modelling of natural structure in this way also has a noticeable effect on computed results for boundary value problems. Increasing sensitivity has a significant

effect on both the magnitude of overall stiffness and the distribution of movements, though this effect is dependant on the type of structure being analysed.

The stage in the history of a deposit at which natural structure is assumed to develop has a subtler effect on predictions of subsequent soil behaviour. Part of this effect is due to differences in the predicted  $K_0$  and part due to the position of the stress state at the start of the loading event with respect to the kinematic surfaces. In the tunnel problem, the  $K_0$  and the position of the stress point relative to the surfaces had a marked effect, whereas for the foundation there was little effect even at large displacements, in contrast to the foundation problem modelled in Chapter 6. Predictions for both problems were significantly affected by the large increase in size of the state boundary surface due to History D, which produced a stiffer response as expected.

### 7.3 THE INFLUENCE OF CREEP ON A BOUNDARY VALUE PROBLEM

To obtain an idea of the influence of modelling creep on a boundary value problem, the geometry and approximate geological history of the Heathrow Express trial tunnel (Deane and Bassett, 1995) were again used as the basis for a finite element analysis. The geometry used is shown in Figure 7.3 and as before consists of five metres of made ground and terrace gravel overlying London clay. The geological history was simulated drained by first swelling the London clay to represent erosion of 200 metres of the clay layer. As for the previous analyses the effect of the re-deposition of the Terrace Gravels was created by building a layer of sand elements modelled using the 3-SKH model with properties similar to those used by Grant (1998) for silica sand. Excavation was again simulated undrained by removing the tunnel elements, replacing them with nodal forces, and reducing these forces by an equal percentage in this case to reach a volume loss of 1.5% at the clay/sand interface. Three finite element analyses were carried out, run 1 simulated the tunnel excavation with no creep, run 2 had a period of creep lasting half a million years, ahead of tunnel construction, and run 3 was the same as run 2 with the addition of one million years creep at the end of erosion of the London clay.

The behaviour predicted by the three different analyses is characterised by the surface settlement profiles in Figure 7.12, settlement profiles at the clay layer follow the same

trend, and have not been presented. These settlement profiles are all for the same volume loss and show a narrowing of the trough and greater maximum settlement as the periods over which creep occurs increase. Nevertheless, the predicted change in trough width is small compared to that which would be required to obtain a Gaussian distribution of vertical settlement, which is usually assumed to represent field displacements (O'Reilly and New, 1982). Normalised surface settlement profiles are presented for comparison in Figure 7.13 and it is clear that the predicted troughs are still somewhat wider than seen in practice.

It is interesting to compare the effect of modelling volumetric creep in this way to the tunnel settlement trough predictions for different geological histories carried out in Section 7.2.1. Changes in predictions for the geological history assumptions were in the range of 6% to 23%, both narrowing and widening the settlement trough respectively. Modelling a long period of creep in this section produced a 6% change in settlement trough centreline displacement causing a narrower normalised trough.

## 7.4 EXCAVATION IN OXFORD CLAY

### 7.4.1 Introduction

This section concerns the detailed analysis of an excavation in Oxford clay situated at Elstow. The excavation has been covered in depth by Pierpoint (1996) and Hird and Pierpoint (1997), and consists of an extensively monitored trial dig which was carried out as part of a site investigation at this location. A diagram of the excavation which is 10 metres deep and 38 metres wide can be seen in Figure 7.14. Also shown in the figure are the monitoring points, which included instrumentation to measure horizontal and vertical movement and pore pressures. Numerical analyses were carried out by Pierpoint (1996) both to examine the sensitivity of predicted movements to parameter selection, and to make a Class A prediction of the ground movements associated with the excavation. The aim of the present analyses is to investigate the effect of assuming different geological histories, consistent with the formation of structure, and structural anisotropy on the prediction of ground movements using the 3-SKH model. The analyses in this section differ from those in Sections 7.2 and 7.3, as real data is available for comparison with predicted results. The Oxford clay is stiffer, more

sensitive, and less influenced by recent stress history (Pierpoint, 1996), than the Boom clay, and work in Chapter 5 concentrated on representing the behaviour of this clay in element tests using the 3-SKH model. The results of the comparisons of model predictions with laboratory element data are described in Section 5.4.

#### 7.4.2 Ground conditions

The geological profile of the site of the trial excavation at Elstow can be seen in Figure 7.14, and consists of a deposit of Oxford clay overlying a series of other soils. For the purposes of the finite element analysis it was assumed, following Pierpoint (1996), that the response of the soil to the excavation would be governed by the behaviour of the Oxford clay deposit. The underlying strata consist of a series of clays and limestones, for which limited material property data was available. For the following finite element analyses, the anisotropic elastic parameters calculated by Pierpoint (1996) are used for these layers. The full set of parameters used for the underlying layers is given in Table 7.3. A set of values for the parameters used in the 3-SKH model were derived in Chapter 5, to describe Oxford clay. From strata profiles the Oxford clay is estimated to have been subjected to a previous overburden of 500 metres (Jackson and Fookes, 1974), and as a consequence is heavily overconsolidated. The clay is therefore stiff to very stiff, and heavily horizontally laminated.

#### 7.4.3 Previous analysis of the Elstow excavation

Pierpoint (1996) carried out an analysis of the Elstow trial excavation using a specially developed model, Model O.C. The model was able to simulate cross anisotropic behaviour with stress path dependant stiffness. A Class A prediction was made using the calculated parameters, as well as a parametric investigation of the predicted response of the excavation. A full set of results are presented in Pierpoint (1996) so only vertical and horizontal movement data will be repeated here. Vertical displacements predicted by model O.C. for both anisotropic (A01) and isotropic (A07) stiffness parameters are shown in Figures 7.15 To 7.20. The predictions were compared with monitoring data at depths of 1.5m, 4.5m, 8m, 11m, 12.5m and 14m below ground

level. A detailed analysis of the model predictions will not be carried out here, but in general, the following statements can be made.

Near to the ground surface the magnitude of settlement in the areas adjacent to the excavation was under-predicted, with the under-prediction becoming less at depth (Figures 7.15 and 7.16).

Heave at the base of the excavation was under-predicted compared to the monitoring data. Predictions were better at the base of the Oxford clay where the influence of the lower strata dominated the movements (Figures 7.16 and 7.17).

The greater horizontal stress changes near to the surface produced the most marked differences between the anisotropic and isotropic analyses, with the results from the two analyses converging at depth (Figure 7.18).

Near to the ground surface (Figure 7.15) the predicted troughs for the isotropic analysis were deeper than for the anisotropic analysis and hence nearer to the monitoring data.

The horizontal displacement predictions for the model were compared with monitoring data along a series of vertical strings and an example comparison can be seen in Figure 7.18. The analysis incorporating cross-anisotropy generally makes a better prediction of the horizontal movement compared to the isotropic analysis. Horizontal movements are, in the main over-predicted by the isotropic analysis, with the results for the anisotropic analysis corresponding close to the upper bound displacements of the monitoring data.

The influence of the value of  $K_0$  at the start of the excavation was investigated. Figures 7.19 and 7.20 show the horizontal and vertical displacement profiles at a variety of positions. The effect of a higher  $K_0$  for these analyses was to increase settlement and increase horizontal movement. The author notes that the effect of changing the value of  $K_0$  was much larger on the horizontal movements, especially along the excavation sides.

#### 7.4.4 Determination of material parameters

A set of material parameters were derived to model the Oxford clay with the 3-SKH model in Section 5.4. Pierpoint (1996) noted that variations in behaviour due to recent stress history were difficult to detect, with strain history possibly being more important. The anisotropy of the heavily layered Oxford clay was thought to dominate the behaviour, so a version of the 3-SKH model incorporating cross-anisotropy of  $G'_{max}$  (Jovicic, 1997) was used along with the standard version of the model. Predictions of element tests made using the anisotropic version of the model better represented the undrained stress paths followed during some of the tests. The values of the model parameters were calculated in a similar way to those for the Boom clay, with the natural behaviour being compared to a reference reconstituted behaviour allowing natural structure to be quantified by sensitivity,  $S_t$ . Values for the full set of parameters for the 3-SKH model are given in table 5.7.

#### 7.4.5 Geometry of the problem

Figure 7.21 shows the mesh used for the finite element analysis of the Elstow excavation. The problem was analysed in plane strain using a total of 1704 linear strain triangular elements. The proportions of the finite element mesh are based on those used by Pierpoint (1996), and no investigation of the effect of the size of the mesh was carried out. The layers used within the mesh were designed to correspond to excavated levels as well as the positions of the instrumentation. The large number of elements used allowed concentrations of elements around the points where stress changes would be at a maximum, although computing time was increased as the paths followed in the analyses required many increments to ensure that the solution was accurate (SSCRISP provides output that enables the precision of the solution to be monitored).

#### 7.4.6 Method of analysis

The excavation was modelled in three stages using the 3-SKH model for four of the analyses, with the fifth analysis requiring an extra stage during the simulation of the

geological history. The first stage of the analysis represented the swelling of the Oxford clay due to the removal of 500 metres of overburden (Jackson and Fookes, 1976). This portion of the analysis was carried out drained over 5500 increments, as the small size of the inner surfaces require small increments of stress to allow them to translate correctly from the high preconsolidation stress. The second stage of the analysis was the building of the head deposits, which was carried out drained over 3000 increments. The third stage of the analysis was the removal of the excavated clay. This stage was carried out undrained in 0.5m layers. The removal of the clay layers took place over a considerable number of increments again to ensure that the model correctly simulated the behaviour of elements undergoing large changes in stress.

The main analysis was carried out in a number of ways to compare predictions from a conventional analysis assuming the clay behaviour is related to a reconstituted normal compression line, to predictions made assuming both that the soil behaves in a manner consistent with a natural normal compression line for the Oxford clay, and that the behaviour is characterised by structural anisotropy. The following analyses were carried out.

- |          |   |
|----------|---|
| Elstow b | Depositional and swelling history consistent with the normal compression line for the reconstituted clay.   |
| Elstow c | Depositional history consistent with the normal compression line for the reconstituted clay and swelling history consistent with the normal compression line for the natural clay (post-depositional formation of natural structure). |
| Elstow e | Depositional and swelling history consistent with the reconstituted normal compression line, with subsequent behaviour related to a natural normal compression line (post erosion formation of structure).                            |
| Elstow a | The same history as for analysis Elstow b, with subsequent cross anisotropic behaviour.   |
| Elstow d | The same history as for analysis Elstow c, with subsequent cross anisotropic behaviour.   |

The five different methods used for the modelling of the Elstow excavation use the same principles as the methods used in the analysis of the two simple boundary value problems in Section 7.2, with the addition of assuming an anisotropic elastic shear

modulus for two of the analyses. Elstow b and Elstow a correspond to history A in Section 7.2, with analyses Elstow c and Elstow d corresponding to history B. Analysis Elstow e has a history created in the same way as for histories C and D. For the analyses where the anisotropic model was used a value of  $\alpha^2 = 2$  was used as in the parametric study in Section 5.4. The elastic shear modulus was assumed to be anisotropic from the onset of the excavation, as this anisotropy was assumed to be caused by the depositional structure resulting from the geological history of deposition and erosion.

In all cases the stage of the analysis recreating the geological history commenced with the erosion of 500m of overburden (Jackson and Fookes, 1976). For the analyses where the behaviour was characterised by the reconstituted normal compression line post deposition Elstow b, Elstow a and Elstow e where structure was assumed to have formed post-erosion the clay was initially considered to be normally consolidated at a  $K_0$  of  $1 - \sin\phi'$  and with a preconsolidation pressure calculated from the intercept of the current elastic wall with the isotropic axis.

The analyses where the behaviour was characterised by the natural normal compression line post-deposition started at the same position in stress space as for the reconstituted analyses but were considered to be at an overconsolidated state. The preconsolidation pressure for these analyses was based on the relative positions of the natural and reconstituted normal compression lines, characterised by sensitivity, and was calculated from,

$$p'_{cn} = \exp\left[\frac{(\lambda - \kappa) \ln p'_c + \lambda \ln S_t}{(\lambda - \kappa)}\right] \quad (7.2)$$

in the manner described in Section 4.2.2. The sensitivity for Oxford clay was calculated as 5.7 (Section 7.2).

Analysis Elstow e was swelled from a preconsolidation pressure calculated from the reconstituted normal compression line. After the swelling stage, i.e. post-erosion the size of the state boundary surface was increased such that the preconsolidation pressure became consistent with the natural normal compression line at a sensitivity of 5.7. The

size of the surface was increased in a similar way to the method described in Section 4.4 which was used to implement the effects of volumetric creep in the 3-SKH model. Instead of the surface increasing with time due to the accumulation of plastic volumetric strains, sensitivity was used in conjunction with Equation 7.2 to determine the size of the surfaces. In the same way as in the creep model, the enlargement of the bounding surface leads to the increase in size of the inner surfaces about their centres, as the three are linked by fixed ratios. The consequence of this increase in size is that the current stress point now lies within the kinematic surfaces and hence the influence of recent stress history is reduced. It was not possible to investigate the anisotropy of elastic shear modulus in association with this method of generating an effect of structure as two different versions of the SSCRISP program are required for these modifications. The 3-SKH model calculates its own value of  $K_0$  during the modelling of the geological history, so no attempt was made to fix the value. Pierpoint (1996) used an average value of  $K_0$  throughout the depth of the mesh equal to 2.25. The value predicted by the 3-SKH model will be discussed with the results of the analysis.

#### 7.4.7 Comparison of results

The results of the analyses of the Elstow excavation are examined in this section in a number of ways.  $K_0$  profiles for the different methods of simulating the geological history are discussed, as are both vertical and horizontal displacements at various sections of the mesh. Figure 7.14 shows a schematic diagram of the area covered by the finite element mesh, with the excavated area highlighted in grey. The vertical dotted lines show the locations of the inclinometers. Data from the inclinometers are used for comparison with the finite element analyses predictions of horizontal displacement. The monitoring strings are located on both sides of the Elstow excavation, so symmetry has been assumed in order to compare measured data with the analysis of the predicted response at various locations as the finite element analysis only modelled one half of the excavation. Vertical displacement data was also available for the Elstow site along the horizons marked as horizontal dotted lines in the figure. Data were only available for the vertical displacement at a limited number of points along these horizons. Nevertheless, these data have been compared to the settlements predicted by the finite element analyses. The simulation of the excavation was carried out undrained and was therefore compared to the measurements taken directly after completion of the

excavation. The monitoring data used for comparison was the data from time I (Pierpoint, 1996) and can be seen along with the full spread of horizontal movements with time for section L in Figure 7.18 to indicate the pattern of further displacement with time recorded.

a) In situ state before excavation

Figure 7.22 shows the  $K_0$  profiles predicted by the model for the analyses swelled from a normally compressed state consistent with the reconstituted state boundary surface for this soil (Elstow a, Elstow b, Elstow e) and those swelled from the same stress state but inside the natural state boundary surface (Elstow c, Elstow d). The predicted values of  $K_0$  are plotted along with a prediction of the  $K_0$  profile made using the relationship proposed by Mayne and Kulhawy (1982) which is given by:

$$K_0 = K_{0nc} \text{OCR}^{(\sin\phi)} \quad (7.3)$$

$K_0$  values for the clay layer predicted for both sets of analyses are much higher than would be expected from the Mayne and Kulhawy (1982) equation, which is more in line with the value of  $K_0$  assumed by Pierpoint (1996) of 2.25, with a maximum  $K_0$  of 10 predicted. A maximum predicted  $K_0$  of 38 for the analyses characterised by the reconstituted normal compression line near the top of the excavation is rather high, with the predicted values more reasonable at greater depth, although still higher than expected. Predictions of  $K_0$  for the analyses where behaviour relates to the larger natural state boundary surface are higher still and somewhat unrealistic. The high values of  $K_0$  predicted by the model for both sets of analyses are controlled by the response of the model to swelling. The values of the model parameters defined for the Oxford clay lead to a one-dimensional unloading curve (Figure 7.23) which is somewhat different to model predictions for other stiff clays, leading to the high  $K_0$  predictions and this is a consequence of the dominant influence of the elastic deformations. As a result of these big differences in computed in situ  $K_0$ , analysis Elstow e will represent the difference in predicted response to excavation caused purely by assuming a natural or a reconstituted state boundary surface. The difference between Elstow e and the other analyses using a natural state boundary surface should be primarily caused by the difference in  $K_0$  as the recent stress history was shown in the

parametric study of stress path tests in Section 5.4 to have little effect on the subsequent stress-strain response for this clay.

b) Overall pattern of displacements

Figure 7.24 shows the displaced profile predicted by the finite element analyses after excavation is complete. Both horizontal and vertical movements are amplified by a factor of 100 to give some idea of the pattern of the predicted displacements. The maximum predicted horizontal movements are for analysis Elstow d and are approximately 55mm. The largest heave at the formation level is 9mm, again predicted by analysis Elstow d. All the model predictions follow the same pattern of movements, which is typical of the undrained behaviour shown as an idealisation by Pierpoint, (1996). Horizontal movements for the analyses using a natural state boundary surface during compression are larger than for the other analyses, in particular Elstow d which was modelled assuming anisotropy of elastic shear modulus. The greater horizontal movements are likely to be caused by the larger change in horizontal stress resulting from the high in-situ  $K_0$  values predicted by the model for the analyses Elstow c and Elstow d. Analysis Elstow e shows the least movement overall, with horizontal movements consistent with the movements predicted by the analyses based on the reconstituted normal compression line. The behaviour of Elstow e is consistent with a key effect of increasing the size of the bounding surface, which is to increase the elastic shear stiffness due to the relationship between stiffness and overconsolidation ratio (elastic deformations dominate the behaviour of Oxford clay - see Section 5.2). Elstow e had predicted  $K_0$  values that were the same as for the reconstituted analyses, and is therefore probably a better comparison of purely the effects of modelling natural structure, without the  $K_0$  complications of Elstow c and Elstow d. Also worthy of note is that analyses Elstow c and Elstow d predict greater movements in the far field than the other analyses with far field vertical displacements exceeding those closer to the excavation edge.

Figures 7.25 to 7.29 show graphs of displacement vectors throughout the mesh for the five analyses. Horizontal displacements near the surface are spread over a large horizontal distance for all the analyses, although less so for the Elstow e analysis. In these plots, analyses Elstow a and Elstow d for which the elastic shear modulus is anisotropic predict patterns of displacements that are similar to the equivalent analyses

with isotropic elastic shear moduli at depth, but with greater horizontal movements at the sides of the excavation. Movements for analyses Elstow c and Elstow d (natural state boundary surface pre-swelling), are deeper seated than for the reconstituted analyses, with larger movements below the excavation base. Movements predicted by analysis Elstow e are smaller than for the other analyses, reflecting the higher stiffness created by this geological history, and the lower  $K_0$  compared to the other analyses using a natural state boundary surface. Figure 7.30 shows displacement vectors for the monitored movements around the excavation. The general pattern of observed movements is comparable with the movements predicted by the analyses, with horizontal movements dominating along the excavation sides, and vertical movements at the base of the excavation and near ground surface away from the excavation. The pattern of the subsurface movements is probably best represented by the natural analyses with post-depositional accumulation of structure Elstow c and Elstow d where the spread of vertical movements is deeper.

c) Vertical displacements at ground surface

Unfortunately, no field data was available for surface settlements but the predicted profiles highlight differences in the computed response of the various analyses. Non-amplified settlement profiles at ground surface are shown in Figure 7.31 and these more clearly show the greater settlement in the far field for analyses Elstow c and Elstow d.

The displacements predicted by the analyses using an anisotropic elastic shear modulus (Elstow a and Elstow d) are similar at the excavation edge despite their different histories, but differ markedly in the form of their profile, with significantly higher far field movements. The same is also true for the two isotropic analyses (Elstow b and Elstow c) although less overall near-excavation displacement is predicted. Assuming an anisotropic elastic shear modulus increases vertical movements but has little effect on the computed surface profile.

The stress anisotropy created by the model which defines  $K_0$  affects the shape of the predicted surface displacement profile, with the higher  $K_0$  computed by the analyses where the behaviour is related to the natural state boundary surface predicting greater far field movement. The three analyses where  $K_0$  was defined by the reconstituted state

boundary surface (Elstow a, Elstow b, and Elstow e) all predict a similar pattern of movement with vertical settlement greatest at the excavation edge. The magnitude of movements predicted by Elstow e are, as expected lowest.

The increased stiffness computed by the analyses where behaviour is related to the natural state boundary surface post deposition (Elstow c and Elstow d) has little effect on movements close to the excavation, but significantly affects predicted far field settlements. The analysis where natural structure was simulated post erosion by increasing the size of the surfaces about their centres (Elstow e) predicted much smaller vertical movements due to the large increase in overall stiffness caused by the current stress point having to traverse the kinematic surfaces for any stress change.

#### d) Vertical settlements below ground surface

The following results are plotted against the monitoring data available from the Elstow site (Pierpoint, 1996) in order to compare measured and computed data. Vertical displacement data in particular is limited, so it is difficult to determine accurately the exact form of the vertical movements. Field displacement data, both horizontal and vertical obtained from the monitoring points are plotted as separate points unconnected by lines. As noted previously data are only plotted for the time immediately after the excavation was completed, as the present analyses were carried out undrained and should therefore reflect the short term movements only. A more complete set of data has been presented by Pierpoint (1996) showing the pattern of displacements with time, confirming that similar patterns of movement occur over time with changing magnitudes. Figure 7.32 shows profiles of vertical displacement for the finite element analyses compared to field data for a depth of 1.5 metres below the ground surface. At this depth, the spread of movements predicted by the analyses is similar to that at ground surface, with greater movements in the far field predicted by analyses Elstow c and Elstow d.

The displacements predicted by the analyses using an anisotropic elastic shear modulus (Elstow a and Elstow d) are again similar at the excavation edge despite their different histories, and again differ in profile, with significantly higher far field movements. The same is again also true for the two isotropic analyses (Elstow b and Elstow c) although less overall near-excavation displacement is predicted. Again, assuming an anisotropic

elastic shear modulus has the effect of increasing vertical movements with little effect on the computed surface profile.

The monitoring data suggests a pattern of behaviour more consistent with the pattern predicted by the lower  $K_0$  analyses (Elstow a, Elstow b, Elstow e) where the spread of movements is less affected than by the higher  $K_0$  predicted by Elstow c and Elstow d. The lack of monitoring points however makes it impossible to be certain about the distribution of movements.

The best prediction of the magnitude and distribution of the monitored movements is made by Elstow a (reconstituted, anisotropic) with Elstow d predicting similar magnitudes. The isotropic analyses (Elstow b and Elstow c) again predict less vertical movement at the excavation edge. Elstow e again predicts a similar distribution of movements to the other analyses with the lower  $K_0$  but under-predicts vertical movements by a significant magnitude.

#### e) Vertical displacements at depth

Figure 7.33 shows predictions of vertical displacements at a depth of 8 metres below the ground surface compared to field data. The model computations predict a much smaller range of magnitude of movements for the different histories. The analyses Elstow c and Elstow d show a similar pattern of behaviour to that shown at shallower depths, with the reconstituted analyses Elstow a and Elstow b showing a different pattern of behaviour with heave at the edge of the excavation. The analyses using a reconstituted state boundary surface before swelling (Elstow a,b) predict less settlement close to the excavation compared to the far field which is a different spread of movements to that at shallower depths. Vertical movements at the edge of the excavation are higher for these analyses along the excavation sides, with the vertical movements for the other analyses probably having been suppressed by the higher horizontal movements - most notably for Elstow d. Analysis Elstow e follows a similar pattern of behaviour to Elstow a and b away from the excavation, but with less movement both in terms of heave near the excavation and settlement further away as a consequence of the stiffer response. Two of the three monitoring points fall within the predictions made by the model and lie closest to analyses Elstow a and b.

The next set of monitoring data is situated at a level just below the formation of the excavation. Monitoring data is available for a point under the centreline of the excavation allowing an assessment of predictions of heave. The measured and predicted vertical displacements are shown in Figure 7.34, for a depth of 11 metres, 1 metre below formation level. Centreline heave is most closely predicted by analysis Elstow c which uses a natural state boundary surface before swelling, with Elstow e predicting the least heave which is in line with the smaller movements predicted by this analysis overall. The general pattern of predicted movements at this horizon seems to represent the limited monitoring data well, with the pattern predicted by the low  $K_0$  analyses appearing to be more convincing.

Figure 7.35 shows the predicted and measured vertical displacements at 14 metres depth, which corresponds to the interface between the Oxford clay and the Kellaways sand. The difference in behaviour at this depth is less marked for the different analyses with all five predicting a deformation profile that is similar in form, although the pattern is more exaggerated for Elstow c and Elstow d indicating the strong effect of the different  $K_0$  even when other changes have little effect. Movements predicted by these analyses are larger, and this is probably due to the wider spread of movements associated with the larger changes in horizontal stress for these two analyses. Heave at the excavation centreline is again under-predicted by all analyses. Movements at this depth are likely to be controlled by the Kellaways sand, the parameters for which are not varied, giving similar movements for all analyses.

#### f) Horizontal displacements

Horizontal movements are compared with monitoring data along vertical sections at discreet distances away from the centreline of the excavation in the positions indicated in Figure 7.14. Figure 7.36 is a plot of horizontal displacement against height for the excavation centreline. The assumption of modelling only half the excavation relies on uniform movements either side of a fixed centreline. The majority of the monitoring points show movements close to the centreline, with the maximum deviation from the line of zero horizontal displacement being in the order of 0.75mm if the top two monitoring points are not taken into account. It is likely that the monitoring points directly under the formation of the excavation may have been disturbed by the excavation process itself and so should not be relied on as accurate. Figure 7.37 shows

the horizontal displacement profiles at section H which is located 4.1 metres from the excavation centreline. Pierpoint (1996) noted that the top two points are likely to have been affected by the excavation process and are not reliable. This seems a reasonable assumption and therefore the good correlation between these points and analyses Elstow a - d is just fortunate, as the horizontal displacements in general are over-predicted. Elstow e is the closest data set to the monitoring data, but still over-predicts movements by approximately a factor of two close to formation level. Data from monitoring sections I, L and M are compared in Figures 7.38 To 7.40 show a similar pattern of horizontal displacements for the finite element predictions with Elstow e again best representing the data, although still around a factor of 2 out. At all the monitoring locations the higher  $K_0$  analyses which used a natural state boundary surface before swelling, predict the greatest horizontal movements, with the analyses with an anisotropic elastic shear modulus predicting larger displacements compared to those where the elastic shear modulus is isotropic. This spread of results was to be expected from examination of the settlement profile (Figure 7.31). In most cases, more movement was predicted within the Kellaways sand and clay layers (14m-20m depth) than was monitored in common with Pierpoint (1996), indicating that model parameters used for this strata did not produce enough resistance to horizontal movement.

#### 7.4.8 Discussion

A set of 3-SKH model parameters have been derived in order to model the trial excavation at Elstow in Oxford clay. The process of identifying values for the model parameters has resulted in values which lead the model predictions to be less affected by recent stress history anisotropy, and more by the depositional anisotropy represented by the anisotropy of elastic shear modulus within the model. Using this combination of parameters along with the state boundary surface defined by tests on natural samples of Oxford clay has enabled reasonable predictions of element tests to be made (Section 5.4). The parameters have been used in conjunction with several methods of simulating the geological history of the clay layer to model the Elstow investigation and to examine the effect of the assumptions on the prediction of ground movements. The assumption that the additional structure exhibited by the natural Oxford clay occurred during deposition (Elstow c and d) produced a profile of in-situ  $K_0$  with very high values of  $K_0$  near the surface compared to the values defined from Mayne and Kulhawy

(1982). These high values of  $K_0$  were reflected in the high lateral movements predicted due to the change in horizontal stress during excavation.

The analyses carried out assuming that the bounding surface was related to the reconstituted normal compression line again predicted values of  $K_0$  higher than might be expected. The horizontal movements computed by these analyses still over-predicted the recorded measurements, although to a lesser degree.

The analysis where the natural soil structure was assumed to form post erosion, Elstow e predicted  $K_0$  values identical to those for the reconstituted analyses, as the deposition and swelling for this analysis was based on the reconstituted normal compression line. The vertical movements for this analysis were less than those for the other analyses indicating that this analysis was behaving in a stiffer manner. Elstow e under-predicted the vertical movements obtained from the monitoring data by a factor of around 2. An over-prediction of horizontal movements by around the same factor was also seen for this analysis with again the response being stiffer than that of the other analyses.

It is difficult to compare the predicted continuous profiles of movement with the monitoring measurements which were at discrete points, but predictions are generally within an order of magnitude of observed movements and for some analyses within 50%. The predicted data seemed to be lacking on two counts. Firstly the pattern of movements was not as localised as for the observed movements pointing to deficiencies in the prediction of mechanisms of movements. Secondly, that the relative accuracy of the predictions in the horizontal and vertical directions was not consistent. Only analysis Elstow e was inaccurate by a similar proportion in both horizontal and vertical directions – but not in the same manner as predictions were too stiff for vertical movements, not stiff enough for horizontal movements. The anisotropy of elastic shear modulus incorporated into the other analyses predicted larger vertical settlements near the surface and larger horizontal movements compared to the equivalent analyses with an isotropic elastic shear modulus, in other words a softer overall response. The single element predictions carried out in Section 5.4.3 also predict a reduction in global stiffness. This was in contrast to Pierpoint (1996) who predicted a stiffer response to excavation for the anisotropic soil model compared to the isotropic soil model. Results from other authors (Addenbrooke et al., 1997, Jovicic, 1997) follow the pattern of the analyses described here in predicting a softer response due to the inclusion of

anisotropy for several boundary value problems. Jovicic (1997) points out that the effect of modelling anisotropy in this way is likely to be history dependant, so the contrast in results may be a subtle effect of the method of modelling. A significantly more detailed analysis of the stress paths followed and the analysis method used by Pierpoint (1996) compared to the method adopted here would be necessary to fully investigate the contrasting predictions.

Had it been possible to combine the versions of the SSCRISP program incorporating an anisotropic elastic shear modulus and the ability for natural structure to develop post-erosion, it is likely that the prediction made using these two assumptions would have been closer to the field data for vertical settlements, but less close for horizontal displacements.

In general, the displacements predicted around the Elstow excavation by the various methods using the 3-SKH model are of the correct order of magnitude and are of similar accuracy to predictions made by Pierpoint (1996) using a cross-anisotropic elastic model despite the very different initial  $K_0$ .

In practice, natural structure in the Oxford clay was likely to have been developed by a variety of processes occurring both during and post deposition affecting both the depositional and stress state anisotropy. In this instance for the Oxford clay which is less affected by the effects of recent stress history the most reasonable analysis could be considered to be Elstow e, as it represents the stiffer behaviour of the natural clay, without the associated effects of the high  $K_0$  predicted by the other natural analyses. The generally high computed values of  $K_0$  are associated with the material parameters identified for the Oxford clay and model predictions of  $K_0$  are generally reasonable for other clays. The need to check the predicted  $K_0$  profile is highlighted here, as the effect of the high values of  $K_0$  predicted by the natural analyses Elstow c and Elstow d is considerable.

The aim of the analyses in this section was to investigate the significance of both allowing for the natural structure of the Oxford clay and also for when that structure was assumed to have formed. It is clear from these analyses that modelling the natural structure of the Oxford clay significantly changes the results compared to analyses assuming that the soil behaves in a manner consistent with the reconstituted clay.

Modelling the increased soil sensitivity affects the magnitude of movements in both the horizontal and vertical planes. It is not clear whether changes in the distribution were primarily caused by the difference in  $K_0$ , but the similarity between the distribution of movements predicted by Elstow e, which was modelled using a state boundary surface consistent with the natural behaviour, to the predictions from analyses assuming a reconstituted state boundary surface, which computed the same  $K_0$  profile, suggest this may be the case.

The stage in the geological history when structure was assumed to have formed also has a significant influence on these predictions. The two different assumptions about when natural structure was formed produced different swelling behaviour leading to different  $K_0$  profiles. This made further comparison of the two assumptions difficult as the different  $K_0$  profiles have a significant effect on the subsequent stress-strain response. When the structure is assumed to form appears to affect the magnitude and distribution of movements (compare Elstow e to Elstow c and Elstow d) but this could be mostly an effect of the different  $K_0$ . It should be noted that a free choice of geological history has been used here to demonstrate the broad effect on predictions. In fact, the in situ state (specific volume, mean effective stress and overconsolidation ratio) will limit the possible geological histories and it may be that the histories leading to the high values of  $K_0$  are unrealistic.

These general findings agree with the analyses carried out in Section 7.2 for two other geotechnical events.

## 7.5 SUMMARY

For element tests the model can be used to make good predictions of the behaviour of stiff clay as accounting for the additional structure of the natural clay in some way, has a real effect on the quality of predictions. For boundary value problems the effects of natural soil structure can be modelled in a relatively simple way and have an effect on predictions that whilst noticeable does not make as significant a difference as in the element tests. This poses several questions, are our methods of testing and hence our soil models missing some aspect of soil behaviour vital to the response of the soils as a

mass? Does the finite element method properly reflect soil behaviour? Are our analyses an over-simplification of the processes involved in the formation of a clay deposit?

Finite element analyses of a foundation and a tunnel modelled in the centrifuge at City University were presented in Chapter 6. These tests were carefully controlled and monitored such that they represent the most complete picture one might be able to have of the formation of a clay deposit and its subsequent response to a geotechnical event. Despite this greater knowledge of the history and processes the clay was subjected to, the finite element prediction was of comparable accuracy to the predictions of the movements around the Elstow excavation. The interaction between soil elements represents a key problem when modelling boundary value problems and is likely to be affected by a combination of the factors highlighted above.

## CHAPTER 8 SUMMARY AND CONCLUSIONS

The overall aim of this work was to improve confidence in predictions of ground movements for field problems. The more specific aim was to devise methods to incorporate features of natural stiff clay behaviour within the 3-SKH model (Stallebrass, 1990), and evaluate the consequences of using these methods for finite element predictions. Aspects of behaviour were investigated which had been found to have significant and wide-ranging effects. Not only were the consequences of the use of these methods investigated by comparison with element test data over a limited number of well defined stress paths, but also the effect on predictions of boundary value problems.

### 8.1 CHARACTERISATION OF STIFF CLAYS FOR MODELLING

The literature review identified features of natural clay behaviour at the macro level which, although not currently accounted for within the formulation of the 3-SKH model, were conceptually possible to incorporate within the current framework. This review concentrated on the behaviour of stiff clays, and recent work that has been predominantly in the UK and Italy.

#### 8.1.1 Natural clay structure

A clay can be thought to exhibit the effects of a natural structure, which is different from its reconstituted structure, when the compression data for the natural clay fall to the right of the compression data for a reconstituted sample of the same clay in volumetric space. The state boundary surface of a clay which has a different natural structure may also be larger than that defined by tests on the reconstituted clay. Sensitivity,  $S_v$ , as defined by Cotecchia (1996) is a useful parameter for describing the difference in structure of a natural clay in compression. Sensitivity can be used as a measure of natural structure in order to normalise shearing data for a natural clay. Several authors have shown that accounting for the difference in structure in compression also accounts for the effect of structure in stress space.

For the purposes of modelling, it is useful to consider two broad components controlling the natural structure, and the manner in which the clay behaves. Natural structure can be split loosely into a stable component caused by the natural clay having a different or enhanced fabric compared to the reconstituted clay, and a meta-stable component caused by bonding of the particles. A stable structure is one that defines a normal compression line parallel to the normal compression line of the reconstituted clay in  $\ln v : \ln p'$  space, whereas a meta-stable structure defines a normal compression line for the natural clay which collapses toward the reconstituted behaviour. In practice natural structure is likely to display both of these types of behaviour simultaneously. Meta-stable clays which exhibit significant destructuration would require the use of a model which predicts this behaviour such as those described by Gens and Nova (1993) and Rouainia and Muir Wood (1998). Clays which have a stable structure fall reasonably well within the current critical state framework as long as the difference in state is accounted for. This work has concentrated on stiff clays where the stable component of structure dominates the response to loading. Hence, the use of a destructuration model is unnecessary. Work by several authors has indicated that it is reasonable to assume that the state boundary surface for the natural clay is similar in shape to that for the reconstituted clay for stiff clays. It is not clear whether the coefficient of friction  $M$  should be the same for both natural and reconstituted samples of the same clay. Tests in which overconsolidated stiff clays are sheared to failure are characterised by the reaching of peak states followed by localisation, which makes the identification of the true critical state difficult.

The very small strain stiffness of a sample can also be related to sensitivity, if the degree of overconsolidation,  $R_0$ , of a natural sample is related to the correct normal compression line. The formula proposed by Viggiani and Atkinson (1995) incorporating  $R_0$  is also valid for natural clays as long as the difference in state is allowed for. Limited data indicate that the formula may become less accurate at high overconsolidation ratios.

### 8.1.2 Anisotropy

Many stiff clays show a response to shearing that is consistent with a form of anisotropy, and this is clearly an important part of their behaviour. Anisotropy can be described using three main groups, structural anisotropy, stress-induced anisotropy and recent stress history anisotropy. Anisotropic behaviour is likely to be a result of a combination of these effects, although the response may be dominated by one of them. Careful testing can isolate each of the three forms of anisotropy in order that their relative importance can be ascertained.

### 8.1.3 Ageing effects

Laboratory tests to characterise ageing effects are likely to be dominated by the effects of creep, as the duration of these tests are insufficient for significant structural bonding to occur (Schmertmann, 1981). Volumetric creep in stiff clays was investigated. Creep rates for stiff clays are likely to be much lower than for soft clays where much work has been carried out. The effects of volumetric creep are to cause a change in volume at a constant stress, which leads to an increase in stiffness and apparent preconsolidation pressure. These features of creep fall conceptually easily within the critical state framework.

## 8.2 METHODOLOGY OF NUMERICAL ANALYSES

The 3-SKH model was to be used as a base to model the behaviour of stiff natural clays. The general methodology was to make modifications to the application of this model to represent features of the observed behaviour, and compare the predictions with predictions using the standard model and laboratory and field data. In particular to check whether the indirect consequences of changes were consistent with the observed response.

The literature review identified three main areas that significantly affect the behaviour of stiff clays. Two of these aspects of behaviour, the effect of a different natural structure and creep could conceptually be modelled by an increase in the size of the

state boundary surface. Analyses were carried out both on element tests and on field problems to investigate the consequences of modelling these effects in this manner.

The 3-SKH model already accounts for stress-induced anisotropy and recent stress history, and has been validated against tests on reconstituted samples. The method proposed by Jovicic (1997) to incorporate cross-anisotropic values of elastic shear modulus within the model was investigated to evaluate any improvement in prediction for a stiff clay where structural anisotropy was thought to dominate response both for element tests and a field problem.

### 8.3 IMPLICATIONS OF RESULTS OF NUMERICAL MODELLING

Numerical analyses were carried out for both element tests and boundary value problems to investigate the three areas of clay behaviour where it had been identified that significant improvements could be made. The purpose of modelling both laboratory element tests and field problems was to investigate not only whether the changes made to the application of the 3-SKH model affected predictions where conditions were well defined and limited, but also when conditions were more complex. For comparison a series of analyses of well-defined centrifuge model tests were also undertaken. In this section the results of the analyses of laboratory tests and boundary value problems will be dealt with together, firstly for the analyses investigating natural structure and anisotropic response, and secondly for the analyses investigating volumetric creep.

#### 8.3.1 Modelling stable structure and anisotropy

This section deals with the analyses carried out to investigate the consequences of modelling natural structure and anisotropy. Stable natural structure was modelled by an increase in the size of the state boundary surface that was consistent with observations. Anisotropy was modelled both explicitly, by assuming anisotropic values of  $G_{\max}$ , and implicitly by the recent stress history predicted by the model.

The 3-SKH model was used to predict the behaviour of Boom clay, a lightly overconsolidated, low sensitivity, stiff marine clay (Coop et al., 1995). The analyses carried out to predict the behaviour of natural samples of Boom clay in triaxial tests highlight the importance of using the correct size of the natural state boundary surface in determining the correct anisotropic response. This leads to an improved prediction of the undrained stress path at both small and large strains. Model predictions carried out using the natural state boundary surface were closer to the laboratory data than those carried out using the state boundary surface defined by the tests on the reconstituted clay particularly at larger strains where the position of the initial state relative to the critical state line is important. The tests on natural samples defined anisotropic stress paths that were distinct from the paths followed in the tests on reconstituted samples particularly at small strains, and this difference was simulated by the model by allowing for the correct stress history which was well defined in the tests. These predictions indicate that much of the anisotropy of the stress paths for the Boom clay was caused by recent stress history and stress state anisotropy, which the standard version of the 3-SKH model is able to simulate. Predictions of initial stiffness were difficult to compare to the laboratory data, as the apparatus used for these tests was unable to measure sufficiently small strains. Stiffness predictions at larger strains were generally improved by allowing for the presence of natural structure by increasing the size of the state boundary surface. In general, predictions made for the tests on natural Boom clay, where the difference in state was allowed for by a change in size of the state boundary surface consistent with sensitivity before the recent stress history was modelled, were of comparable accuracy to the model predictions for the reconstituted Boom clay, where the entire stress history was more clearly defined.

In contrast to laboratory element tests, where the recent stress history of the problem is clearly defined by the paths followed in the test prior to shearing, the recent stress history for a field problem is the geological history, which is less well defined. No data from a field problem in Boom clay data was available, so it was not possible to test whether the improvement in prediction was significant for more complex interactions between load paths. Data for Oxford clay, another stiff clay with a stable structure, were available from both element tests and the field problem of an open excavation so these data could be used to compare any improvements in laboratory test predictions with improvements in the prediction of ground movements for a field problem. For the field problems, it was first necessary to determine the influence of when the natural

structure was assumed to form during the geological history of the deposit, as the intention was to incorporate the formation of additional natural structure as a simple stage in addition to a standard stress history defined by changes in overburden stress.

Analyses described in Section 7.2 were carried out to assess whether modelling natural structure simply by increasing in the size of the state boundary surface for stiff clays with stable structure also produced significant differences in the prediction of movements around two typical field problems. Modelling natural structure in this way produced noticeable effects on the predictions for both a tunnel and a foundation problem with similar histories. In order to model the formation of natural structure during the geological history of the soil in a relatively straightforward way it is necessary to make some assumptions about when the natural structure was formed. A range of scenarios were investigated, and it was found that the choice of when the natural structure formed had consequences for the predictions. The simple histories investigated showed that simulating the development of natural structure for the model had effects on both the predicted  $K_0$  profile and the relative configuration of the kinematic surfaces which control the anisotropic response of the model to further loading.

In order to model the excavation in Oxford clay which was described by Pierpoint (1996) it was necessary to determine 3-SKH model parameters for this clay. An evaluation of a series of triaxial tests carried out on natural samples of Oxford clay by Pierpoint (1996) defined a set of parameters not strongly affected by recent stress history which was in agreement with earlier observations by Pierpoint (1996). The behaviour of the Oxford clay is thought to be strongly affected by structural anisotropy, and the simple inclusion of an anisotropic initial shear stiffness, consistent with observations of stiffness by Pierpoint, allowed the model to predict anisotropic stress paths similar to those observed in undrained triaxial tests and not predicted by the standard version of the 3-SKH model. It is encouraging that the model seems able to distinguish between the relative influence of different forms of anisotropy when it is applied to test results in a consistent way.

Both the standard and anisotropic (Jovicic, 1997) versions of the 3-SKH model were used to model the excavation in Oxford clay. A range of histories incorporating the development of natural structure were employed which were similar to those used for

the analyses of the tunnel and the foundation. The different histories again influenced the profile of predicted  $K_0$  as well as the configuration of the kinematic surfaces.  $K_0$  predictions in general were rather high.

It was not clear from these analyses which scenarios might be the most realistic method of simply incorporating the accumulation of natural structure within model predictions, but it is likely that in practice it will be possible to use in situ measurements of water content, current state and  $K_0$  profile to partially determine when natural structure may have formed for a particular stratum.

Predictions made by analyses that assumed that the soil behaved in a manner consistent with the natural state boundary surface for the soil computed a stiffer overall response, which would have been expected by inspection. The wider effects of doing this were more subtle, with changes to the distributions of movements, but it was not clear what the contributing influence of the difference in predicted  $K_0$  profiles was, and whether this was a true effect.

The effect of assuming anisotropic values of  $G_{\max}$  was to reduce the global stiffness compared to the isotropic analyses, which was in contrast to predictions made by Pierpoint (1996), but in agreement with work by other authors (Addenbrooke et al., 1997, Jovicic, 1997). Incorporating anisotropy in this manner had little effect on the distributions of movements.

In general, 3-SKH model predictions were within an order of magnitude of the field measurements, but were unable to reproduce the more localised mechanisms of movement observed. This was the same as for the centrifuge test analyses in Chapter 6, even though the stress history was well defined in these tests, reducing the range of possible predictions. In practice, the formation of natural structure is likely to be characterised by more complex interactions than the simple assumptions made here, and a more complex assessment of likely scenarios may be required to more accurately fix the point or points in the geological history of the soil when the structure forms.

### 8.3.2 Modelling volumetric creep

Volumetric creep was accounted for in the model by allowing the size of the state boundary surface to increase with the logarithm of time at set periods within the stress history of both element tests and the boundary value problem of a tunnel in stiff clay. This method of including creep within the analyses allowed several of the key features of the response associated with creep to be predicted by the model. For a series of single element simulations of typical triaxial paths, the model predicted an increase in initial tangent shear stiffness where creep was allowed, which is consistent with observations. The model did predict a drop in tangent stiffness at small strains for some tests, but generally an increase in secant stiffness was observed. In agreement with measurements made by Richardson (1998) the model predicts an interaction between volumetric creep and recent stress history that could be considered additive. For the analysis of the tunnel problem, the analyses where creep was allowed to occur produced transverse settlement troughs which were noticeably steeper than those predicted when creep was not modelled at the same volume loss. Whilst an improvement on the predictions made without creep, the troughs were still not as narrow as the Gaussian profiles seen in practice. The modelling of periods of creep for laboratory tests where conditions are again well defined, is likely to be simpler than allowing for this phenomena within boundary value problems. Complex stress paths and processes undergone by natural deposits prior to any geotechnical event make decisions about when to allow for periods of creep at discreet points difficult. Perhaps allowing for ageing phenomena in a more evolutionary way throughout a soils stress history in the manner described by some authors (Yin and Graham, 1989, Burghignoli et al., 1994) may be conceptually easier to use over geological time. It is clear however that modelling creep, even in a simple way can significantly influence predicted ground movements in a manner that is consistent with observations in element tests.

## 8.4 LIMITATIONS OF THE CURRENT RESEARCH AND FURTHER WORK

The method used to incorporate natural structure within the analyses carried out in this work are limited to stable stiff clays only, and may not be appropriate for clays where natural structure degrades significantly. The measure of natural structure may not be as great as in the field, due to the influence of sample disturbance, but will be more

representative than the reconstituted behaviour. Limited histories have been investigated here for the formation of natural structure, when in practice, conditions are likely to be more complicated.

It is clear that modelling the formation of natural structure is a complex process, with a large number of unknowns concerning the geological history. A study such as that carried out by Cotecchia (1996) for Pappadai clay to more precisely define the geological history of a deposit would be a useful method of adding further constraints to a problem with a large number of degrees of freedom.

Model predictions of boundary value problems were, in some cases, strongly affected by predictions of in situ  $K_0$  made by the model for different assumptions. Model predictions of in situ stresses for centrifuge tests where conditions are clearly defined lead to  $K_0$  values which are consistent with predictions by Mayne and Kulhawy (1982) and Al Tabbaa (1988) (Section 6.2). It is however, unclear whether these predictions accurately reflect conditions in the centrifuge, as no measurements have been taken. Model predictions of  $K_0$  are also clearly affected by parameter choice, and this may add a further constraint to parameter choice where values of  $K_0$  can be estimated from in situ testing for a given soil.

The relationship proposed by Viggiani and Atkinson (1995) is clearly a useful method to compute values of initial stiffness for modelling. Atkinson (2000) highlighted the usefulness of this parameter and the relative ease with which it can be measured. It would be helpful to extend the charts presented by Viggiani and Atkinson (1995) to include a number of other measurements of other soils at a variety of states, to increase the confidence with which this method can be applied.

## 8.5 CONCLUSIONS

The main aim of this work was to improve confidence in the prediction of ground movements for field problems by more fully accounting for observed features of natural clay behaviour. This has been carried out by making a series of relatively straightforward changes to the application of the 3-SKH model. The work carried out here has in part helped to improve confidence, but in part highlighted other difficulties

associated with the modelling of natural phenomena. It is clear from the analyses of element tests, that allowing for some of the observed features of the behaviour of natural stiff clays, even in this relatively simple way, can cause a significant improvement in predictions. The stress paths followed in these tests are clearly defined, and this simplifies their analysis. The analyses of element tests indicate that correct simulation of the recent history as well as using the appropriate state boundary surface can be important for predicting the observed response. The stress history of field problems is less clearly defined, making the modelling of the accumulation of natural structure conceptually difficult. It is difficult to closely monitor the effects of the methods of incorporating natural structure, as sufficiently detailed field measurements are scarce. It is also difficult to assess the effects of modelling anisotropy and volumetric creep for field problems for the same reasons. In order to improve confidence in the response of the analysis of field problems, it may be necessary to more clearly define their geological history in the manner attempted by Cotecchia (1996).

The modelling of the natural structure, seen as a real effect in laboratory tests is clearly important for model predictions. For element tests natural structure must be accounted for in order to be able to model the shear/volumetric response observed in undrained stress paths. For boundary value problems, allowing for natural structure in similar ways has a noticeable influence on predictions, however, the recent stress history is less clearly defined as it incorporates the geological history which makes the choices more complex. It seems that studying evidence for the accumulation of natural structure rather than just its degradation would be useful if further improvement to predictions of ground movements when modelling boundary value problems are required.

# APPENDIX

## A.1 STANDARD VERSION OF SSCRISP SUBROUTINE VARTRI

```
1  SUBROUTINE VARTRI(IP,MR,KM,ICS,INGP,JEL,NIP,NEL,NPMT,NVRS,NS,NPR,
2    1 NMT,IEL,NCODE,VARC,PR,VARINT,VARPMT,NTY,P,DEVIA,XP,XDEV,DP,SDEV,
3    2 PO,AVECT,HMOD,SS,ED,LED,DEV,SSE,DPE,SDEVE)
4  C
5  C.... subroutine to determine position of stress point relative to
6  C.... surfaces and translate surfaces if necessary
7  C
8  IMPLICIT DOUBLE PRECISION (A-H,O-Z)
9  DOUBLE PRECISION VARC,PR,VARPMT,ED,SS,VARINT,QA,DEV,RP,RH,RY,XPPO
10 DOUBLE PRECISION P,DEVIA,XP,XDEV,DP,SDEV,PO,AVECT,HMOD,PB,BDEV
11 DOUBLE PRECISION RKPPA,RLMDA,RMU,TVALU,SVALU,GAMMA,BK,XPHO
12 DOUBLE PRECISION PPO,PHO,PYO,RMCON,UNLOAD,CONS,DPO,DEVP,WARN,XPYO
13 DOUBLE PRECISION GRADA,MGRADA,MSIG,DEPSE,CE,DEVE,SSE,DPE,SDEVE
14 C
15 DIMENSION NCODE(NIP,NEL),VARC(10,NIP,NEL),PR(NPR,NMT),
16 1 VARINT(NVRS,NIP,NEL),CE(6,6),DEPSE(6),GRADA(6)
17 DIMENSION VARPMT(NPMT,NIP,NEL),NTY(NMT),ED(LED),SS(NS),SSE(NS)
18 DIMENSION DEVIA(NS),XDEV(NS),SDEV(NS),AVECT(NS),BDEV(6),SDEVE(NS)
19 C
20 C.... material properties
21 C
22 RKPPA=PR(2,KM)
23 c SHEAR=PR(1,KM)
24 RLMDA=PR(4,KM)
25 RMU=PR(3,KM)
26 TVALU=PR(11,KM)
27 SVALU=PR(12,KM)
28 GAMMA=PR(5,KM)
29 RMCON=1.5D0/(RMU*RMU)
30 C
31 IST=NCODE(IP,JEL)
32 C
33 C.... yield surfaces through current and old stress point
34 C
35 CALL CURYLD(IP,JEL,NS,NPMT,NIP,NEL,VARPMT,P,PO,DEVIA,RMU,PPO,PHO
36 1 ,PYO)
37 CALL CURYLD(IP,JEL,NS,NPMT,NIP,NEL,VARPMT,XP,PO,XDEV,RMU,XPPO,XPHO
38 1 ,XPYO)
39 C
40 C.... calculate limits for collecting surfaces
41 C
42 DS=PYO-XPYO
43 RY=(1.0D0-(DS/(SVALU*TVALU*PO)))
44 C
45 DS=PHO-XPHO
46 RH=(1.0D0-(DS/(TVALU*PO)))
47 C
48 DS=PPO-XPPO
49 RP=(1.0D0-(DS/PO))
50 C
51 C.... still elastic
52 C
53 IF(IST.NE.0) GOTO 20
54 IF(PYO.GE.RY*PO*TVALU*SVALU) THEN
55   IST=1
56   CALL ADJUST(1,IP,JEL,NIP,NEL,NS,NPMT,VARPMT,PO,P,DEVIA,PHO,PYO,
57 1 TVALU,SVALU)
58 ELSE IF(PHO.GE.RH*PO*TVALU) THEN
59   IST=2
60   CALL ADJUST(3,IP,JEL,NIP,NEL,NS,NPMT,VARPMT,PO,P,DEVIA,PHO,PYO,
61 1 TVALU,SVALU)
62 ELSE IF(PPO.GE.RP*PO) THEN
63   IST=3
64   CALL ADJUST(3,IP,JEL,NIP,NEL,NS,NPMT,VARPMT,PO,P,DEVIA,PHO,PYO,
65 1 TVALU,SVALU)
66 ELSE
67   GOTO 10
68 END IF
69 10 GOTO 100
70 C
71 C.... was element unloaded? - If yes don't translate
72 C
```

```

73      20 PB=VARPMT(6,IP,JEL)
74      DO 21 JJ=1,4
75      BDEV(JJ)=VARPMT(6+JJ,IP,JEL)
76      21 CONTINUE
77      C
78      IF(NS.EQ.4) GOTO 22
79      BDEV(5)=VARPMT(13,IP,JEL)
80      BDEV(6)=VARPMT(14,IP,JEL)
81      C
82      22 DO 23 JJ=1,NS
83      23 GRADA(JJ)=RMCON*(XDEV(JJ)-BDEV(JJ))
84      C
85      DO 24 JJ=1,3
86      24 GRADA(JJ)=GRADA(JJ)+((XP-PB)/3.0D0)
87      GRADA(4)=2*GRADA(4)
88      IF(NS.EQ.4) GOTO 25
89      GRADA(5)=2*GRADA(5)
90      GRADA(6)=2*GRADA(6)
91      C
92      25 MGRADA=0.0D0
93      DO 26 JJ=1,NS
94      26 MGRADA=MGRADA+(GRADA(JJ)**2)
95      MGRADA=SQRT(MGRADA)
96      C
97      MSIG=(SS(1)**2)+(SS(2)**2)+(SS(3)**2)+2*(SS(4)**2)
98      IF(NS.EQ.4) GOTO 27
99      MSIG=MSIG+2*(SS(5)**2)+2*(SS(6)**2)
100     27 MSIG=SQRT(MSIG)
101     C
102     UNLOAD=(DPE*(XP-PB))+RMCON*((SDEVE(1)*(XDEV(1)-BDEV(1)))
103     1 +(SDEVE(2)*(XDEV(2)-BDEV(2)))+(SDEVE(3)*(XDEV(3)-BDEV(3)))+
104     2 4.0D0*(SDEVE(4)*(XDEV(4)-BDEV(4))))
105     IF(NS.EQ.4) GOTO 28
106     C
107     UNLOAD=UNLOAD+RMCON*4.0D0*((SDEVE(5)*(XDEV(5)-BDEV(5)))+(SDEVE(6)*
108     1 (XDEV(6)-BDEV(6))))
109     C
110     28 UNLOAD=UNLOAD/(MSIG*MGRADA)
111     28 IF(UNLOAD.GT.-0.001) GOTO 29
112     IST=0
113     CC PRINT*, 'UNLOADED'
114     GOTO 100
115     C
116     C.... if not elastic, calculate DPO from DEVP
117     C
118     29 CONS=0.0D0
119     DO 30 JJ=1,NS
120     CONS=CONS+AVECT(JJ)*SS(JJ)
121     30 CONTINUE
122     DEVP=(CONS/HMOD)*(AVECT(1)+AVECT(2)+AVECT(3))
123     DPO=PO*DEVP/(RLMDA-RKPPA)
124     CC 28 BK=XP/RKPPA
125     CC CALL CEL(CE,NS,BK,SHEAR)
126     CC DO 30 II=1,NS
127     CC DEPSE(II)=0.0D0
128     CC DO 29 JJ=1,NS
129     CC DEPSE(II)=DEPSE(II)+CE(II,JJ)*SS(JJ)
130     CC 29 CONTINUE
131     CC 30 CONTINUE
132     CC DEVE=DEPSE(1)+DEPSE(2)+DEPSE(3)
133     CC DEVP=DEV-DEVE
134     CC DPO=PO*DEVP/(RLMDA-RKPPA)
135     C
136     C.... translate when on yield surface
137     C
138     IF(IST.NE.1) GOTO 40
139     CALL TRANSL(IST,IP,JEL,NS,NIP,NEL,NPMT,VARPMT,XP,XDEV,DP,SDEV,PO,
140     1 DPO,RMU,TVALU,SVALU)
141     CALL CRYLD(IP,JEL,NS,NPMT,NIP,NEL,VARPMT,P,PO,DEVIA,RMU,PPO,PHO
142     1 ,PYO)
143     IF(PHO.GE.RH*PO*TVALU) THEN
144         IST=2
145         CALL ADJUST(3,IP,JEL,NIP,NEL,NS,NPMT,VARPMT,PO,P,DEVIA,PHO,PYO,
146     1 TVALU,SVALU)
147     ELSE IF(PPO.GE.RP*PO) THEN
148         IST=3
149         CALL ADJUST(3,IP,JEL,NIP,NEL,NS,NPMT,VARPMT,PO,P,DEVIA,PHO,PYO,
150     1 TVALU,SVALU)
151     ELSE

```

```

152          GOTO 32
153      END IF
154      32 GOTO 100
155      C
156      C.... translate when on history surface
157      C
158      40 IF(IST.NE.2) GOTO 50
159          CALL TRANSL(IST,IP,JEL,NS,NIP,NEL,NPMT,VARPMT,XP,XDEV,DP,SDEV,PO,
160      1 DPO,RMU,TVALU,SVALU)
161          CALL CURLD(IP,JEL,NS,NPMT,NIP,NEL,VARPMT,P,PO,DEVIA,RMU,PPO,PHO
162      1 ,PYO)
163          IF(PPO.GE.RP*PO) IST=3
164          GOTO 100
165      C
166      C.... translate when on bounding surface
167      C
168      50 CALL TRANSL(IST,IP,JEL,NS,NIP,NEL,NPMT,VARPMT,XP,XDEV,DP,SDEV,PO,
169      1 DPO,RMU,TVALU,SVALU)
170      C
171      C.... calculate 'cam clay' parameters and check for warnings
172      C
173      100 CONTINUE
174          QT=QA(VARINT(1,IP,JEL),P,NS)
175          PC=2.0D0*PO
176          WARN=QT/P
177          IF(WARN.LT.0.95D0*RMU) WARN=0.0D0
178          WARN=(WARN-RMU)/RMU
179          IF(ABS(WARN).LT.0.05D0.AND.IST.EQ.3) ICS=1
180      C
181          IF(P.GT.0.0D0) GOTO 110
182          INGP=1
183          GOTO 120
184      110 EE=(GAMMA*(PO**(RKPPA-RLMDA)))/(P**RKPPA))-1.0D0
185      120 CONTINUE
186      C
187          VARC(1,IP,IEL)=P
188          VARC(2,IP,IEL)=QT
189          VARC(4,IP,IEL)=PC
190          VARC(5,IP,IEL)=QT/P
191          VARC(6,IP,IEL)=QT/(P*RMU)
192          VARC(7,IP,IEL)=PO/(PO-DPO)
193          VARC(8,IP,IEL)=EE
194          NCODE(IP,JEL)=IST
195      C
196          RETURN
197      END

```

## A.2 VERSION OF VARTRI INCORPORATING VOLUMETRIC CREEP (NEW LINE NO.S INDICATED)

```

3      2 PO,AVECT,HMOD,SS,ED,LED,DEV,SSE,DPE,SDEVE,ctime,icreep)
50      C
50a     C.... Creep occurs...
50b     C
50c     IF(icreep.EQ.0) GOTO 9
50d     C
50e     spv=(GAMMA*(PO**(RKPPA-RLMDA)))/(P**RKPPA))
50f     dvol=calpha*LOG(ctime)
50g     DEVP=(dvol/spv)
50h     DEVPN=-LOG(1-DEV)
50i     C
50j     C.... incremental approach, looping until p'o is within 1kPa
50k     C
50l     N=1
50m     POI=PO
50n     POL=0
50o     DO 6 I=1,10
50p     DO 4 J=1,N
50q     DPO=((POI*(DEVPN/N))/(RLMDA-RKPPA))
50r     POI=POI+DPO
50s     4 CONTINUE
50t     IF(POL.GE.(POI-1)) GOTO 8
50u     N=N*10
50v     POL=POI
50w     POI=PO

```

```

50x      6 CONTINUE
50y      C
50z      8 PO=POI
50aa     C
50ab     IST=0
50ac     GOTO 100
53       9 IF(IST.NE.0) GOTO 20

```

### A.3 VERSION OF VARTRI INCORPORATING INCREASE OF NATURAL STRUCTURE CONTROLLED BY SENSITIVITY (NEW LINE NO.S INDICATED)

```

3        2 PO,AVECT,HMOD,SS,ED,LED,DEV,SSE,DPE,SDEVE,isens)
50a     C.... sensitivity applied...
50b     C
50c     IF(isens.EQ.0) GOTO 9
50d     C
50e     pco=2.0d0*po
50f     pc=exp((((r1mda-rkppa)*log(pco))+ (r1mda*(log(sens))))
50g     1 /(r1mda-rkppa))
50h     po=pc/2.0d0
50i     C
50j     IST=0
50k     GOTO 100
53      9 IF(IST.NE.0) GOTO 20

```

Test	Test type	$v_i$	$p'$ (kPa)	$p'_c$ (kPa)	$p'_{cn}$ (kPa)
Boom l	UE ISO OC	1.625	2228	3342	5276
Boom n	UC ISO OC	1.704	1118	2081	3286
Boom o	UC ISO OC	1.667	2247	2549	4025
Boom q	UC ISO OC	1.701	2234	2058	3250

UE Undrained extension test  
 UC Undrained compression test  
 ISO Shearing commences from isotropic state  
 OC Shearing commences from overconsolidated state

Table 5.1 Table of initial states and calculated preconsolidation pressures for tests carried out on natural samples of Boom clay based on both the reconstituted and natural normal compression lines

Test	Test type	$v_i$	$p'$ (kPa)	$p'_c$ (kPa)
Boom 1	UC ISO NC	2.01	397.6	397.6
Boom 10	DRC $K_0$ OC	2.07	166.2	339.4
Boom 11	DRC $K_0$ OC	2.08	161.3	325.1
Boom mrc	UC ISO OC	1.98	205.0	447.5
Ruth	UC ISO OC	2.04	105	320.7

DRE Drained extension test  
 DRC Drained compression test  
 UE Undrained extension test  
 UC Undrained compression test  
 ISO Shearing commences from isotropic state  
 OC Shearing commences from overconsolidated state  
 $K_0$  Shearing commences from a  $K_0$  consolidated state

Table 5.2 Table of initial states and calculated preconsolidation pressures for tests carried out on reconstituted Boom clay

$\lambda$	N	$\kappa$	A	n	m	M	$\phi$	T	S
0.0984	3.605	0.004	180	0.97	0.2	1.03	1.6	0.2	0.04

Table 5.3 Summary of Boom clay parameters for the 3-SKH model

test	$\lambda$	N	$\kappa$	A	n	m	M	$\phi$	T	S
bcp1	0.0984	3.605	0.004	180	0.97	0.2	1.03	2.5	0.4	0.08
bcp2	0.0984	3.605	0.004	180	0.97	0.2	1.03	2.2	0.4	0.08
bcp3	0.0984	3.605	0.004	180	0.97	0.2	1.03	2	0.4	0.08
bcp4	0.0984	3.605	0.004	180	0.97	0.2	1.03	1.8	0.4	0.08
bcp5	0.0984	3.605	0.004	180	0.97	0.2	1.03	1.6	0.4	0.08
bcp6	0.0984	3.605	0.004	180	0.97	0.2	1.03	2.5	0.2	0.08
bcp7	0.0984	3.605	0.004	180	0.97	0.2	1.03	2.2	0.2	0.08
bcp8	0.0984	3.605	0.004	180	0.97	0.2	1.03	2	0.2	0.08
bcp9	0.0984	3.605	0.004	180	0.97	0.2	1.03	1.8	0.2	0.08
bcp10	0.0984	3.605	0.004	180	0.97	0.2	1.03	1.6	0.2	0.08
bcp11	0.0984	3.605	0.004	180	0.97	0.2	1.03	2.5	0.4	0.04
bcp12	0.0984	3.605	0.004	180	0.97	0.2	1.03	2.2	0.4	0.04
bcp13	0.0984	3.605	0.004	180	0.97	0.2	1.03	2	0.4	0.04
bcp14	0.0984	3.605	0.004	180	0.97	0.2	1.03	1.8	0.4	0.04
bcp15	0.0984	3.605	0.004	180	0.97	0.2	1.03	1.6	0.4	0.04
bcp16	0.0984	3.605	0.004	180	0.97	0.2	1.03	2.5	0.2	0.04
bcp17	0.0984	3.605	0.004	180	0.97	0.2	1.03	2.2	0.2	0.04
bcp18	0.0984	3.605	0.004	180	0.97	0.2	1.03	2	0.2	0.04
bcp19	0.0984	3.605	0.004	180	0.97	0.2	1.03	1.8	0.2	0.04
bcp20	0.0984	3.605	0.004	180	0.97	0.2	1.03	1.6	0.2	0.04

Table 5.4 Summary of parameters used for the parametric study to determine the parameters defining the behaviour of the kinematic surfaces in the 3-SKH model for Boom clay

$\lambda$	N	$\kappa$	A	n	m	M	$\phi$	T	S
0.097	3.557	0.006	407	0.76	0.25	1	2.5	0.2	0.08

Table 5.5 3-SKH model parameters for London clay (Stallebrass and Viggiani, 1994)

test	$\lambda$	N	$\kappa$	A	n	m	M	$\phi$	T	S
P1	0.1265	3.962	0.0033	980	0.67	0.235	0.88	3.0	0.06	0.08
P2	0.1265	3.962	0.0033	980	0.67	0.235	0.88	3.0	0.06	0.05
P3	0.1265	3.962	0.0033	980	0.67	0.235	0.88	3.0	0.03	0.05
P4	0.1265	3.962	0.0033	980	0.67	0.235	0.88	2.5	0.03	0.05

Table 5.6 Variations used for the parametric study to determine T, S and  $\phi$  for Oxford clay

$\lambda$	N	$\kappa$	A	n	m	M	$\phi$	T	S
0.1265	3.962	0.0033	980	0.67	0.235	0.88	3.0	0.03	0.05

Table 5.7 3-SKH model parameters for Oxford clay

M	$\lambda$	$e_{cs}$	$\kappa$	$\nu$	$k_v$	$k_h$
0.89	0.18	1.97	0.035	0.3	$0.47 \times 10^{-6}$	$1.37 \times 10^{-6}$

Table 6.1 Modified Cam Clay Parameters for Speswhite kaolin (Morrison 1994)

M	$\lambda^*$	$e_{cs}$	$\kappa^*$	$G_{ec}$	T	S	$\psi$	$k_v$	$k_h$
0.89	0.073	1.994	0.005	60000	0.25	0.08	2.5	$0.47 \times 10^{-6}$	$1.37 \times 10^{-6}$

Table 6.2 3-SKH model parameters for Speswhite kaolin (Stallebrass 1990) (Viggiani 1992)

$\lambda^*$	$\kappa^*$	$l$	$\nu$	$\mu$	$\beta\gamma$	$\beta\phi$
0.073	0.02	0.0032	0.2	1.3	4	2

Table 6.3 Brick model parameters for Speswhite kaolin (Ingram, 2000)

No.	Length	$G/G_{max}$
1	0.00008	0.80882
2	0.00010	0.61765
3	0.00015	0.48529
4	0.00020	0.36765
5	0.00030	0.22059
6	0.00050	0.11765
7	0.00100	0.07353
8	0.00300	0.04412
9	0.00700	0.01765
10	0.08000	0.00000

Table 6.4 Brick model stepwise curve string data for Speswhite kaolin (Ingram, 2000)

$\lambda$	N	$\kappa$	A	n	m	M	$\phi$	T	S
0.06	3.17	0.000375	6000	0.63	0.0	1.42	9.0	0.001	0.2

Table 7.1 3-SKH model parameters for Silica sand (after Grant, 1998)

	$p'$	q	$K_0$	$p'_c$
History A	159.2	-134.7	2.9	764.9
History B	211.0	-212.2	4.1	1176.3
History C	159.2	-134.7	2.9	1178.5
History D	159.2	-134.7	2.9	4252.8

Table 7.2 Stress states prior to geotechnical event for various geological histories defining natural soil structure

Strata	$E'_h$ MPa	$E'_v$ MPa	$\nu'_{hh}$	$\nu'_{vh}$	$G'_{hv}$ MPa	$\gamma$ kN/m <sup>3</sup>
Kellaways sand	620	207	0.25	0.14	143	19.5
Kellaways clay	613	204	0.25	0.14	142	19.5
Cornbrash	7768	2589	0.25	0.14	1794	19.5
Blisworth limestone/clay	1503	501	0.25	0.14	347	19.5

Table 7.3 Parameters used for the soil strata underlying the excavation in Oxford clay

## REFERENCES

- Addenbrooke T.I., Potts D.M. and Puzrin A.M. (1997) The influence of pre-failure soil stiffness on the numerical analysis of tunnel construction. *Geotechnique*. Vol 47, No.3, pp. 693-712
- Agah S. (1996) The measurement of soil stiffness using bender elements. Final year undergraduate project report. City University
- Al Tabbaa A. (1987) Permeability and stress-strain response of speswhite kaolin. PhD Thesis, University of Cambridge
- Al Tabbaa A. and Wood D.M. (1989) An experimentally based 'bubble' model for clay. *Proc. Third Int. Conf. On Numerical Methods in Geomechanics*, pp. 91-99
- Amorosi A. (1996) Il comportamento meccanico di una argilla naturale consistente. PhD thesis, University of Rome 'La Sapienza'.
- Amorosi A. and Rampello S. (1998) The influence of natural soil structure on the mechanical behaviour of a stiff clay. *The Geotechnics of hard soils - soft rocks*, Evangelista and Picarelli. (eds). Balkema, Rotterdam. pp. 395-402
- Atkinson J.H. (1973) The deformation of undisturbed London clay. PhD thesis, University of London
- Atkinson (2000) Non-linear soil stiffness in routine design, 40<sup>th</sup> Rankine lecture. In preparation.
- Atkinson J. and Richardson D. (1987) The effect of local drainage in shear zones on the undrained strength of overconsolidated clay. *Geotechnique* Vol 37, No. 3. pp. 393-403
- Atkinson J.H and Cherill H.E. (1988) Normal consolidation and ultimate strength of clay soils at medium stress levels. research report GE/88/28, City University
- Atkinson J.H., Richardson D. and Stallebrass S.E. (1990) Effect of recent stress history on the stiffness of overconsolidated soil. *Geotechnique*. Vol. 40, No. 4, pp. 531-540

- Atkinson J.H. and Salfors G. (1991) Experimental determination of stress-strain-time characteristics in laboratory and in situ tests. Proc. 10<sup>th</sup> Eur. Conf. on Soil Mech. and Found. Eng. Florence. Vol. 3, pp. 915-956
- Banerjee P.K. and Yousif N.B. (1986) A plasticity model for the mechanical behaviour of anisotropically consolidated clay. International Journal for Numerical and Analytical methods in Geomechanics, Vol. 10, pp. 521-541
- Bishop A.W. (1966) Sixth Rankine lecture: The strength of soils as engineering materials. Geotechnique. Vol 16, No.2, pp. 91-130
- Bjerrum L. (1967) Engineering geology of Norwegian normally consolidated marine clays as related to the settlement of buildings. Geotechnique. Vol 17, No.2, pp. 83-118
- Borja R.I. and Kavazanjian Jr, E. (1985) A constitutive model for the stress-strain-time behaviour of 'wet clays'. Geotechnique. Vol 35, No.3, pp. 283-298
- Britto A.N. and Gunn M.J. (1987) Critical state soil mechanics via finite elements. Ellis Horwood
- Burghignoli A. et al (1994) Modelling stress-strain-time behaviour of natural soils. Rivista Italiana di geotechnica 4. pp. 267-283
- Burland J.B. (1990) On the compressibility and shear strength of natural clays. Geotechnique. Vol. 40, No. 3, pp. 329-378
- Burland J.B. Rampello S. Georgiannou V.N. and Calabresi G. (1996) A laboratory study of the strength of four stiff clays. Geotechnique. Vol. 46, No. 3, pp. 491-514
- Butterfield R. (1979) A natural compression law for soils. Geotechnique. Vol. 29, No. 4, pp. 469-480
- Chazallon C. and Hicher P. Y. (1995) An elastoplastic model with damage for bonded geomaterials. Numerical models in Geomechanics. NUMOG V, Rotterdam
- Coop M.R. and Cotecchia F. (1995) The compression of sediments at the archaeological site of Siberi. Proc. XI ECSMFE. Copenhagen, Vol 8, pp. 19-27
- Coop M.R. Atkinson J.H. and Taylor R.N. (1995) Strength and stiffness of structured and unstructured soils. Proc. ECSMFE. Vol1, pp. 55-62

- Cotecchia F. (1996) The effects of structure on the properties of an Italian pleistocene clay. PhD Thesis, University of London
- Cotecchia F. and Chandler R.J. (1997) The influence of structure on the pre-failure behaviour of a natural clay. *Geotechnique*. Vol 47, No.3, pp. 523-544
- Cotecchia F. and Chandler R. (1998) One-dimensional compression of a natural clay: Structural changes and mechanical effects. *The Geotechnics of hard soils - soft rocks*, Evangelista and Picarelli. (eds). Balkema, Rotterdam. pp. 103-114
- D'Onfario A. et al (1998) Influence of soil structure on the behaviour of two natural stiff clays in the pre-failure range. *The Geotechnics of hard soils - soft rocks*, Evangelista and Picarelli. (eds). Balkema, Rotterdam. pp. 497-505
- Davies M. C. R. and Newson T. A. (1993) A critical state constitutive model for anisotropic soil. *Predictive soil mechanics* (Eds G. T. Houlsby and A. N. Schofield), pp. 219-229. London: Thomas Telford
- Deane and Basset (1995) The Heathrow express trial tunnel. *Proc. Instn. Civ. Engrs. Geotechnical Engineering*, 113, pp. 114-156
- Fearon R. (1998) The behaviour of a structurally complex clay from an Italian landslide. PhD thesis. City University
- Gens A. and Nova R. (1993) Conceptual bases for a constitutive model for bonded soil and weak rocks. *Proc. Conf. on Hard soils Soft rocks*, Athens
- Graham J. and Houlsby G. T. (1983) Anisotropic elasticity of a natural clay. *Geotechnique* 33, No. 2, pp. 165-180
- Grant R.J. (1998) Movements around a tunnel in two-layer ground. Ph.D. thesis. City University
- Grant R.J., Stallebrass S.E. and Taylor R.N. (1997) Prediction of pre-failure ground movements: Physical and numerical techniques. *Proc. 14<sup>th</sup> Int. Conf. Soil Mechanics and Foundation Engineering*, Hamburg, September 1997, pp. 663-668. Balkema Rotterdam

- Grant, R.J., Stallebrass, S.E. and Taylor, R.N. (1999) Modelling soil deformation at a tunnel heading using physical and numerical techniques. Proc. 12<sup>th</sup> Eur. Conf. Soil Mech. And Geo. Eng. Amsterdam, June 1999. Vol 3, pp. 2045-2052. Balkema, Rotterdam
- Hird C.C and Pierpoint N.D. (1997) Stiffness determination and deformation analysis for a trial excavation in Oxford clay. Geotechnique. Vol 47, No.3, pp. 665-692
- Ingram P. (2000) Brick model analysis of a rigid circular foundation. Research report GE/00/01, City University
- Jackson J. and Fookes P. (1974) The relationship of the estimated former burial depth of the lower Oxford clay to some soil properties. Quarterly Journal of Engineering Geology. Vol. 7, pp. 137-179
- Jaky J. (1944) The coefficient of earth pressure at rest. Journal of the Union of Hungarian Engineers and Architects. pp. 355-358
- Jamiolkowski M., Lancellotta R., Marchetti S., Nova R., Pasqualini E. (1979) General report: Design parameters for soft clays. Proc VII ECSMFE, Brighton. Vol 5, pp. 27-57
- Jamiolkowski M., Lancellotta R., and Lo Presti D.C.F. (1995) Remarks on the stiffness at small strains of six Italian clays. Pre-failure deformation of geomaterials. Shibuya, Mitachi and Miura (eds) Balkema, Rotterdam. pp. 817-836
- Jardine R.J., Potts D.M., Fourie A.B. and Burland J.B. (1986) Studies of the influence of non-linear stress-strain characteristics in soil-structure interaction. Geotechnique. Vol. 36, No. 2, pp. 377-396
- Jovicic V. (1997) The measurement and interpretation of small strain stiffness of soils. PhD Thesis, City University
- Kavvas M. and Amorosi A. (1998) A plasticity approach for the mechanical behaviour of structured soils. The Geotechnics of hard soils - soft rocks, Evangelista and Picarelli. (eds). Balkema, Rotterdam. pp. 603-613
- Leonards G.A and Ramiah B.K. (1960) Time effects in the consolidation of clays. ASTM STP, 254, pp. 116-130

- Leroueil S. and Vaughan P.R. (1990) The general and congruent effects of structure in natural soils and weak rocks. *Geotechnique*. Vol. 40, No. 3, pp. 467-488
- Mair R.J. (1993) Unwin memorial lecture 1992 Developments in geotechnical engineering research: application to tunnels and deep excavations. *Proc. Instn Civ. Engrs. Civil Engineering*, 93, pp. 27-41
- Mayne P.W. and Kulhawy F.H. (1982)  $K_o$ -OCR relationships in soil. *Journal of the Geotechnical Eng. Div. ASCE*. Vol. 108 (GT6), pp. 851-872
- Mesri G. and Choi Y.K. (1985) Settlement analysis of embankments on soft clays. *ASCE Journal of Geotechnical Engineering*. Vol 111, No.4, pp. 441-464
- Mitchell J.K. (1976) *Fundamentals of soil behaviour*, New York, Wiley
- Morrison P.R.J. (1994) Performance of foundations in a rising groundwater environment. PhD Thesis. City University
- Mroz Z., Norris V. A. and Zienkiewicz O. C. (1978) An anisotropic hardening model for soils and its application to cyclic loading. *Int. J. Num. Anal. Methods in Geomech.* 2, pp. 203-221
- Mroz Z., Norris V.A. and Zienkiewicz O.C. (1979) Application of an anisotropic hardening model in the analysis of elasto-plastic deformation of soils. *Geotechnique*. Vol. 29, No. 1, pp. 1-34
- O'Reilly M.P. and New B.M. (1982) Settlements above tunnels in the United Kingdom – their magnitude and prediction. *Proc. Tunnelling '82 Symp.*, Institution of mining and metallurgy, London (ed. M.J. Jones), pp. 173-181
- Pennington D.S. Nash D.F.T and Lings M.L. (1997) Anisotropy of  $G_0$  shear stiffness in Gault clay. *Geotechnique*. Vol 47, No.3, pp. 391-398
- Pierpoint N.D. (1996) The prediction and back analysis of excavation behaviour in Oxford clay. PhD thesis, University of Sheffield
- Powrie W. and Li E.S.F (1991) Finite element analyses of an in situ wall propped at formation level. *Geotechnique*, Vol 41, N0.4, pp. 499-514
- Powrie W., Chandler R.J., Carder R. and Watson G.V.R. (1999) Back-analysis of an embedded retaining wall with a stabilizing base slab. *Geotechnical Engineering*, Vol 137, No.2, pp. 75-86

- Puzrin A.M. and Burland J.B. (1998) Non-linear model of small-strain behaviour of soils. *Geotechnique*. Vol 48 No.2, pp. 217-233
- Rampello S. (1991) Some remarks on the mechanical behaviour of stiff clays: The example of Todi clay. *Experimental characterisation and modelling of soils and soft rocks*. Workshop, Naples, 29-31<sup>st</sup> October 1991. pp. 131-190
- Rampello S. and Silvestri F. (1993) The stress strain behaviour of natural and reconstituted samples of two overconsolidated clays. *Geotechnical engineering of hard soils - soft rocks*, Anagnostopoulos et al. (eds). Balkema, Rotterdam. pp. 769-778
- Rampello S. Viggiani G. and Georgiannou V.N. (1993) Strength and dilatancy of natural and reconstituted Vallericca clay. *Geotechnical engineering of hard soils - soft rocks*, Anagnostopoulos et al. (eds). Balkema, Rotterdam. pp. 761-768
- Rampello S. Viggiani G. and Silvestri F. (1994) The dependence of small strain stiffness on stress state and history for fine grained soils: The example of Vallericca clay. *Pre-failure deformation of geomaterials*. Shibuya, Mitachi and Miura (eds) Balkema, Rotterdam. pp. 273-278
- Rampello S. Silvestri F. and Viggiani G. (1995) Panellist discussion: The dependence of  $G_0$  on stress state and history in cohesive soils. *Pre-failure deformation of geomaterials*. Shibuya, Mitachi and Miura (eds) Balkema, Rotterdam. pp. 1155-1160
- Rampello S. Viggiani G. and Amorosi A. (1997) Small strain stiffness of reconstituted clay compressed along constant triaxial effective stress ratio paths. *Geotechnique* Vol 47, No. 3, pp. 475-489
- Richardson D. (1988) *Investigations of threshold effects in soil deformations*. PhD Thesis. City University
- Roscoe K.H. and Burland J.B. (1968) On the generalised stress-strain behaviour of "wet" clay. *Engineering Plasticity* (ed. J. Heyman and F.A. Leckie) pp. 535-609. Cambridge University Press
- Rouainia M. and Muir Wood D (1998) A kinematic hardening model for structured clays. *The Geotechnics of hard soils - soft rocks*, Evangelista and Picarelli. (eds). Balkema, Rotterdam. pp. 817-824

- Schmertmann J.H. (1981) A general time-related soil friction increase phenomenon. Laboratory shear strength of soil ASTM STP, 740, pp. 456-484
- Schofield A.N and Wroth C.P. (1968) Critical State Soil Mechanics, McGraw-Hill, London
- Simpson B. (1992) Retaining structures - displacement and design. Geotechnique. Vol. 42, No. 4, pp. 541-576
- Simpson B. (1997) Personal communication
- Skempton A. W. and Northey R. D. (1952) The sensitivity of clays. Geotechnique 3, pp. 30-53
- Skempton A.W. (1970) The consolidation of clays by gravitational compaction. Quarterly Journal of the Geological Soc. No. 125, pp. 373-411
- Smith P. R., Jardine R. J. and Hight D. W. (1992) On the yielding of Bothkennar clay. Geotechnique 42, No. 2, pp. 257-274
- Som N.N. (1968) The effect of stress path on the deformation and consolidation of London clay. Ph.D. thesis, University of London
- Stallebrass S.E. (1990) The effect of recent stress history on the deformation of overconsolidated soils. PhD Thesis. City University
- Stallebrass S. E. (1992) Final report for SERC postdoctoral fellowship. Ref no. B/90/RFH/8970
- Stallebrass, S.E., Grant, R.J. & Taylor, R.N. (1996) A finite element study of ground movements measured in centrifuge model tests of tunnels. Proc. Int. Symp. Geotechnical Aspects of Underground Construction in Soft Ground, London: Balkema, pp. 595-600
- Stallebrass S.E. and Taylor R.N. (1997) Prediction of ground movements in overconsolidated clay. Geotechnique Vol. 47, No. 2, pp. 235-253
- Taylor R.N. (ed.) (1995) Geotechnical centrifuge technology. Blajkie academic and professional
- Vatsala A. Nagendra Prasad K. Srinivasa Murthy B.R. and Sitharam T.G. (1998) A rational approach to model the behaviour of bonded soils. The Geotechnics of hard soils - soft rocks, Evangelista and Picarelli. (eds). Balkema, Rotterdam. pp. 923-928

- Viggiani G. (1992) Small strain shear stiffness of fine grained soils. PhD Thesis. City University
- Viggiani G. and Stallebrass S.E. (1994) Shear test data for reconstituted London clay. Research report GE/94/04, City University
- Viggiani G. and Atkinson J.H. (1995) Stiffness of fine-grained soil at very small strains. *Geotechnique*. Vol. 45, No. 2, pp. 249-265
- Wheeler S. J. (1997) A rotational hardening elasto-plastic model for clays. Proc. 14th ICSMFE, Hamburg.
- Whittle A.J. (1993) Evaluation of a constitutive model for overconsolidated clays. *Geotechnique*. Vol. 43, No. 2, pp. 289-313
- Yin J.H. and Graham J. (1989) Viscous-elastic-plastic modelling of one-dimensional time-dependent behaviour of clays. *Can. Geotechnical Journal*. Vol 26, pp. 199-209

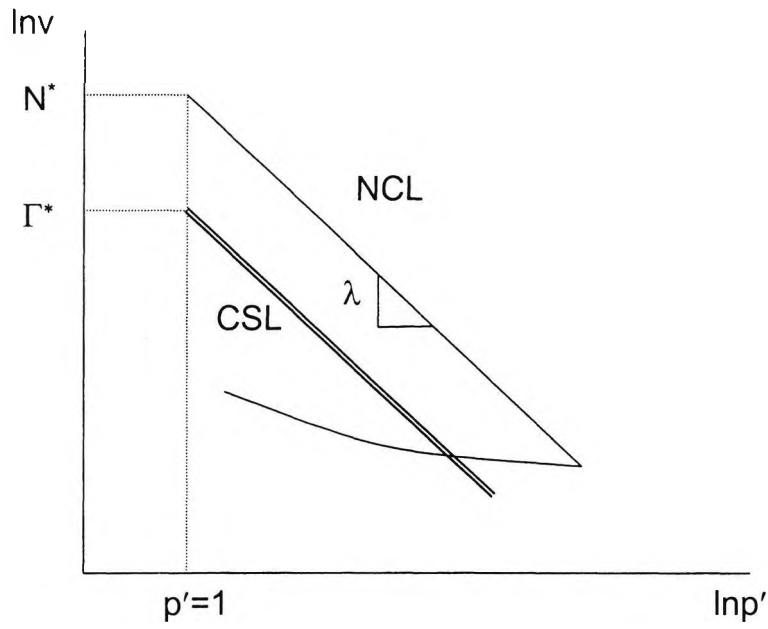


Figure 1.1 Framework for the behaviour of reconstituted clay in volumetric space

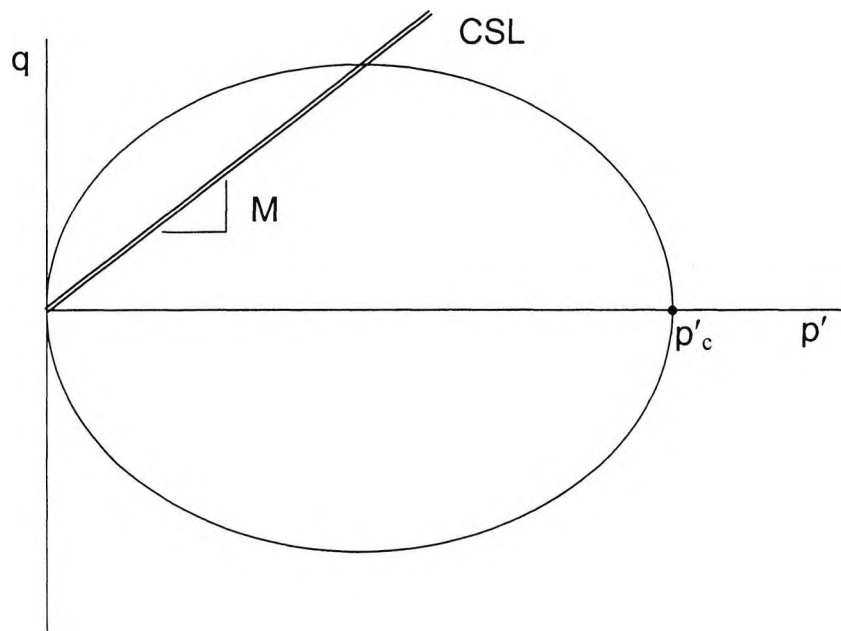


Figure 1.2 Framework for the behaviour of reconstituted clay in stress space

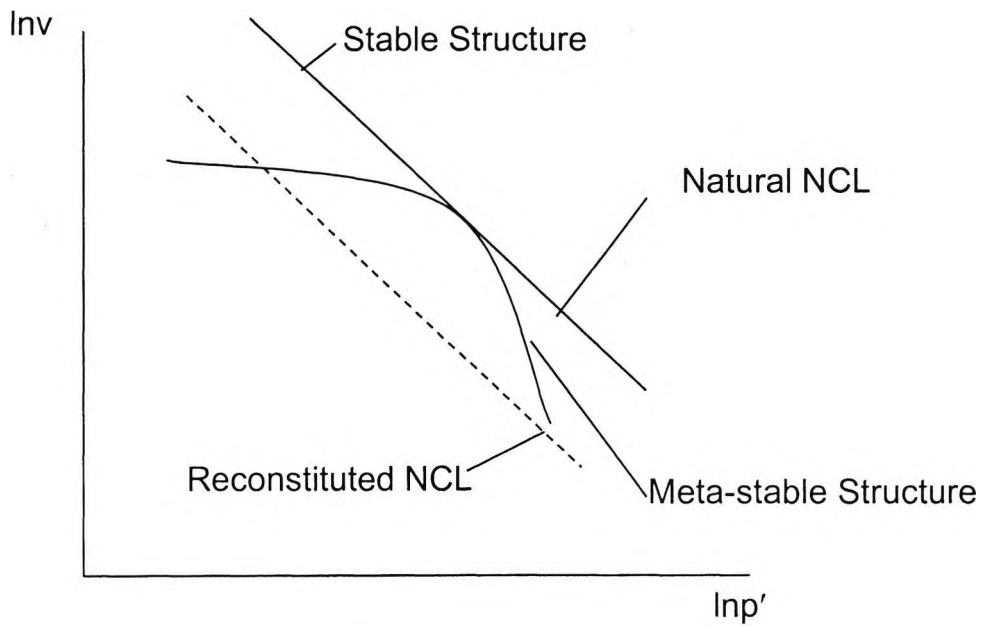


Figure 1.3 Framework for the behaviour of natural clay in volumetric space

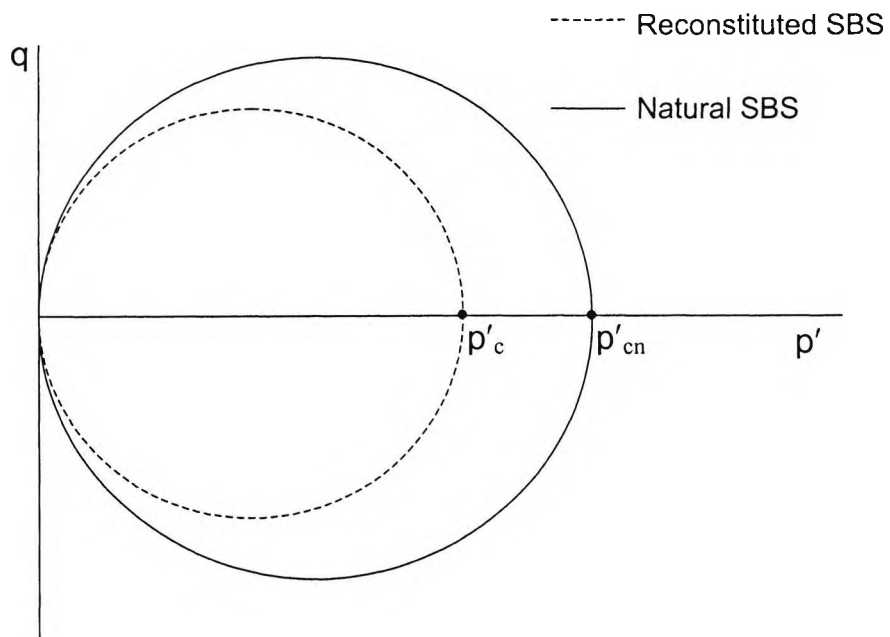


Figure 1.4 Framework for the behaviour of natural clay in stress space

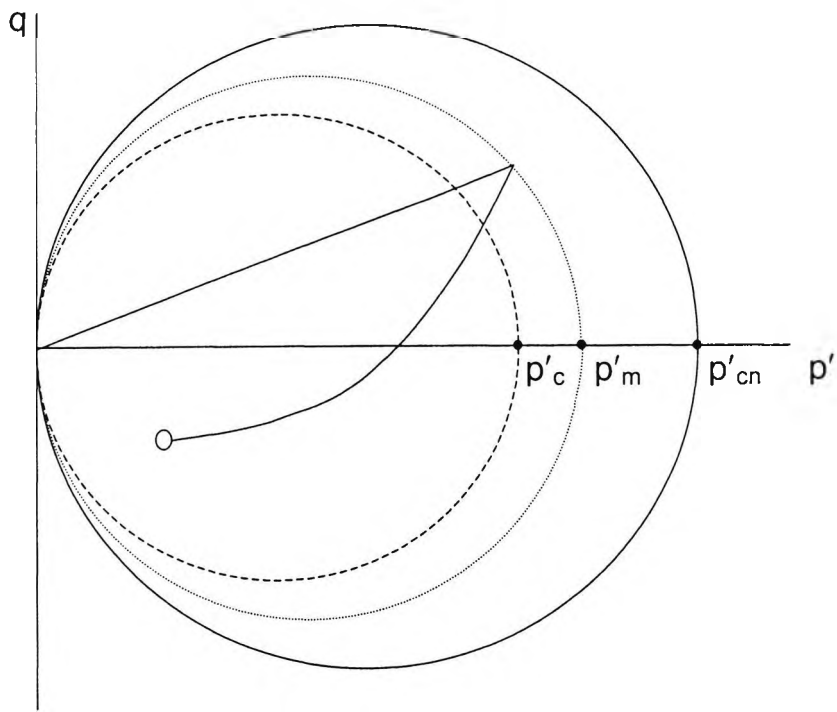


Figure 1.5 Description of initial state for a stiff clay





Figure 2.3 Scanning electron micrograph of reconstituted Pappadai clay compressed to  $\sigma'_v = 22$  Mpa (after Cotecchia, 1996)

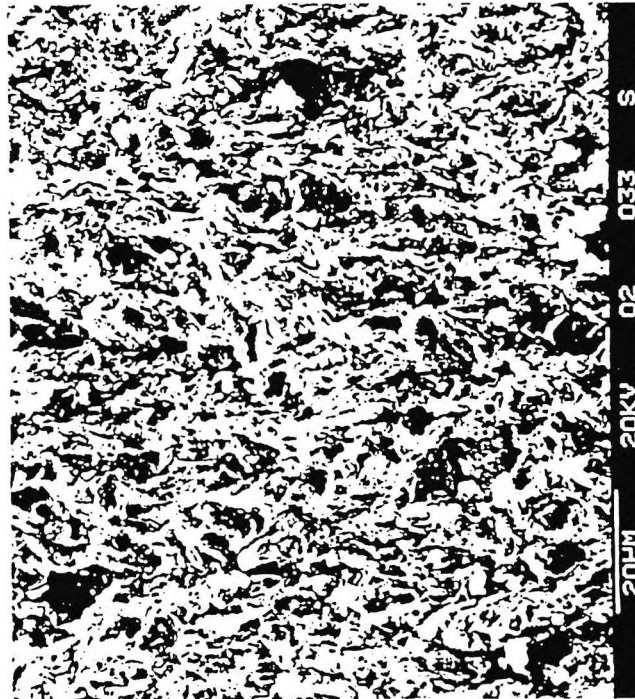


Figure 2.4 Scanning electron micrograph of natural Pappadai clay compressed to  $\sigma'_v = 22$  Mpa (after Cotecchia, 1996)

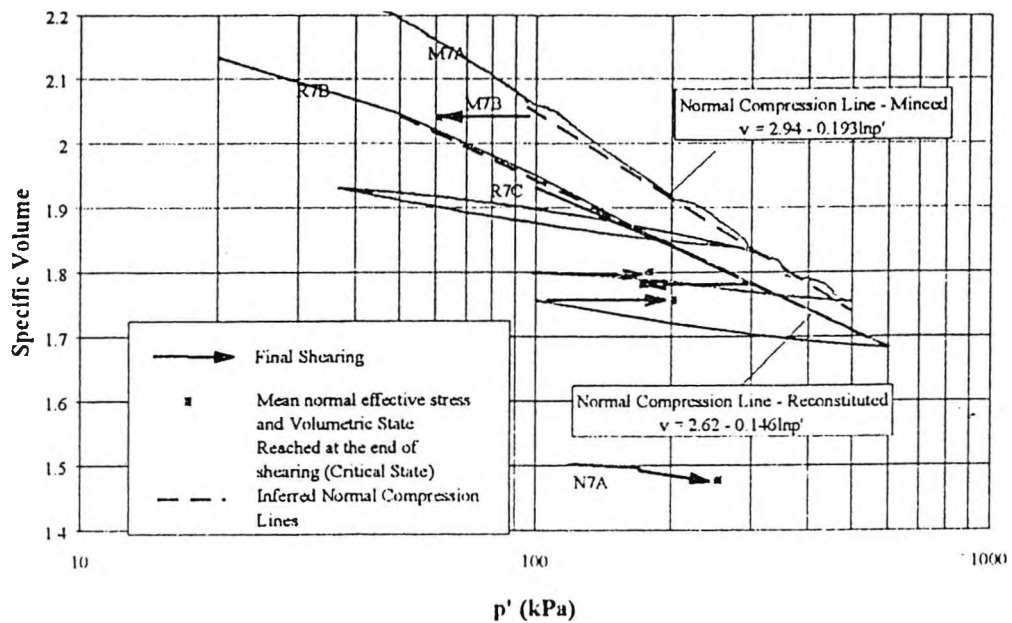


Figure 2.5 Compression data for reconstituted and minced samples of a structurally complex clay (after Fearon, 1998)

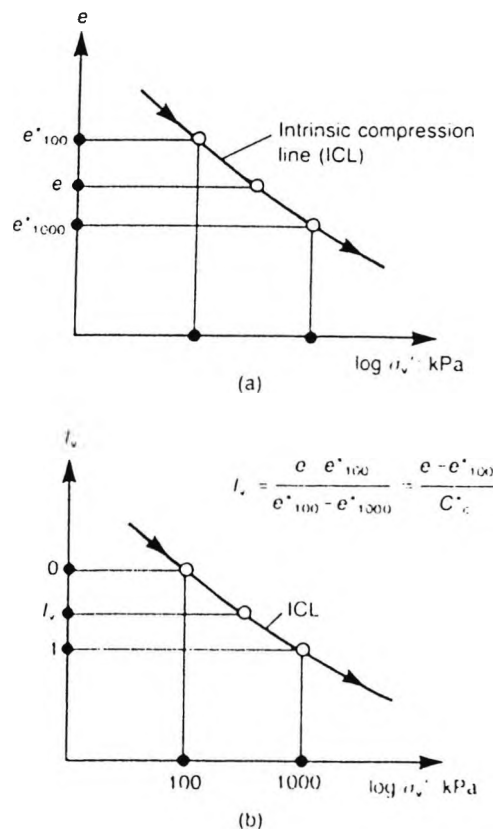


Figure 2.6 Normalising compression data by the use of void index  $I_v$  to identify the Intrinsic compression line (ICL) (after Burland, 1990)

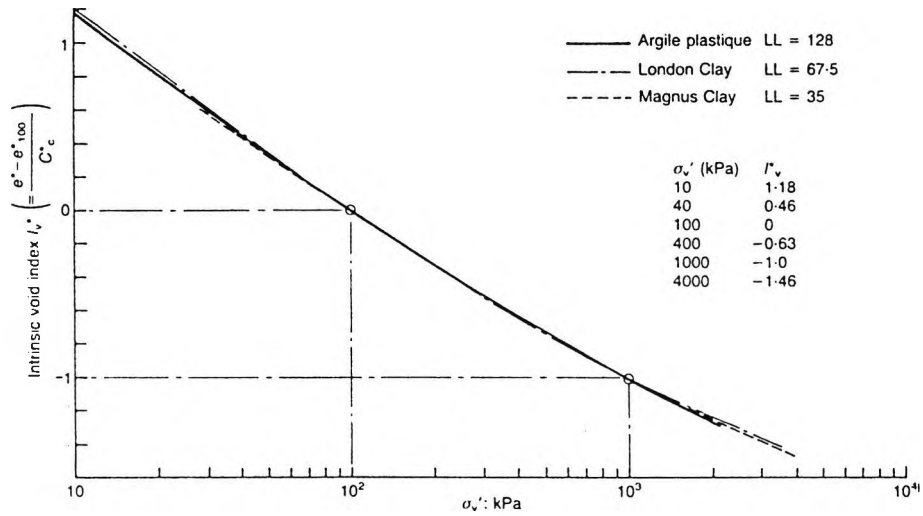


Figure 2.7 Normalised reconstituted compression curves, identifying the Intrinsic compression line (ICL) (after Burland, 1990)

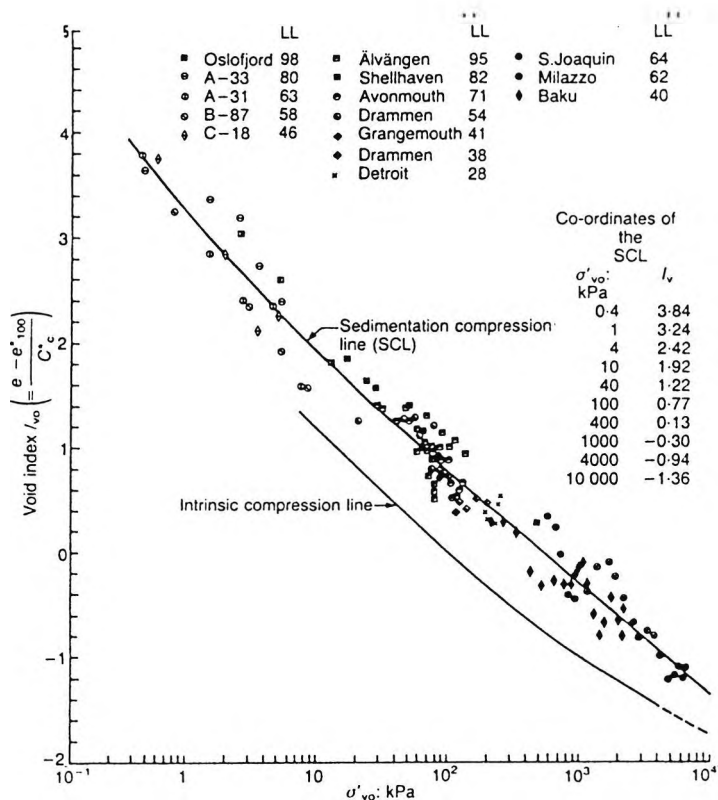


Figure 2.8 The intrinsic compression line (ICL) and the sedimentation compression line (SCL) for normally consolidated clays (after Burland, 1990)

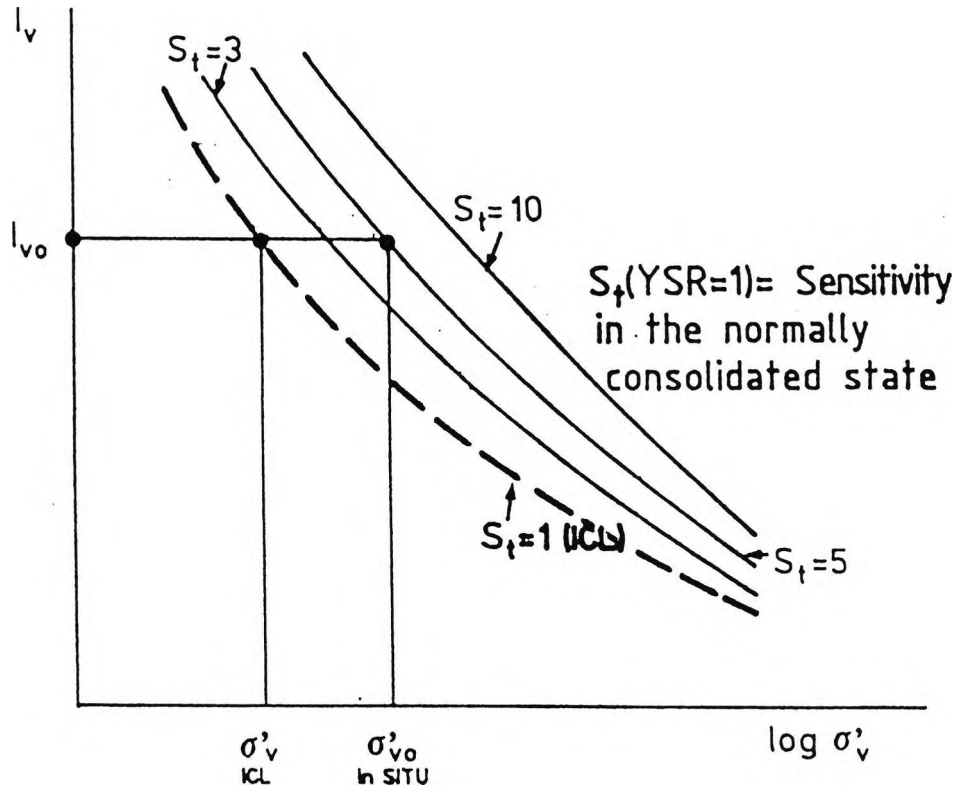


Figure 2.9 The sensitivity framework, showing sedimentation compression curves for clays of equal sensitivities (after Cotecchia, 1996)

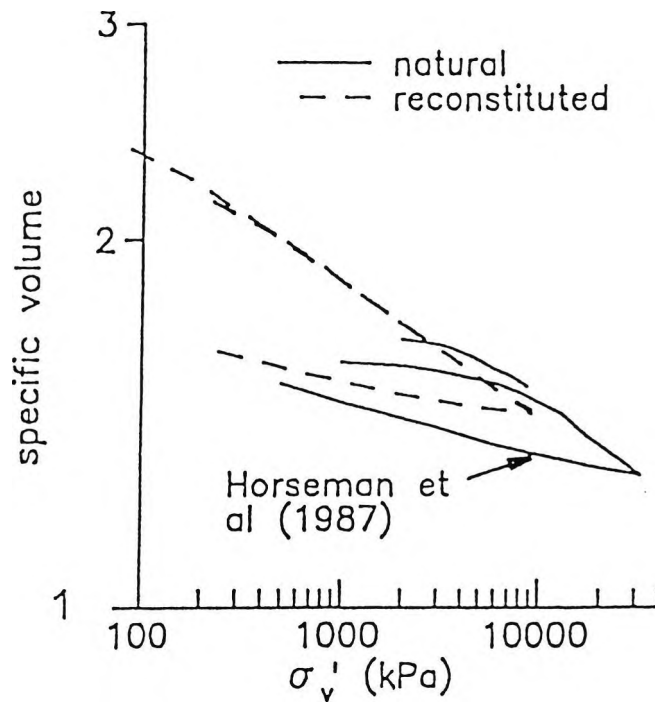


Figure 2.10 One dimensional compression of Boom clay (after Coop et al., 1995)

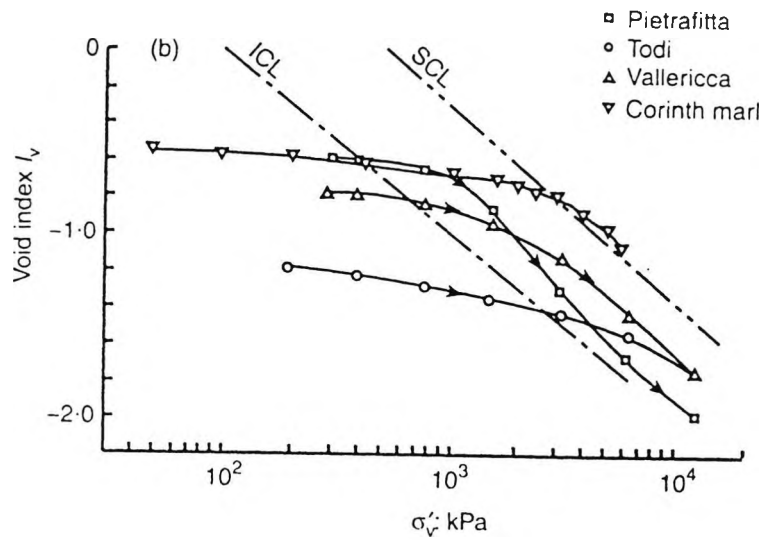


Figure 2.11 One dimensional compression data for reconstituted samples of clay plotted in terms of void index  $I_v$  (after Burland et al, 1996)

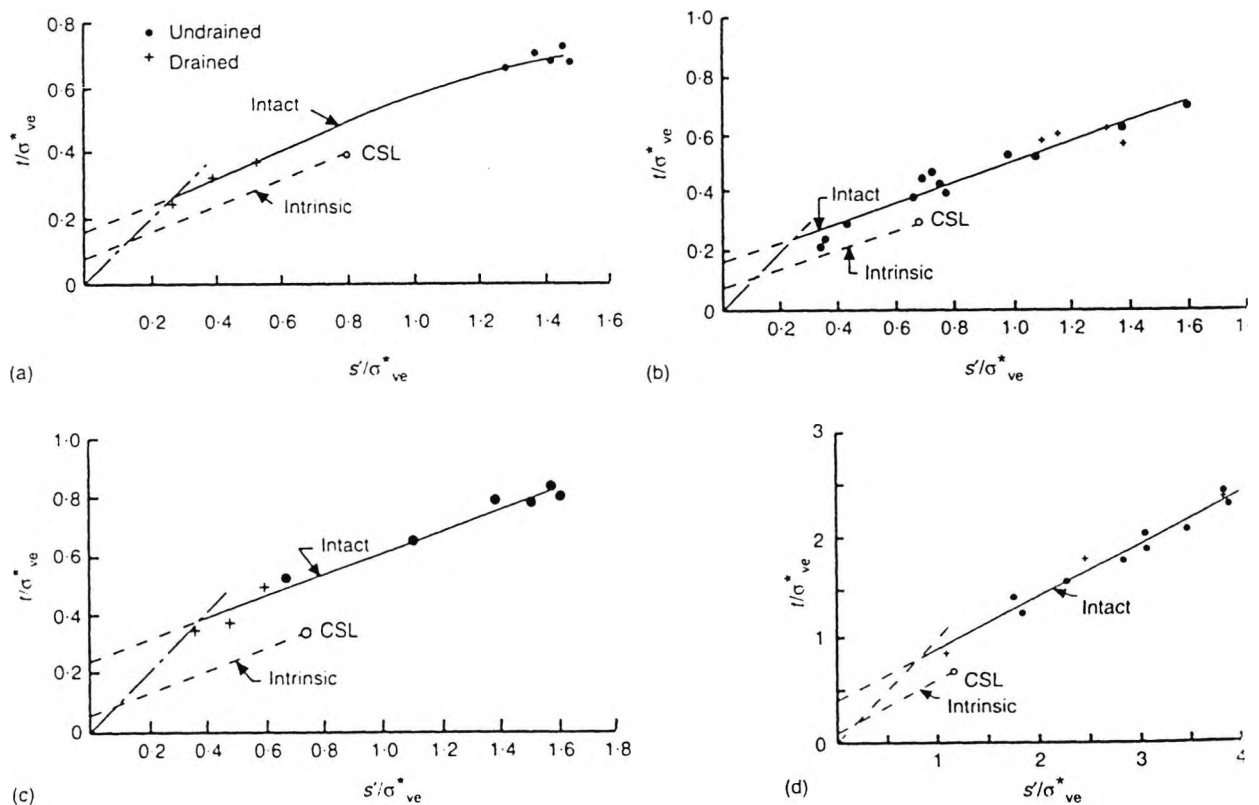


Figure 2.12 Comparison of natural (intact) and reconstituted (intrinsic) Hvorslev surfaces: a) Pietrafitta clay; b) Todi clay; c) Vallericca clay; d) Corinth marl (after Burland et al, 1996)

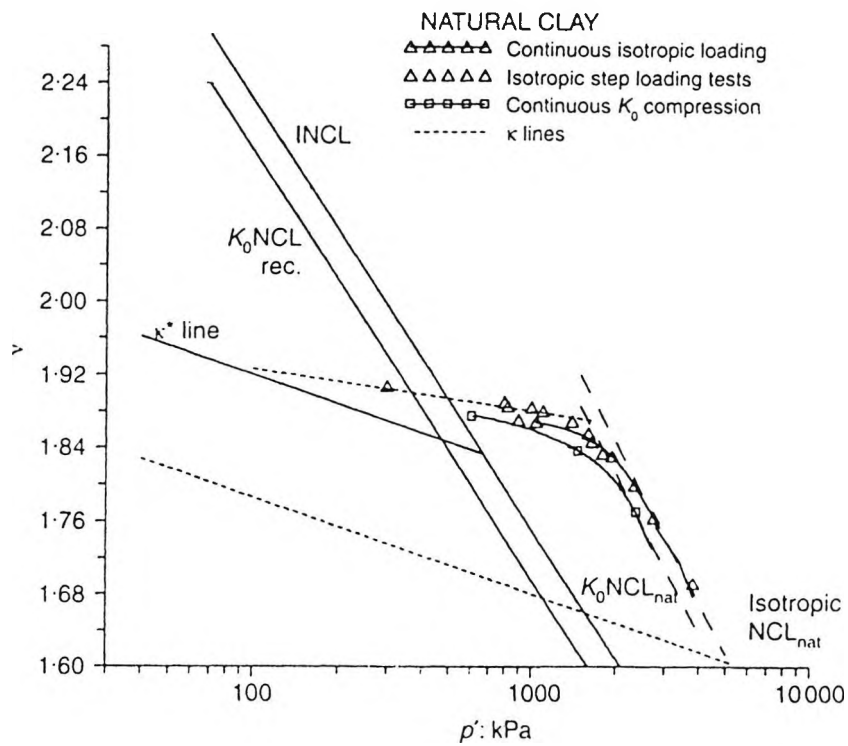


Figure 2.13 Isotropic and  $K_0$  compression and swelling data for reconstituted and natural samples of Pappadai clay (after Cotecchia and Chandler, 1997)



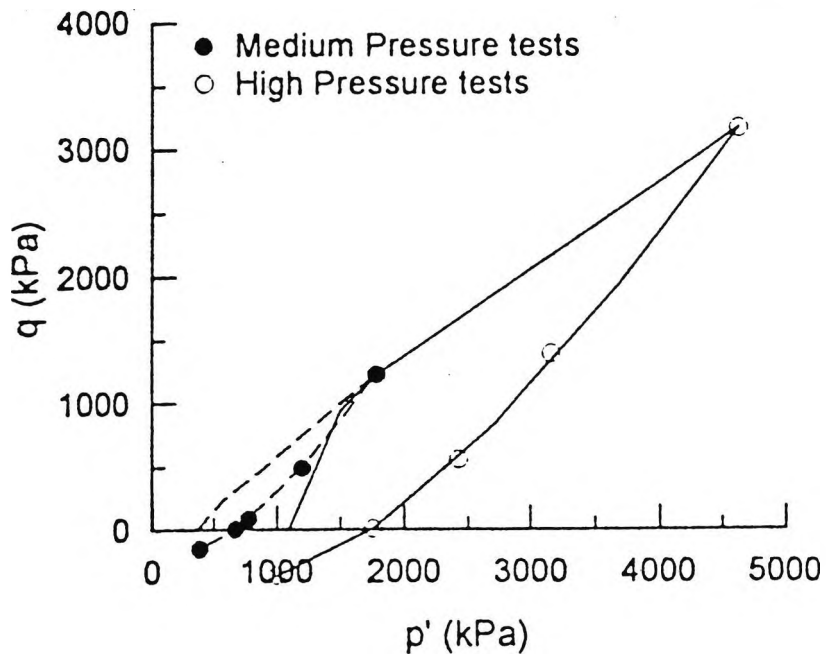


Figure 2.16 Initial states for shearing tests carried out on Vallericca clay, medium and high pressure tests (after Amorosi and Rampello, 1998)

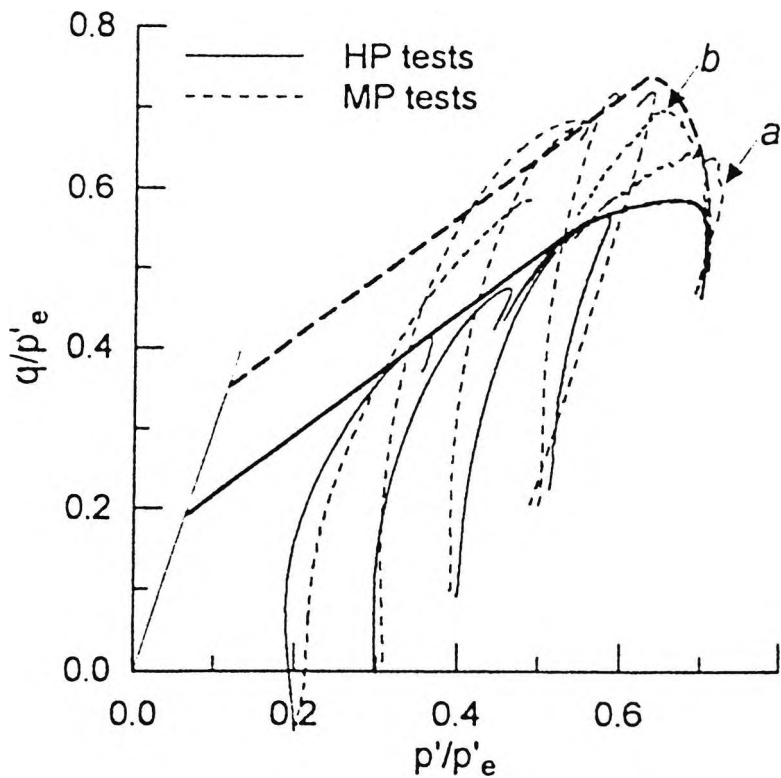


Figure 2.17 Normalised stress paths for medium and high pressure shearing stages (after Amorosi and Rampello, 1998)

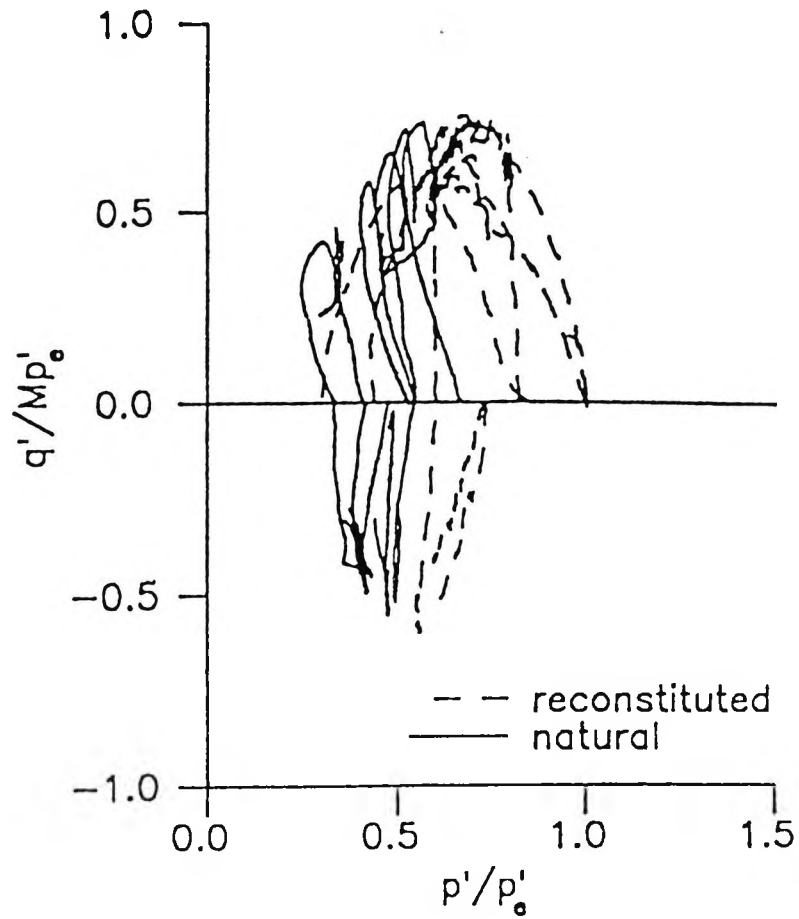


Figure 2.18 Normalised stress paths for Boom clay in triaxial compression and extension (after Coop et al, 1995)

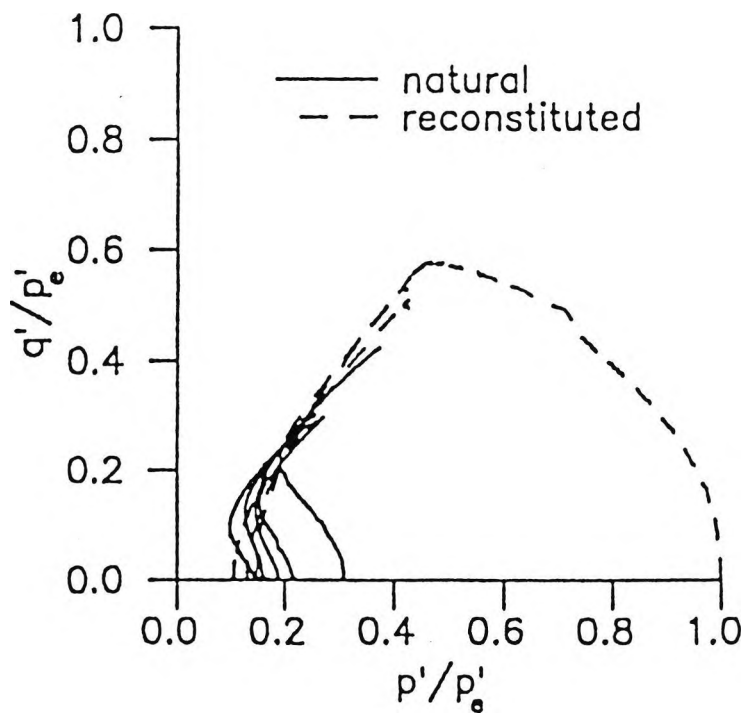


Figure 2.19 State paths for boulder clay from Chapel cross (after Coop et al, 1995)

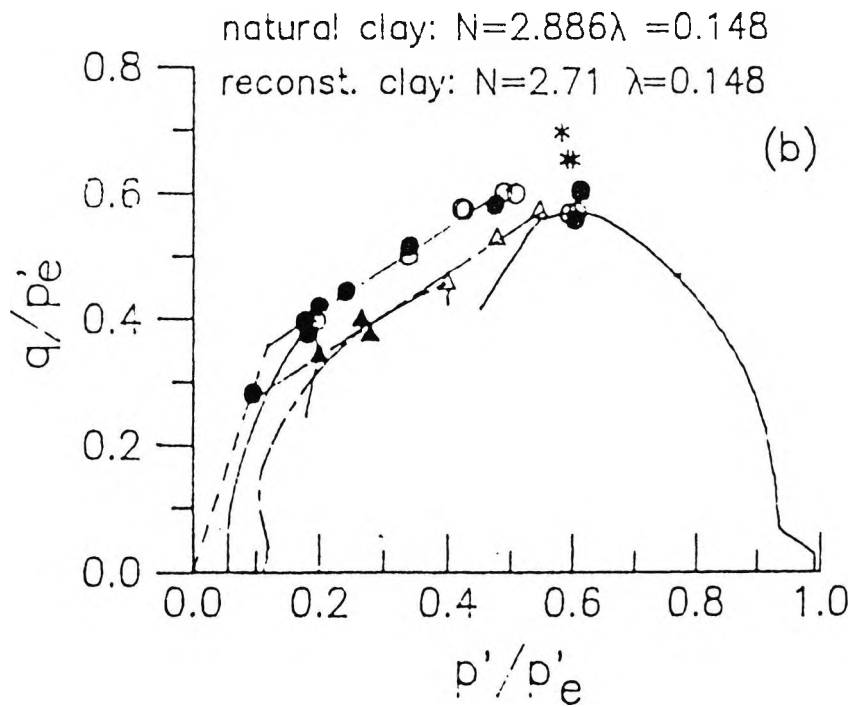
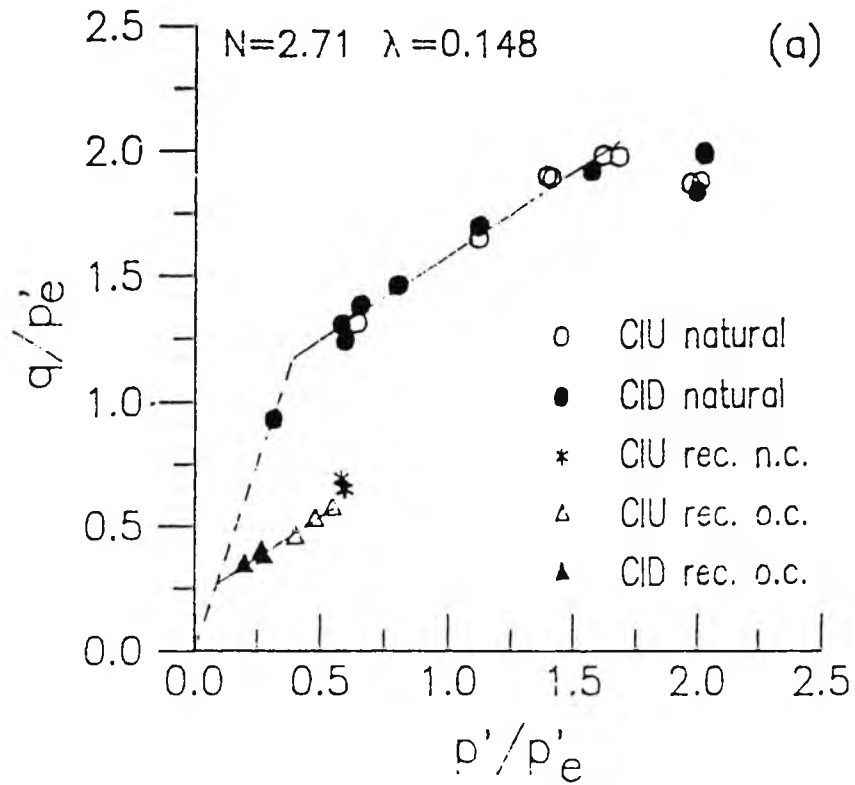


Figure 2.20 State boundary surfaces for natural and reconstituted Vallericca clay, normalised by the equivalent pressure at failure (after Rampello et al, 1993)

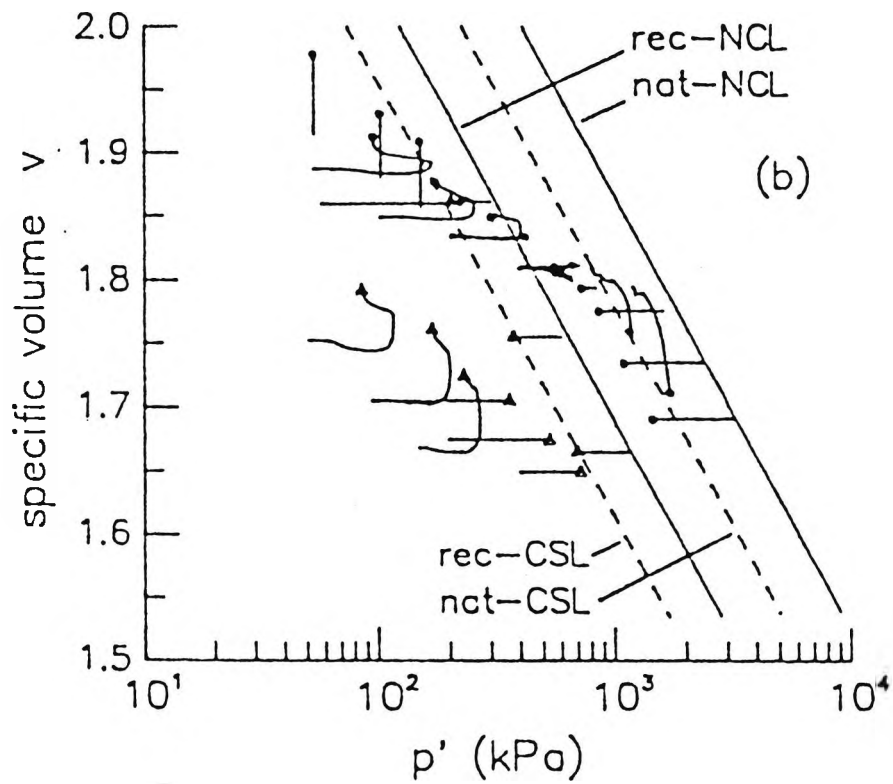


Figure 2.21 Shearing paths of reconstituted and natural samples in the compression plane: (after Rampello et al, 1993)

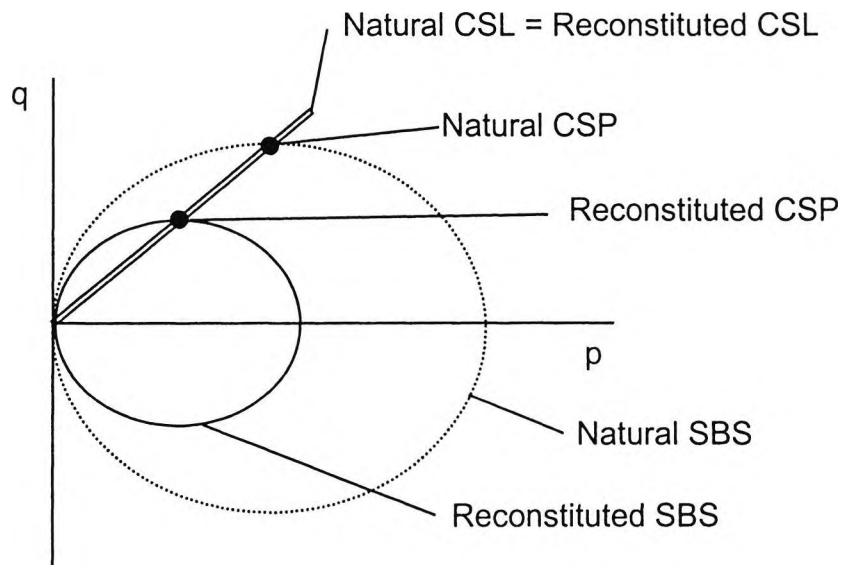


Figure 2.22 Schematic of state boundary surfaces for reconstituted and natural samples of clay, showing location of critical states.

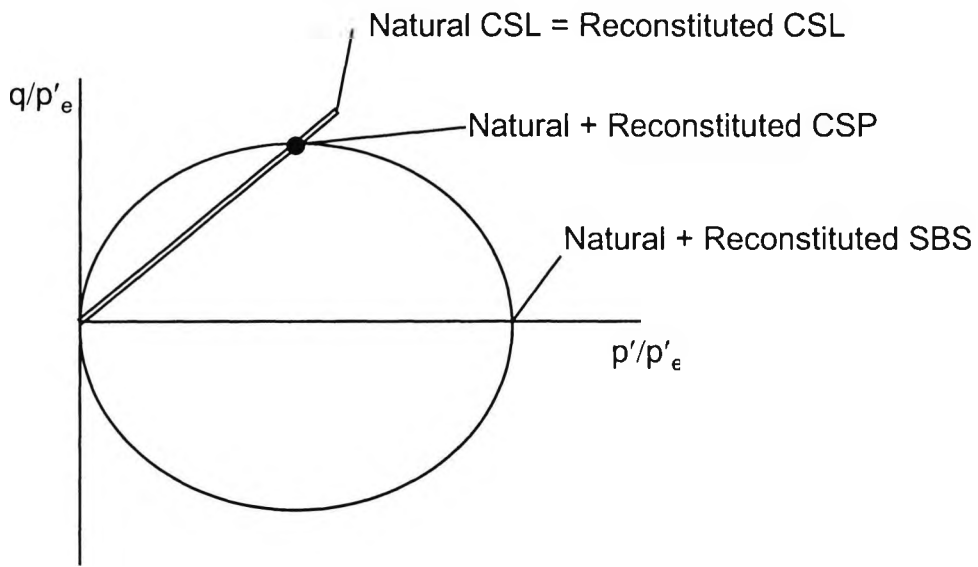


Figure 2.23 Schematic of normalised state boundary surfaces for reconstituted and natural samples of clay, showing location of critical states.

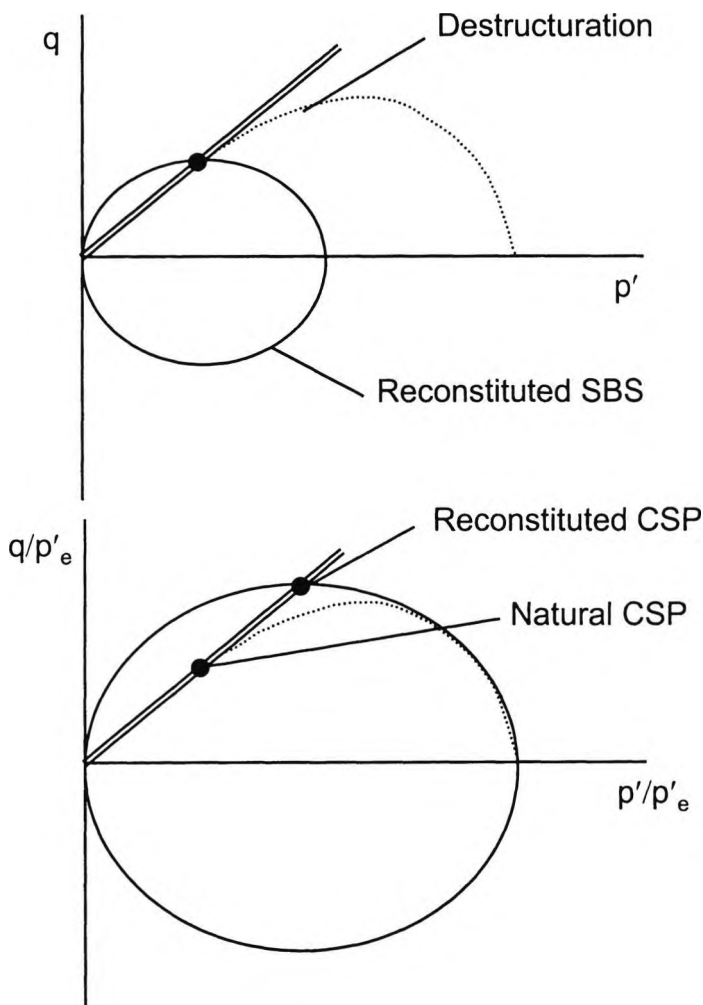


Figure 2.24 Schematic of normalised state boundary surfaces for reconstituted and destructuring natural samples of clay, showing location of critical states.

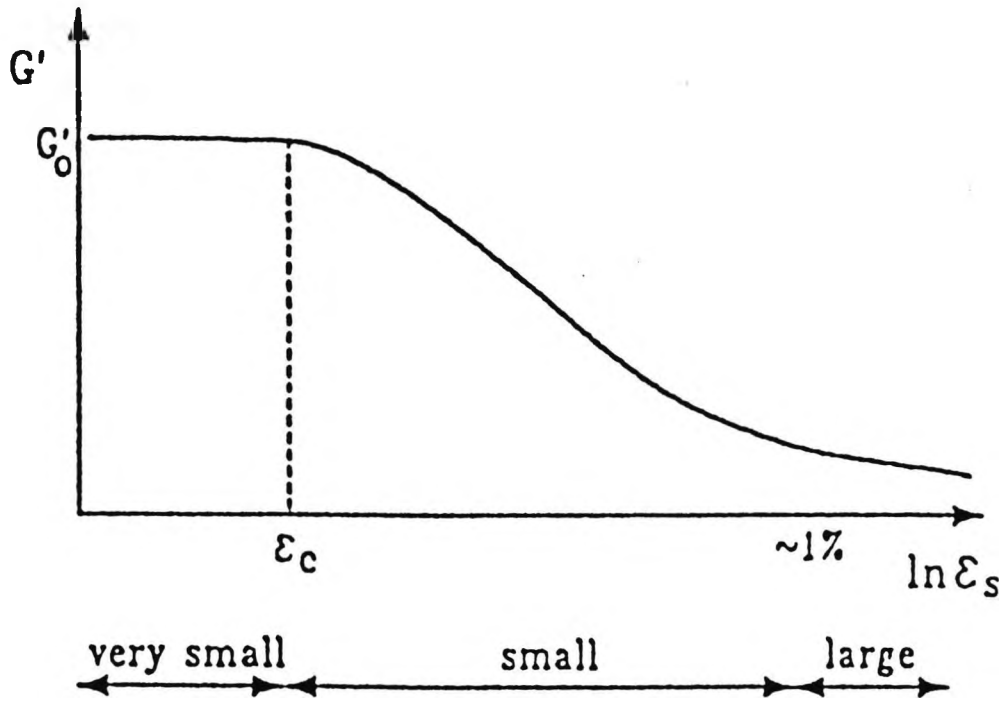


Figure 2.25 An idealisation of the variation of stiffness with strain for soil (after Atkinson and Salfors, 1991)

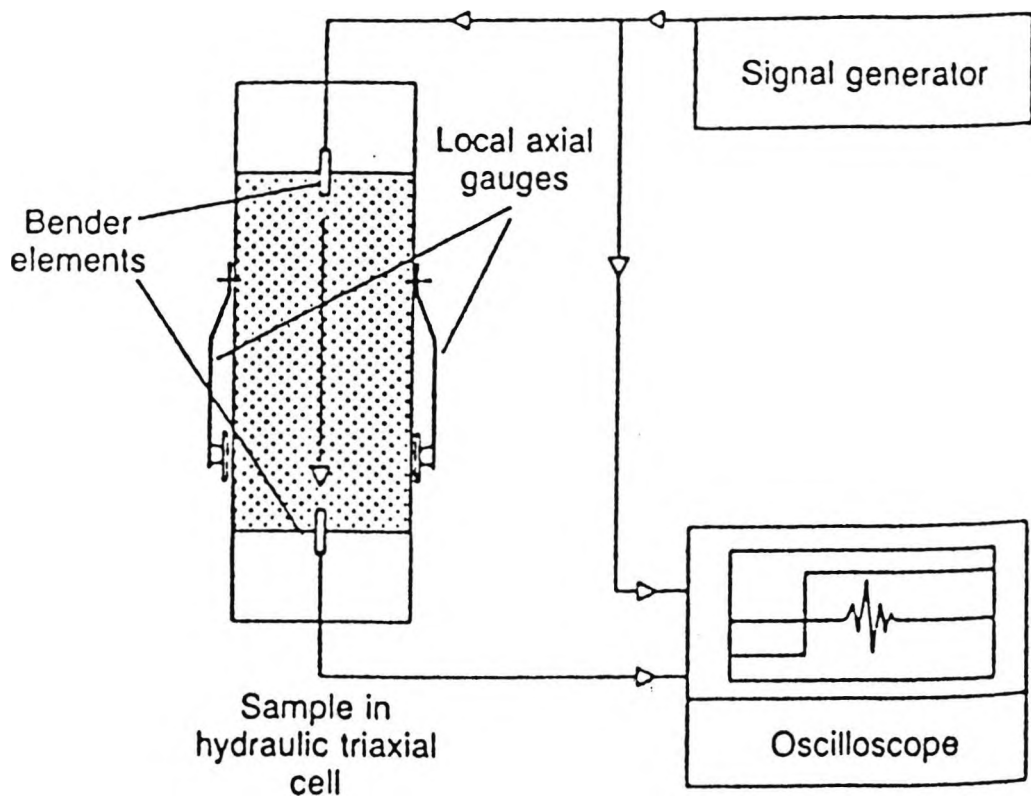


Figure 2.26 Triaxial cell incorporating bender elements (after Viggiani and Atkinson, 1995)

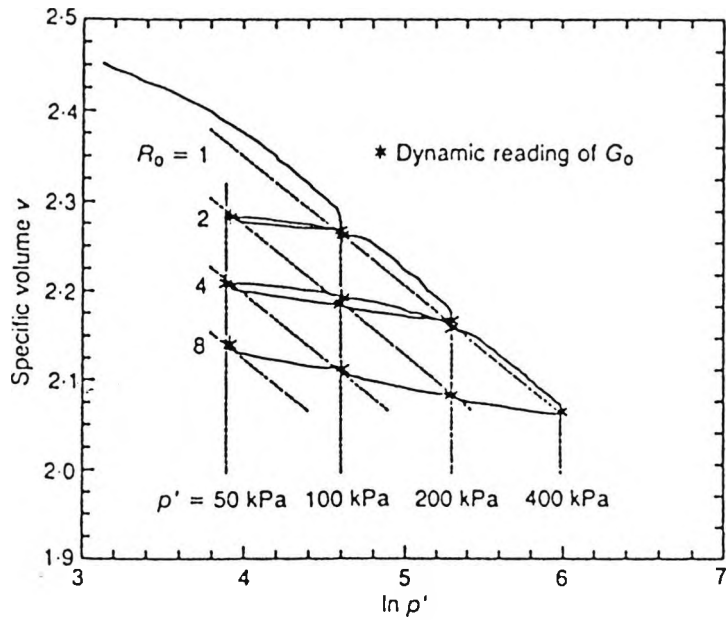


Figure 2.27 Isotropic stress states at which bender element tests were carried out (after Viggiani and Atkinson, 1995)

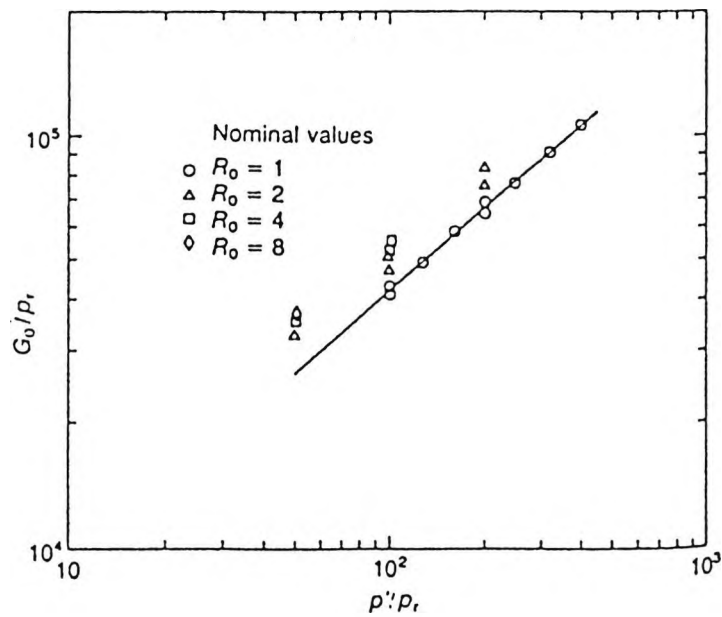


Figure 2.28 Variation of  $G_0$  with stress and overconsolidation ratio,  $R_0$ , for reconstituted samples of Speswhite kaolin (after Viggiani and Atkinson, 1995)

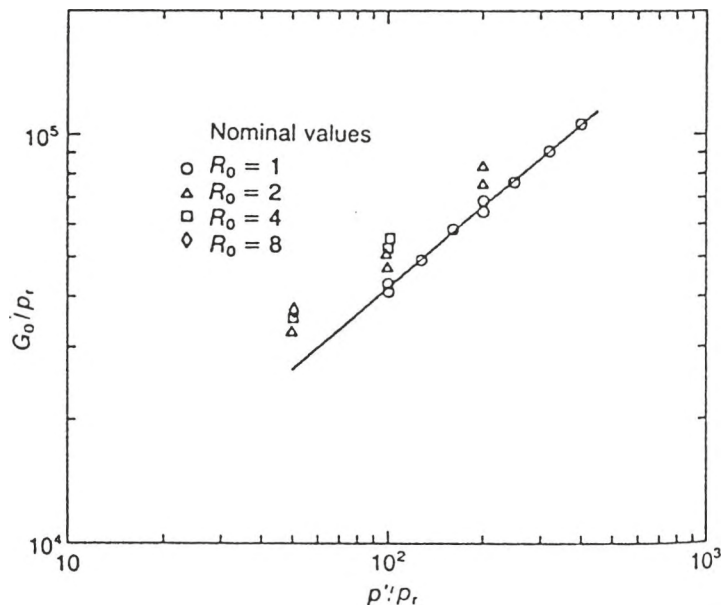


Figure 2.29 Variation of  $G_0$  with stress and overconsolidation ratio,  $R_0$ , for reconstituted samples of Speswhite kaolin (after Viggiani and Atkinson, 1995)

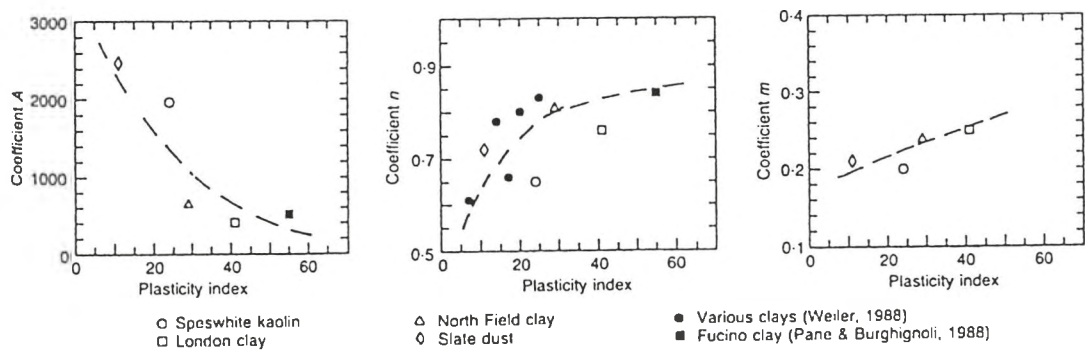


Figure 2.30 Charts showing the variation of coefficients  $A$ ,  $n$ , and  $m$  for the relationship for  $G_0$  (after Viggiani and Atkinson, 1995)

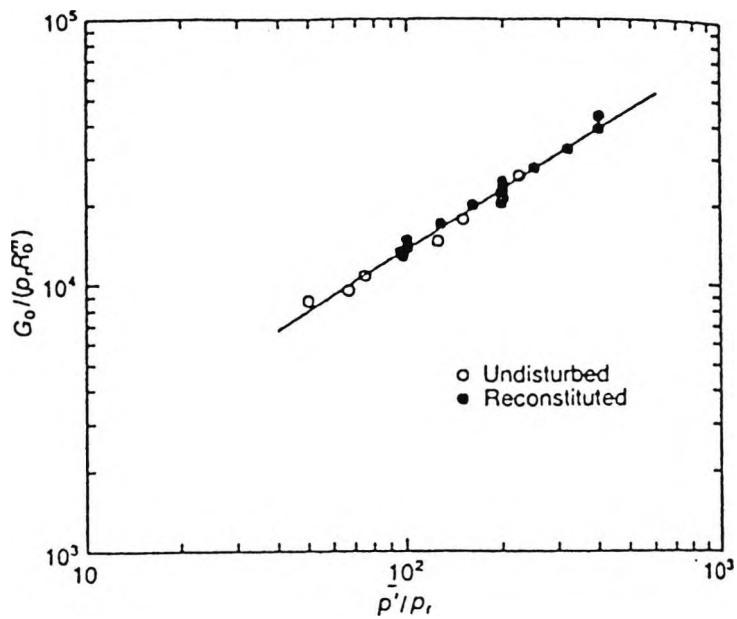


Figure 2.31 Variation of normalised  $G_0$  with mean effective stress and overconsolidation ratio,  $R_0$ , for natural and reconstituted samples of London clay (after Viggiani and Atkinson, 1995)

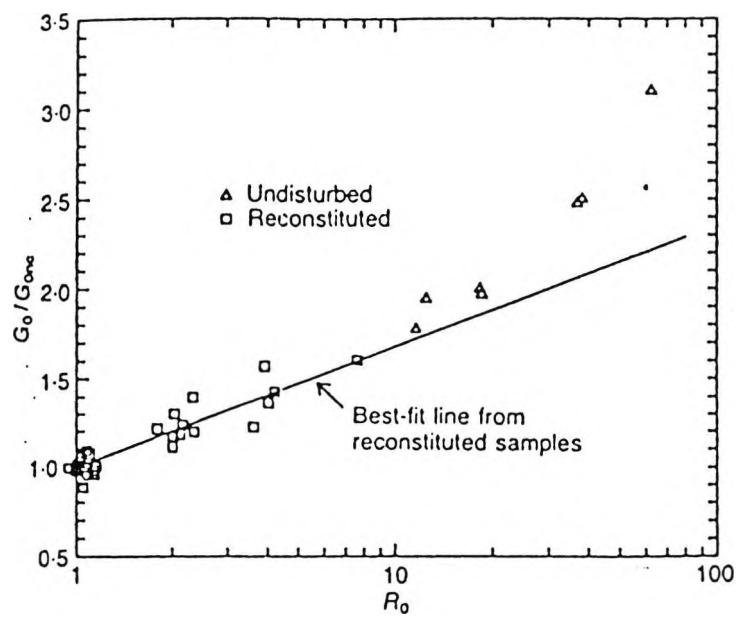


Figure 2.32 Variation of normalised  $G_0$  with overconsolidation ratio,  $R_0$ , for natural and reconstituted samples of London clay (after Viggiani and Atkinson, 1995)

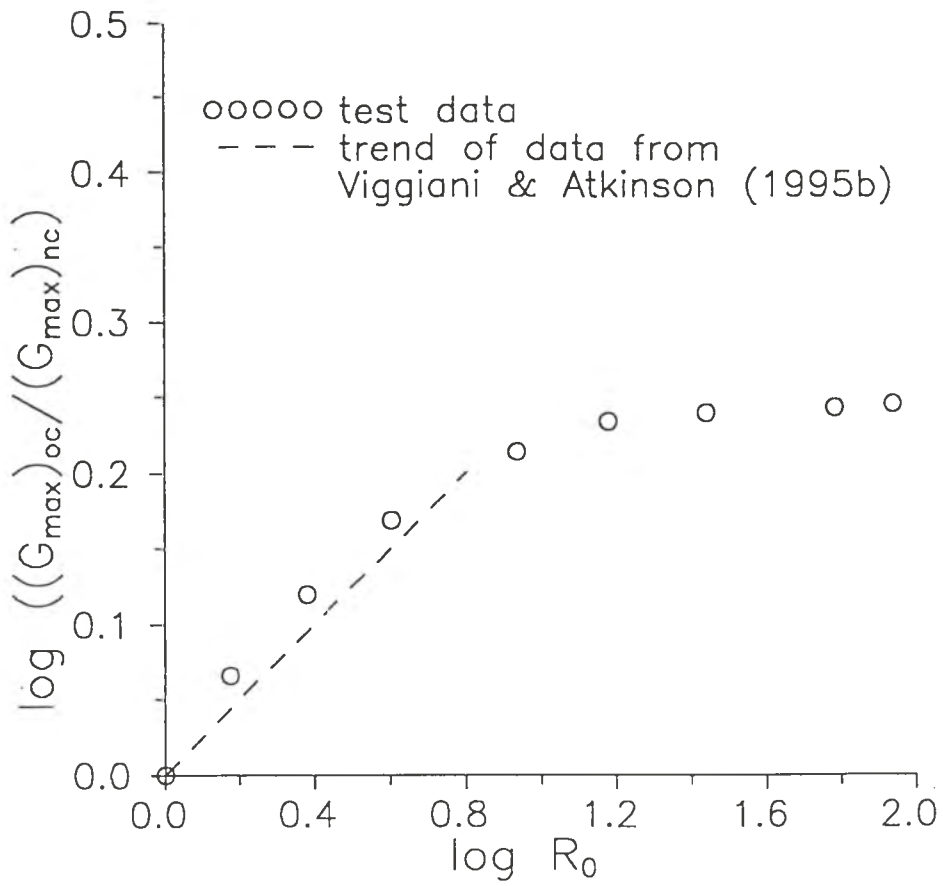


Figure 2.33 Variation of normalised stiffness with overconsolidation ratio for reconstituted Speswhite kaolin (after Jovicic, 1997)

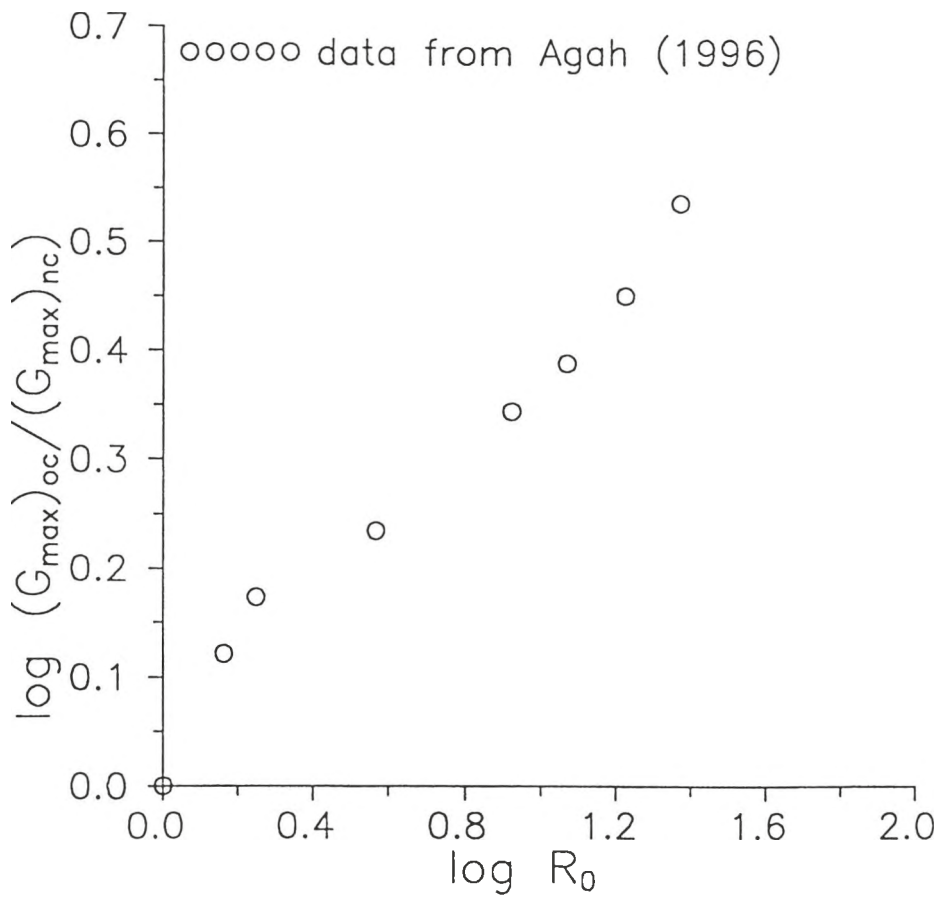


Figure 2.34 Variation of normalised stiffness with overconsolidation ratio for reconstituted Boom clay (after Jovicic, 1997)

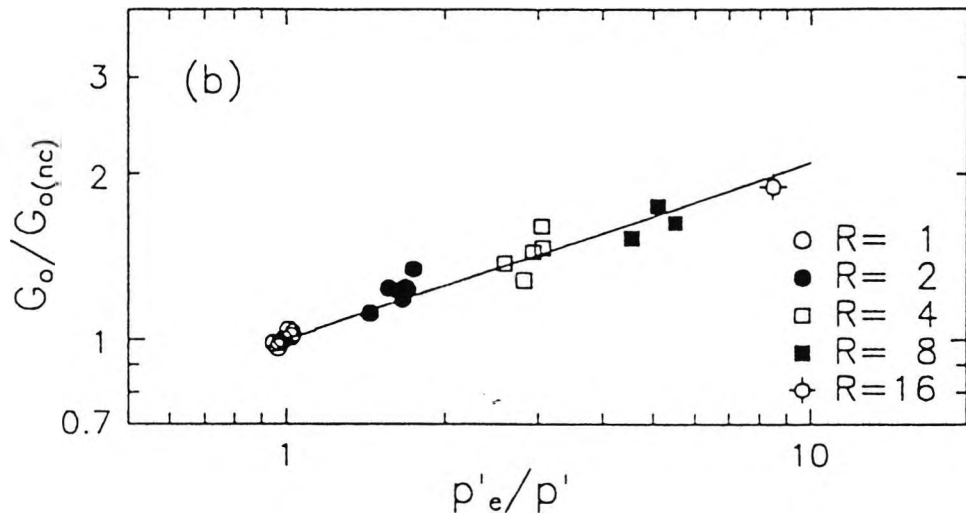


Figure 2.35 Variation of normalised  $G_0$  with mean effective stress and overconsolidation ratio,  $R_0$ , for natural and reconstituted samples of Vallericca clay (after Rampello et al, 1994)

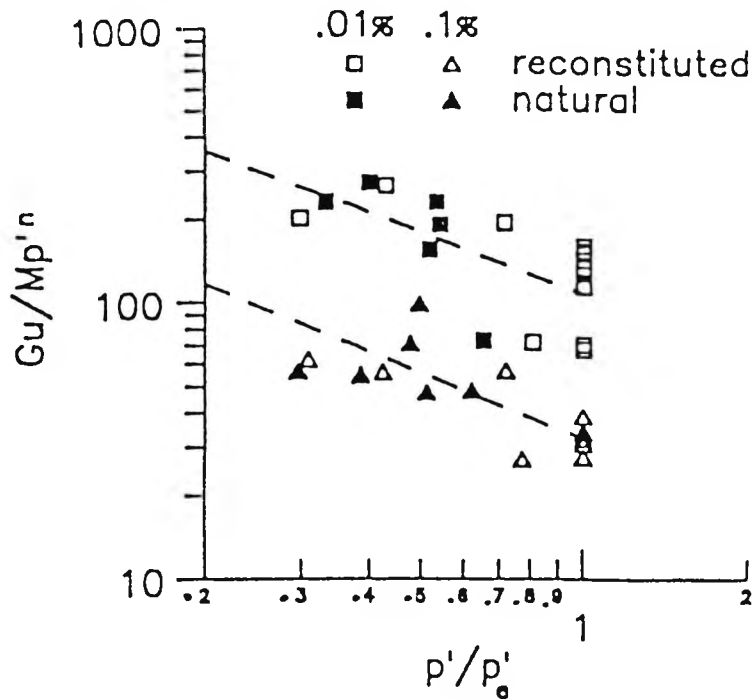


Figure 2.36 Undrained shear modulus of natural and reconstituted Boom clay (after Coop et al, 1995)

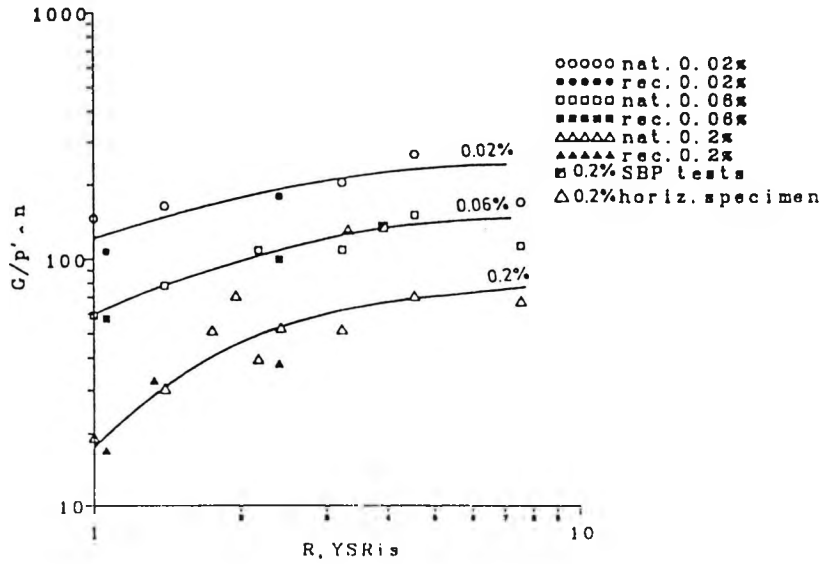


Figure 2.37 Normalised shear stiffness against yield stress ratio for natural and reconstituted samples of Pappadai clay (after Cotecchia, 1996)

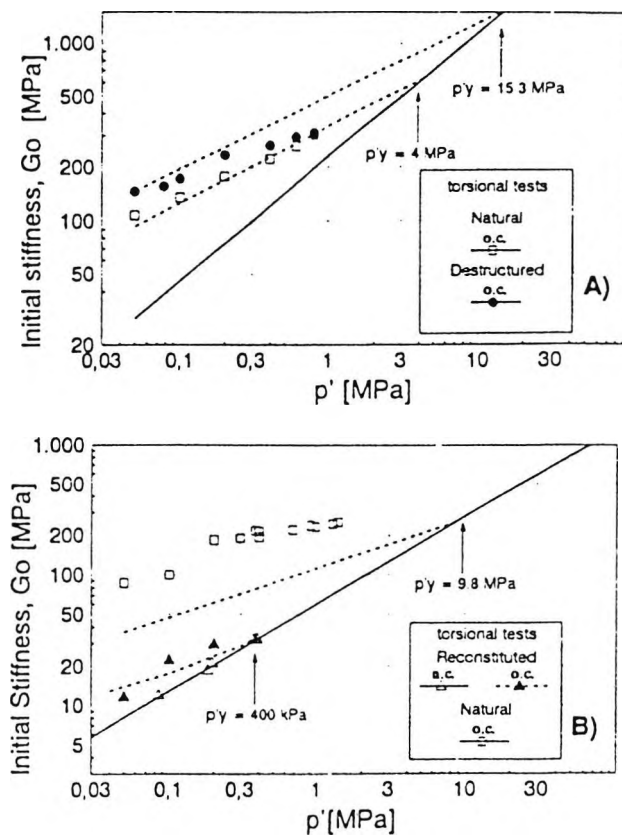


Figure 2.38 Variation of  $G_0$  with mean effective stress for a) Vallericca clay; b) Bisaccia clay (after D-Onafrio et al, 1998)

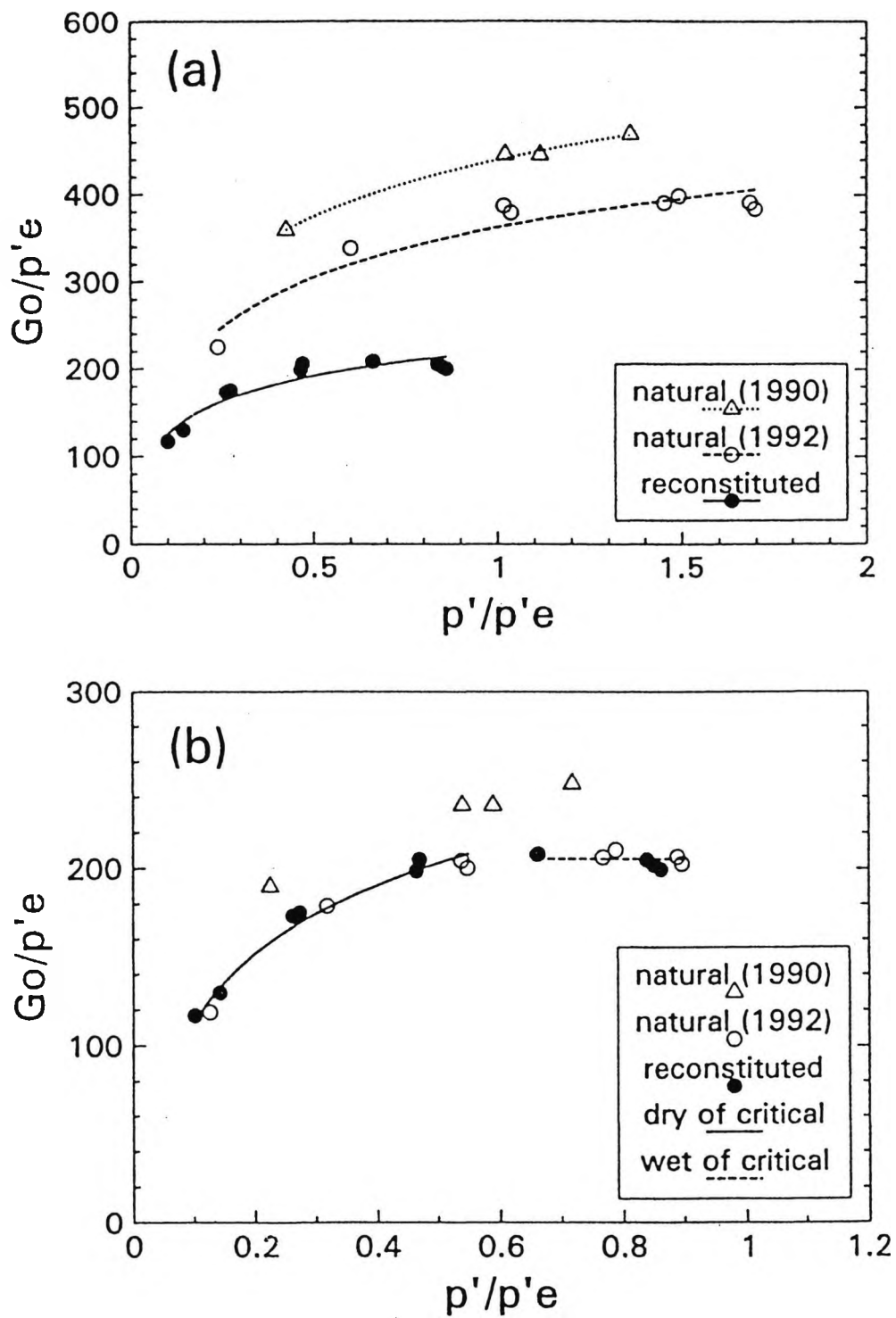


Figure 2.39 Initial shear stiffness,  $G_0$ , normalised by: a) the reconstituted equivalent pressure; b) the appropriate equivalent pressure (after Rampello and Silvestri, 1993)

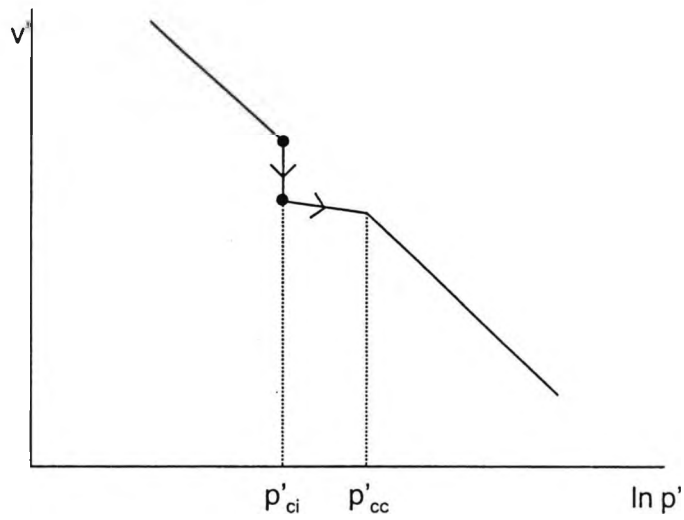


Figure 2.40 Schematic diagram in volumetric space showing possible state path for soil subject to creep

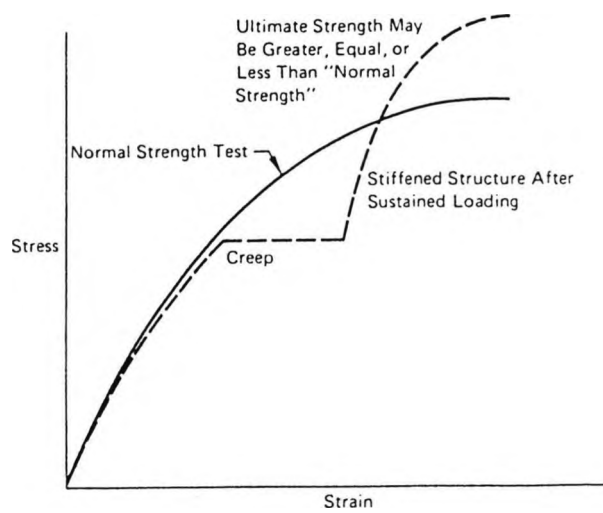


Figure 2.41 The effect of sustained loading on stress-strain and strength behaviour (after Mitchell, 1976)

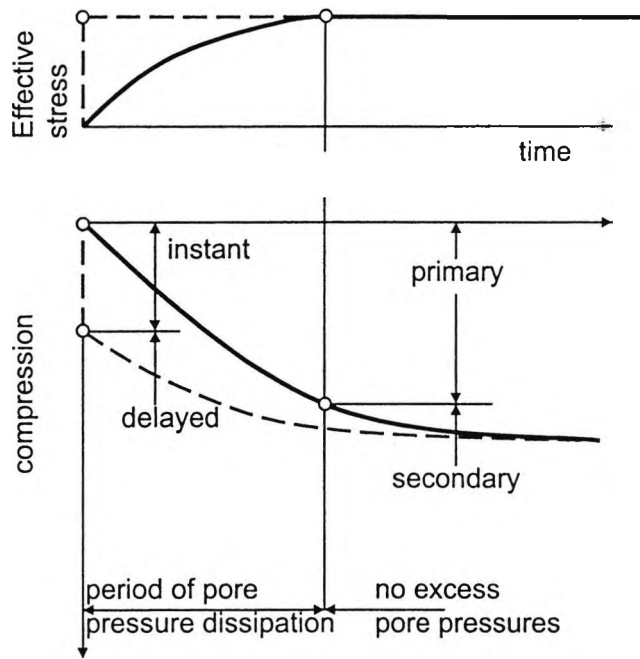


Figure 2.42 Definition of instant and delayed compression compared with primary and secondary compression (after Bjerrum, 1967)

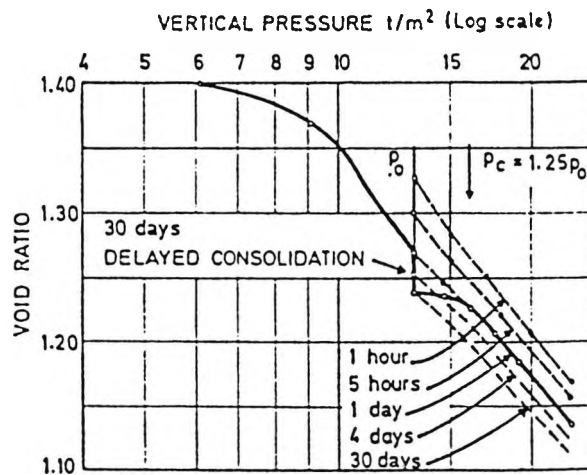


Figure 2.43 Laboratory creep test on Drammen clay (after Bjerrum, 1967)

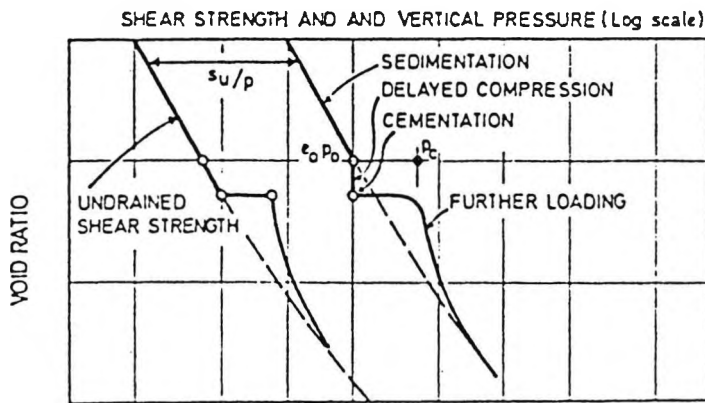


Figure 2.44 The effect of cementation in volumetric space (after Bjerrum, 1967)

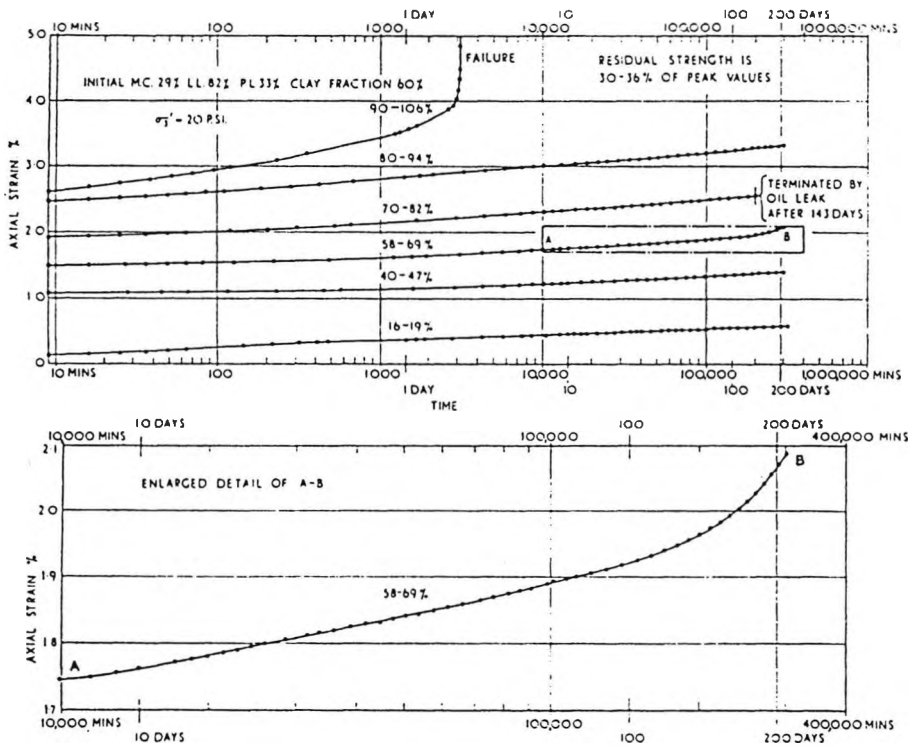


Figure 2.45 Drained creep tests on natural samples of London clay (after Bishop, 1966)

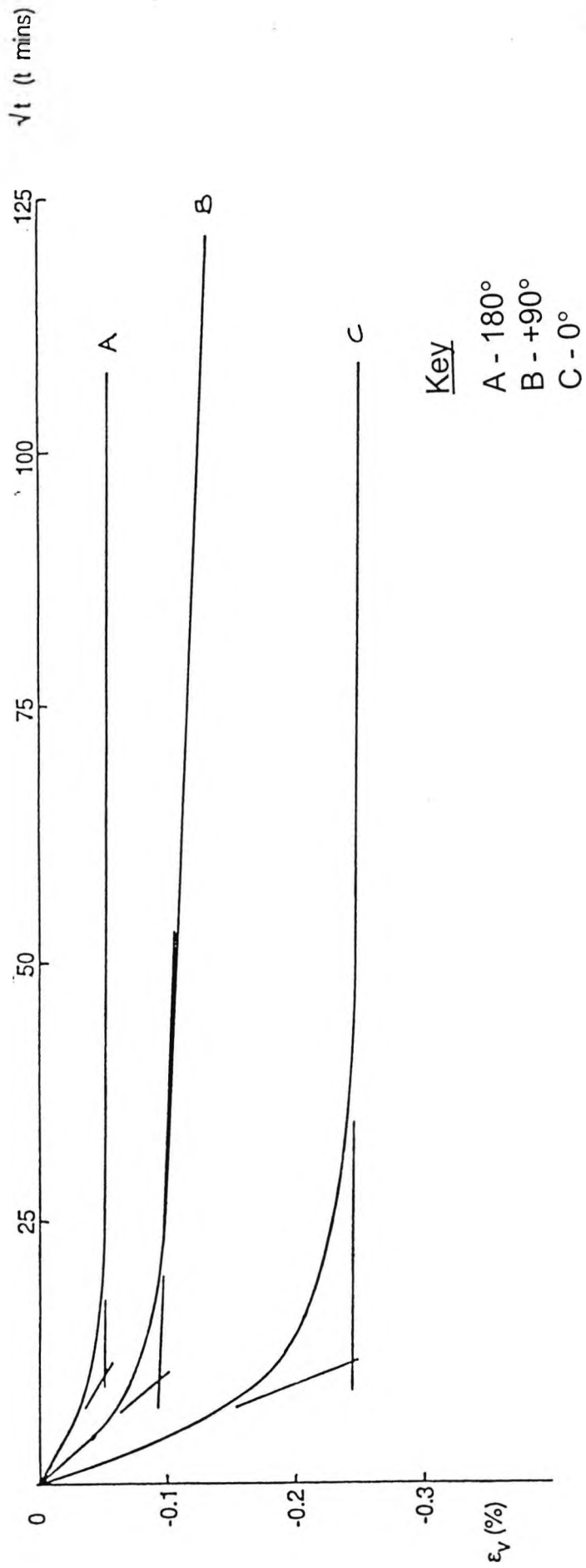


Figure 2.46 Rest periods for London clay following different approach paths (after Richardson, 1988)

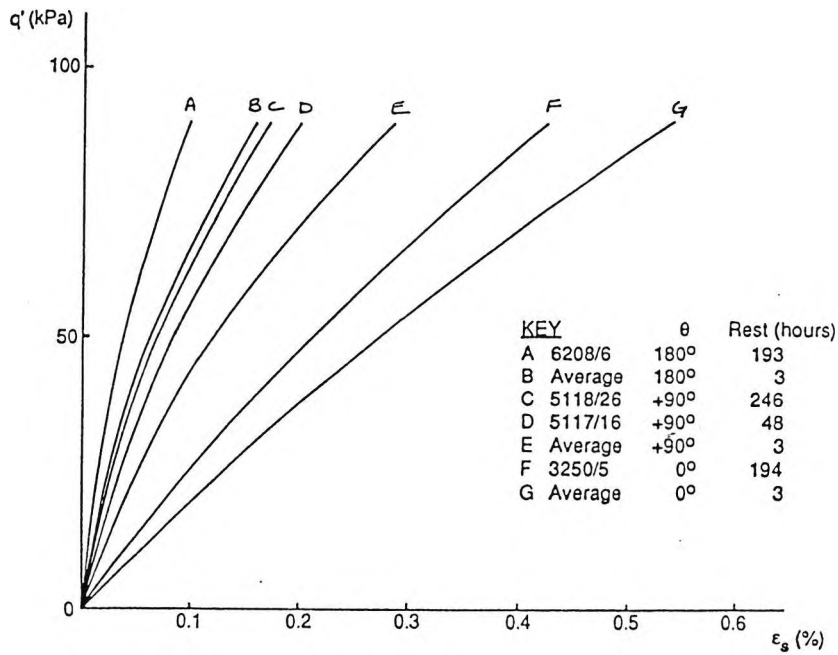


Figure 2.47 Graph of deviator stress against shear strain for constant  $p'$  tests with different rest periods and approach paths (after Richardson, 1988)

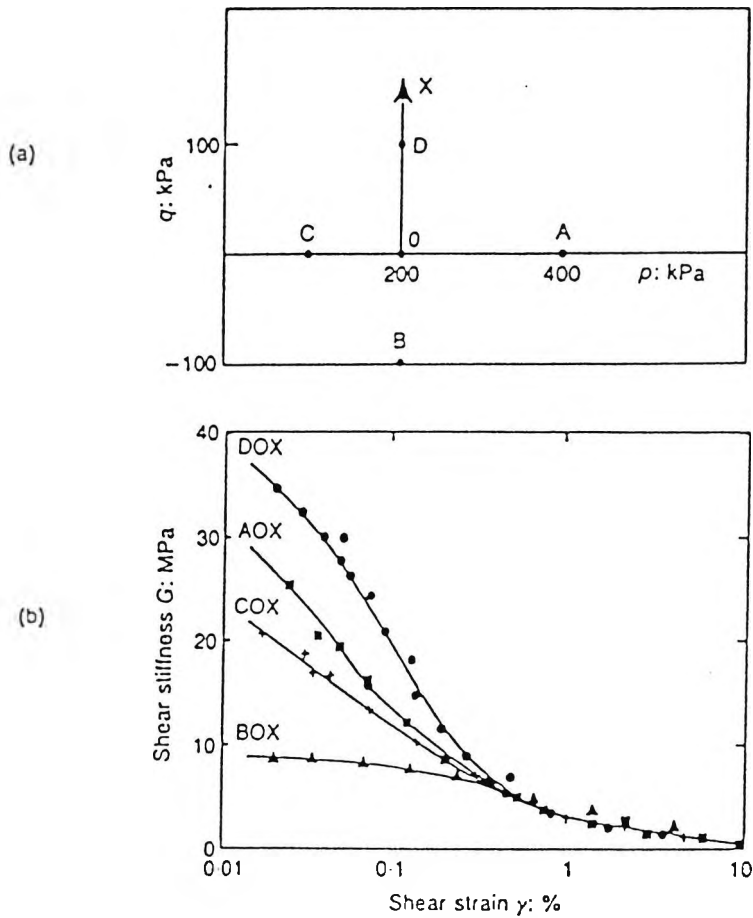


Figure 2.48 Results from recent stress history tests for path OX: a) approach paths; b) stiffness curves for different stress path rotations (after Richardson, 1988)

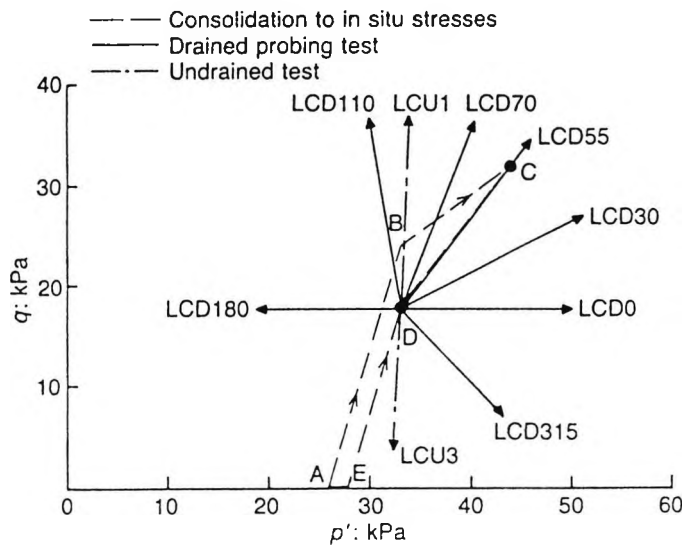


Figure 2.49 Stress probes to investigate recent stress history (after Smith et al, 1992)

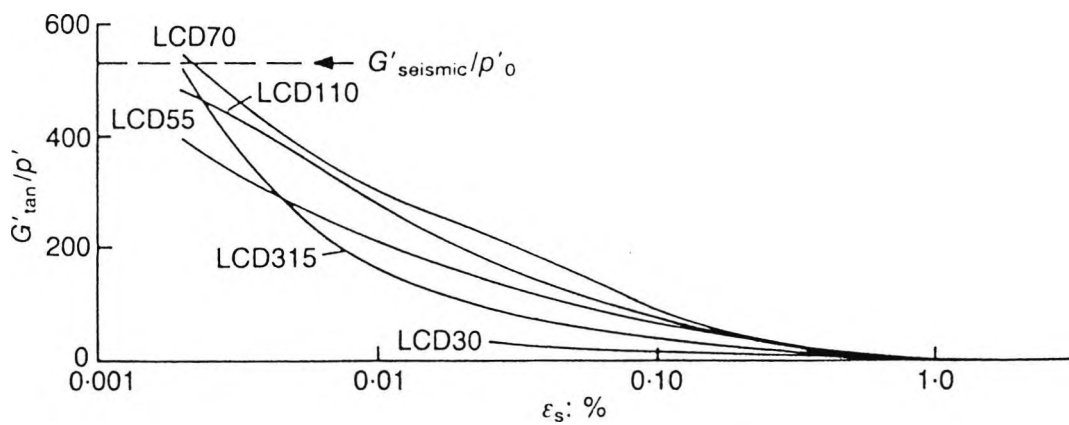


Figure 2.50 Stiffness curves following various stress path rotations (after Smith et al, 1992)

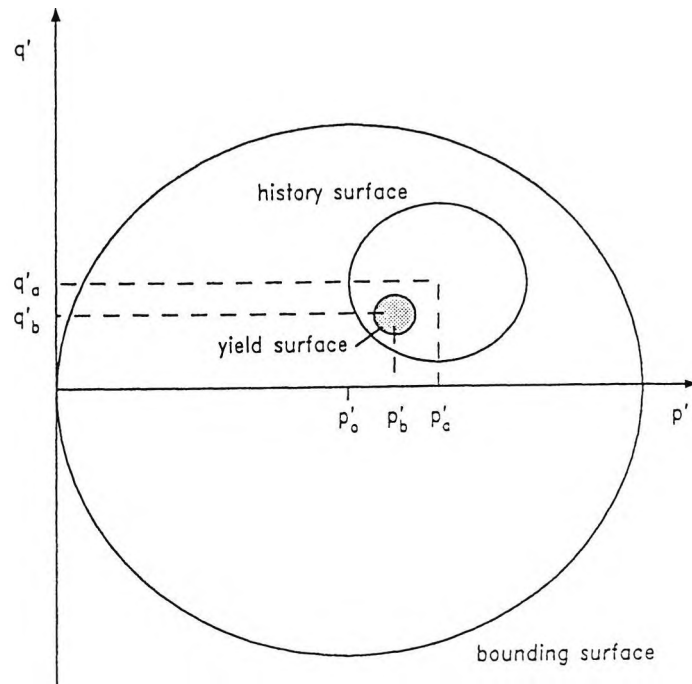


Figure 3.1 The three surface kinematic hardening model in stress space (after Stallebrass, 1990)

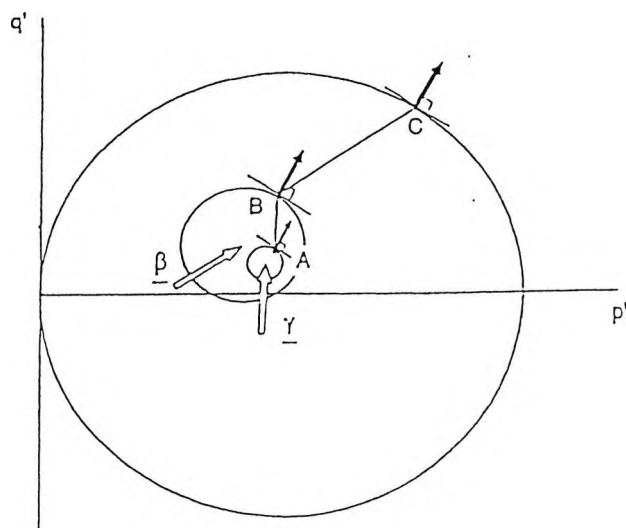


Figure 3.2 The principal of the translation rule for the kinematic surfaces in the 3-SKH model (after Stallebrass, 1990)

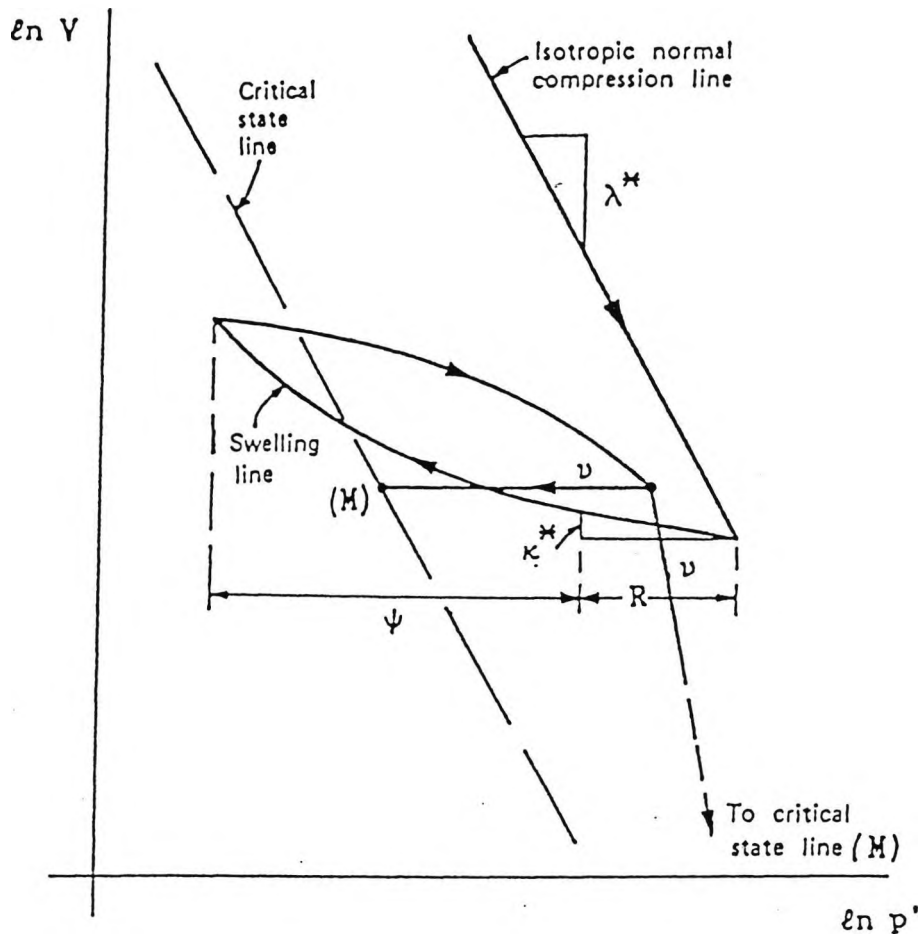


Figure 3.3 Normal compression line and swelling line in  $\ln v$ : $\ln p'$  space (after Al Tabbaa, 1987)

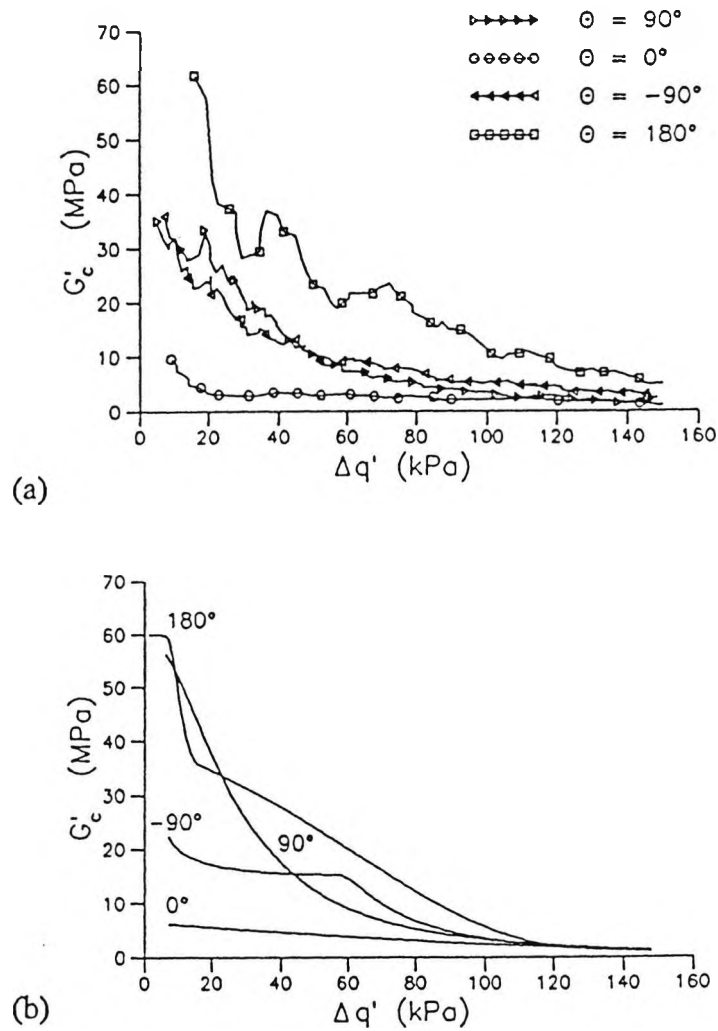


Figure 3.4 3-SKH model predictions for different stress path rotations (after Stallebrass and Taylor, 1997)

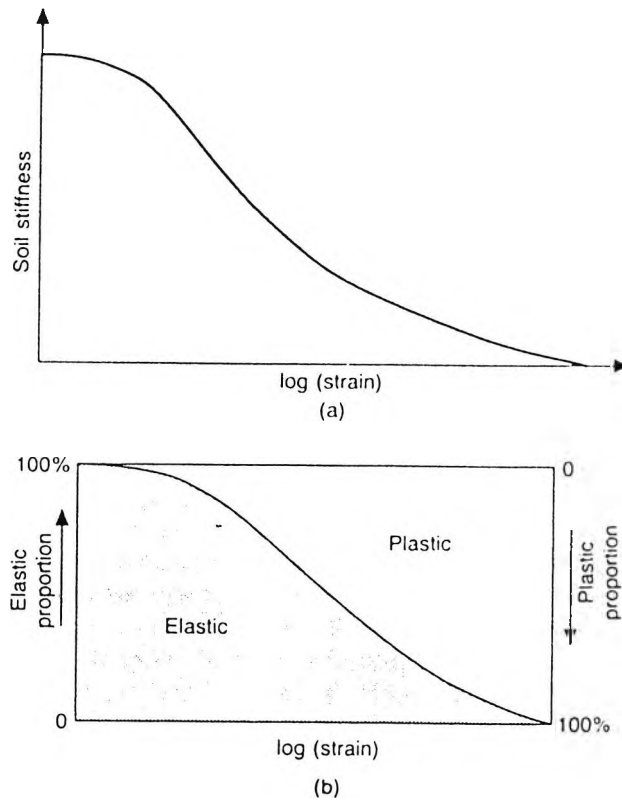


Figure 3.5 The s-shaped curve of stiffness against strain (after Simpson, 1992)

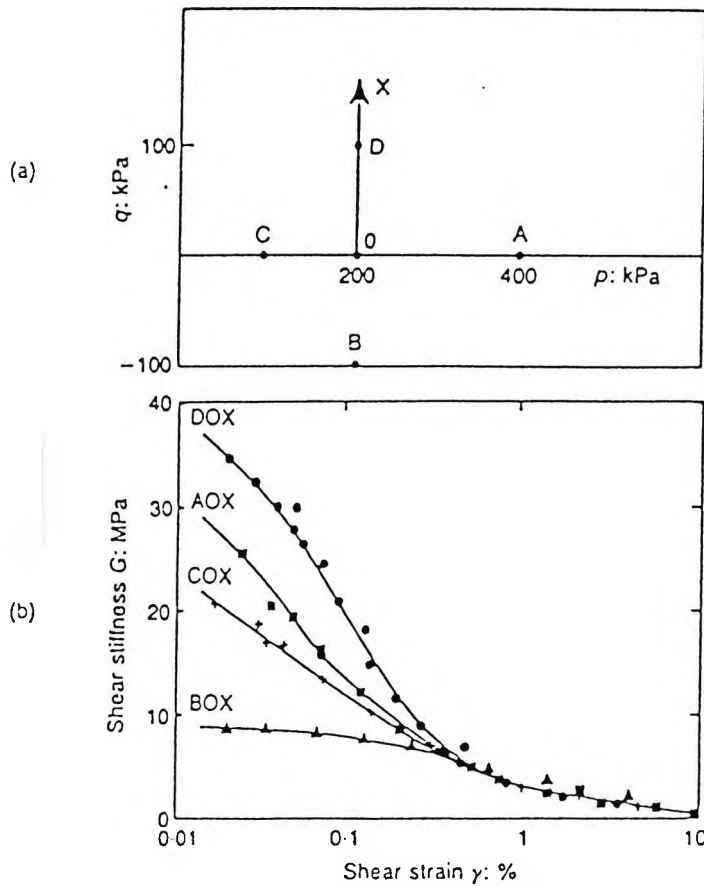


Figure 3.6 Recent stress history tests, results for path OX: a) stress paths; b) stiffness curves (after Richardson, 1988)

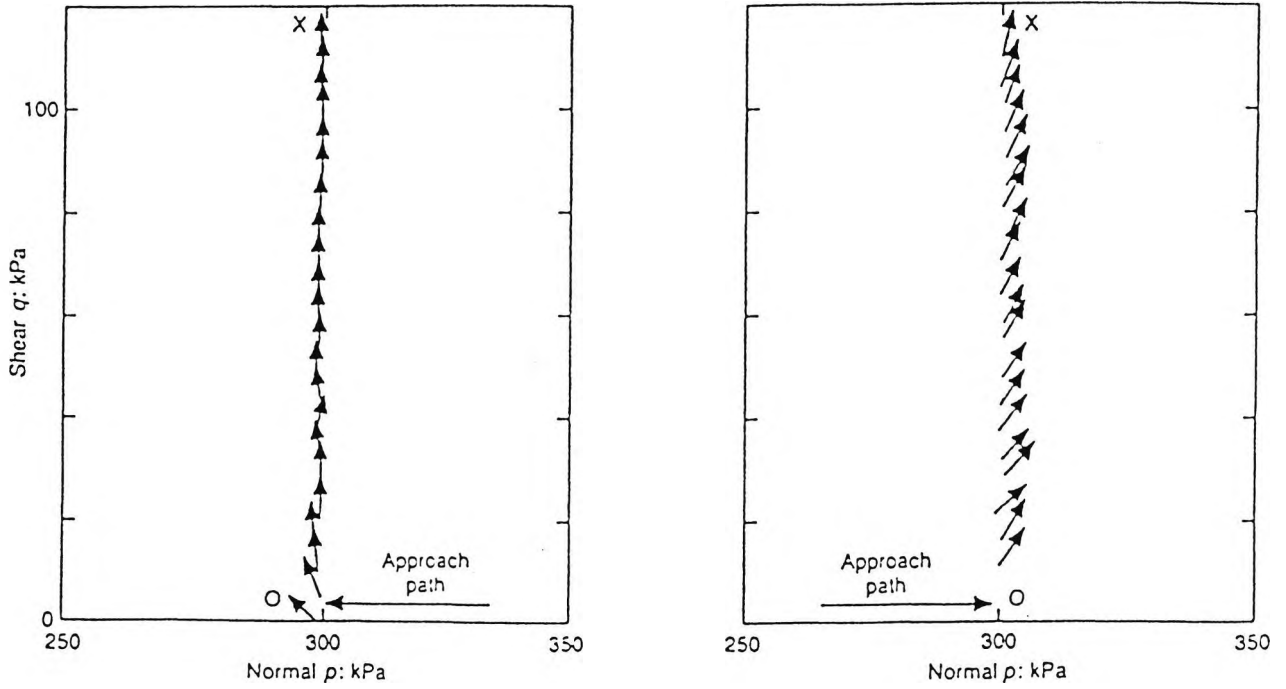


Figure 3.7 Strain vectors following different approach paths in stress space (after Stallebrass, 1990)

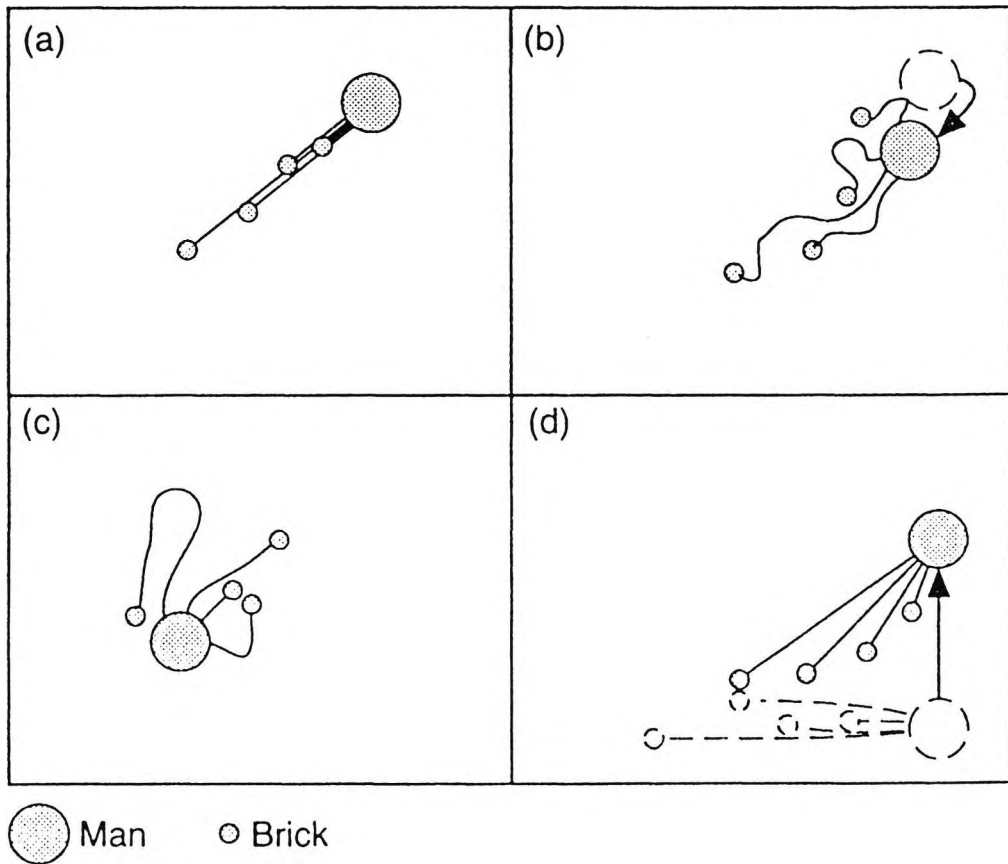


Figure 3.8 A man pulling bricks attached to him by strings in strain space (after Simpson, 1992)

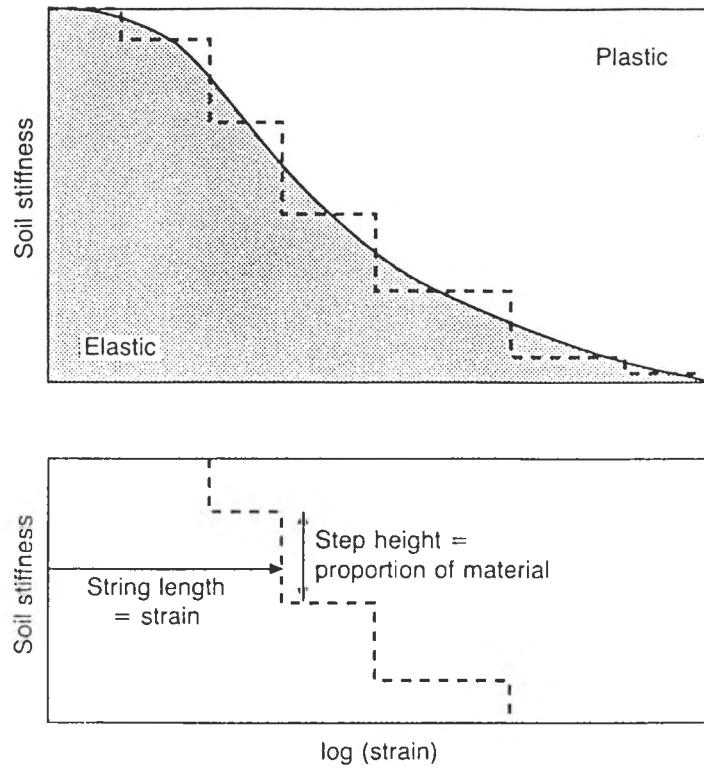


Figure 3.9 The s-shaped curve represented in a stepwise fashion by the brick concept (after Simpson, 1992)

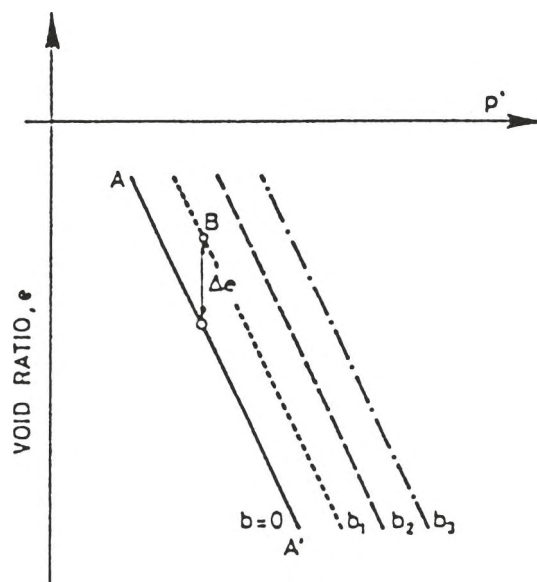


Figure 3.10 Isotropic normal compression lines for materials with various degrees of bonding (after Gens and Nova, 1993)

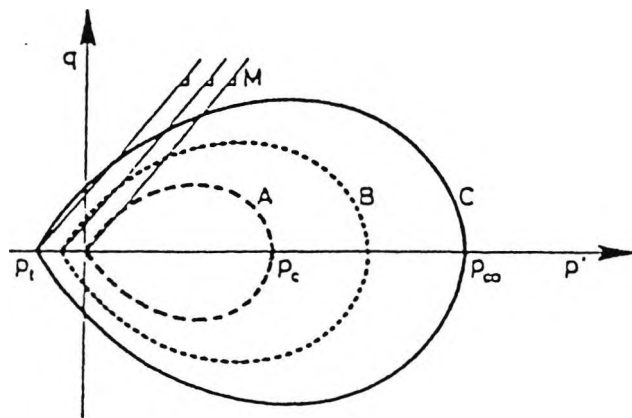


Figure 3.11 Successive yield surfaces for increasing degrees of bonding, with surface a representing the unbonded material (after Gens and Nova, 1993)

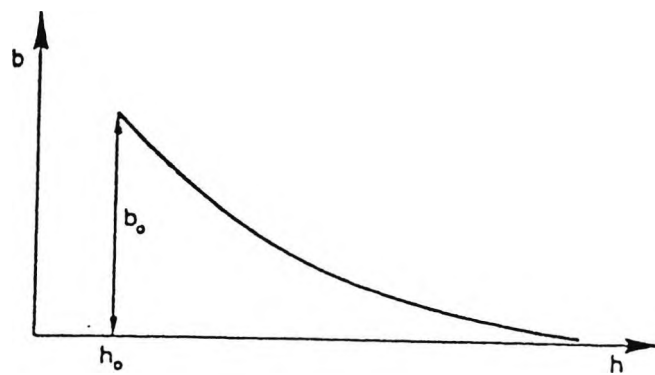


Figure 3.12 The reduction of bonding,  $b$ , with increasing damage (after Gens and Nova, 1993)

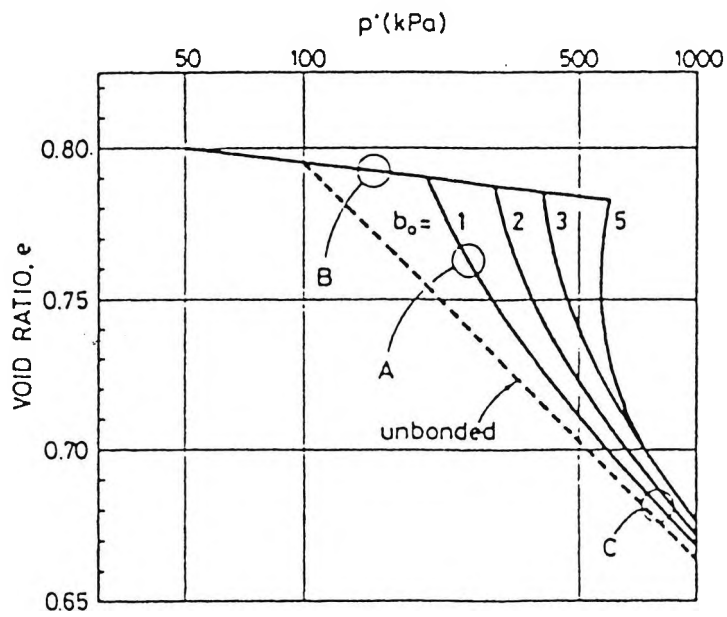


Figure 3.13 Predicted isotropic normal compression lines for materials with various degrees of bonding (after Gens and Nova, 1993)

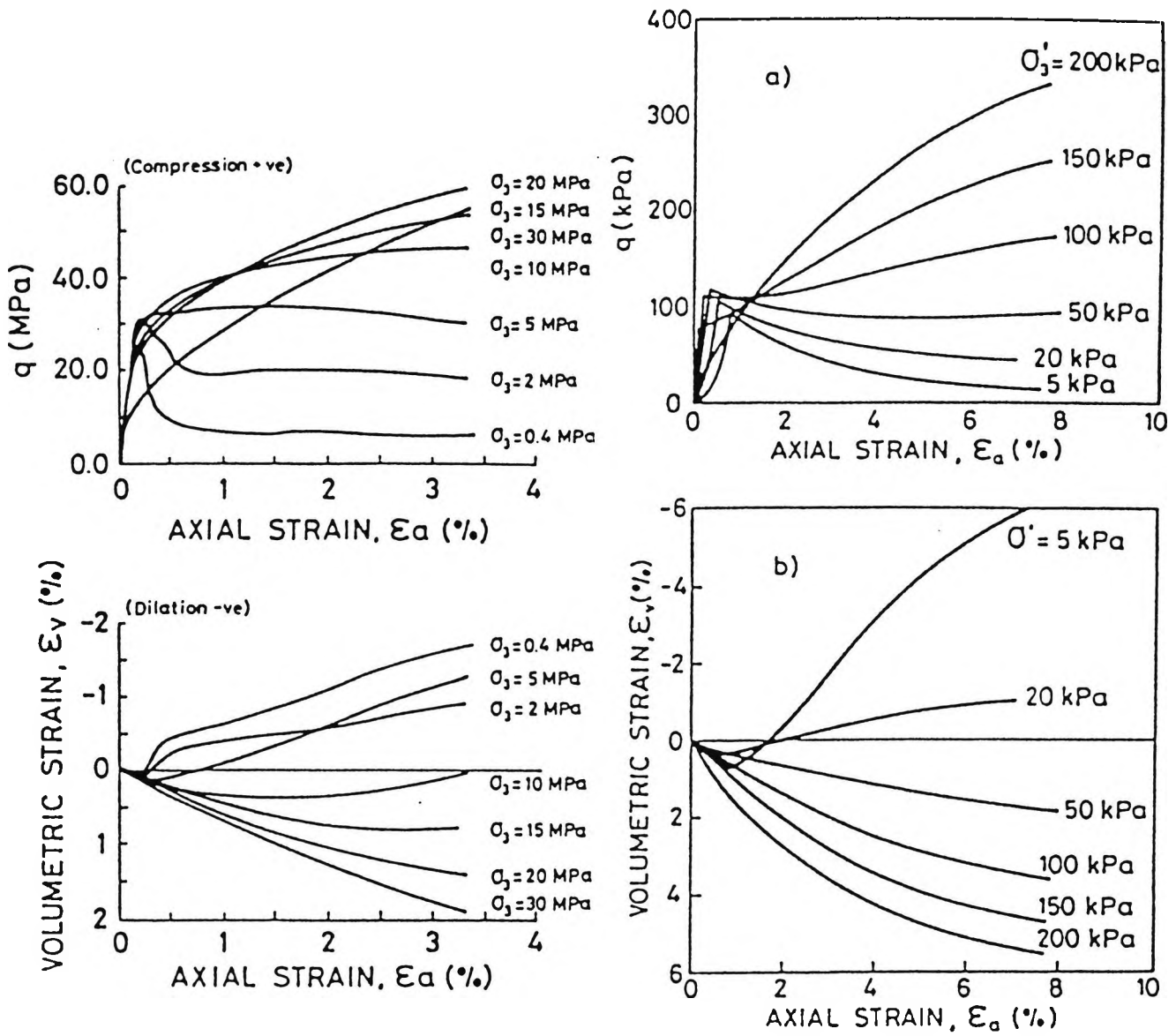


Figure 3.14 Measured and computed triaxial shearing test data: a) deviator stress versus axial strain; b) volumetric strain versus axial strain (after Gens and Nova, 1993)

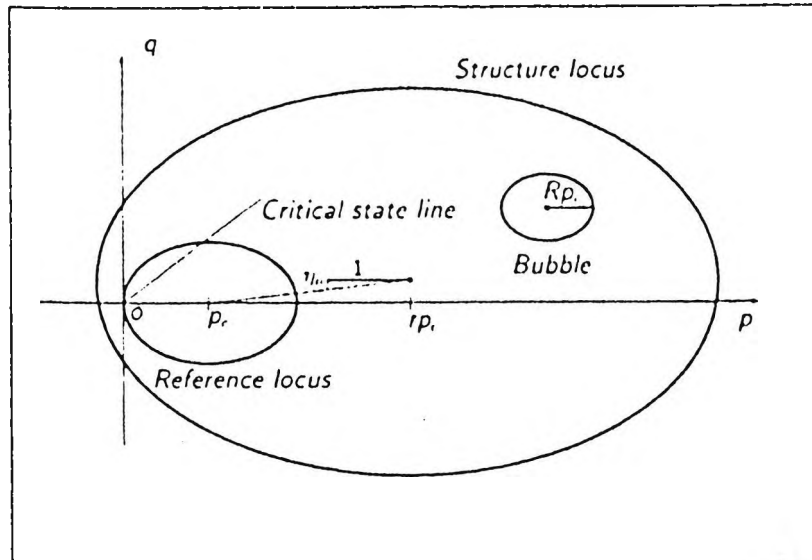


Figure 3.15 Model for destructurection of clays represented in stress space (after Rouainia and Muir Wood, 1998)

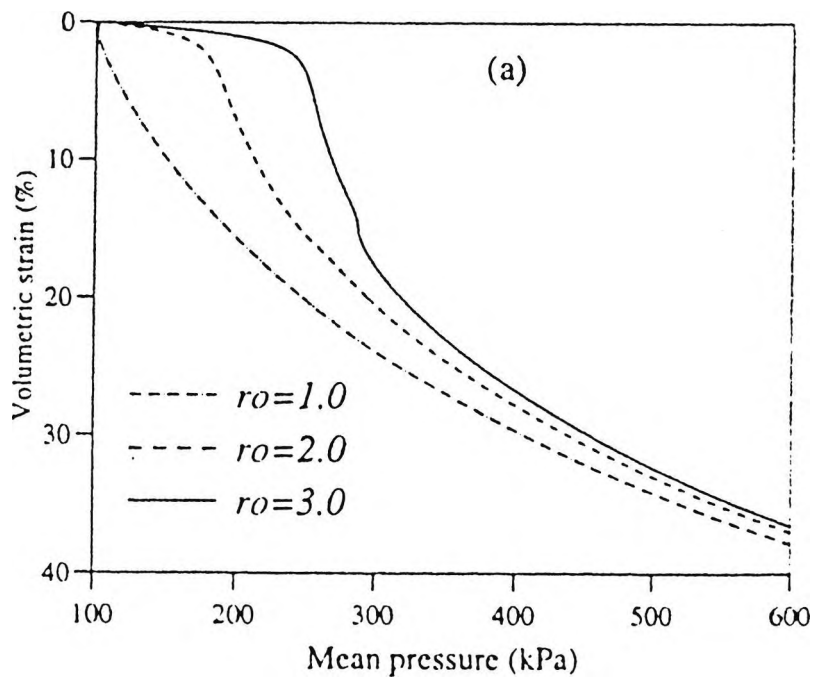


Figure 3.16 Predictions of one dimensional compression for various amounts of initial structure  $r_0$  (after Rouainia and Muir Wood, 1998)

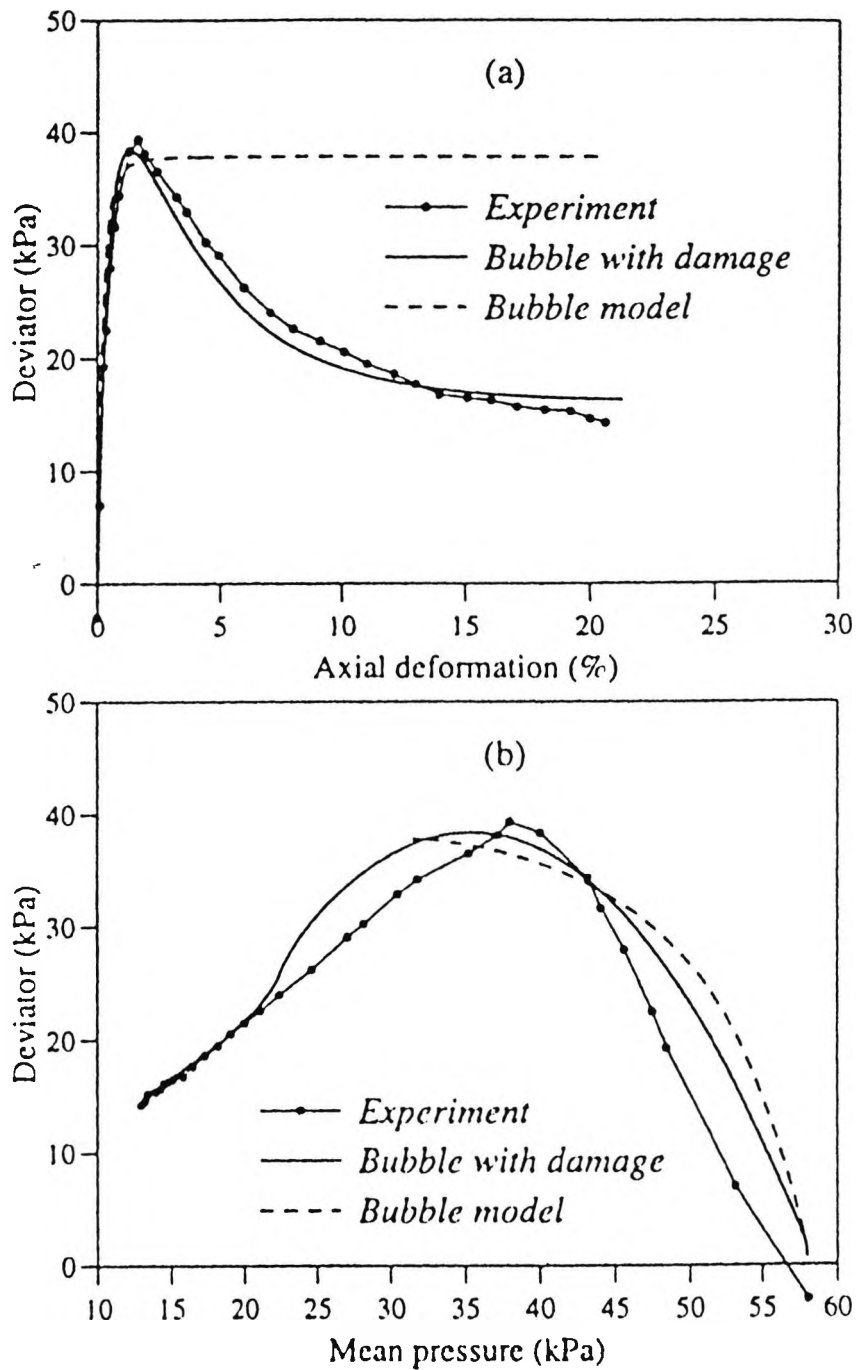


Figure 3.17 Comparison of model predictions and experimental data for an undrained triaxial test on Norrköping clay showing: a) stress-strain response; b) stress path (after Rouainia and Muir Wood, 1998)

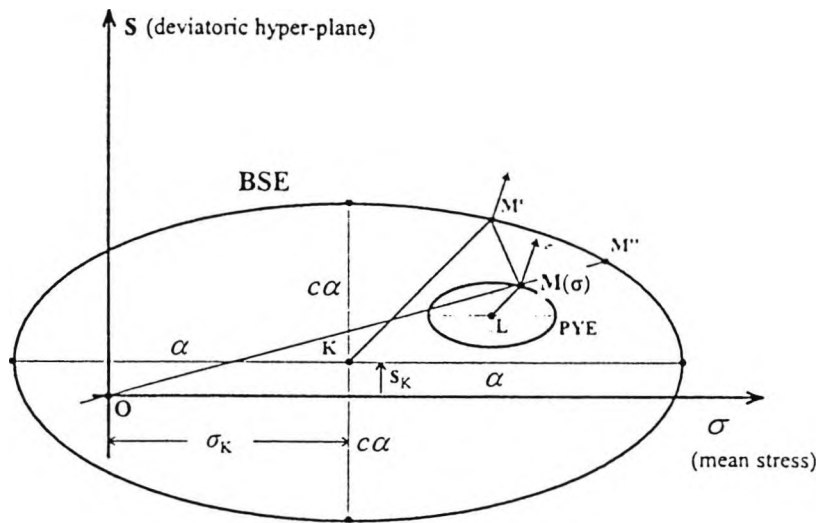


Figure 3.18 Characteristic surfaces of the MSS model (after Kavvadas and Amorosi, 1998)

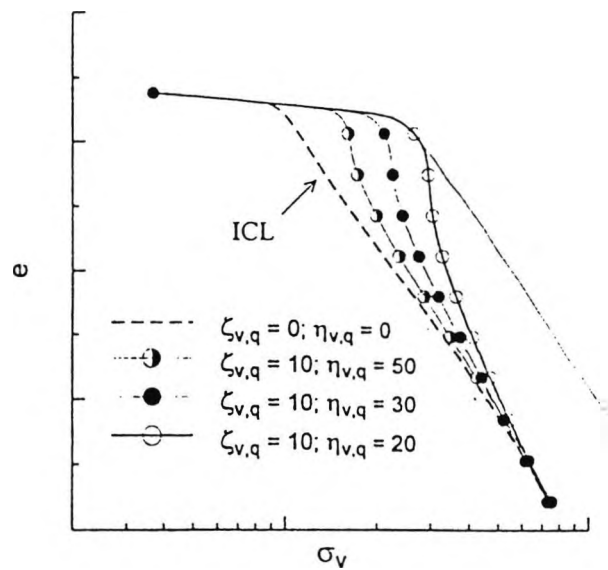


Figure 3.19 One dimensional compression curves computed by the MSS model for Various parameter combinations (after Kavvadas and Amorosi, 1998)

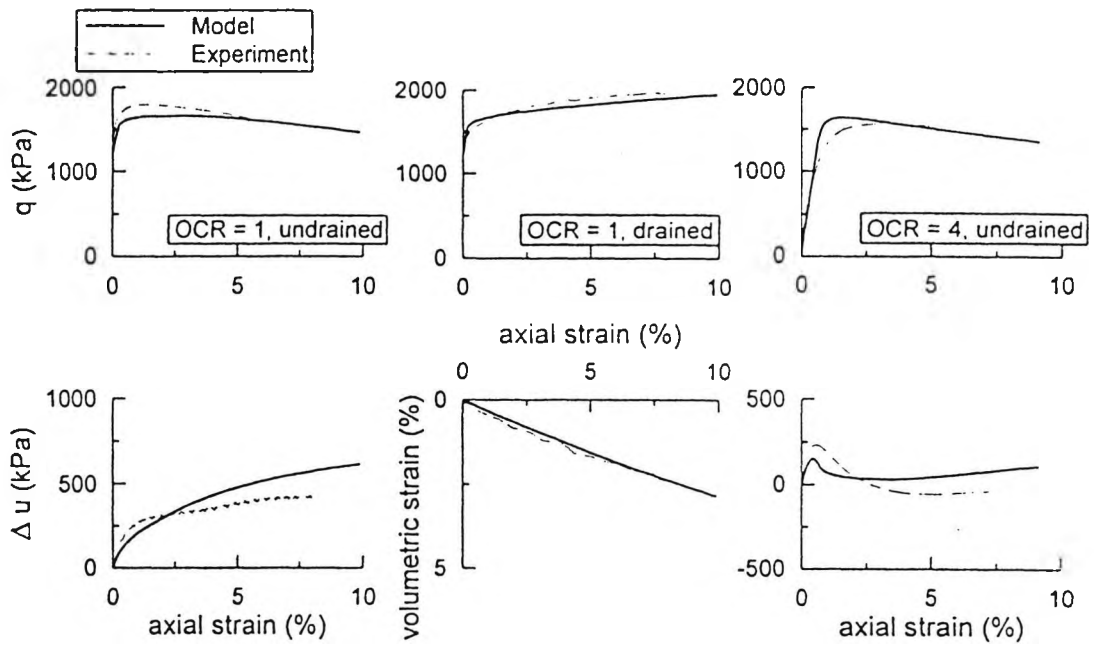


Figure 3.20 Comparison between experimental results and model predictions for medium pressure drained and undrained tests on anisotropically consolidated Vallericca clay (after Kavvadas and Amorosi, 1998)

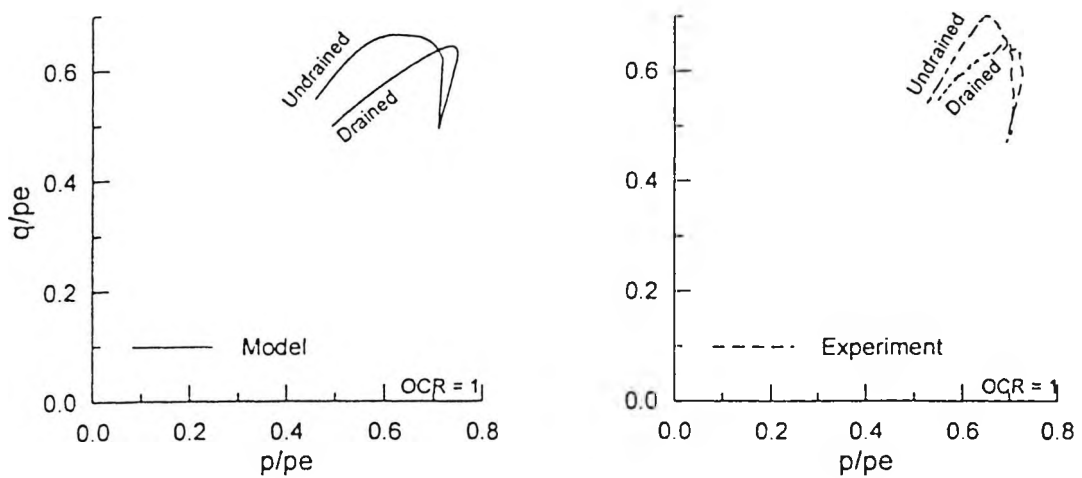


Figure 3.21 Comparison between normalised stress paths of experimental results and model predictions for medium pressure drained and undrained tests on anisotropically consolidated Vallericca clay (after Kavvadas and Amorosi, 1998)

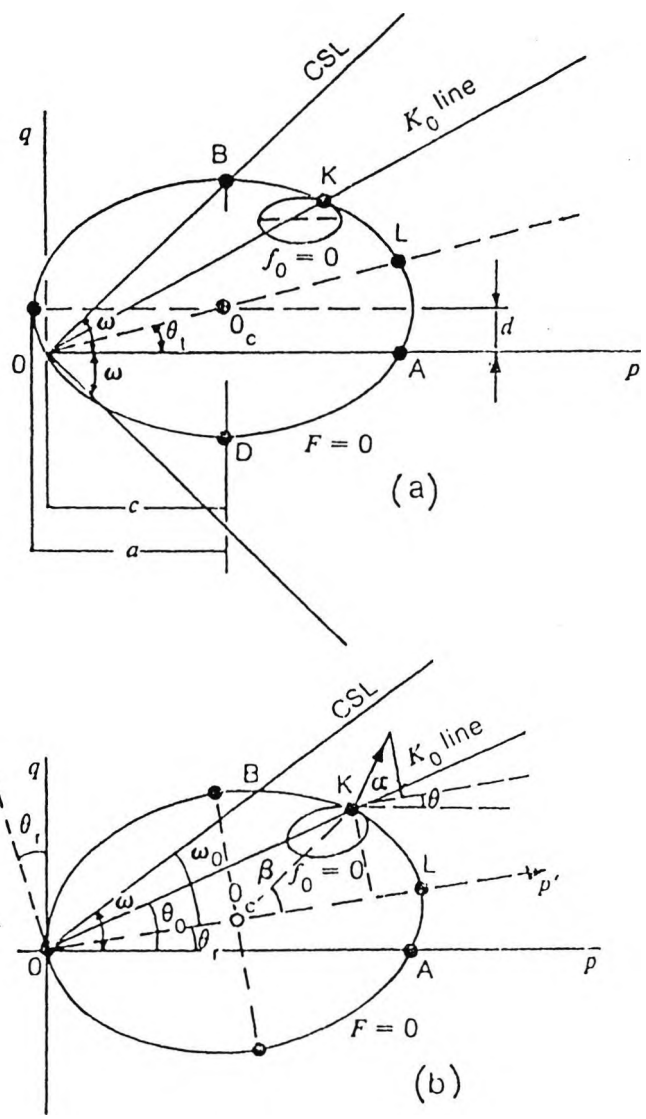


Figure 3.22 Proposed anisotropic bounding surfaces: a) translated; b) rotated (after Mroz et al., 1979)

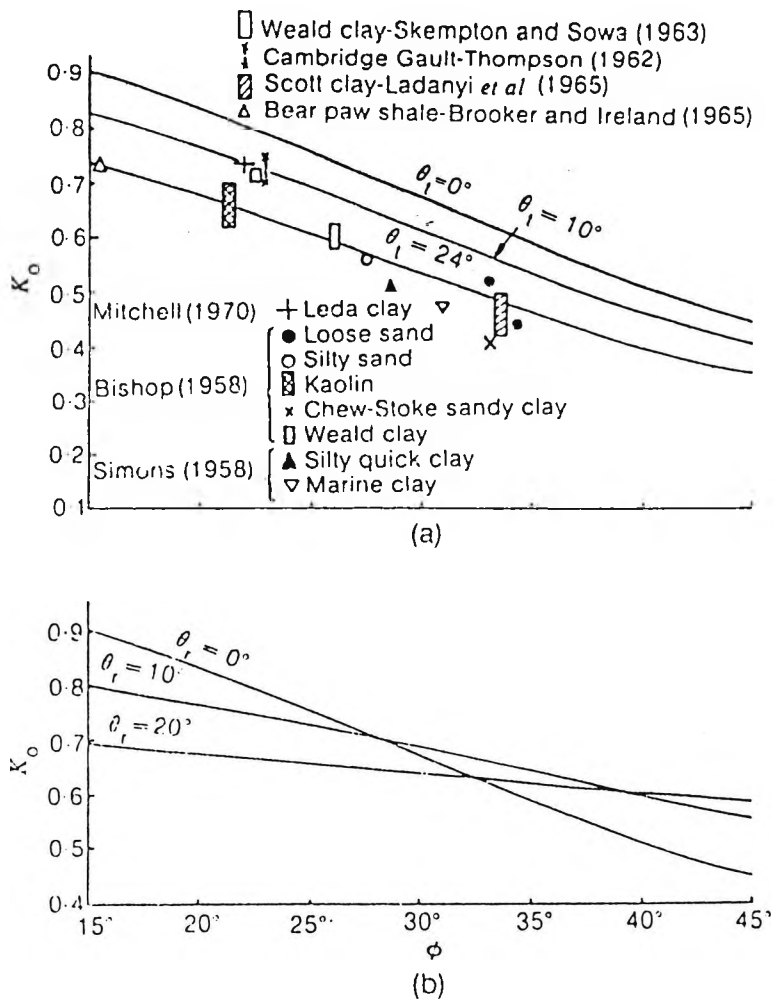


Figure 3.23 Model predictions of  $K_0$  for; a) translated bounding surface; b) rotated bounding surface (after Mroz *et al*, 1979)

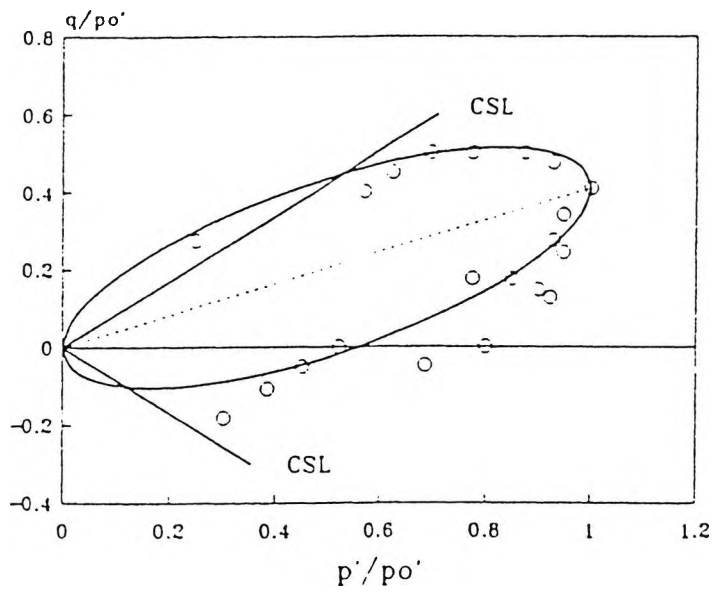


Figure 3.24 Proposed yield surface compared with experimental results (after Davies and Newson, 1993)

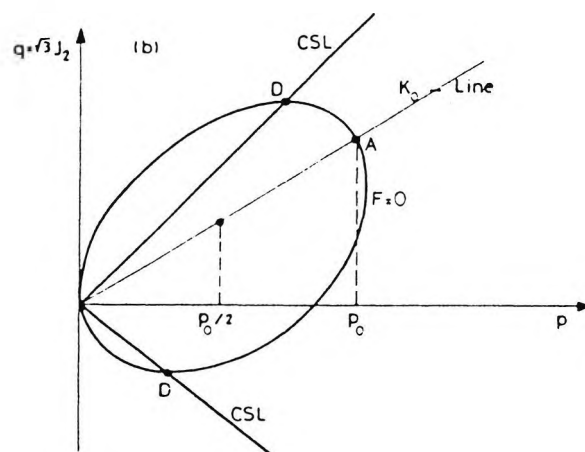


Figure 3.25 Yield surface for anisotropic model in stress space (after Banerjee and Yousef, 1986)

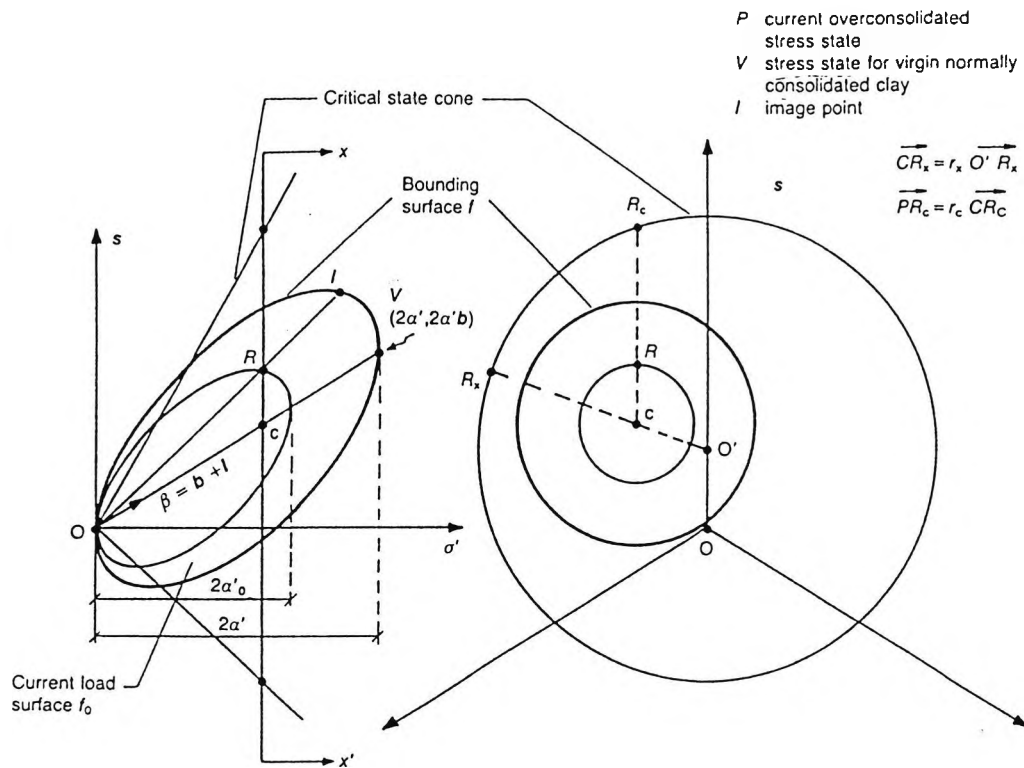


Figure 3.26 Yield, failure and loading surfaces for MIT-E3 model (after Whittle, 1993)

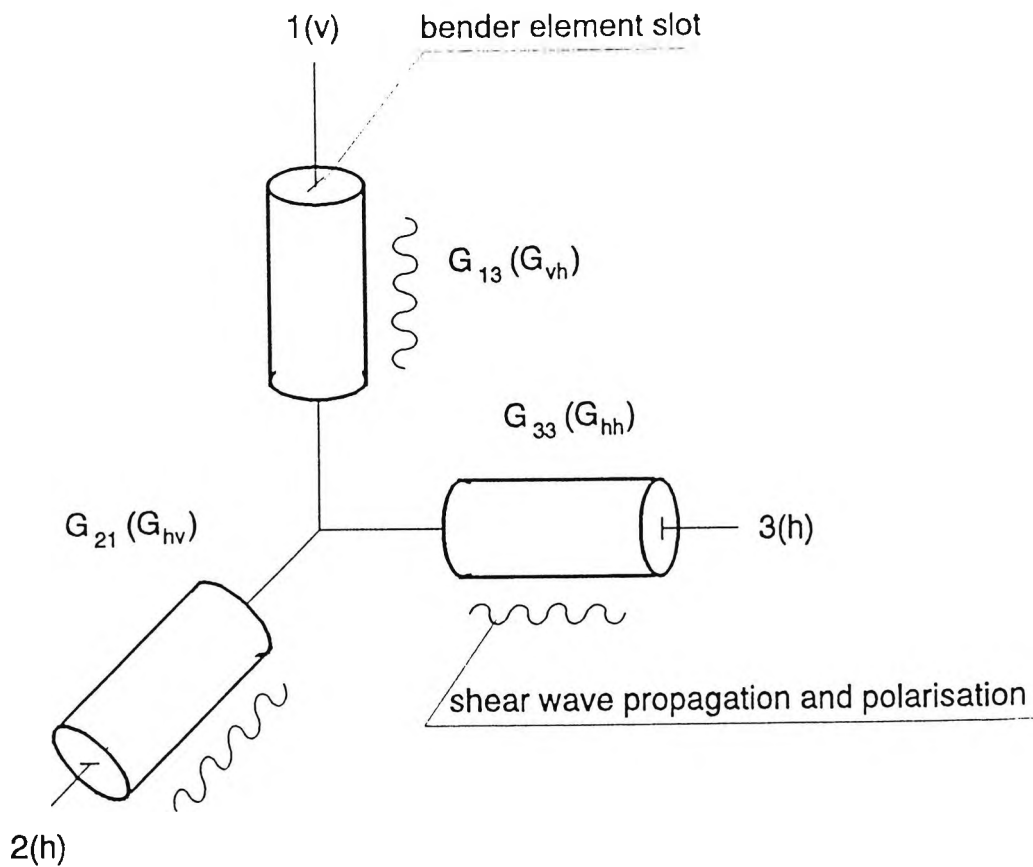
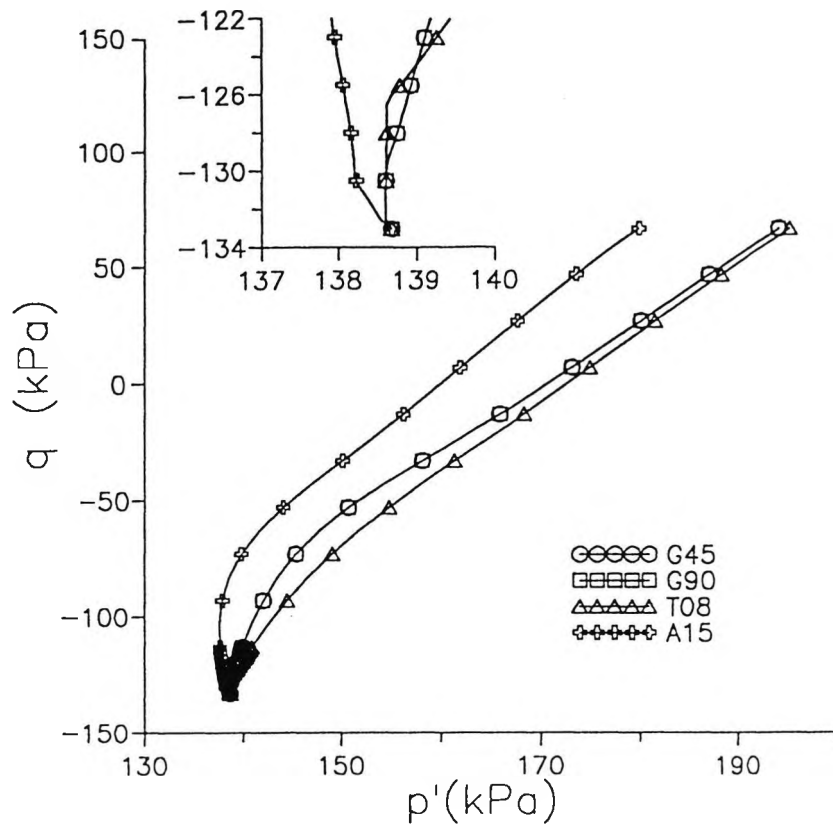
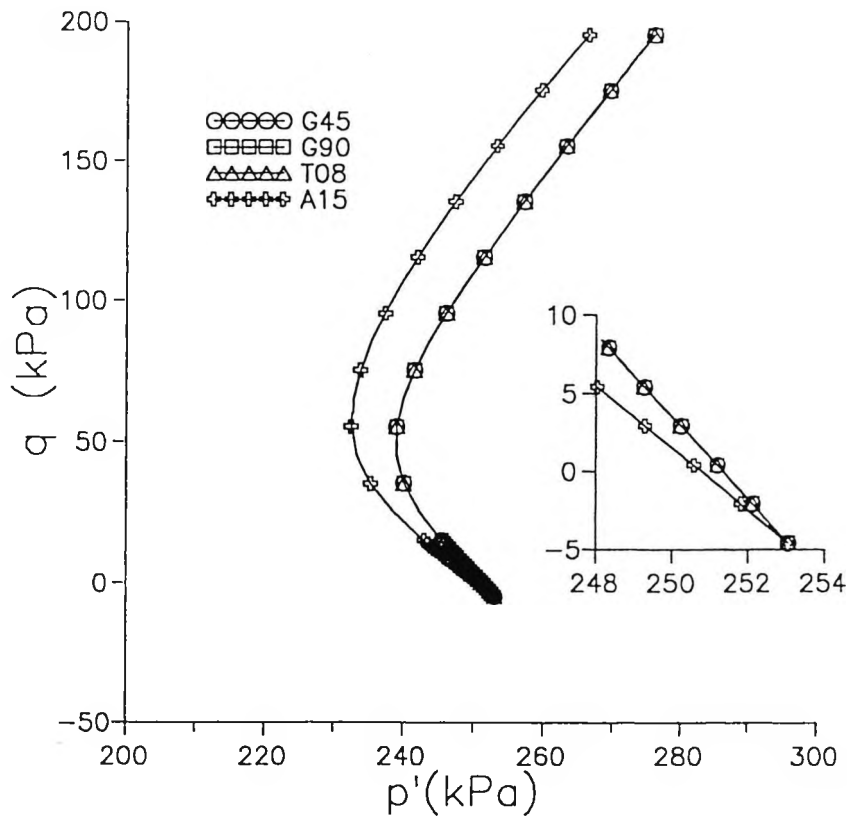


Figure 3.27 Definition of anisotropic parameters for  $G_{\max}$



a) after History 1



b) after History 2

Figure 3.28 Stress paths during undrained shearing for the version of the 3-SKH model incorporating anisotropic values of  $G_{max}$  (after Jovicic, 1997)

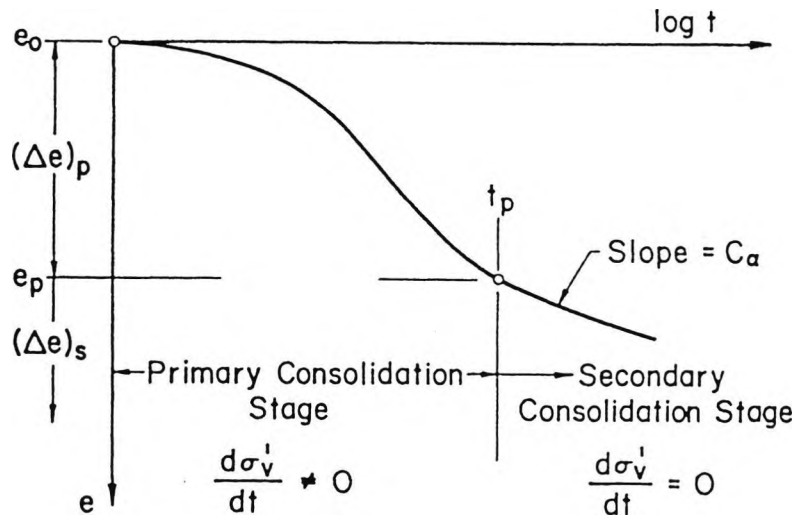


Figure 3.29 Definition of primary and secondary consolidation (after Mesri and Choi, 1985)

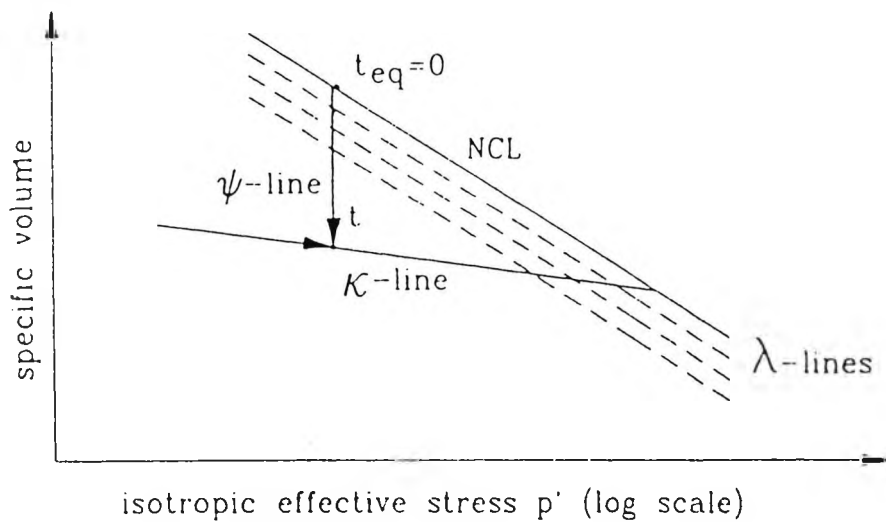


Figure 3.30 Definition of equivalent time (after Burhignoli et al, 1994)

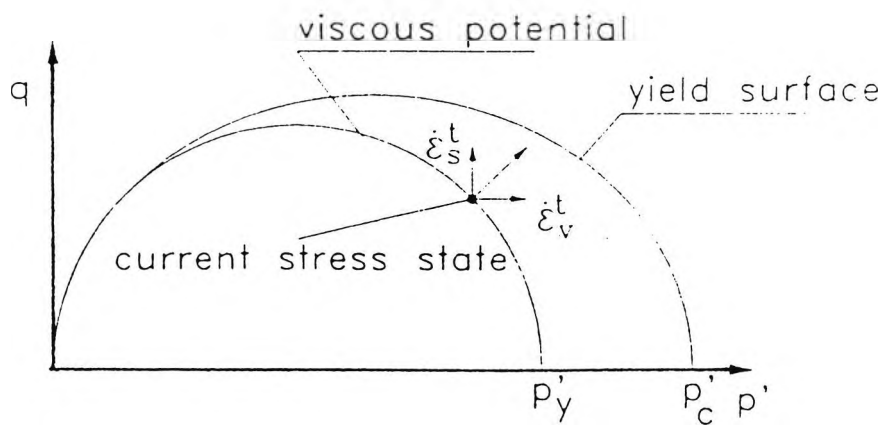


Figure 3.31 Definition of creep model in stress space (after Burghignoli et al, 1994)

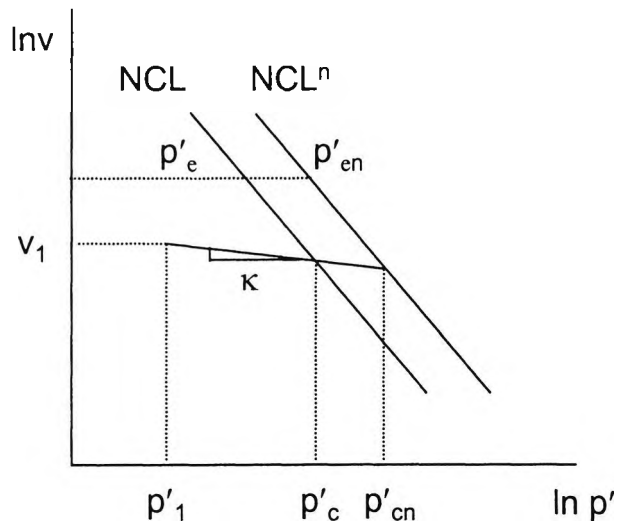


Figure 4.1 Schematic showing location of reconstituted and natural normal compression lines in  $\ln v:\ln p'$  space for a natural clay with stable fabric and  $S_t > 1$

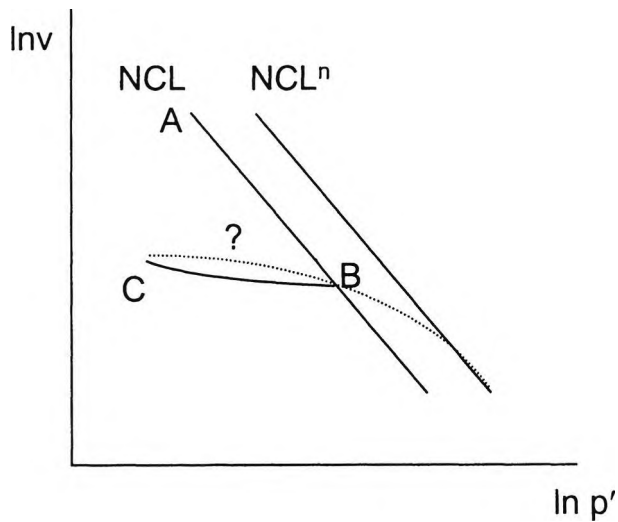


Figure 4.2 Schematic showing possible path taken in  $\ln v:\ln p'$  space during deposition of a clay deposit

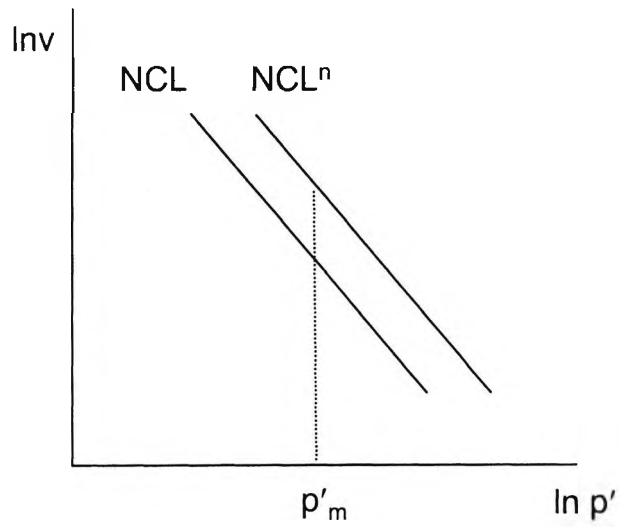


Figure 4.3 Schematic showing the relative locations of points defined on the reconstituted and natural normal compression lines by the mean effective stress due to overburden

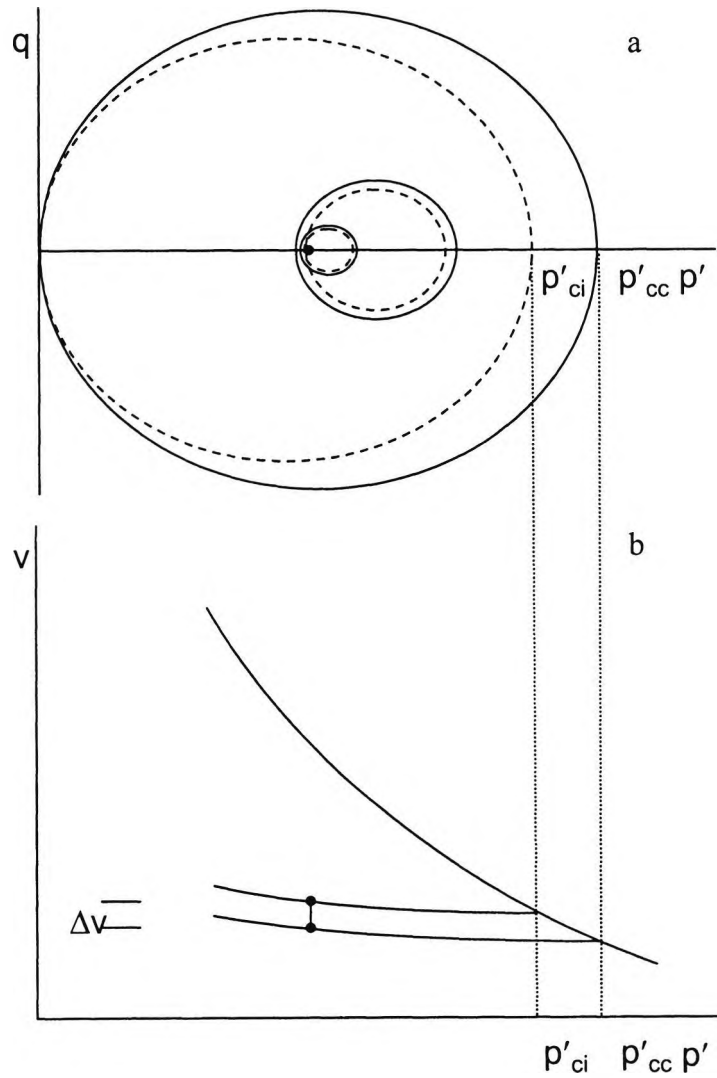


Figure 4.4 The inclusion of volumetric creep in the 3-SKH model; a) in stress space; b) in volumetric space

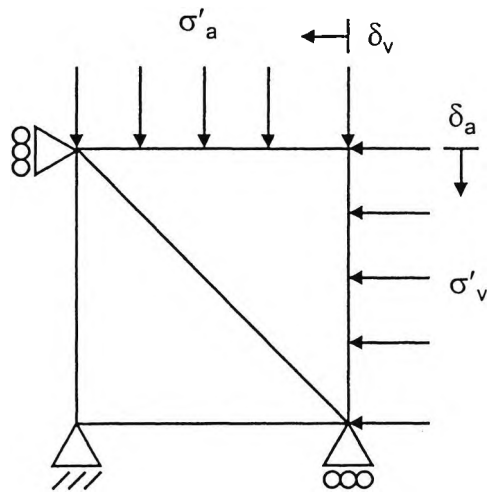


Figure 5.1 Finite element mesh representing a 'single element' of uniform soil for the analysis of triaxial tests.

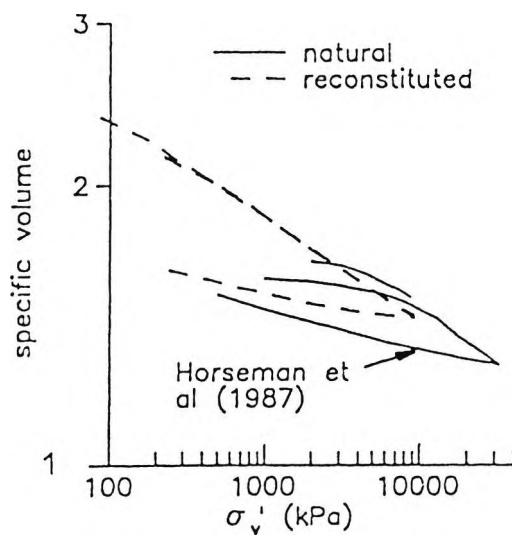


Figure 5.2 One dimensional normal compression lines of natural and reconstituted Boom clay (after Coop et al., 1995)

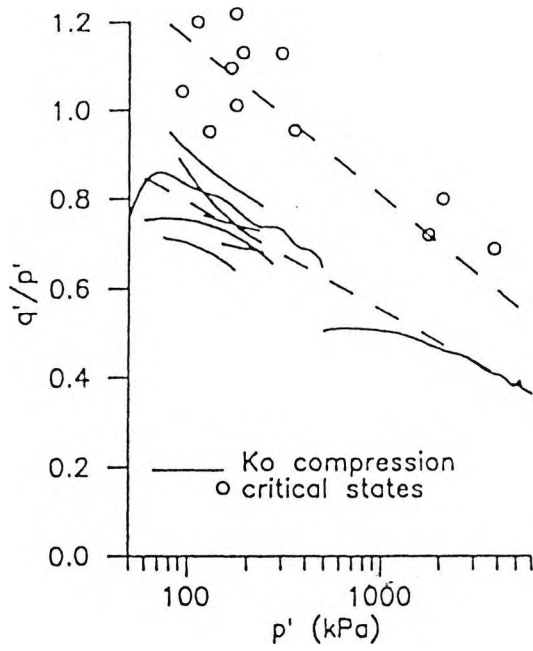


Figure 5.3 Variation of stress ratio at failure with mean effective stress for Boom clay (after Coop et al., 1995)

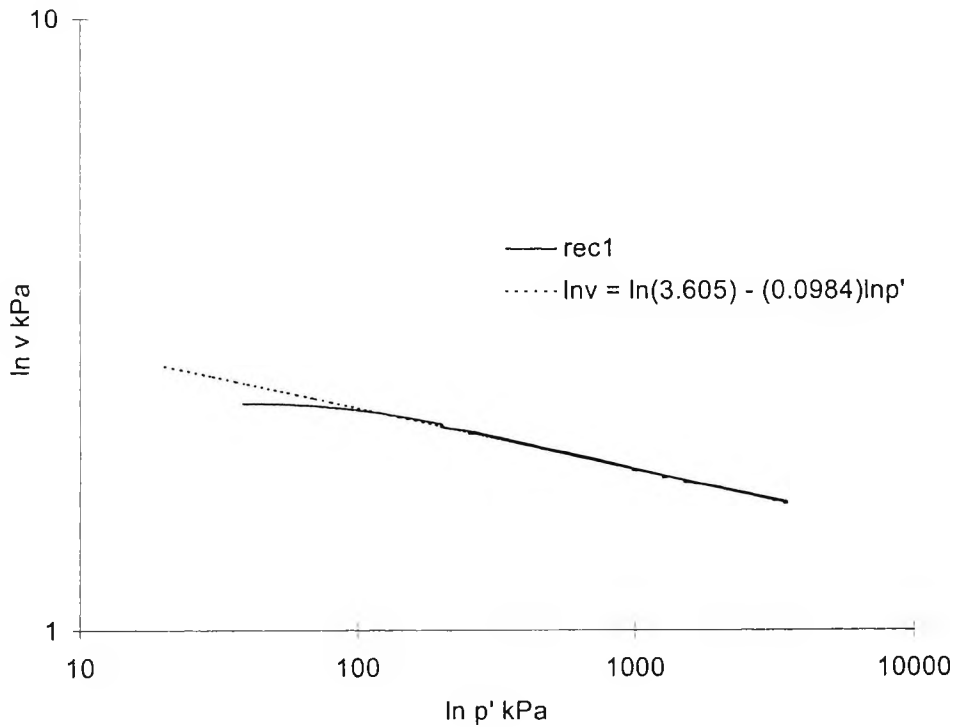


Figure 5.4 Reconstituted isotropic normal compression data for test *rec1* showing calculated normal compression line

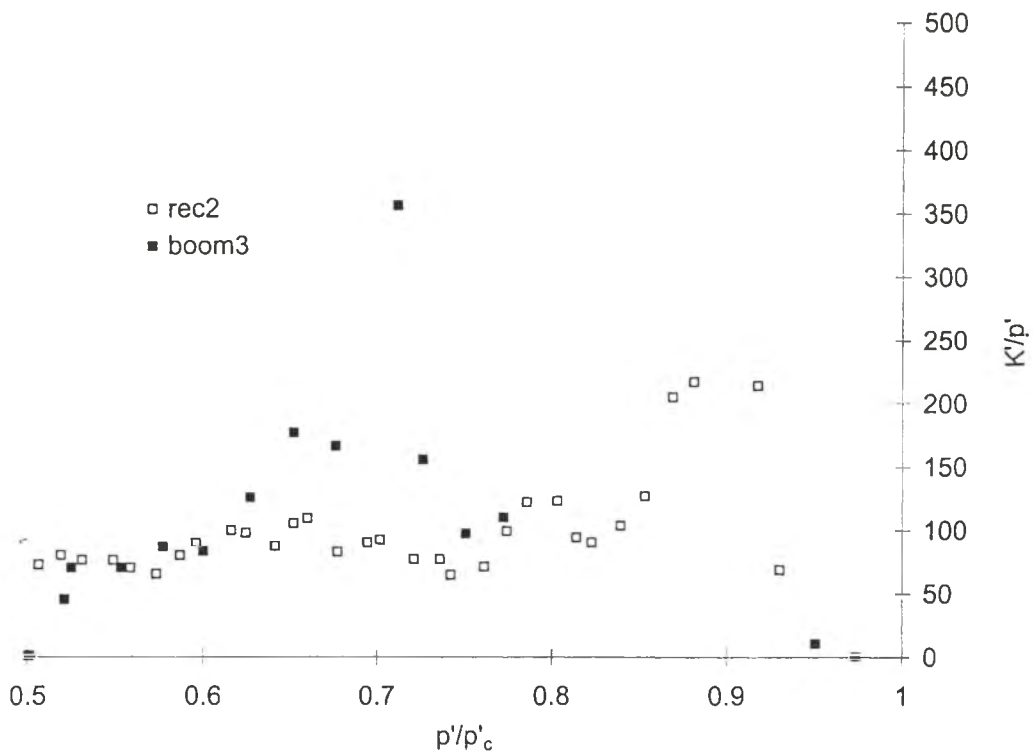


Figure 5.5 Isotropic swelling stages for tests rec2 and boom3 plotted as bulk modulus divided by mean effective stress against mean effective stress normalised by the preconsolidation pressure on the reconstituted normal compression line.

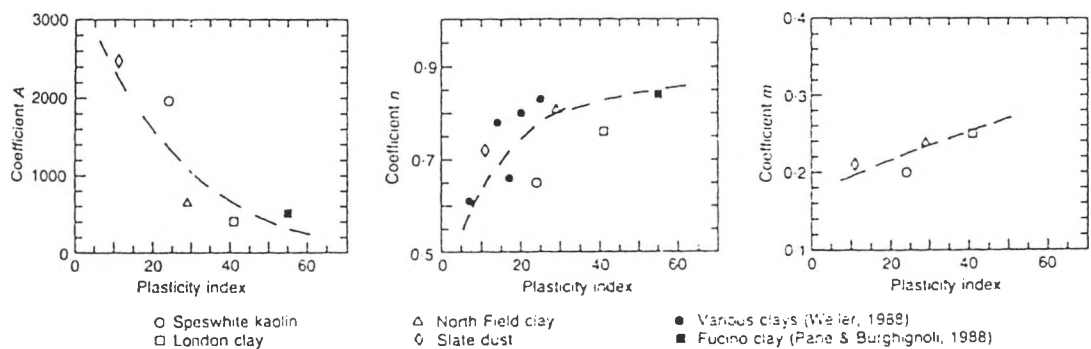


Figure 5.6 Charts linking the plasticity index with the stiffness coefficients A, n, m (after Viggiani and Atkinson, 1995)

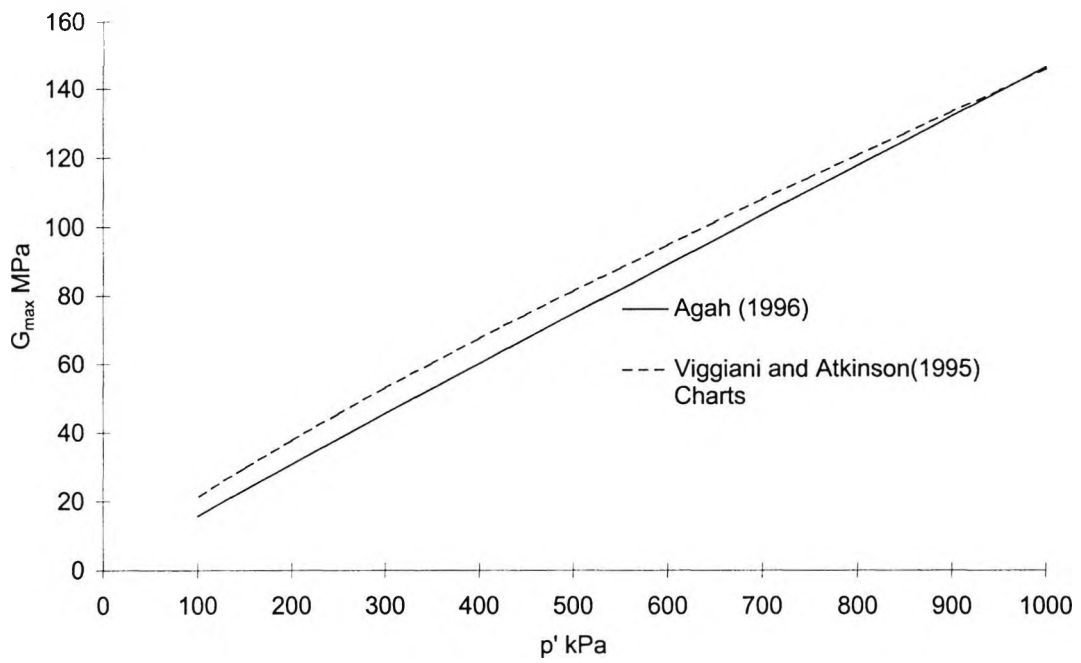


Figure 5.7 Predictions of  $G_{max}$  against mean effective stress using parameters derived from Agah (1996) and from charts presented by Viggiani and Atkinson (1995)

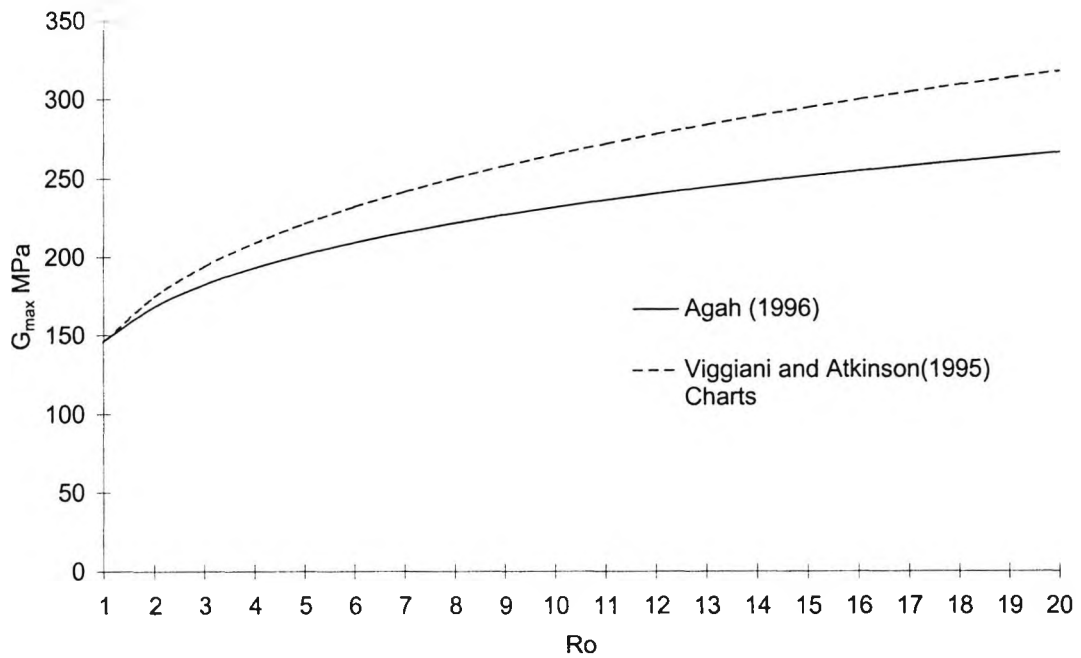


Figure 5.8 Predictions of  $G_{max}$  against overconsolidation ratio using parameters derived from Agah (1996) and from charts presented by Viggiani and Atkinson (1995)

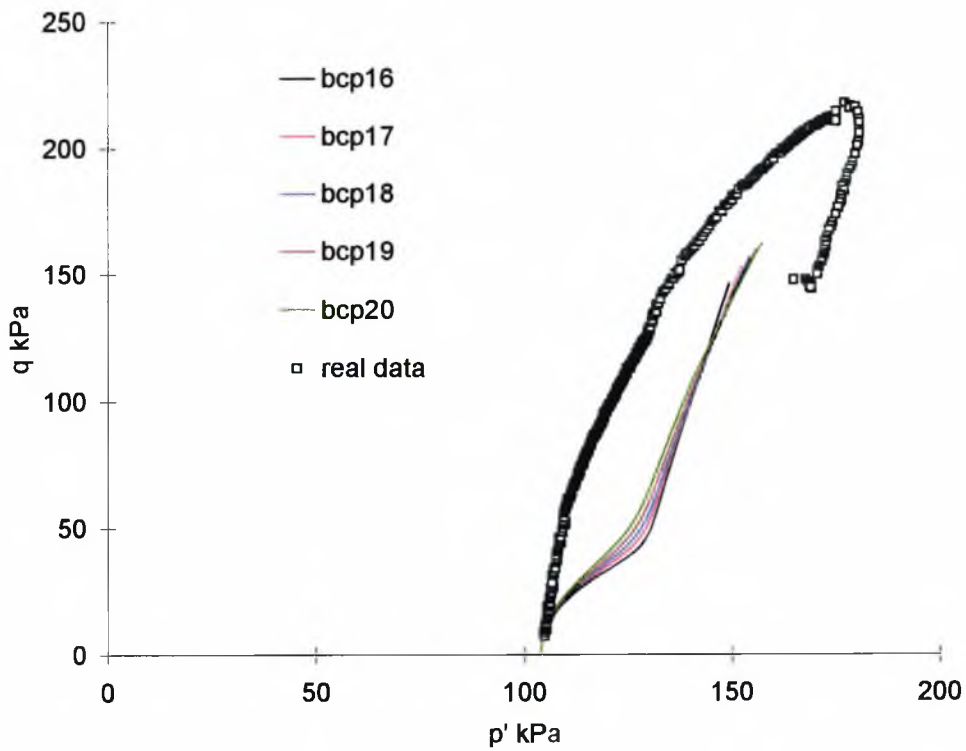


Figure 5.9 Stress path predictions for test *ruth* for parameter sets 16-20

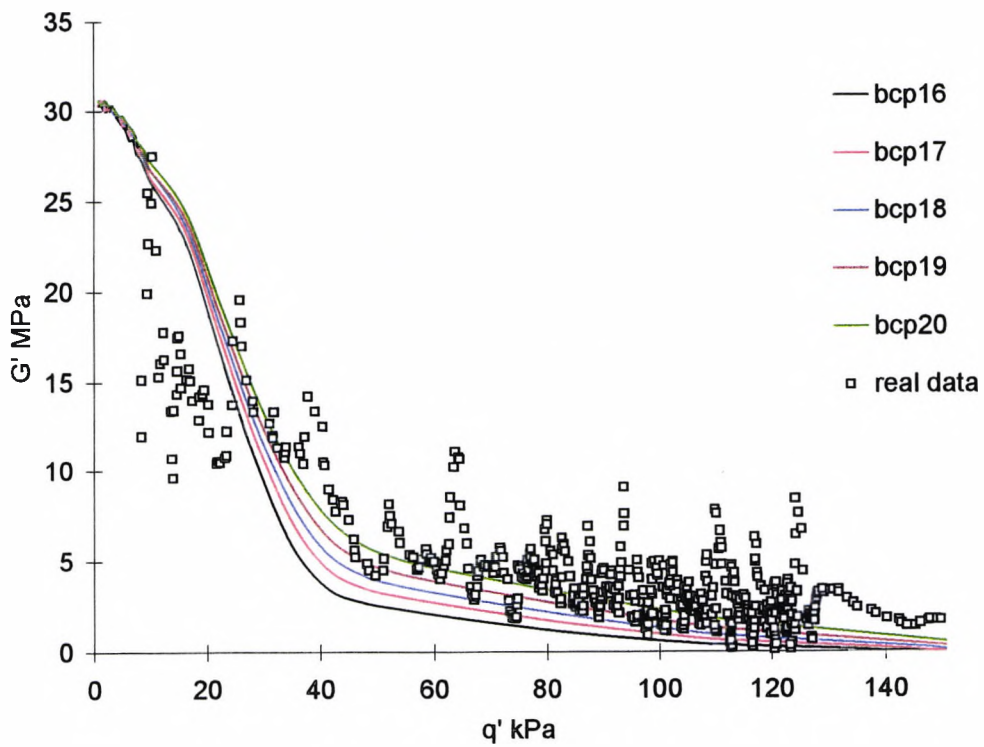


Figure 5.10 Shear stiffness predictions for test *ruth* for parameter sets 16-20

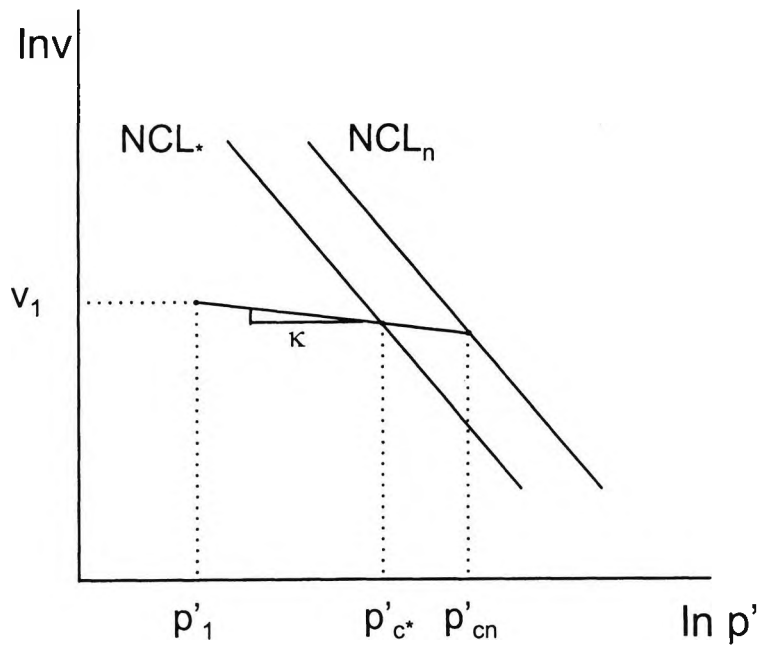


Figure 5.11 Schematic diagram showing the relative positions of the reconstituted and natural normal compression lines in volumetric space.

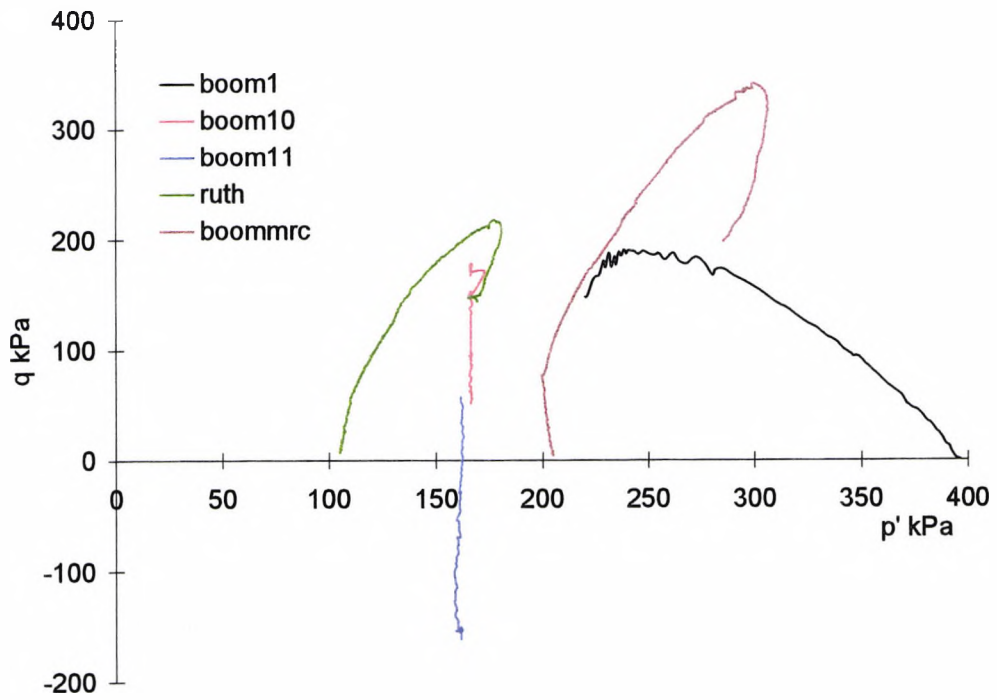


Figure 5.12 Drained and undrained stress paths for reconstituted samples of Boom clay

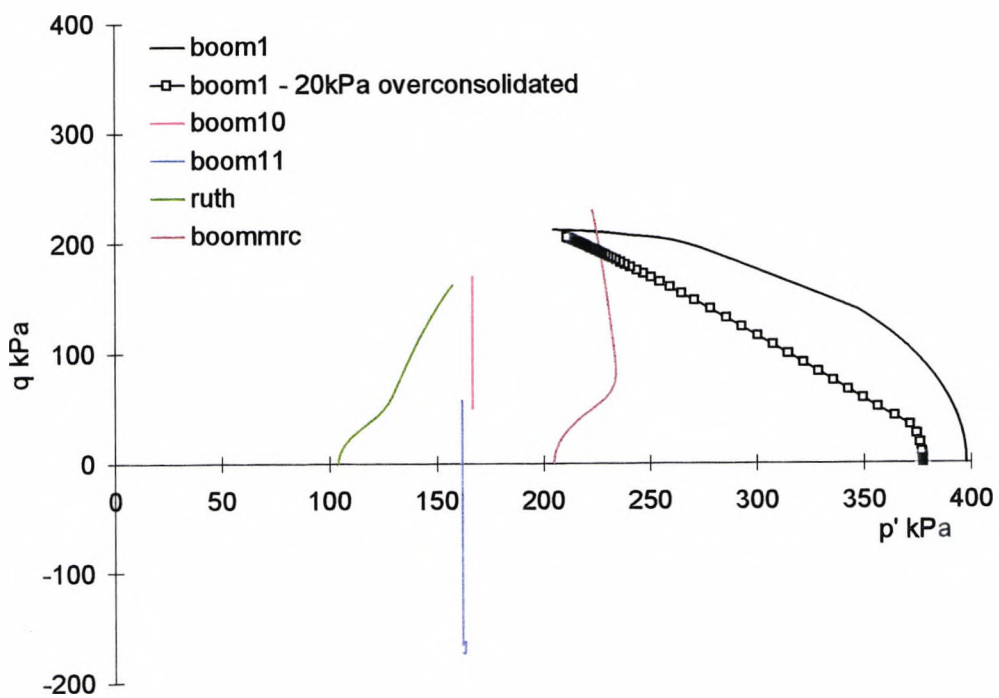


Figure 5.13 3-SKH model predictions of drained and undrained stress paths for reconstituted samples of Boom clay

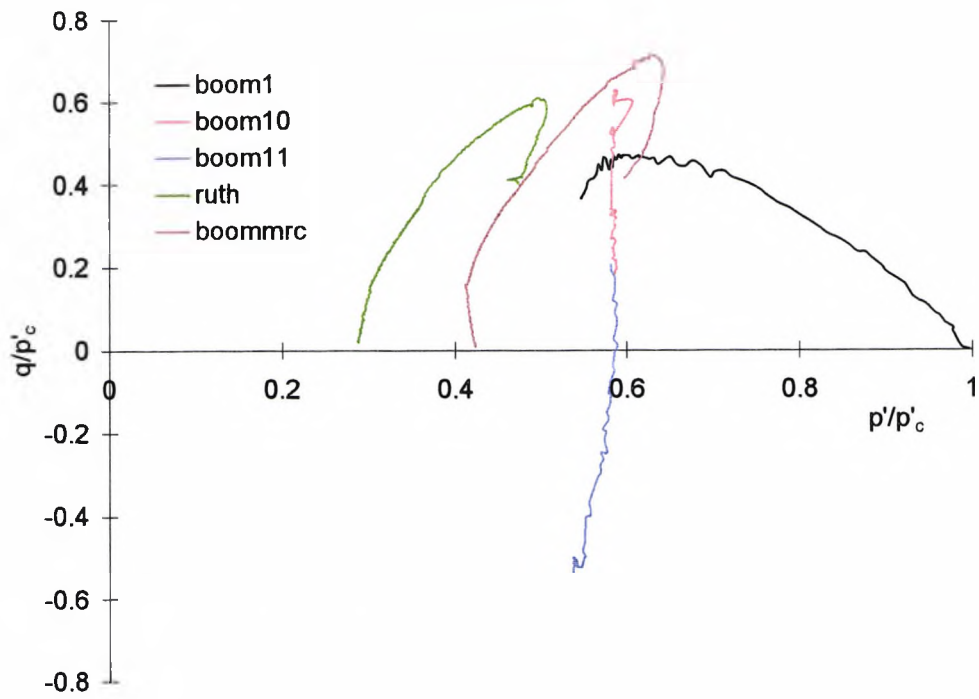


Figure 5.14 Drained and undrained stress paths for reconstituted samples of Boom clay normalised by the current preconsolidation pressure

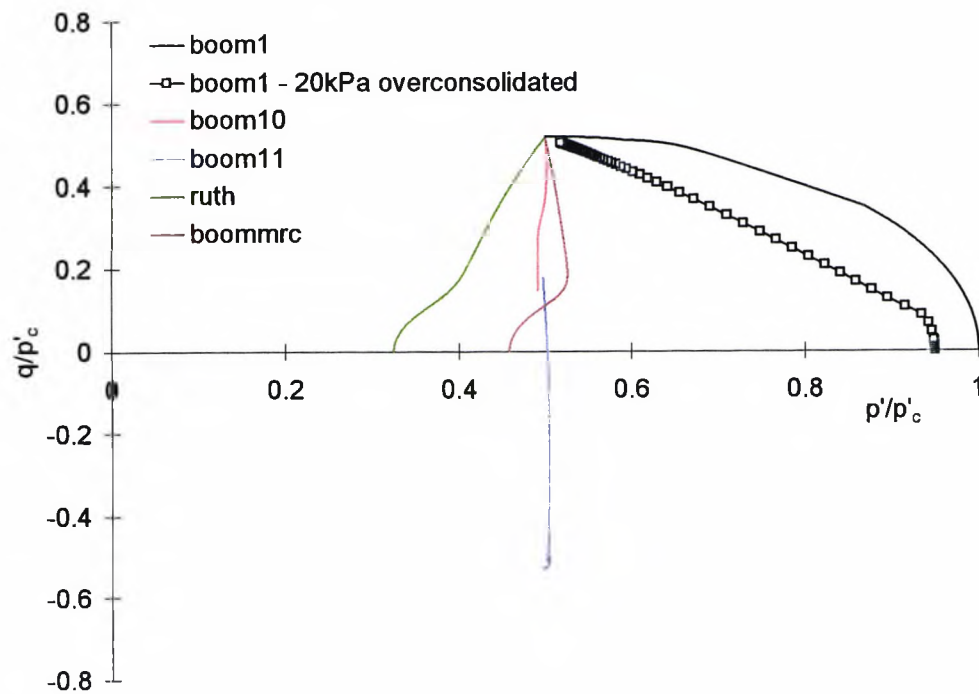


Figure 5.15 3-SKH model predictions of drained and undrained stress paths for reconstituted samples of Boom clay normalised by the current preconsolidation pressure

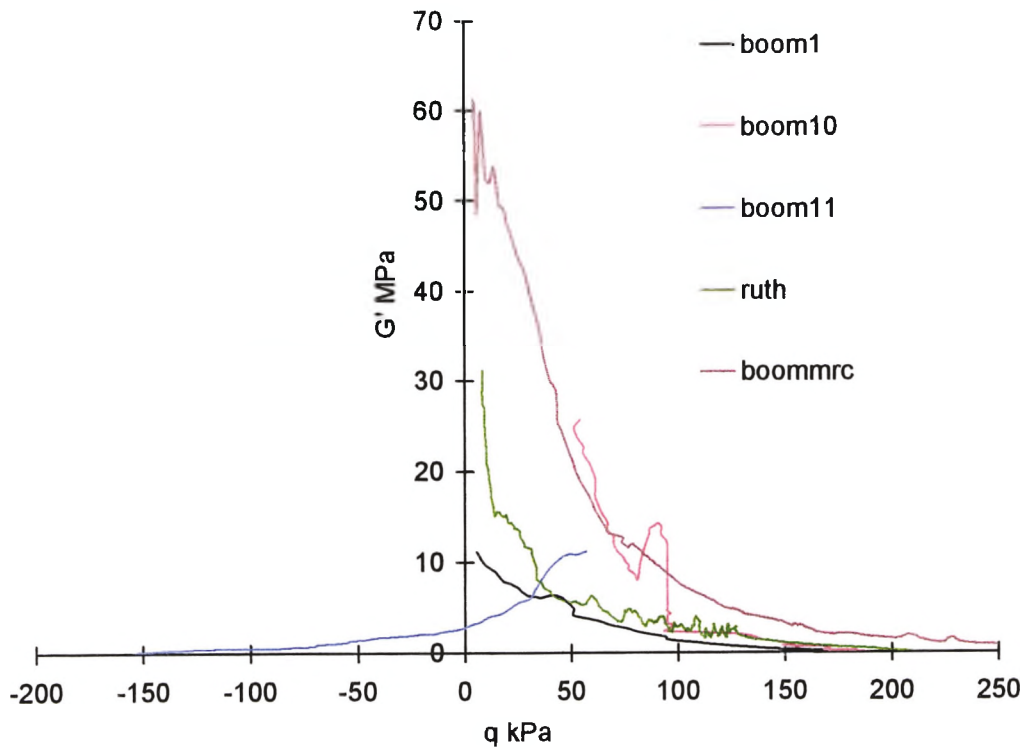


Figure 5.16 Shear stiffness behaviour for reconstituted samples of Boom clay

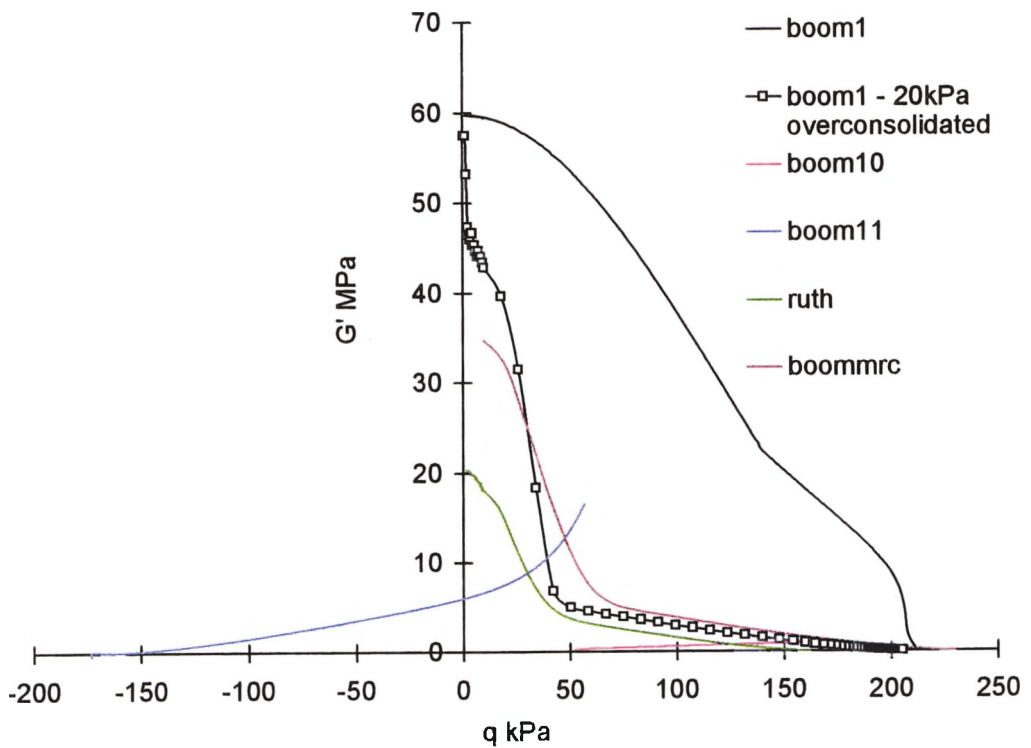


Figure 5.17 3-SKH model predictions of shear stiffness behaviour for reconstituted Boom clay

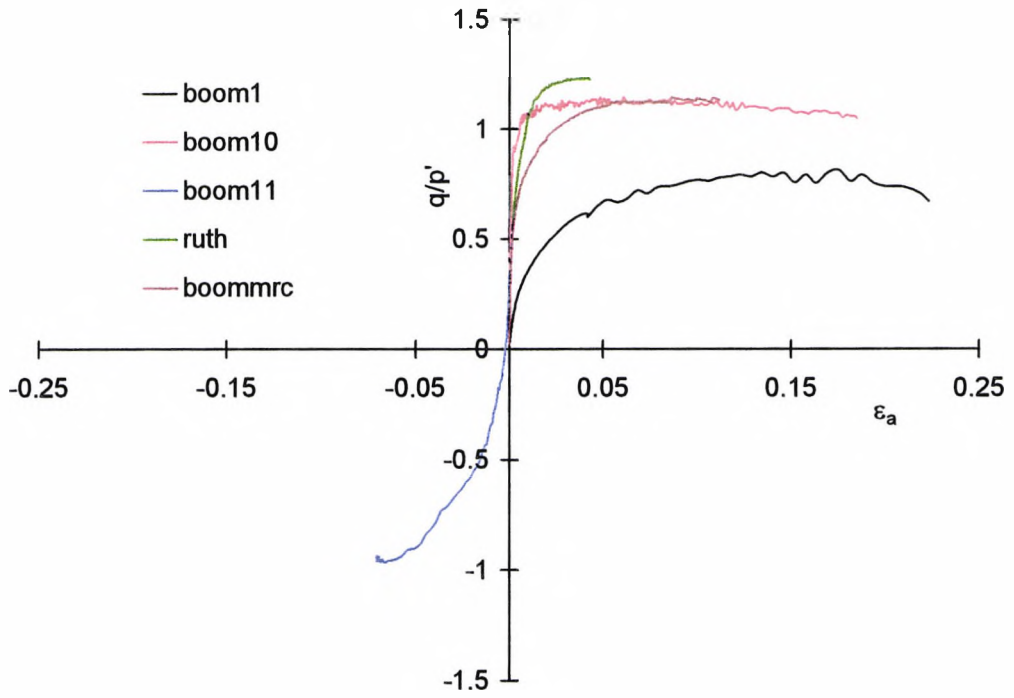


Figure 5.18 Graph of stress ratio against axial strain for reconstituted Boom clay

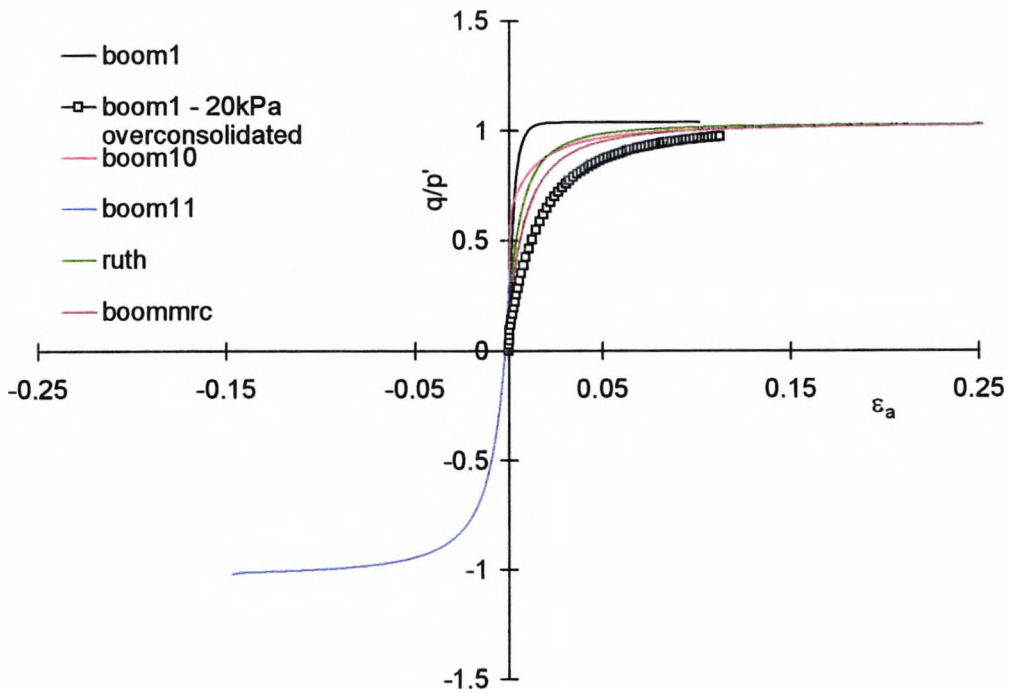


Figure 5.19 3-SKH model predictions of stress ratio against axial strain for reconstituted Boom clay

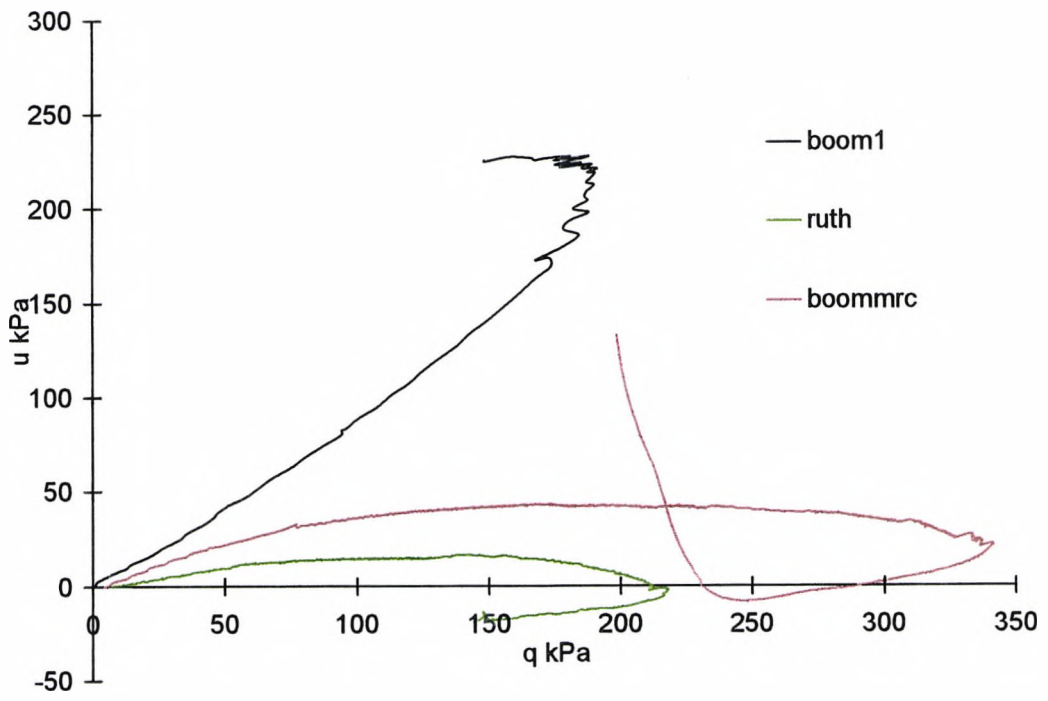


Figure 5.20 Graph of pore water pressure against deviator stress for reconstituted samples of Boom clay

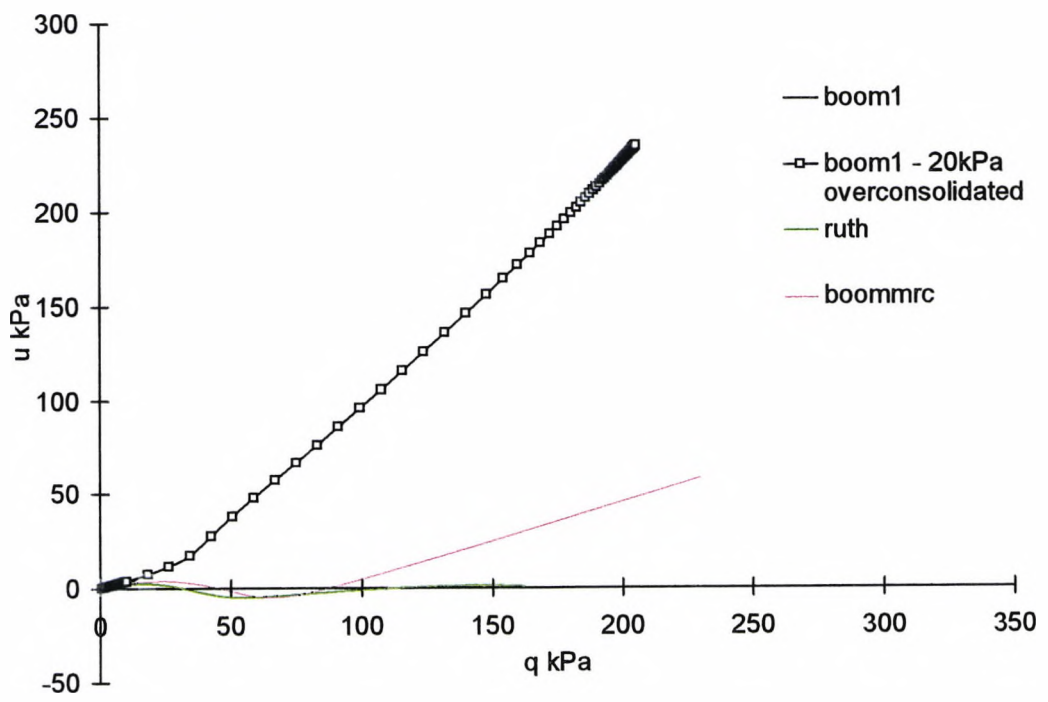


Figure 5.21 Graph of 3-SKH model predictions of pore water pressure against deviator stress for reconstituted Boom clay

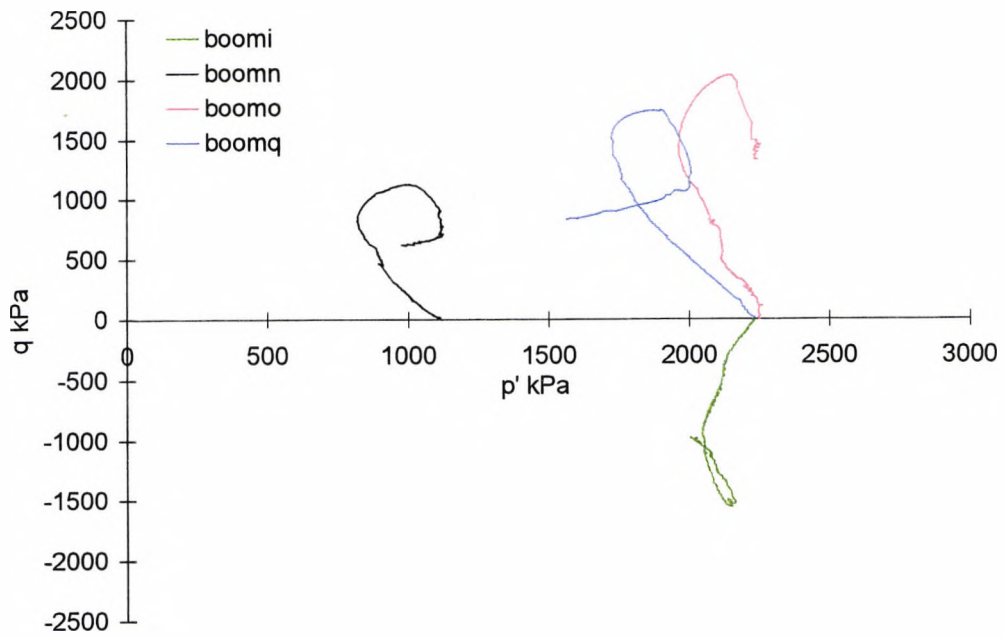


Figure 5.22 Undrained stress paths for natural samples of Boom clay

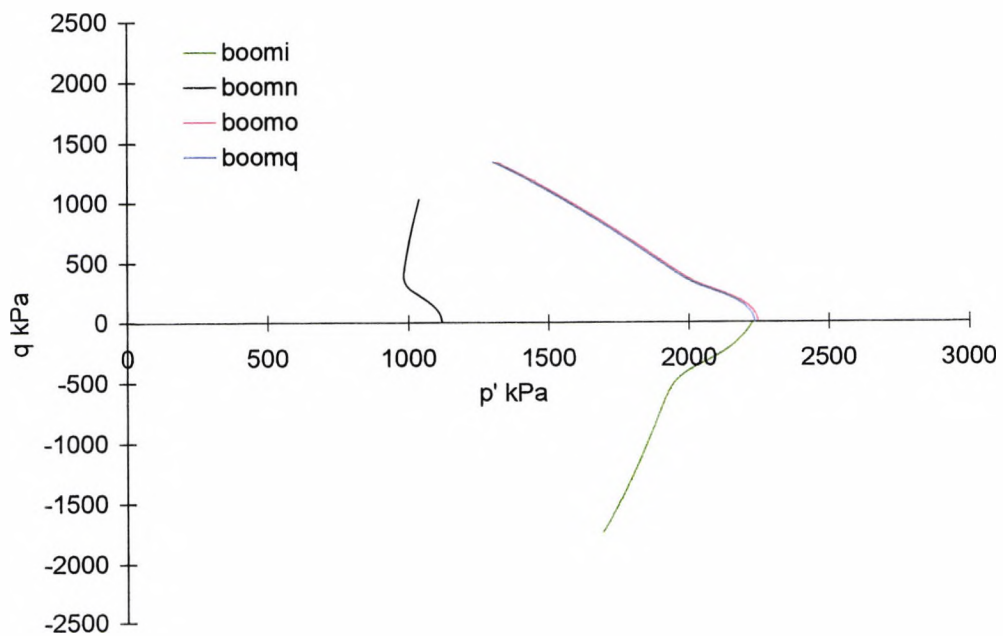


Figure 5.23 3-SKH model predictions of undrained stress paths for natural Boom clay using an initial state boundary surface computed from the reconstituted compression behaviour

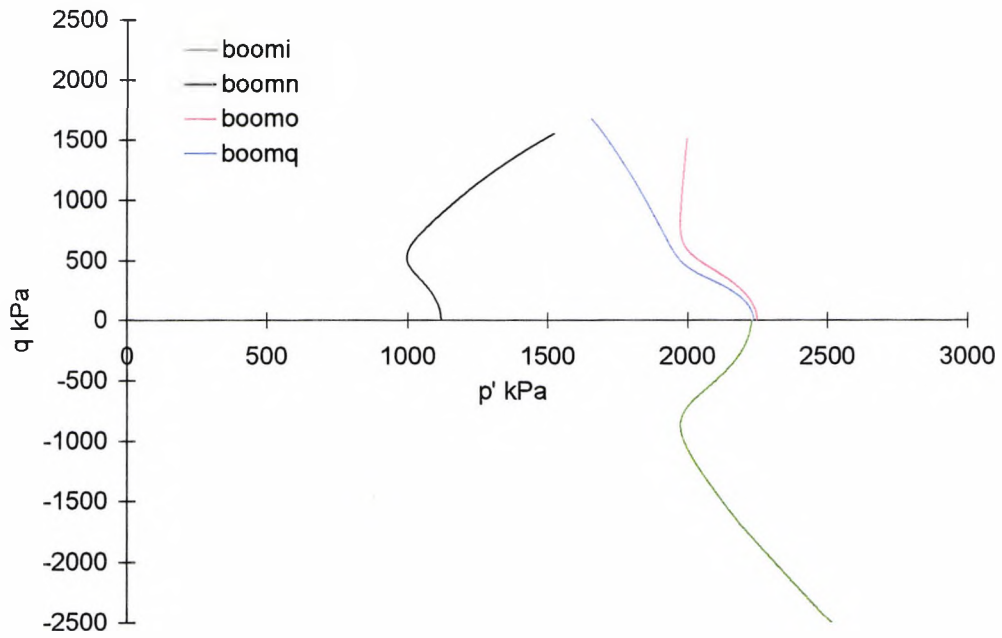


Figure 5.24 3-SKH model predictions of undrained stress paths for natural Boom clay using an initial state boundary surface computed from the natural compression behaviour

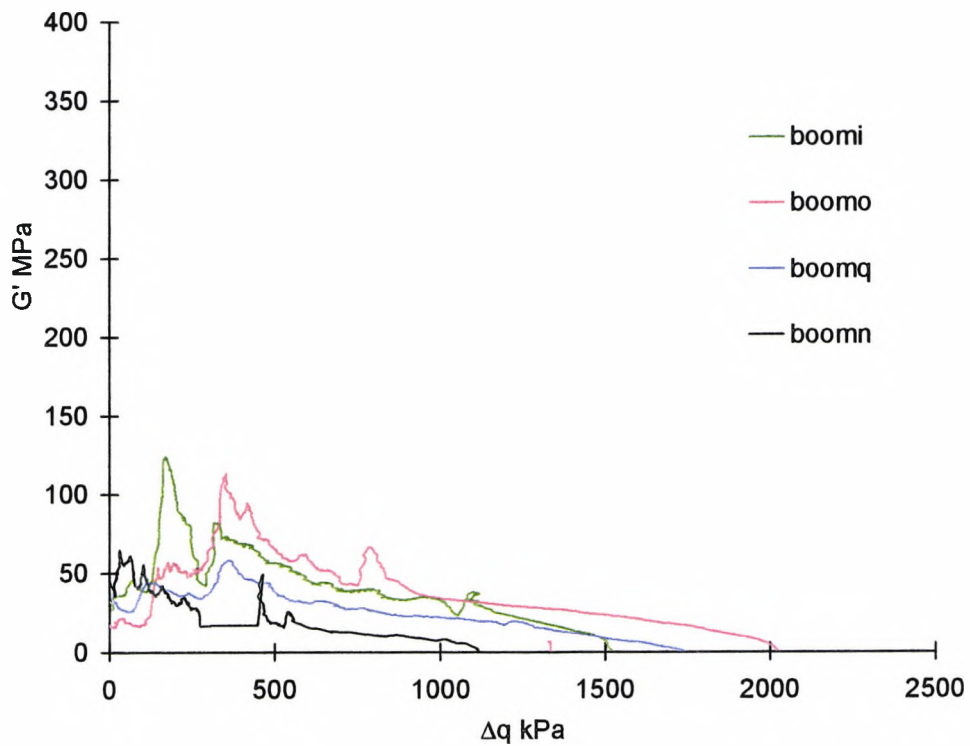


Figure 5.25 Shear stiffness behaviour for natural samples of Boom clay

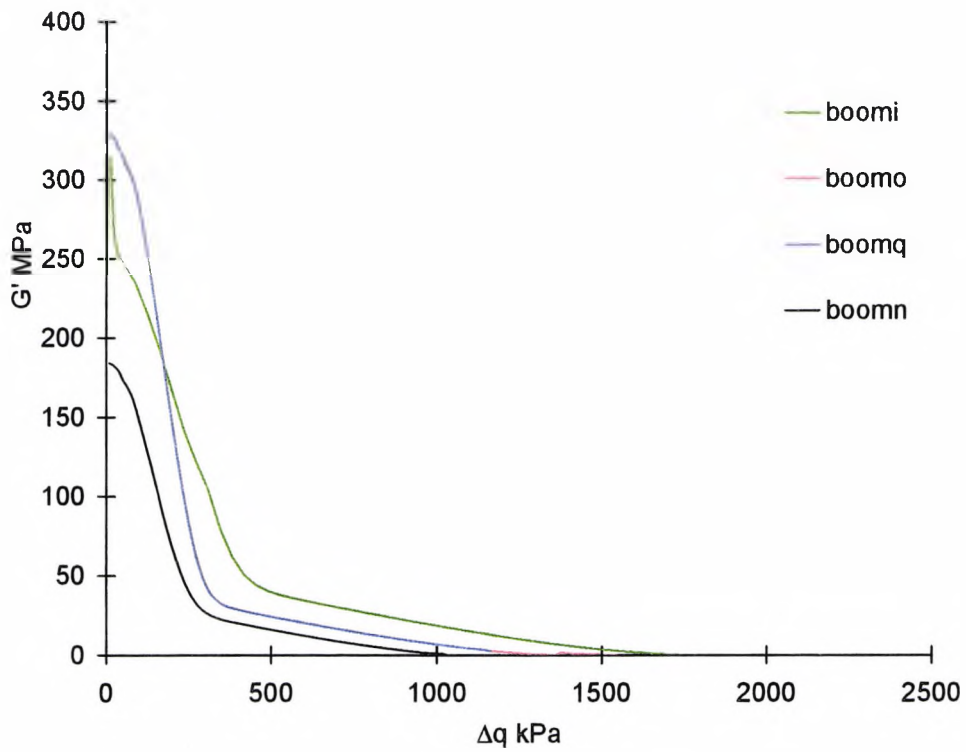


Figure 5.26 3-SKH model predictions of shear stiffness behaviour for natural Boom clay using an initial state boundary surface computed from the reconstituted compression behaviour

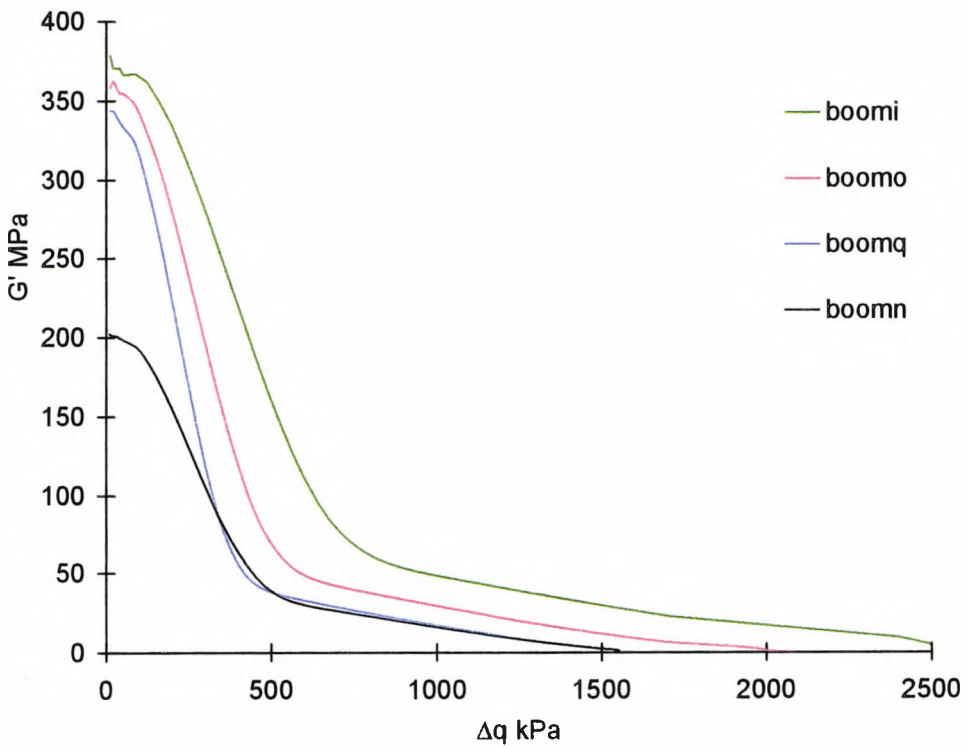


Figure 5.27 3-SKH model predictions of shear stiffness behaviour for natural Boom clay using an initial state boundary surface computed from the natural compression behaviour

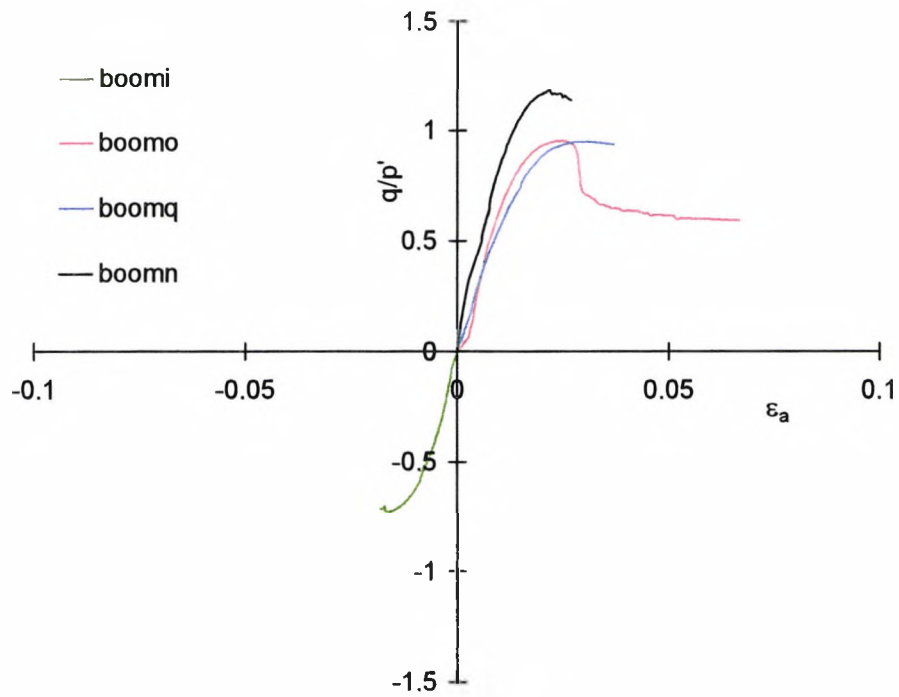


Figure 5.28 Graph of stress ratio against axial strain for natural Boom clay

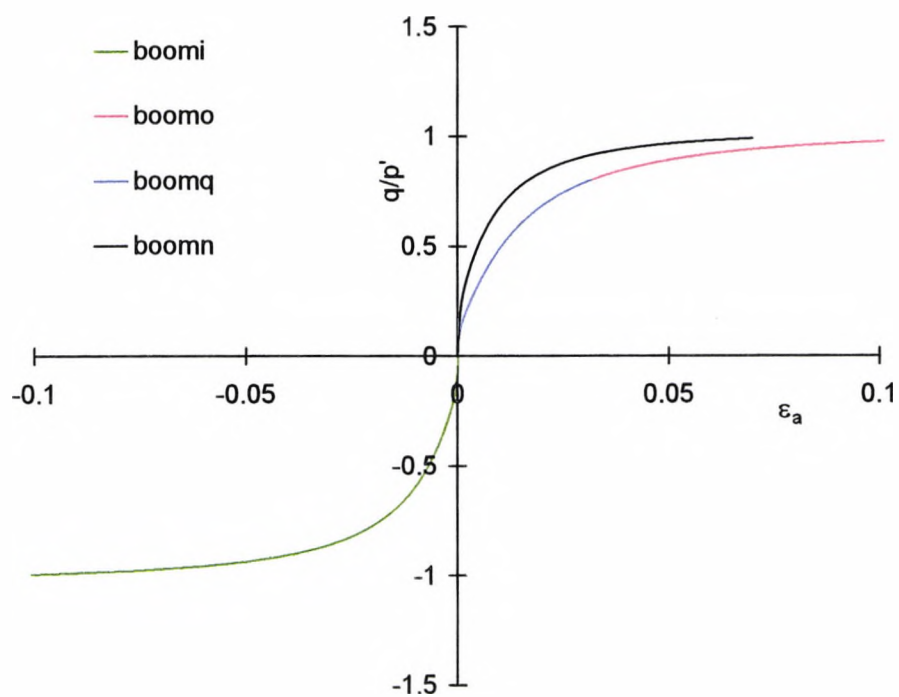


Figure 5.29 3-SKH model predictions of stress ratio against axial strain for natural Boom clay using an initial state boundary surface computed from the reconstituted compression behaviour

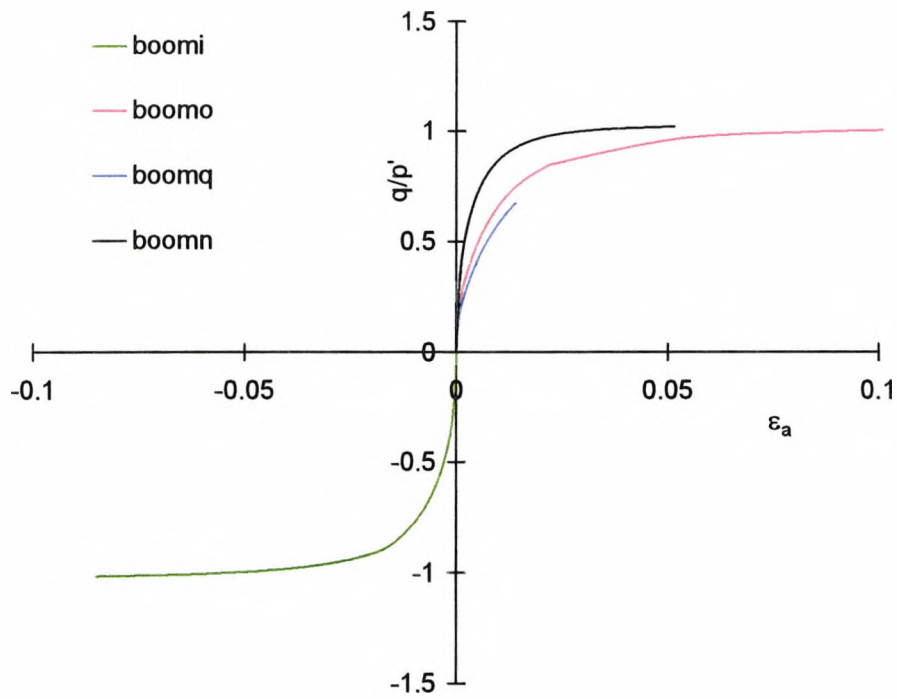


Figure 5.30 3-SKH model predictions of stress ratio against axial strain for natural Boom clay using an initial state boundary surface computed from the natural compression behaviour

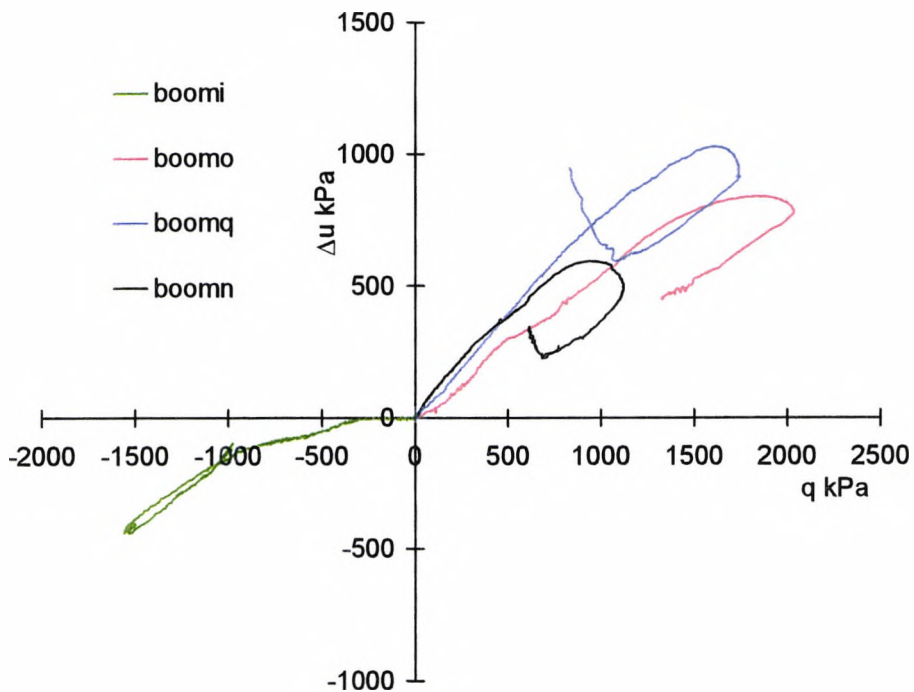


Figure 5.31 Graph of pore water pressure against normalised deviator stress for reconstituted samples of Boom clay

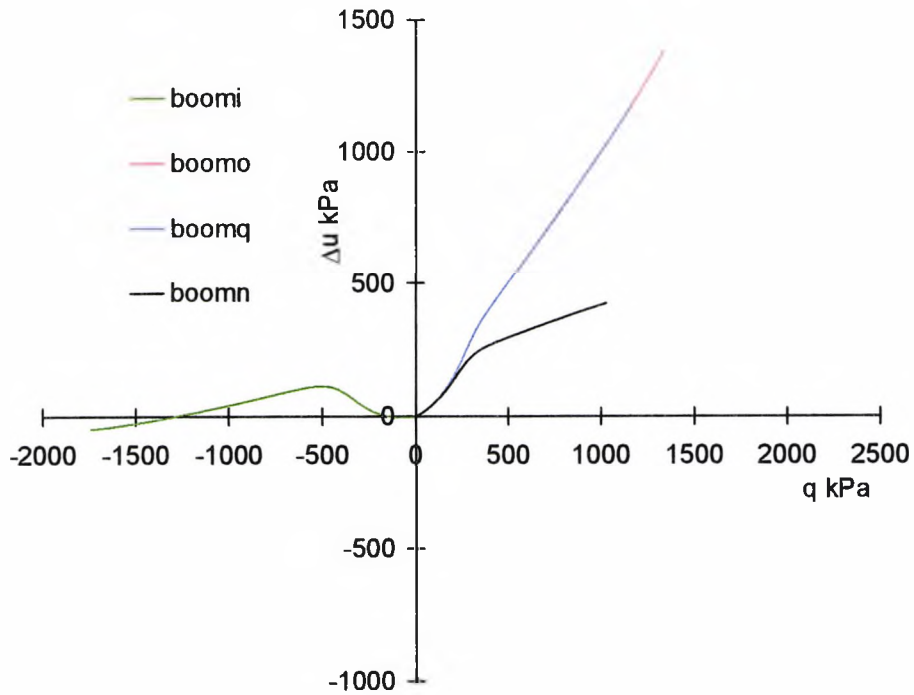


Figure 5.32 Graph of 3-SKH model predictions of pore water pressure against deviator stress for natural Boom clay using an initial state boundary surface computed from the reconstituted compression behaviour

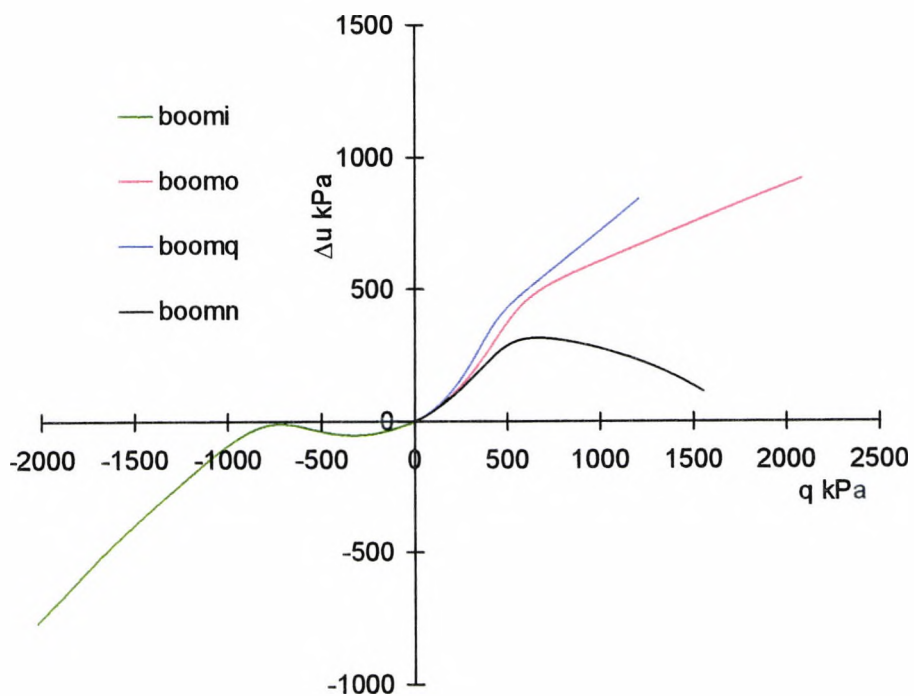


Figure 5.33 Graph of 3-SKH model predictions of pore water pressure against deviator stress for natural Boom clay using an initial state boundary surface computed from the natural compression behaviour

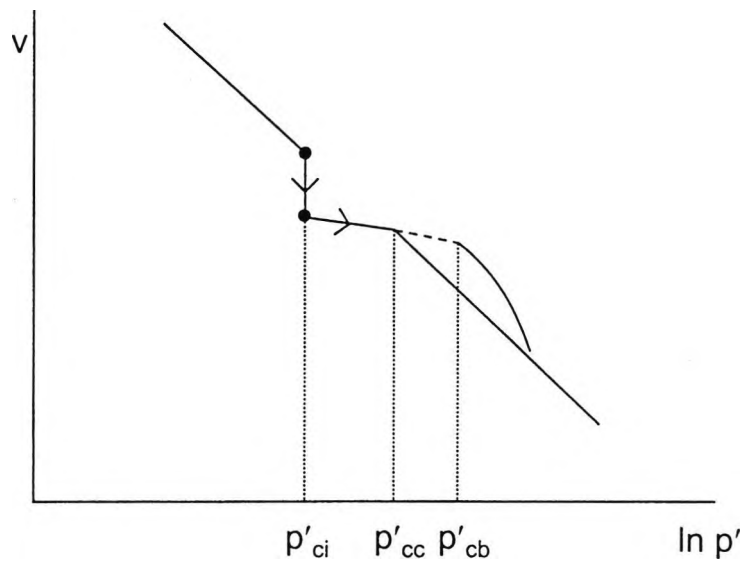


Figure 5.34 Schematic diagram in volumetric space showing possible state paths for soil subject to ageing effects distinguishing creep and bonding.

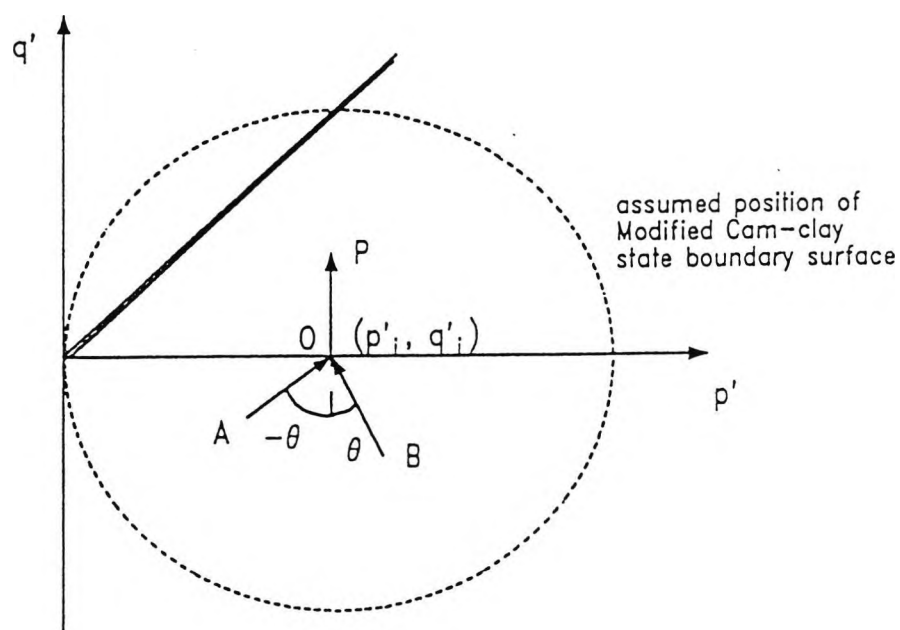


Figure 5.35 Stress probes followed during test to establish the influence of recent stress history (after Stallebrass, 1990)

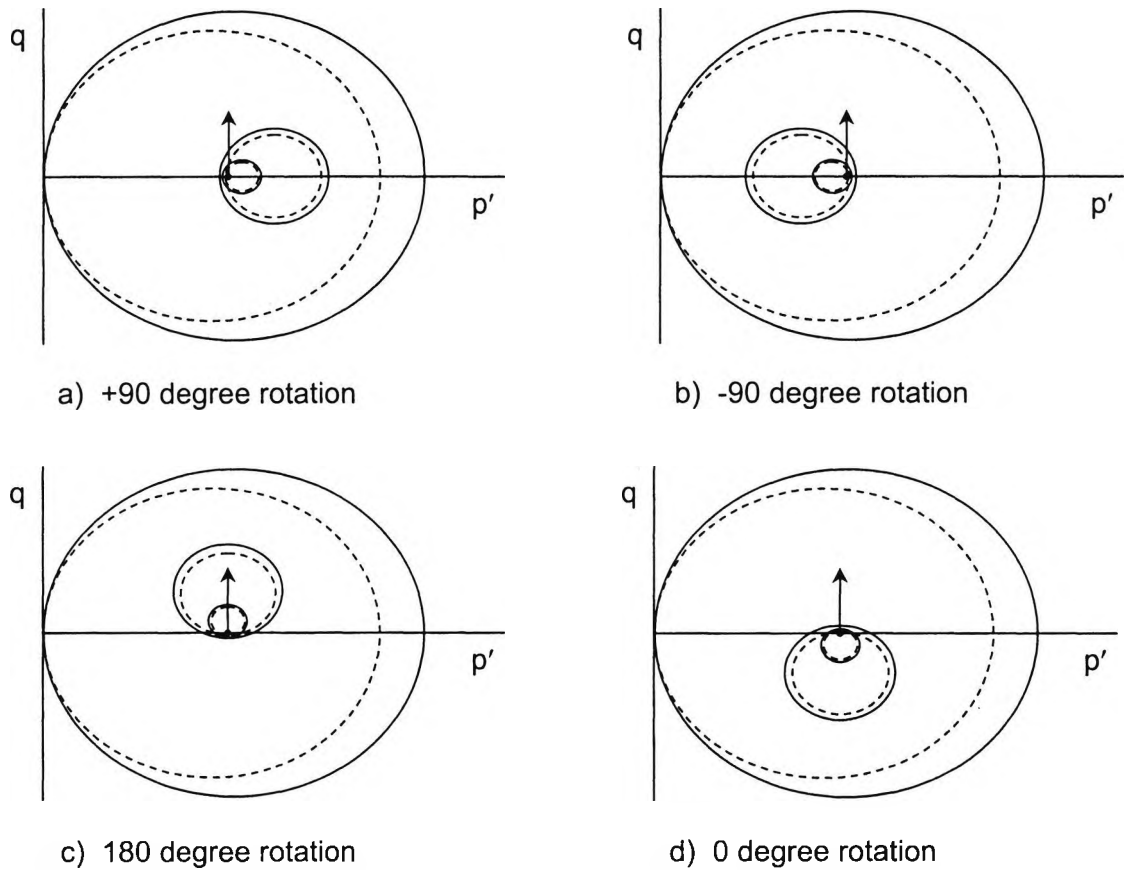


Figure 5.36 Schematic diagrams showing the configuration of the surfaces of the 3-SKH model after following paths corresponding to various recent stress histories and being allowed to creep

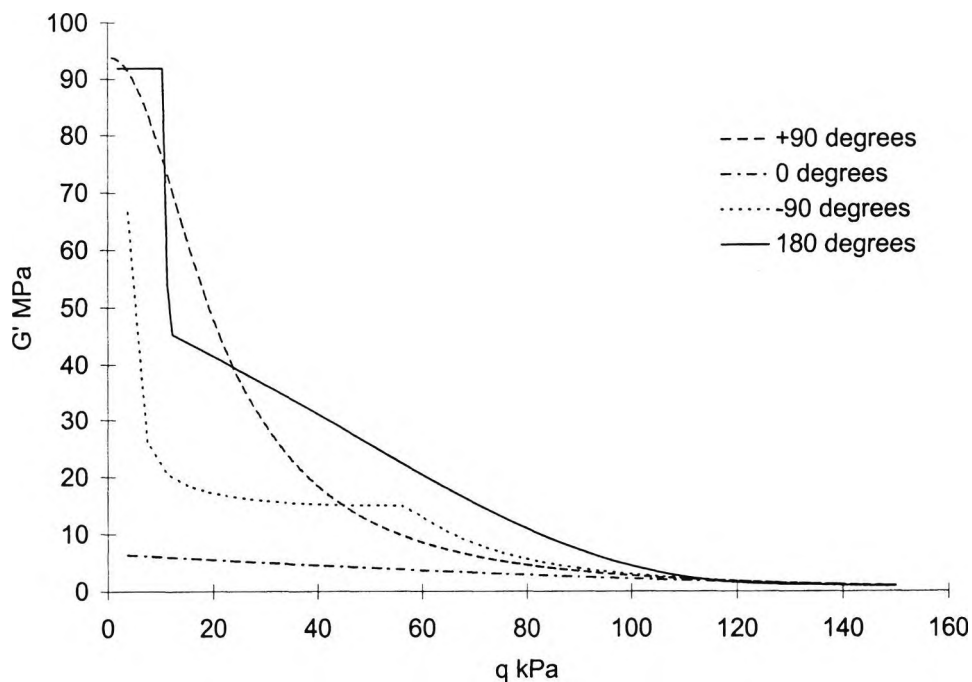


Figure 5.37 Graph of shear stiffness against deviator stress for various stress path rotations where no creep has been modelled

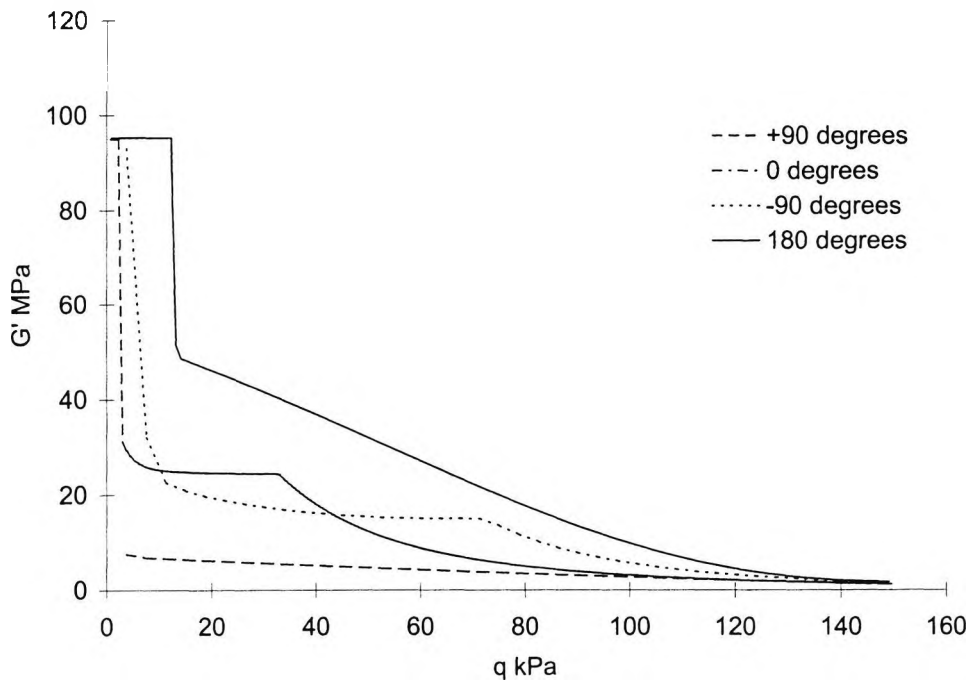


Figure 5.38 Graph of shear stiffness against deviator stress for various stress path rotations where a period of 1 year of creep has been modelled

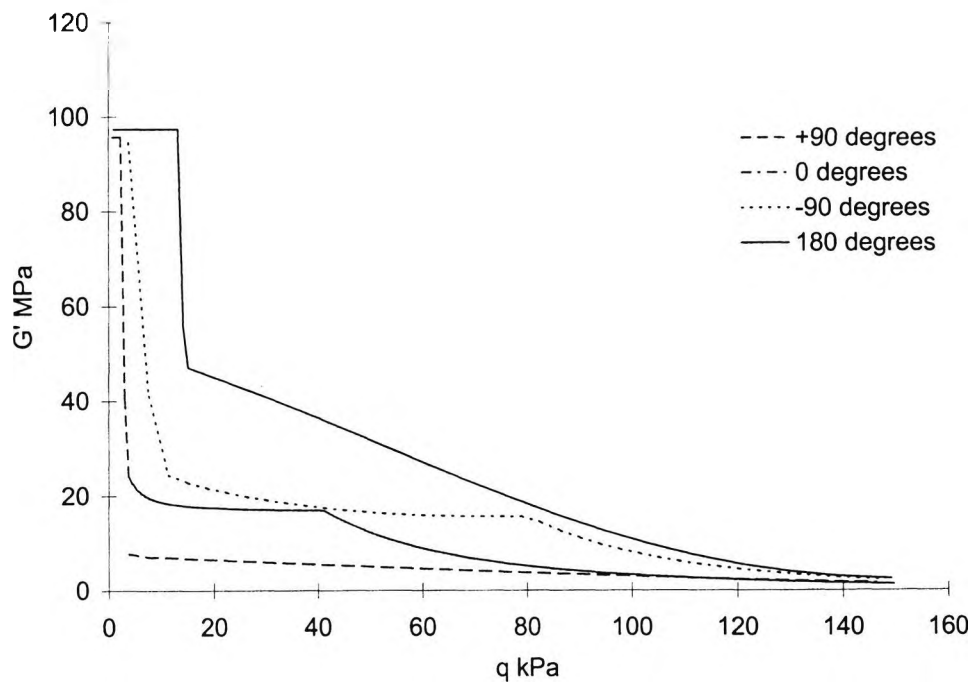


Figure 5.39 Graph of shear stiffness against deviator stress for various stress path rotations where a period of 1000 years of creep has been modelled

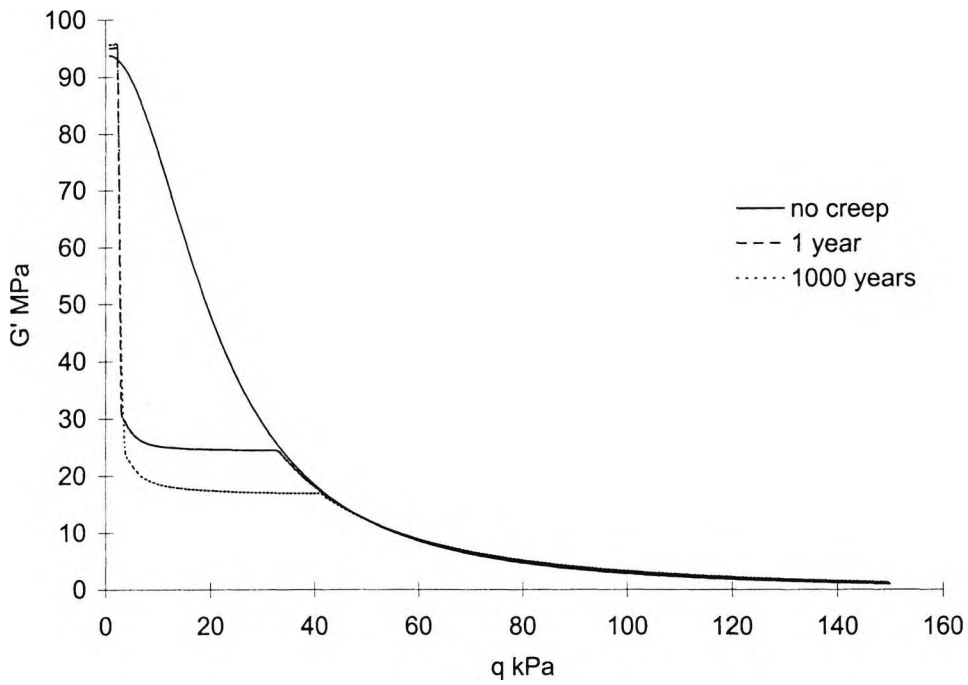


Figure 5.40 Graph of shear stiffness against deviator stress for a 90 degree stress path rotation showing predictions for various modelled periods of creep

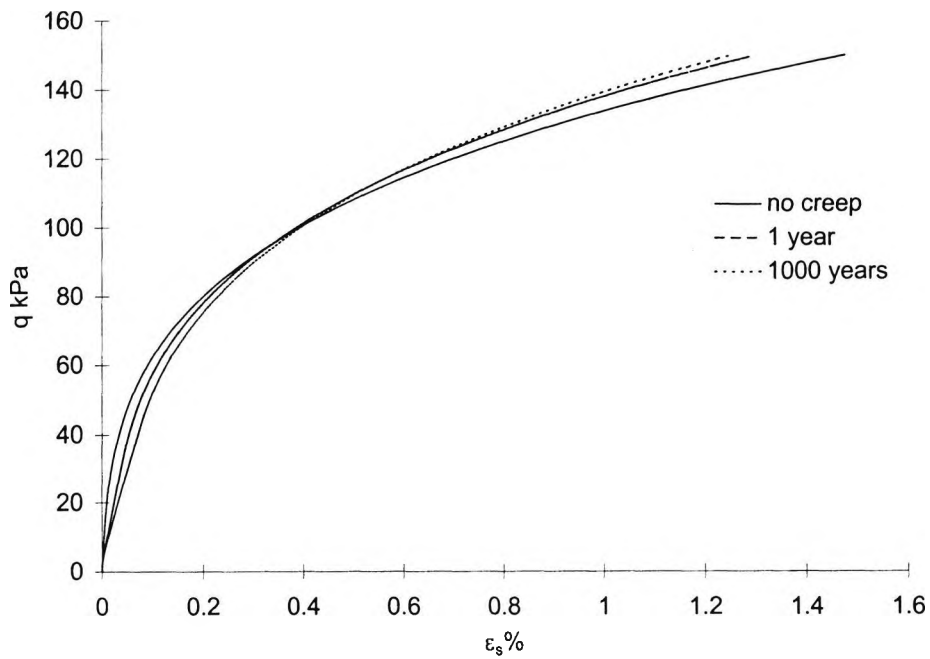


Figure 5.41 Graph of deviator stress against percentage shear strain for a 90 degree stress path rotation showing predictions for various modelled periods of creep

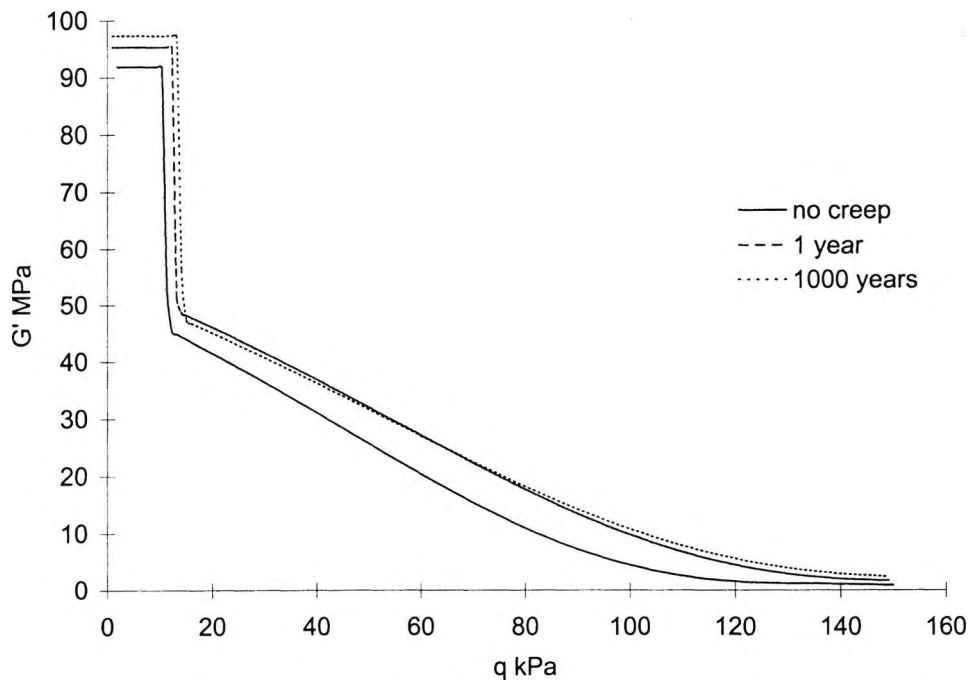


Figure 5.42 Graph of shear stiffness against deviator stress for a 180 degree stress path rotation showing predictions for various modelled periods of creep

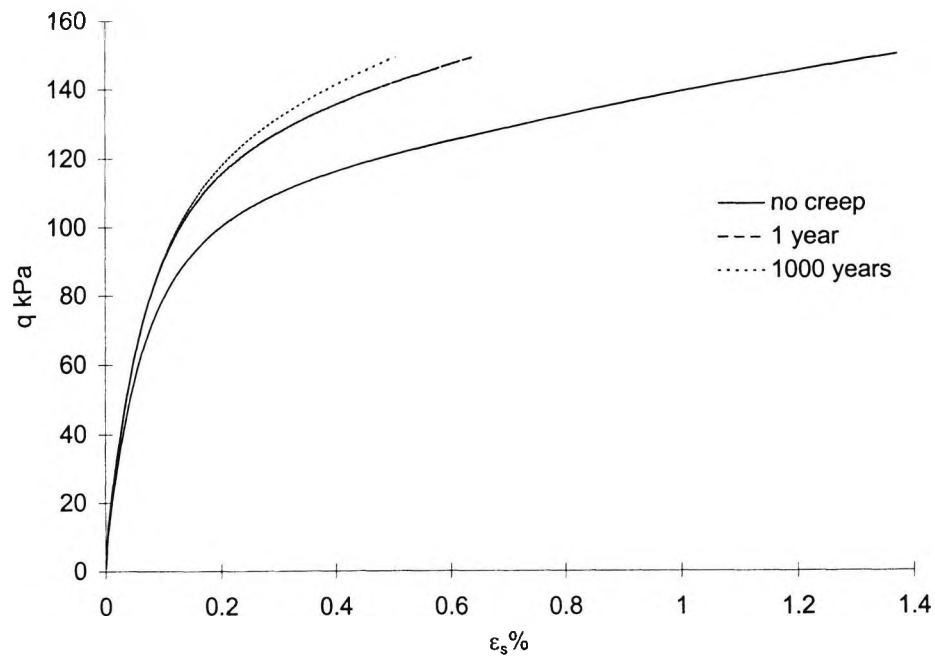


Figure 5.43 Graph of deviator stress against percentage shear strain for a 180 degree stress path rotation showing predictions for various modelled periods of creep

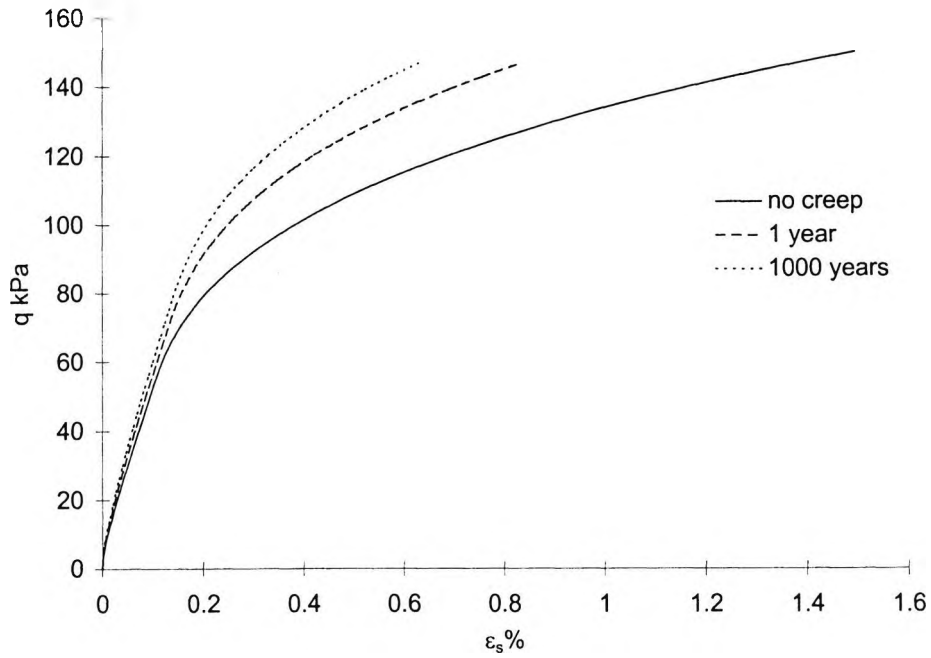


Figure 5.44 Graph of deviator stress against percentage shear strain for a -90 degree stress path rotation showing predictions for various modelled periods of creep

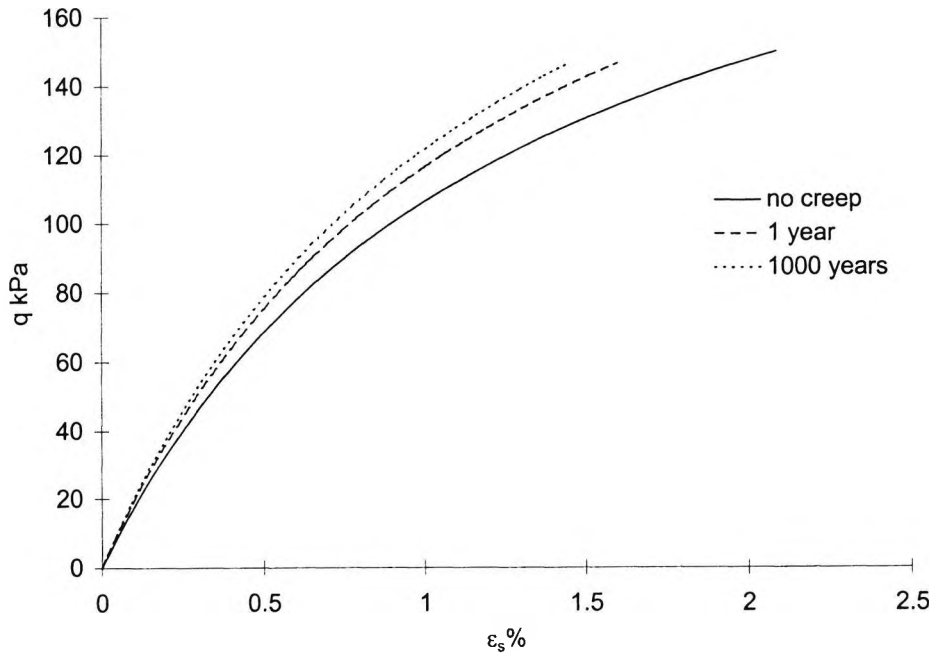


Figure 5.45 Graph of deviator stress against percentage shear strain for a 0 degree stress path rotation showing predictions for various modelled periods of creep

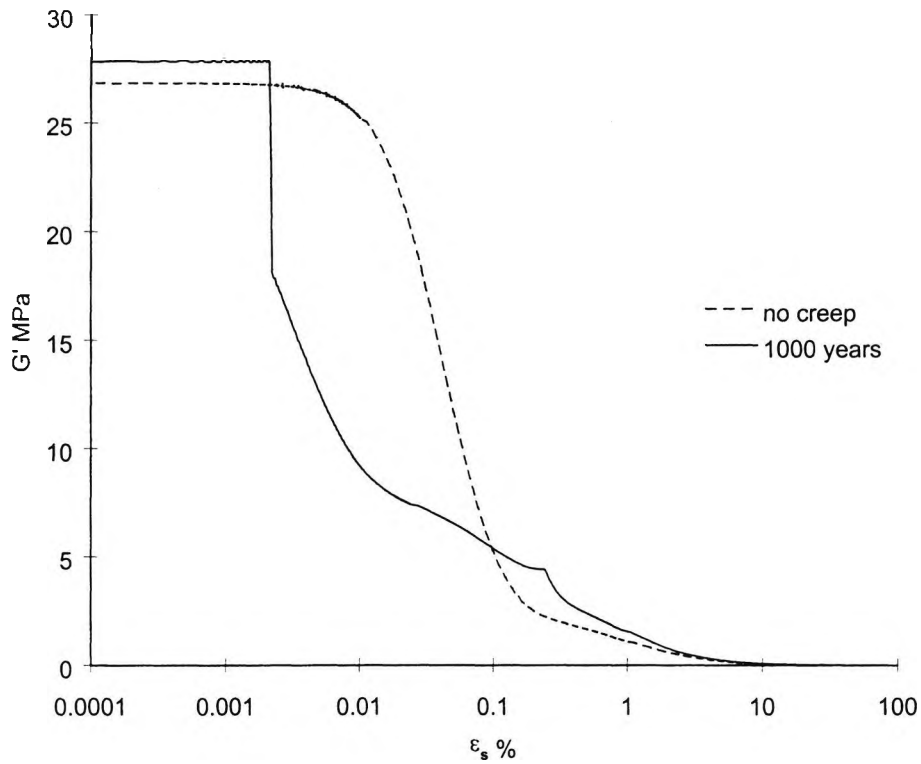


Figure 5.46 Graph showing the effect of creep on shear stiffness during undrained shearing.

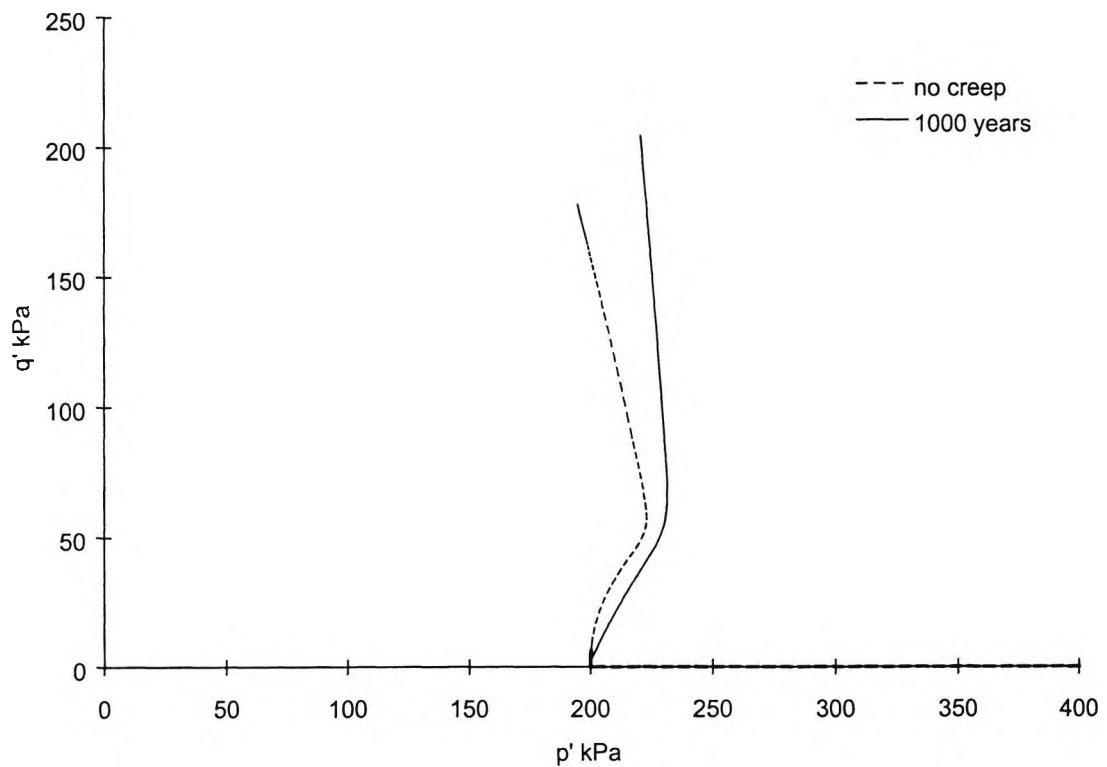


Figure 5.47 Graph showing the effect of creep on stress paths during undrained shear.

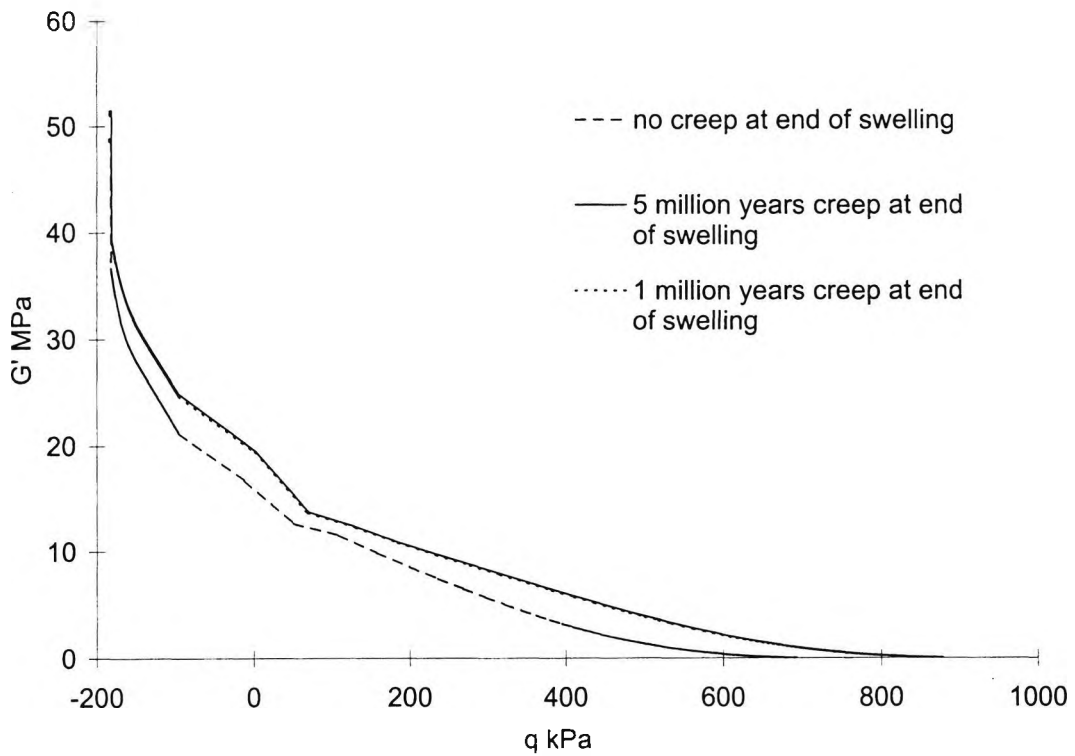


Figure 5.48 The effect of different periods of creep on shear stiffness for a single element simulation of the geological history of a deposit of London clay.

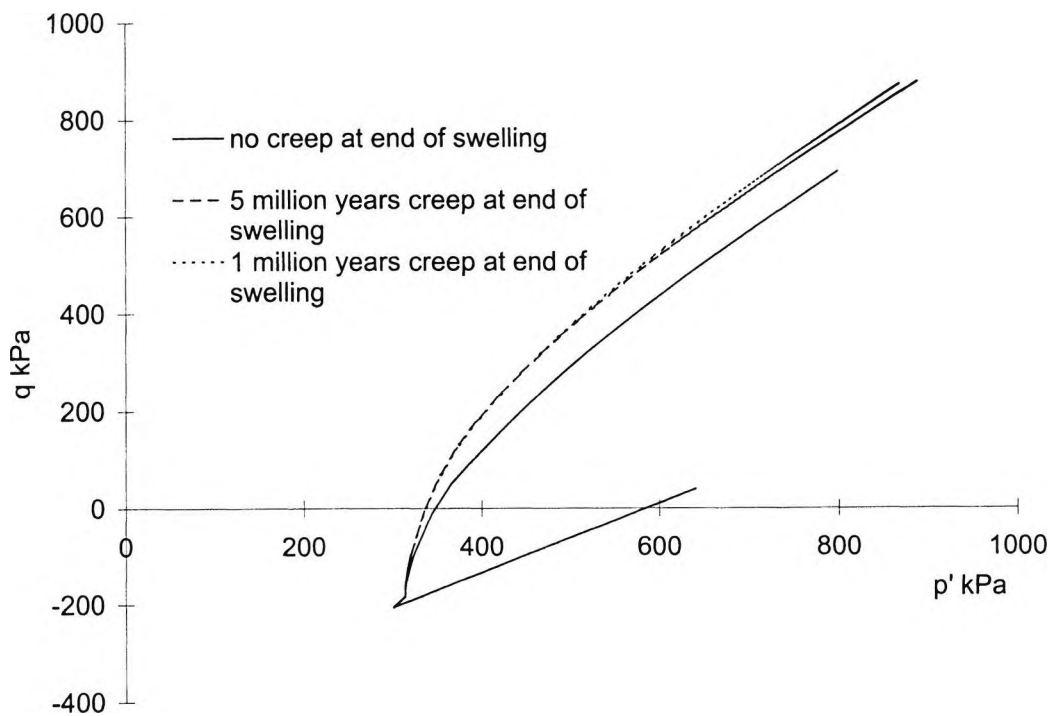


Figure 5.49 The effect of different periods of creep on stress path direction for a single element simulation of the geological history of a deposit of London clay.

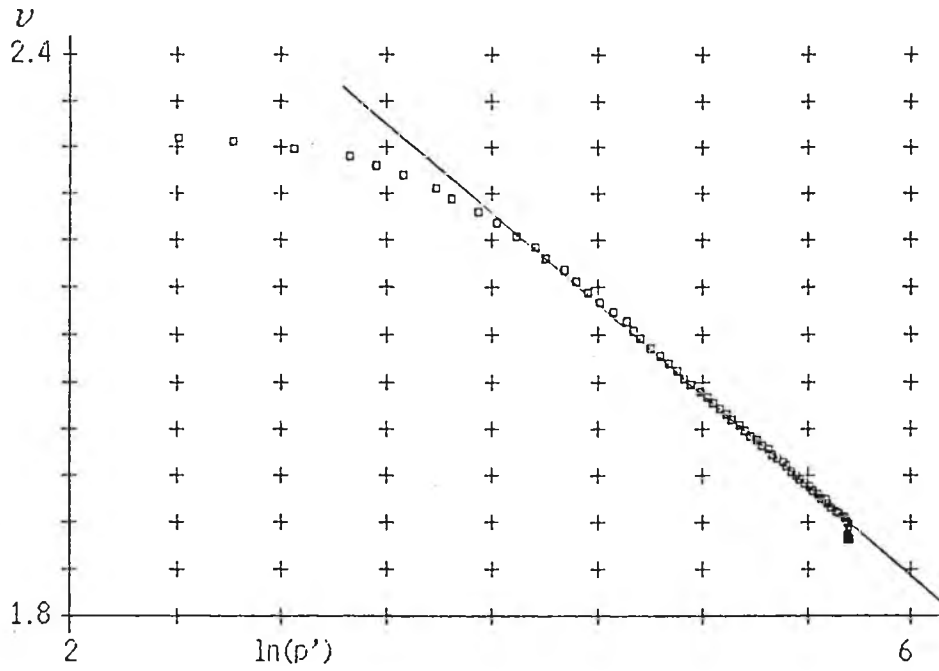


Figure 5.50 Isotropic normal compression line data for reconstituted Oxford clay (after Atkinson and Cherrill, 1988)

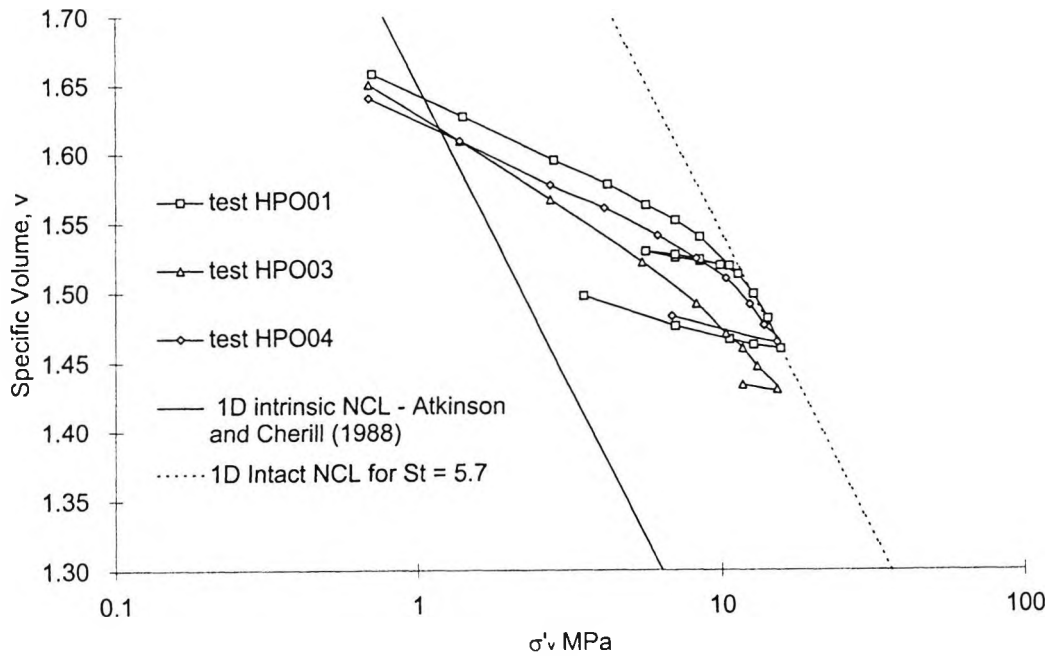


Figure 5.51 One dimensional normal compression lines for reconstituted and natural samples of Oxford clay

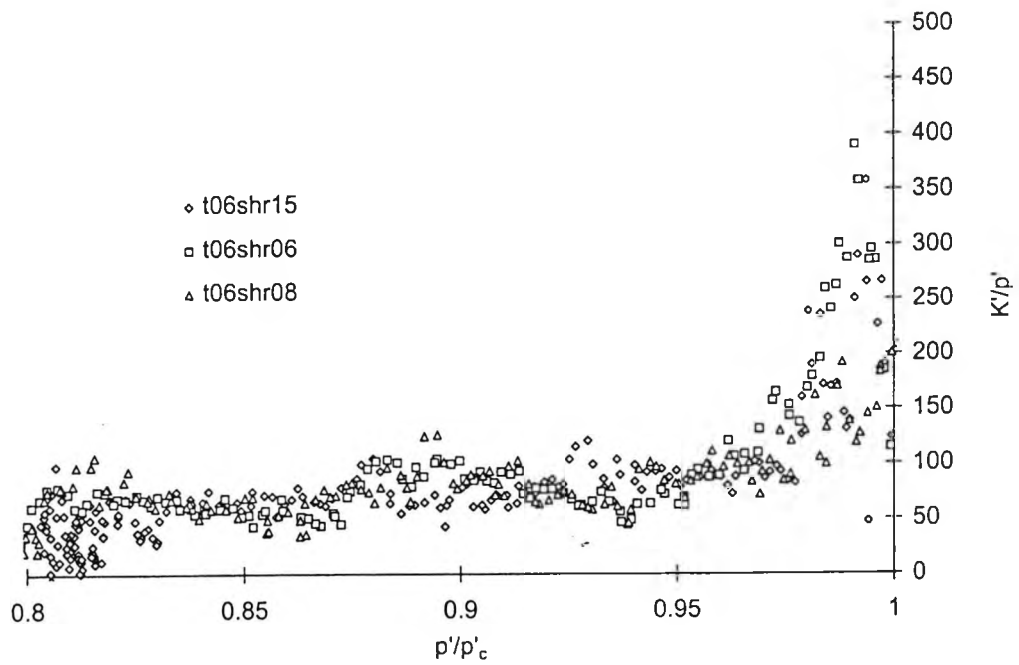


Figure 5.52 Graph of  $K'/p'$  against  $p'/p'_c$  for three constant  $q$  swelling stages for test t06 on natural Oxford clay

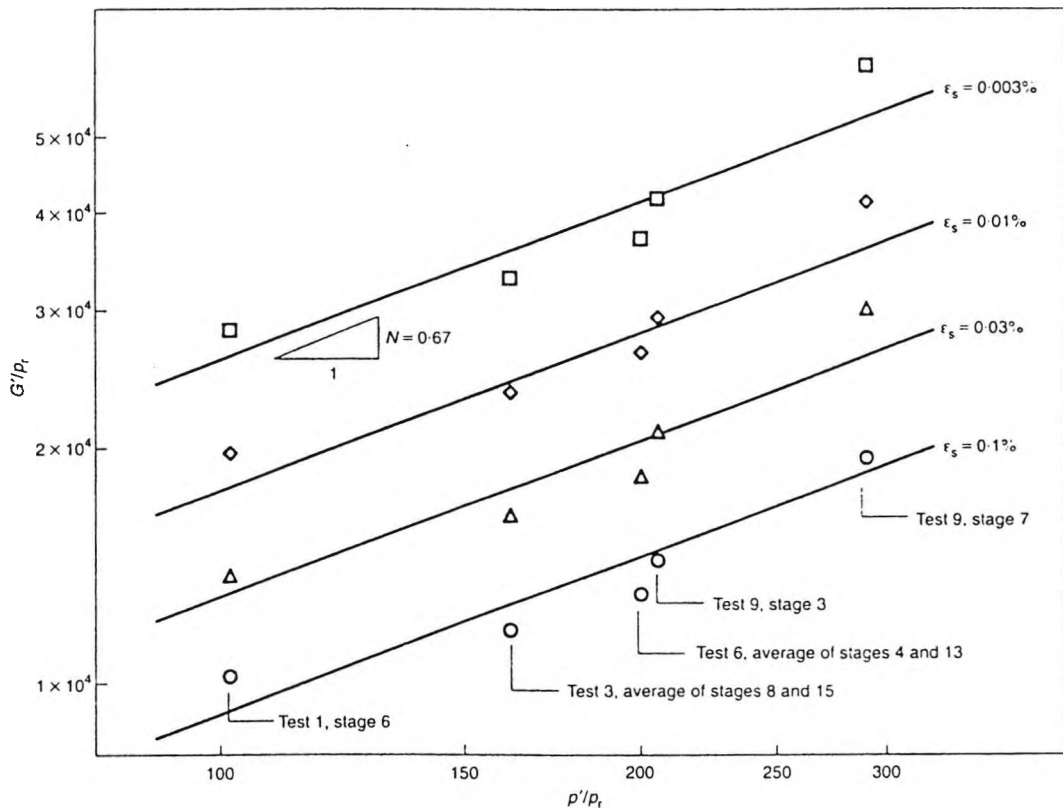


Figure 5.53 Graph of Shear stiffness at various strain levels (after Hird and Pierpoint, 1997)

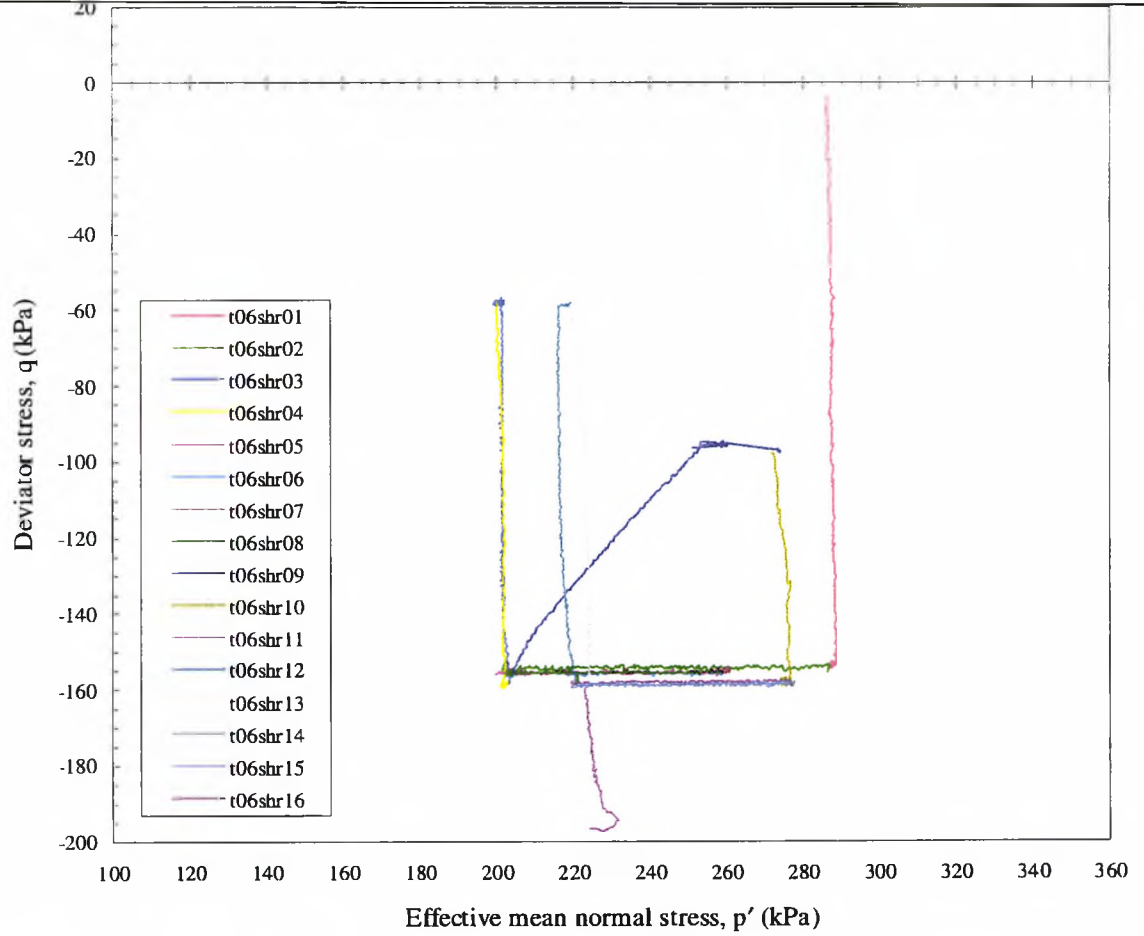


Figure 5.54 Stress probes followed during test T06 on natural Oxford clay (after Pierpoint, 1997)

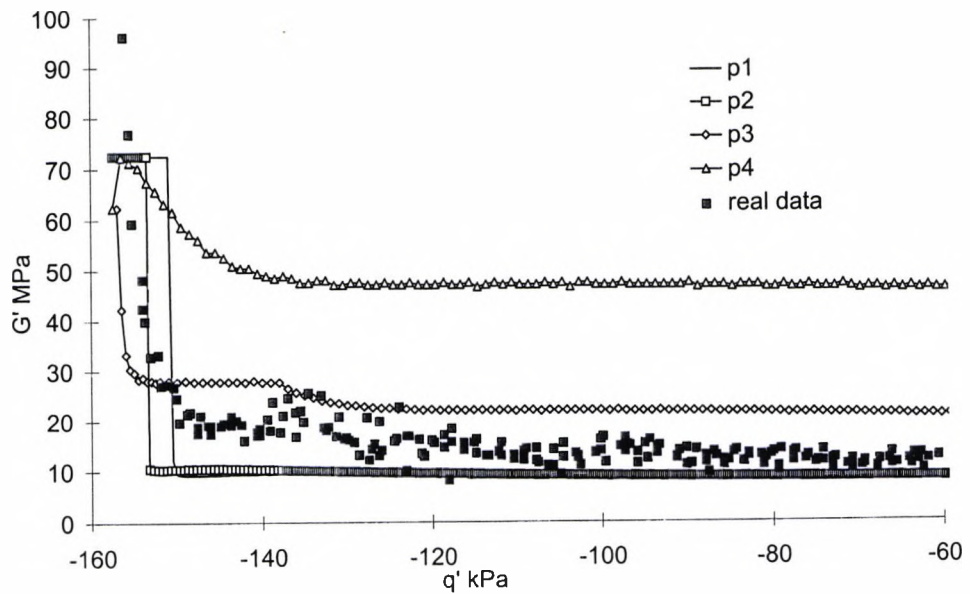


Figure 5.55 Stiffness curve for Oxford clay constant  $p'$  test T06SHR03 plotted against model predictions for varying values of  $T$ ,  $S$  and  $\phi$ .

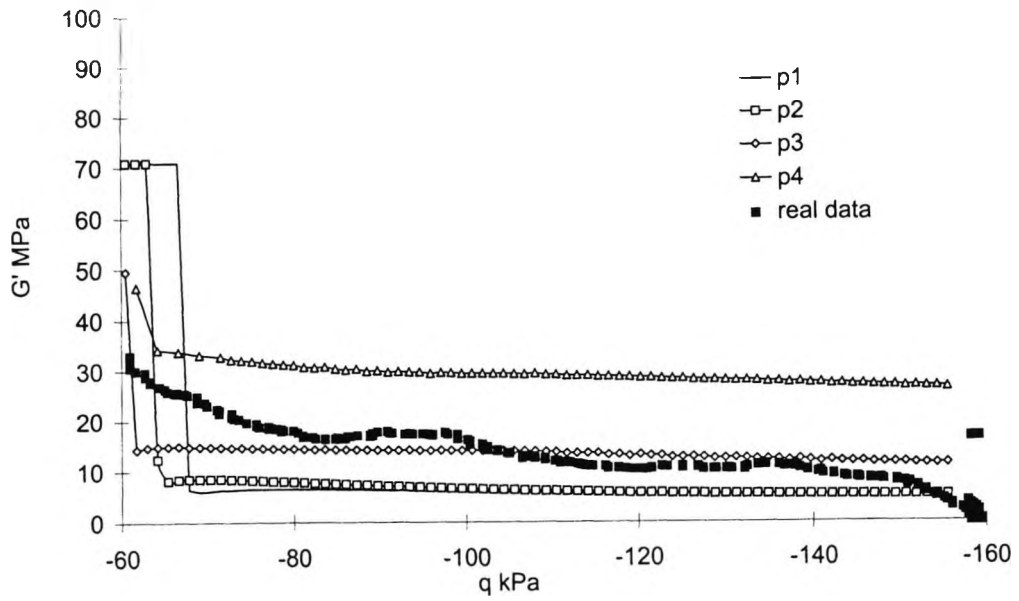


Figure 5.56 Stiffness curve for Oxford clay constant  $p'$  test T06SHR04 plotted against model predictions for varying values of  $T$ ,  $S$  and  $\phi$ .

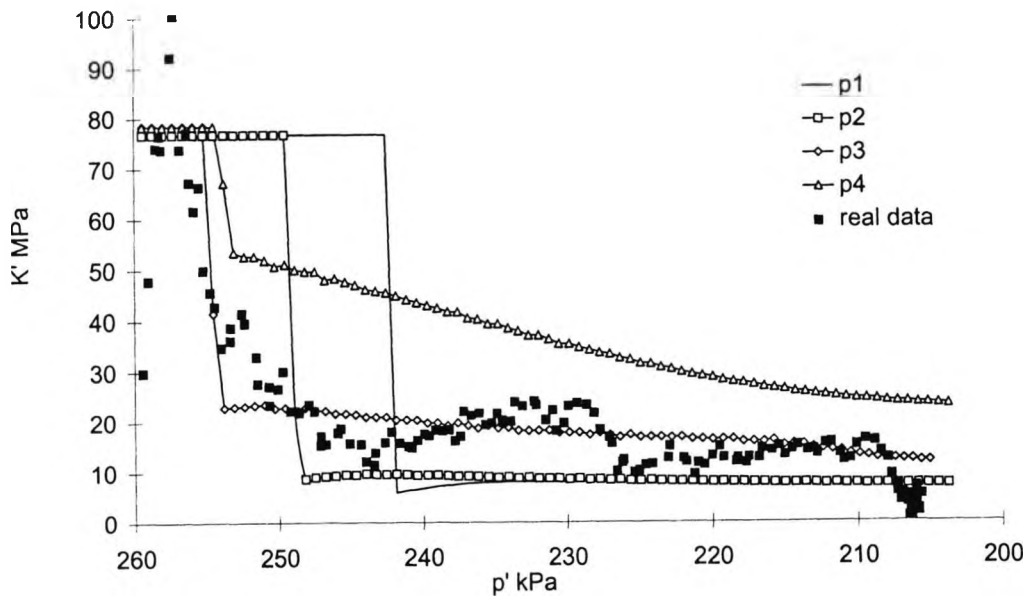


Figure 5.57 Stiffness curve for Oxford clay constant  $p'$  test T06SHR06 plotted against model predictions for varying values of  $T$ ,  $S$  and  $\phi$ .

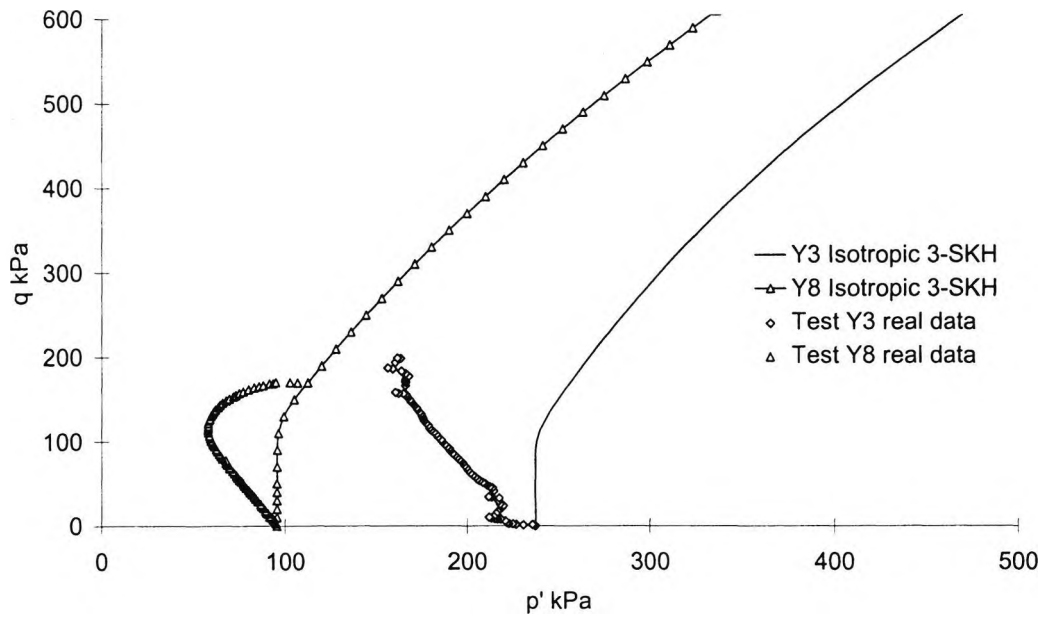


Figure 5.58 Undrained stress paths for tests on Oxford Clay plotted against model predictions for isotropic parameters

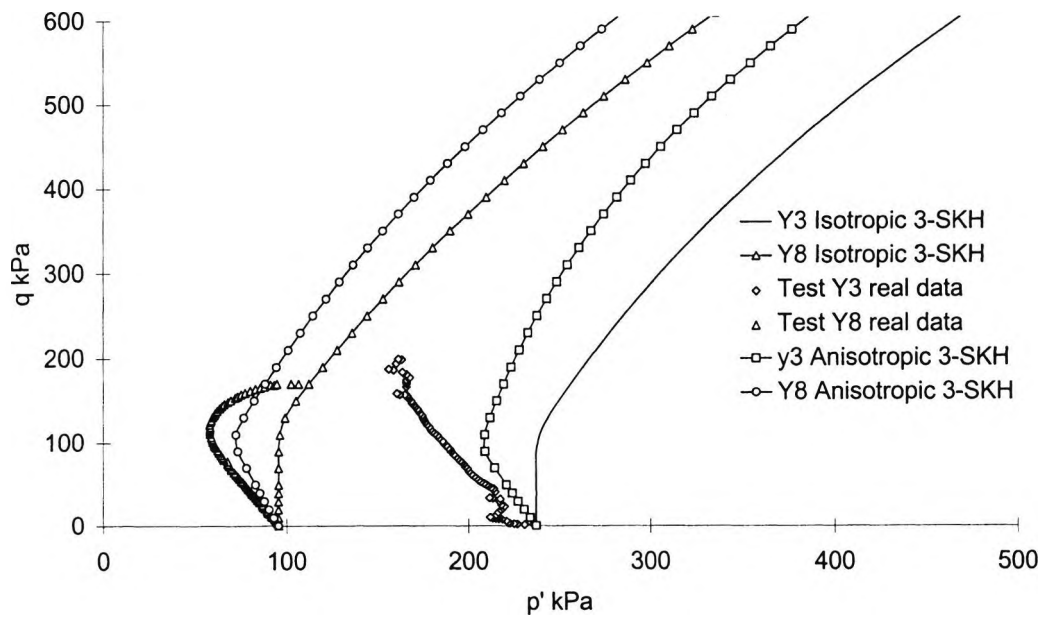


Figure 5.59 Undrained stress paths for tests on Oxford Clay plotted against model predictions for both isotropic and anisotropic parameters

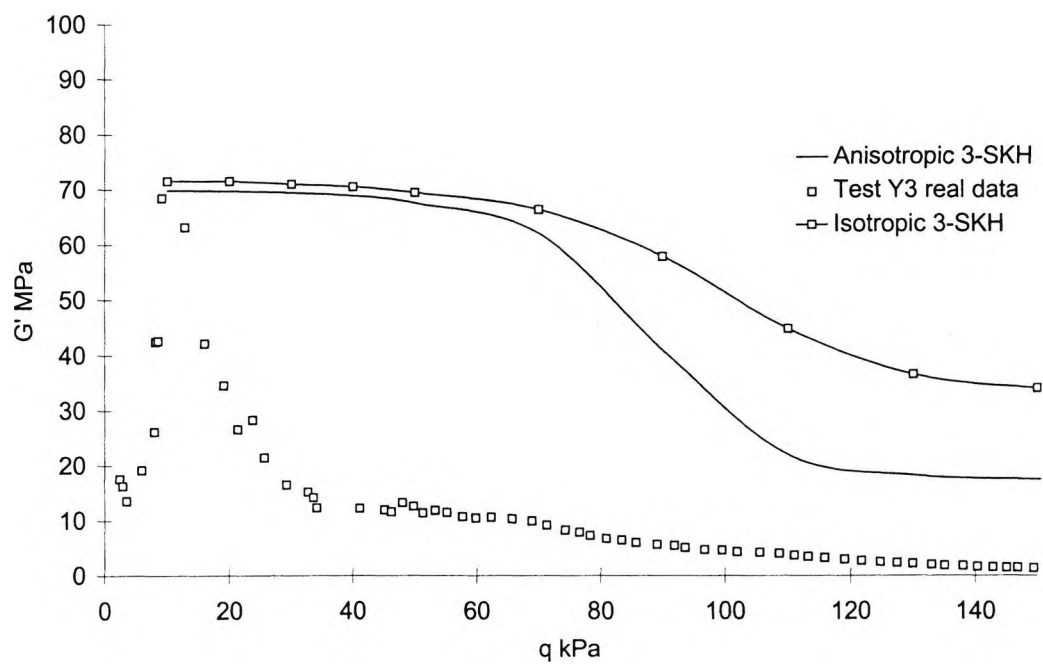


Figure 5.60 Stiffness curve for Oxford Clay undrained test 'Y3' plotted against model predictions for both isotropic and anisotropic parameters

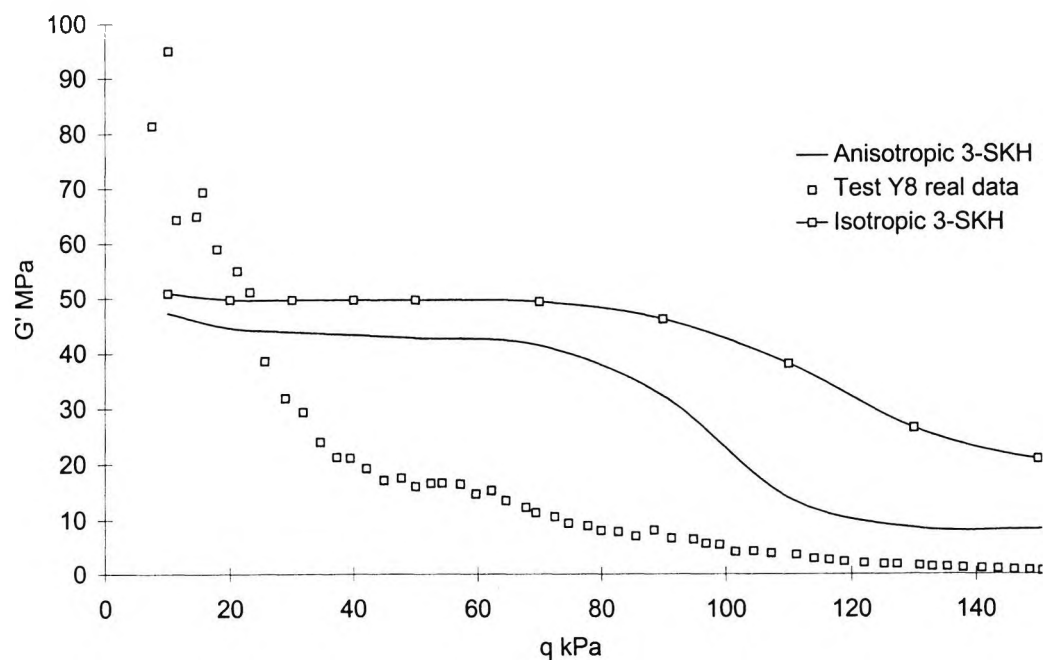


Figure 5.61 Stiffness curve for Oxford Clay undrained test 'Y8' plotted against model predictions for both isotropic and anisotropic parameters

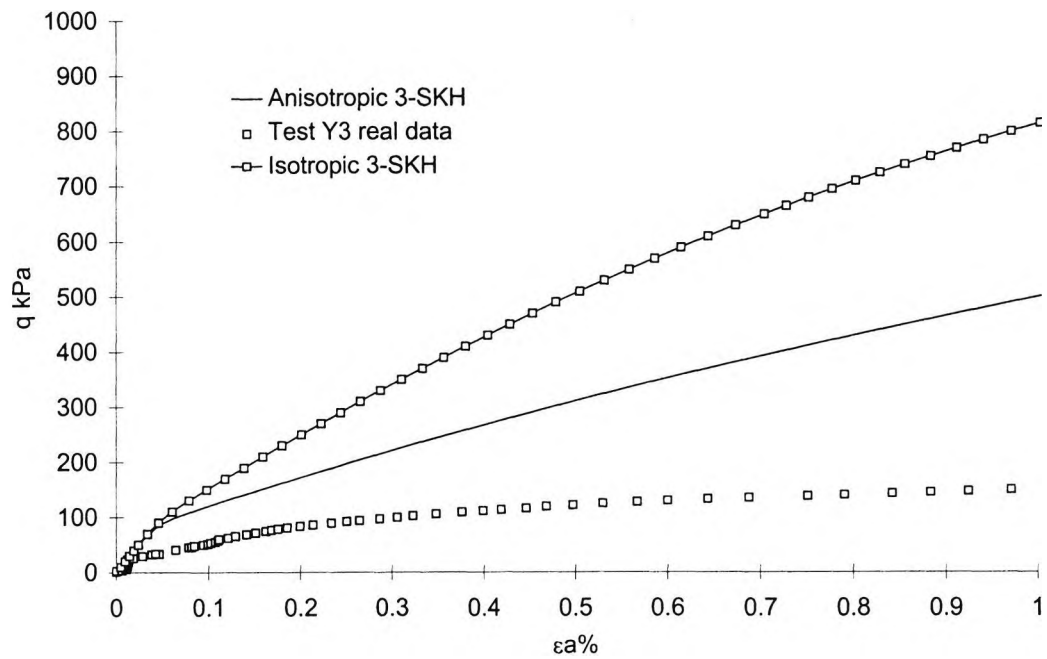


Figure 5.62 Deviator stress against axial strain for Oxford Clay undrained test 'Y3' plotted against model predictions for both isotropic and anisotropic parameters

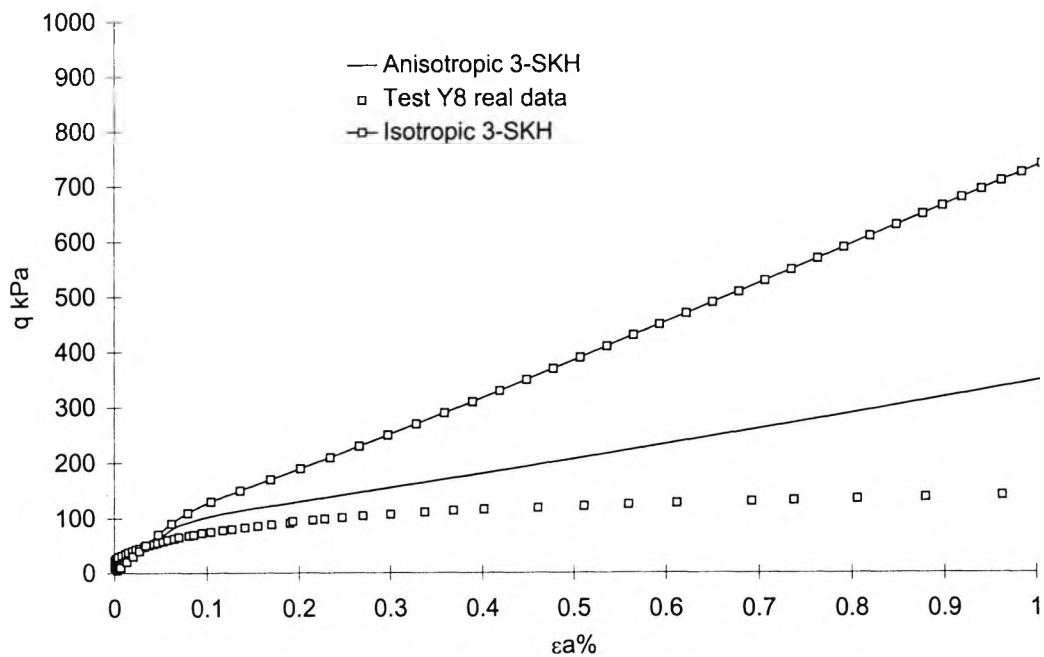


Figure 5.63 Deviator stress against axial strain for Oxford Clay undrained test 'Y8' plotted against model predictions for both isotropic and anisotropic parameters

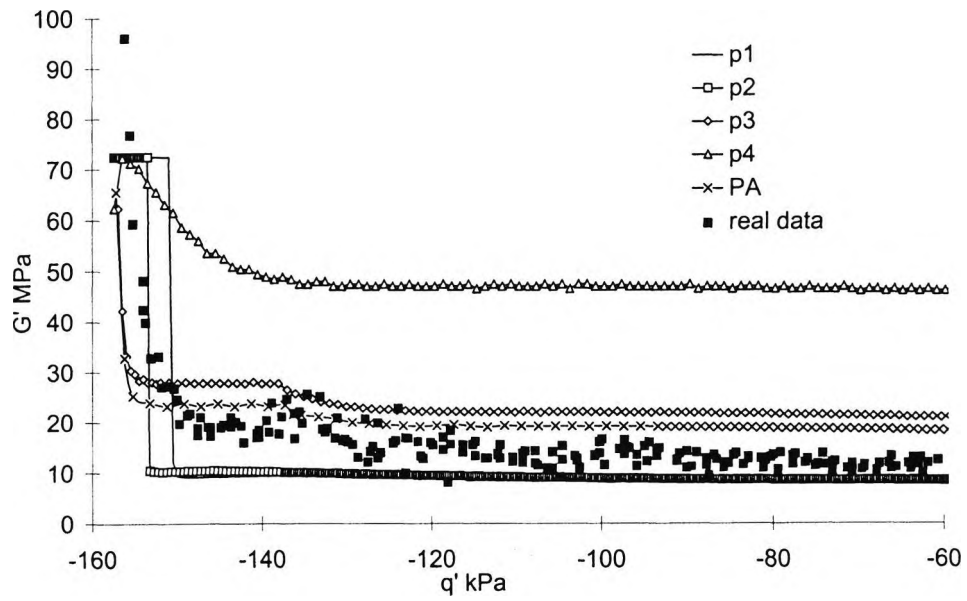


Figure 5.64 Stiffness curve for Oxford clay constant  $p'$  test T06SHR03 plotted against model predictions for varying values of  $T$ ,  $S$  and  $\phi$  and for anisotropic model prediction.

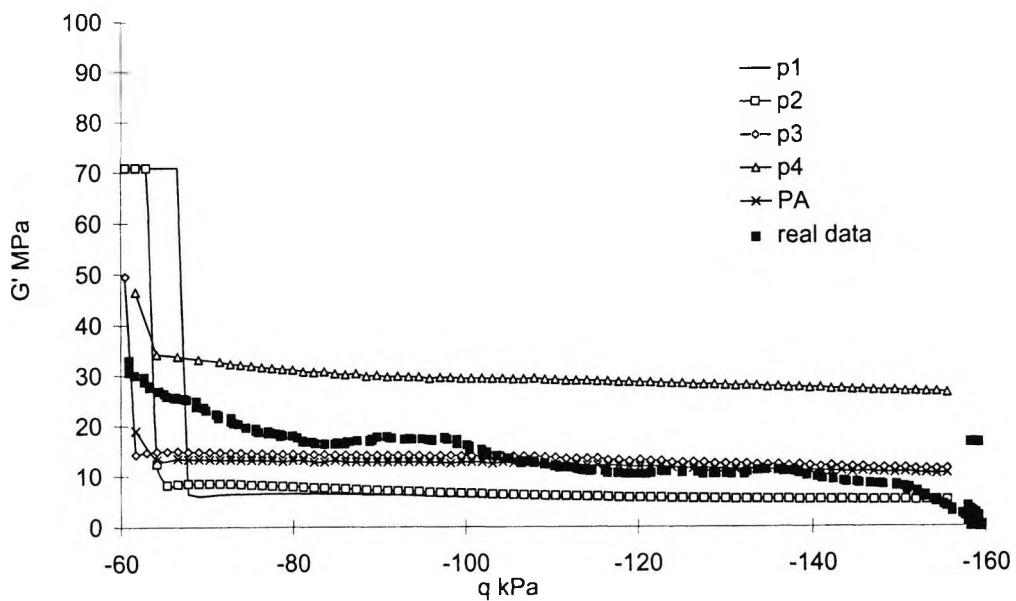


Figure 5.65 Stiffness curve for Oxford clay constant  $p'$  test T06SHR04 plotted against model predictions for varying values of  $T$ ,  $S$  and  $\phi$  and for anisotropic model prediction.

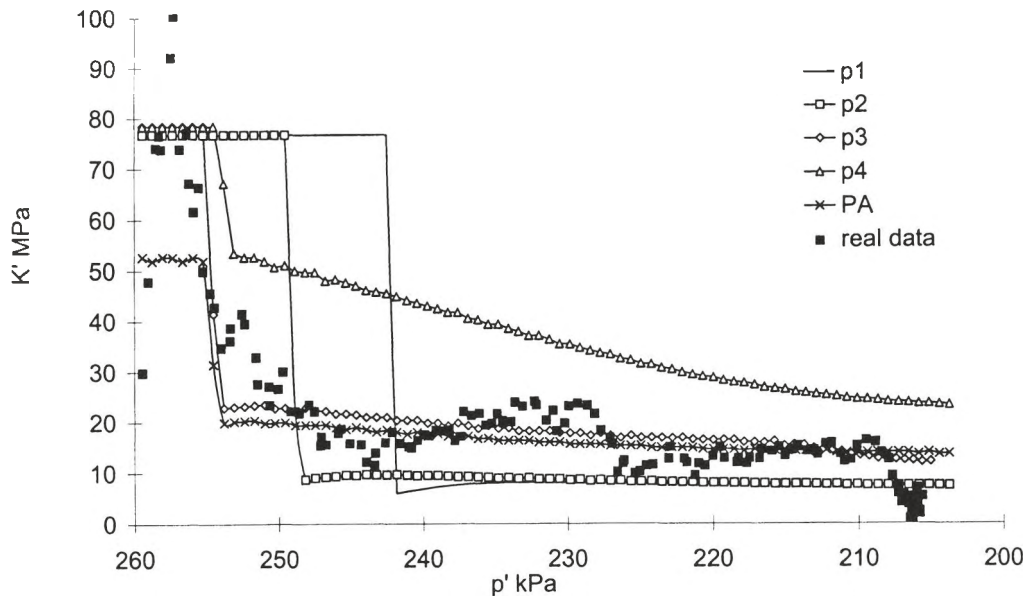


Figure 5.66 Stiffness curve for Oxford clay constant  $p'$  test T06SHR06 plotted against model predictions for varying values of  $T$ ,  $S$  and  $\phi$  and for anisotropic model prediction.

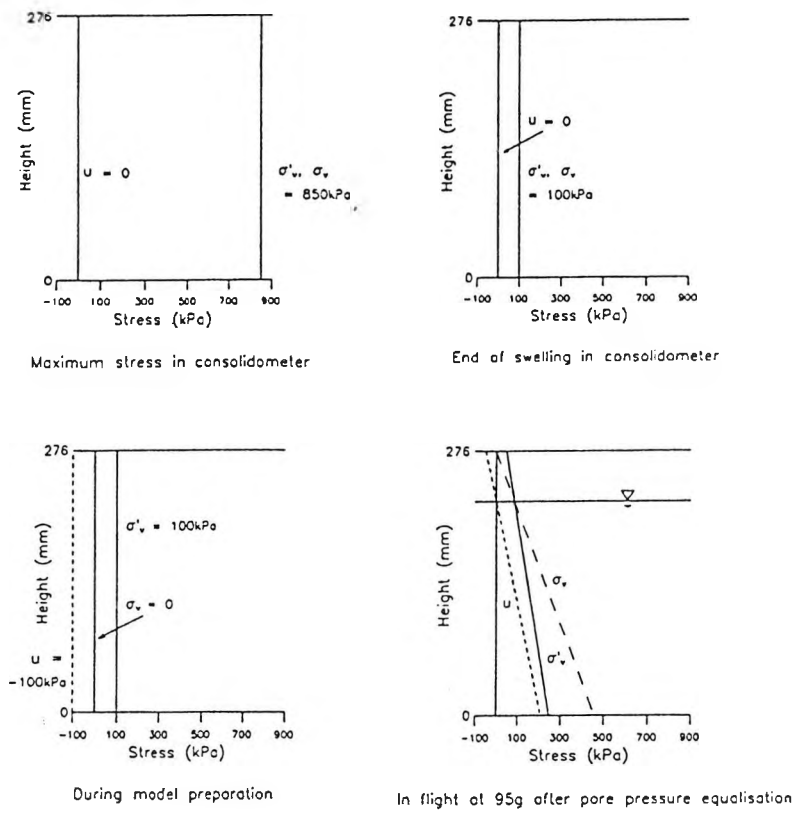
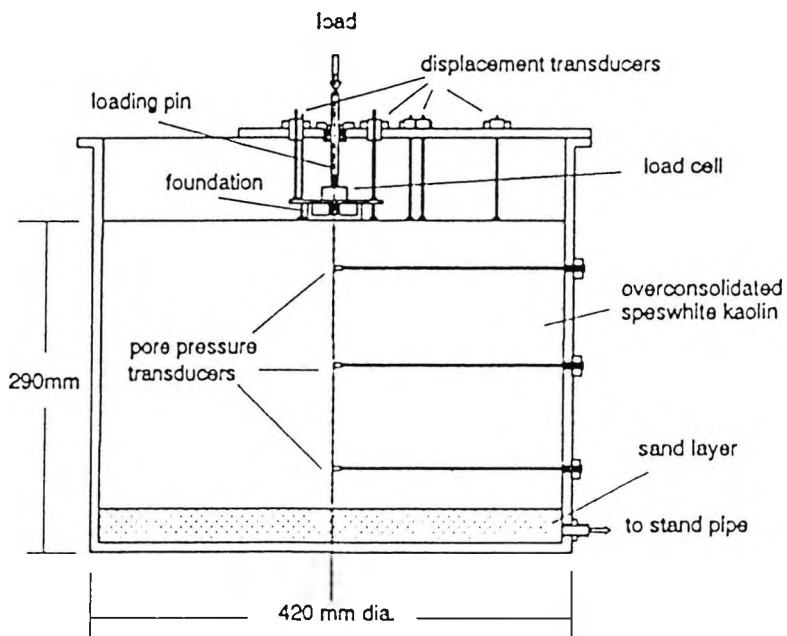


Figure 6.1 The change in stress distribution in the clay layer during consolidation, preparation and testing of the centrifuge foundation model (after Stallebrass and Taylor, 1997)



Cross section

Figure 6.2 Diagram showing general layout of the centrifuge foundation model (after Stallebrass and Taylor, 1997)

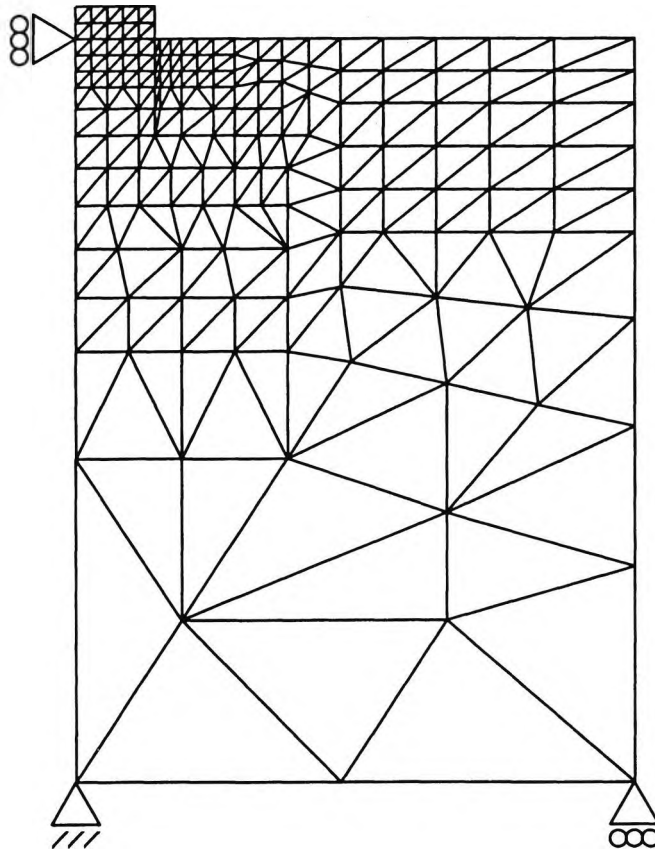


Figure 6.3 Finite element mesh used for analyses carried out using the CriSP finite element program for the 3-SKH model and Modified Cam clay

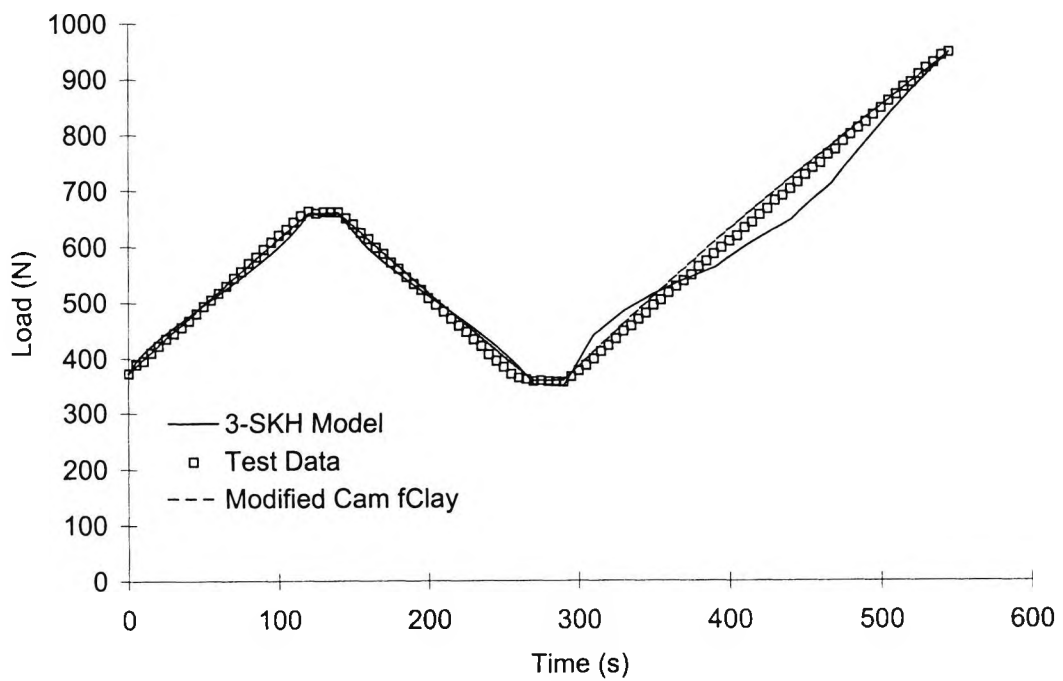


Figure 6.4 Load/time ramps applied during the centrifuge foundation test, showing 3-SKH model and Modified Cam clay simulations.

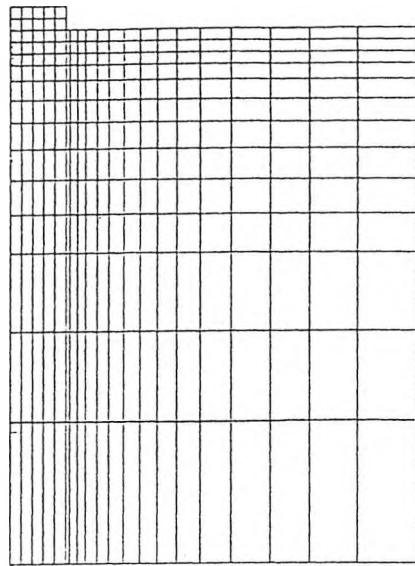


Figure 6.5 Finite element mesh used for analyses carried out using the SAFE finite element program for the Brick model

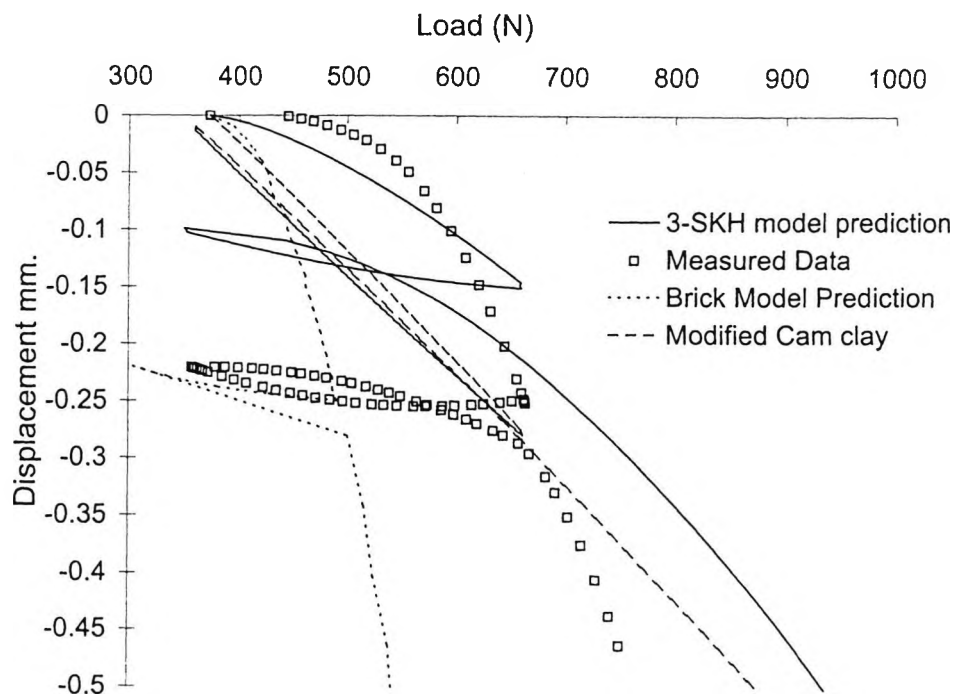


Figure 6.6 Load-displacement curves comparing measured data with 3-SKH model and Brick model predictions at the centre of the foundation

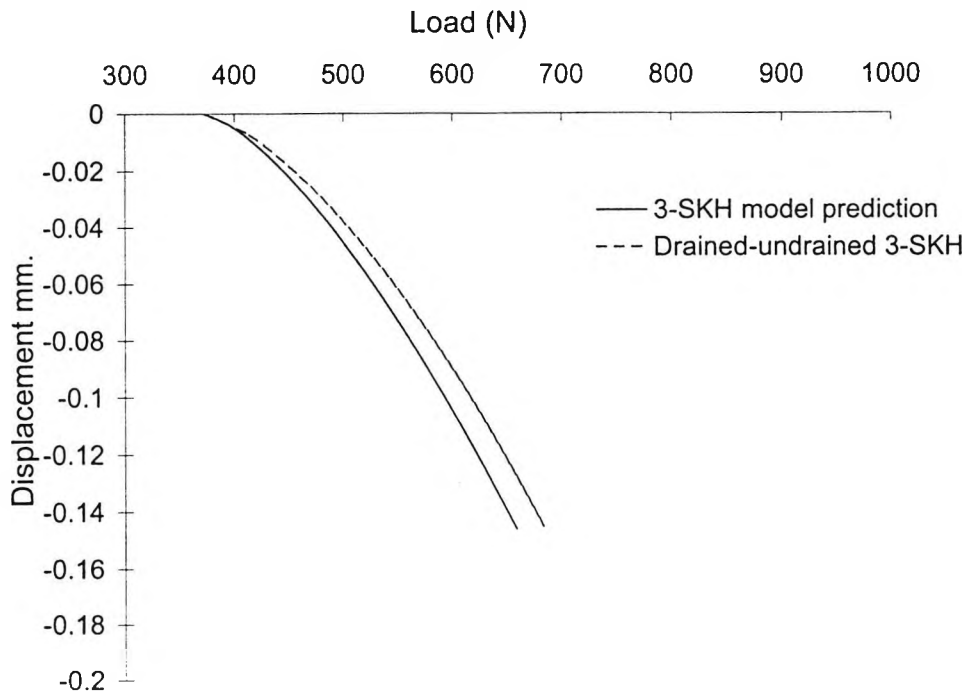


Figure 6.7 Comparison of predicted 1<sup>st</sup> load-displacement curves predicted using the 3-SKH model for consolidation and drained/undrained assumptions

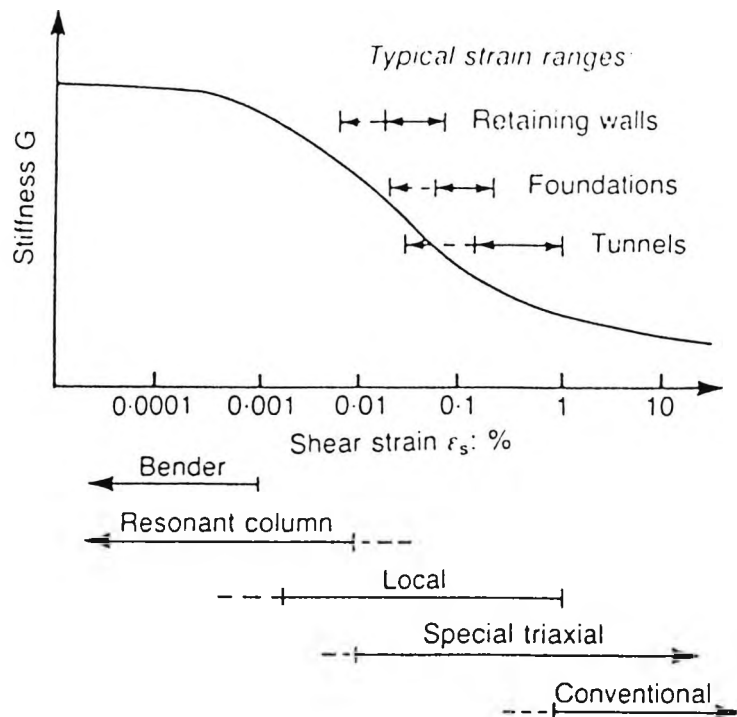


Figure 6.8 Typical strain ranges around geotechnical structures (after Mair, 1993)

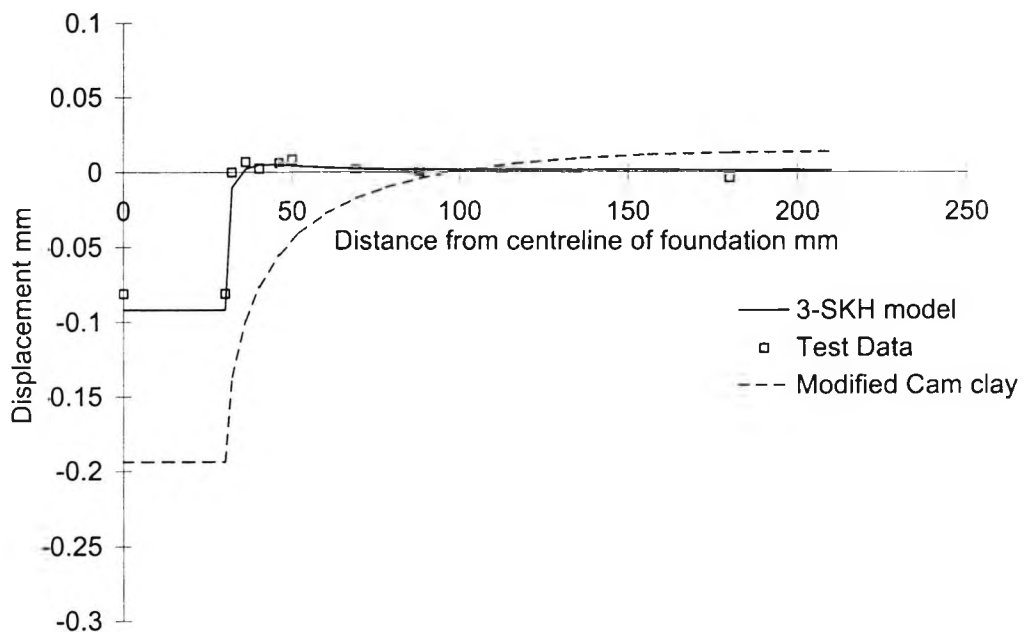


Figure 6.9 Settlement profile at 580N first loading comparing measured data and 3-SKH model and Modified Cam clay predictions

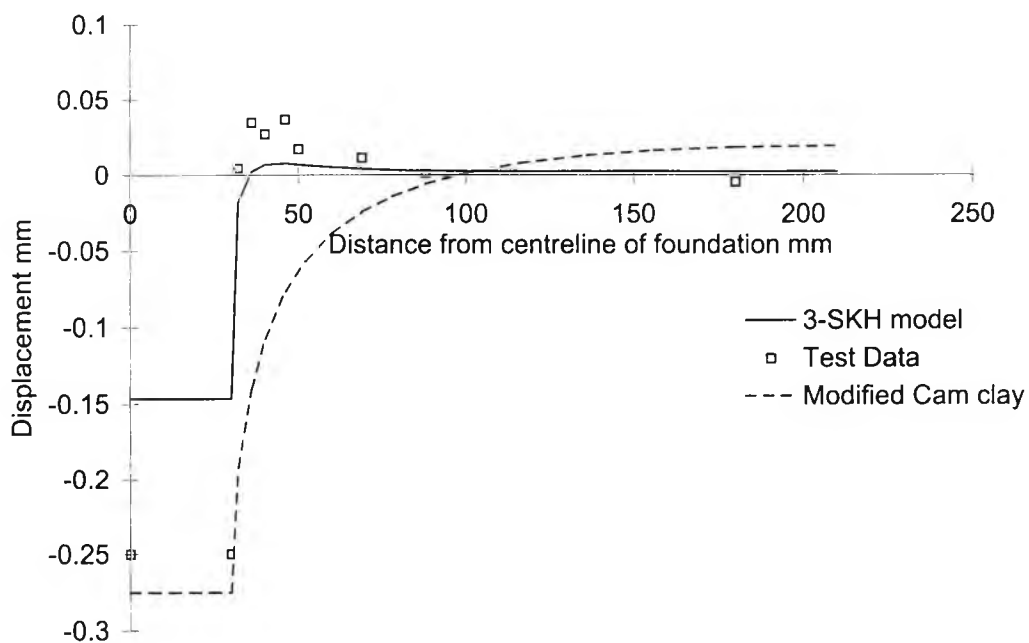


Figure 6.10 Settlement profile at 660N first loading comparing measured data and 3-SKH model and Modified Cam clay predictions

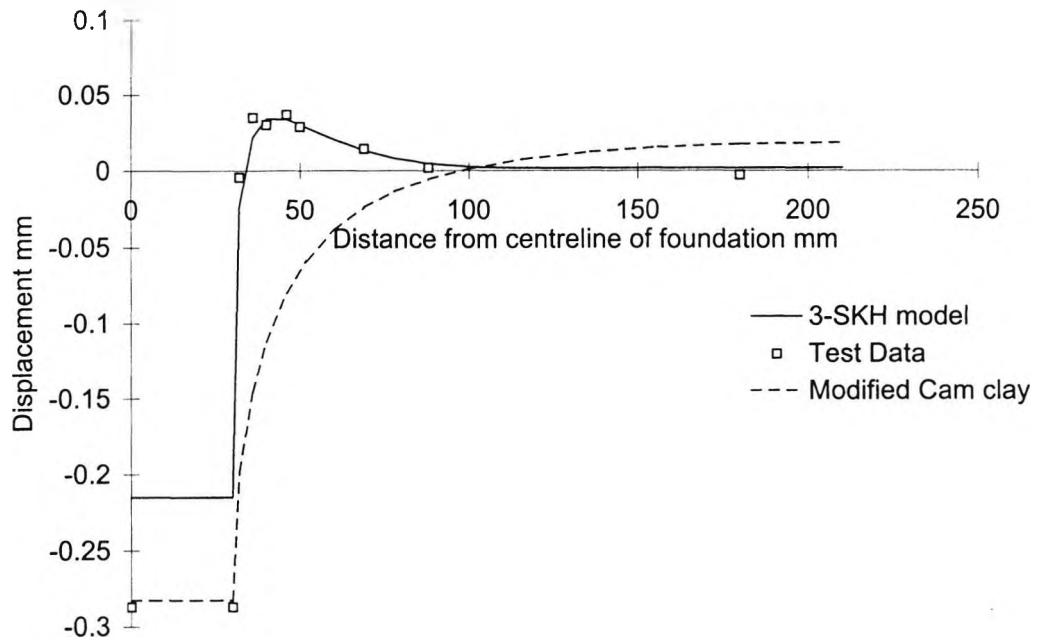


Figure 6.11 Settlement profile at 660N re-loading comparing measured data and 3-SKH model and Modified Cam clay predictions

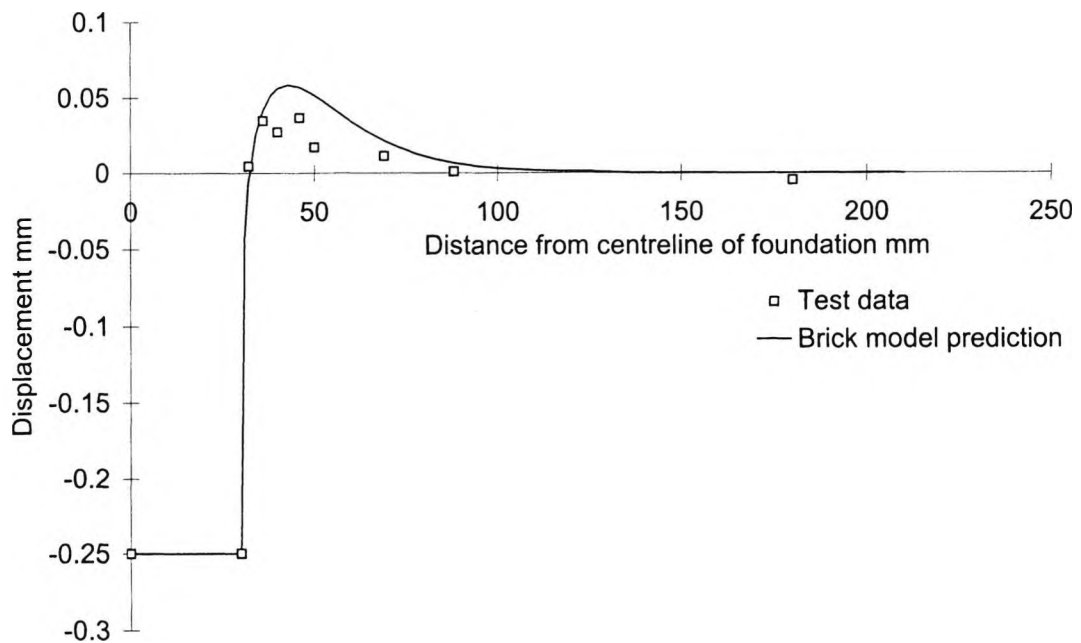


Figure 6.12 Settlement profile at end of first loading comparing measured data and Brick model prediction

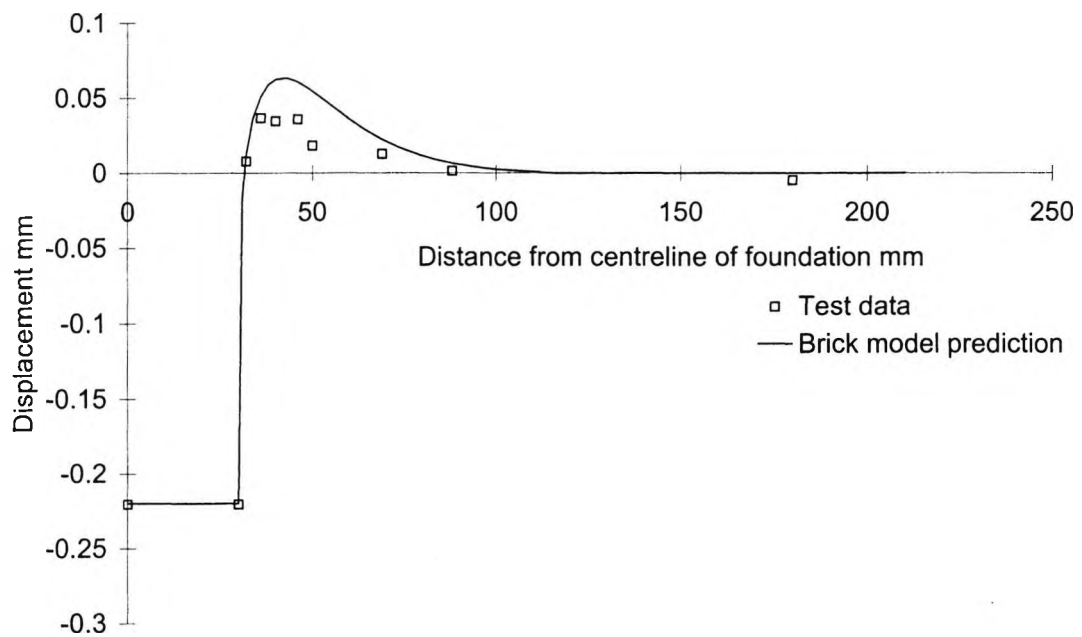


Figure 6.13 Settlement profile at end of swelling comparing measured data and Brick model prediction

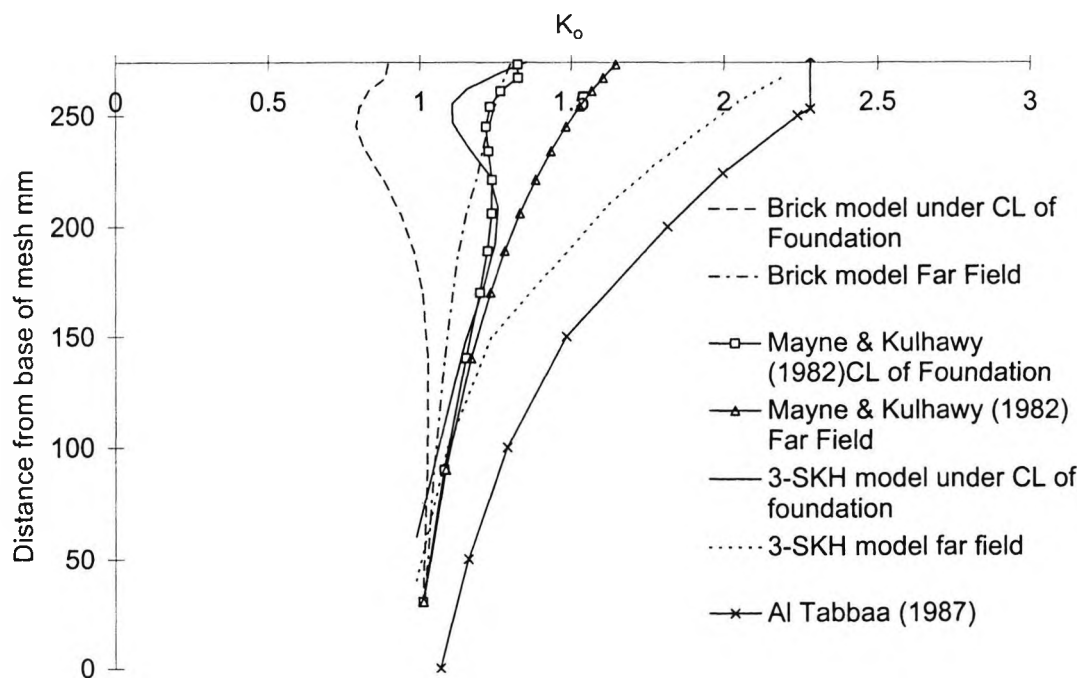


Figure 6.14  $K_0$  profiles predicted from finite element analyses compared to various methods of estimating  $K_0$  from the literature

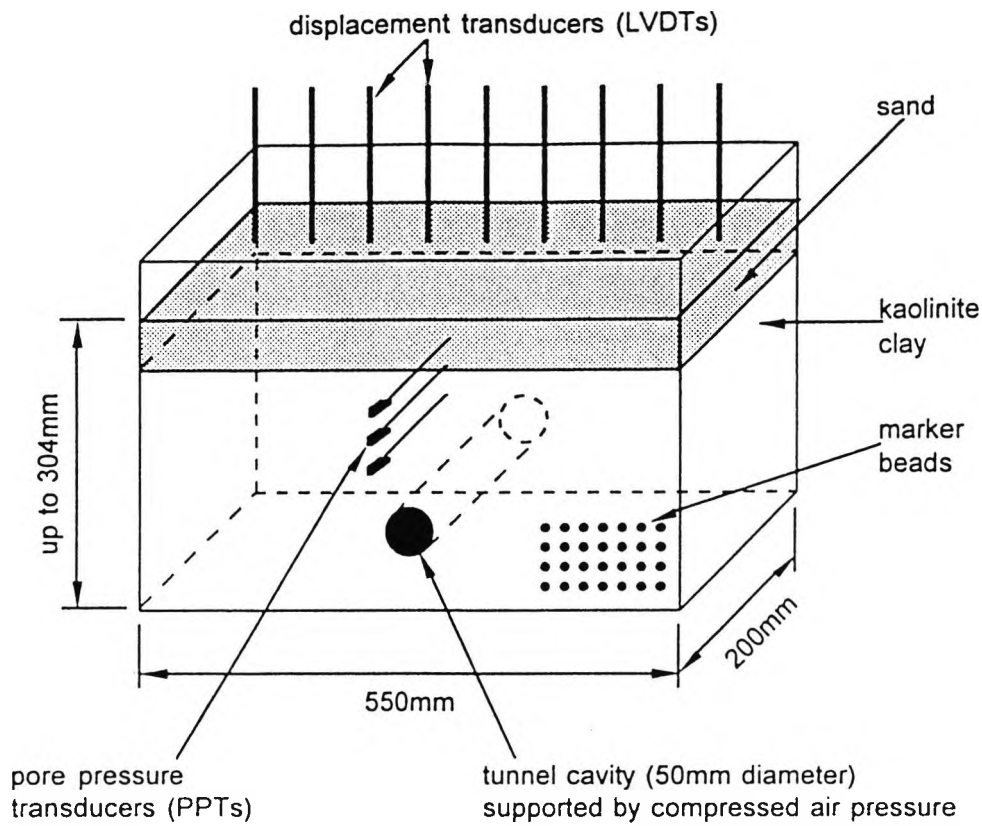


Figure 6.15 The centrifuge tunnel model (after Grant, 1998)

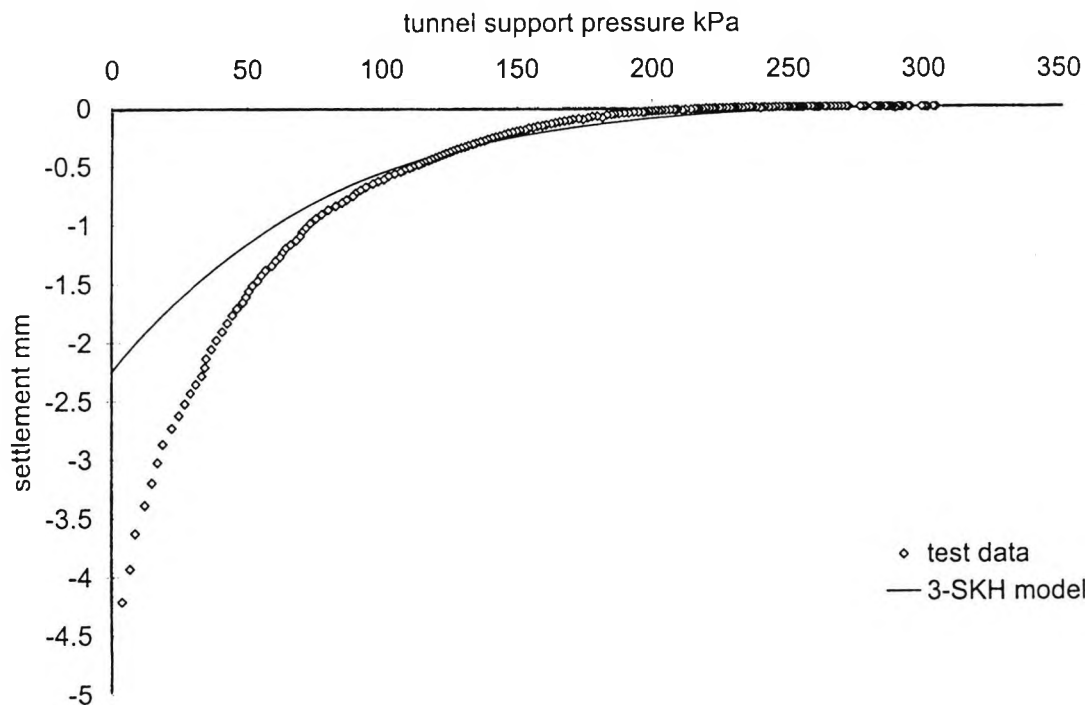


Figure 6.16 Surface settlement plotted against reduction in tunnel support pressure for centrifuge tunnel test

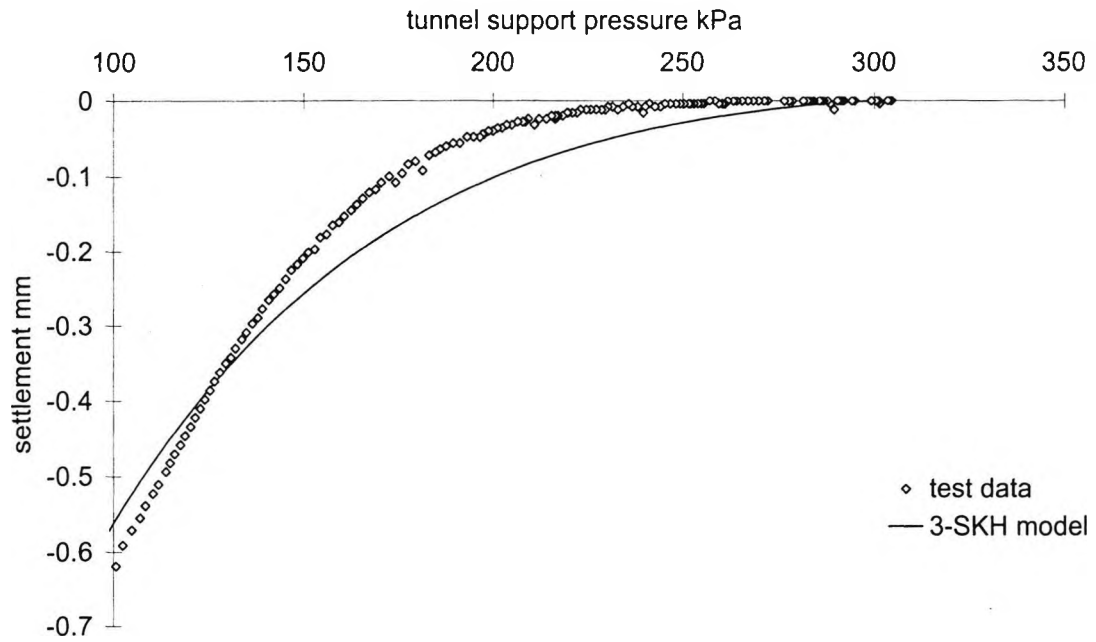


Figure 6.17 Enlargement of the initial part of the graph of surface settlement plotted against reduction in tunnel support pressure.

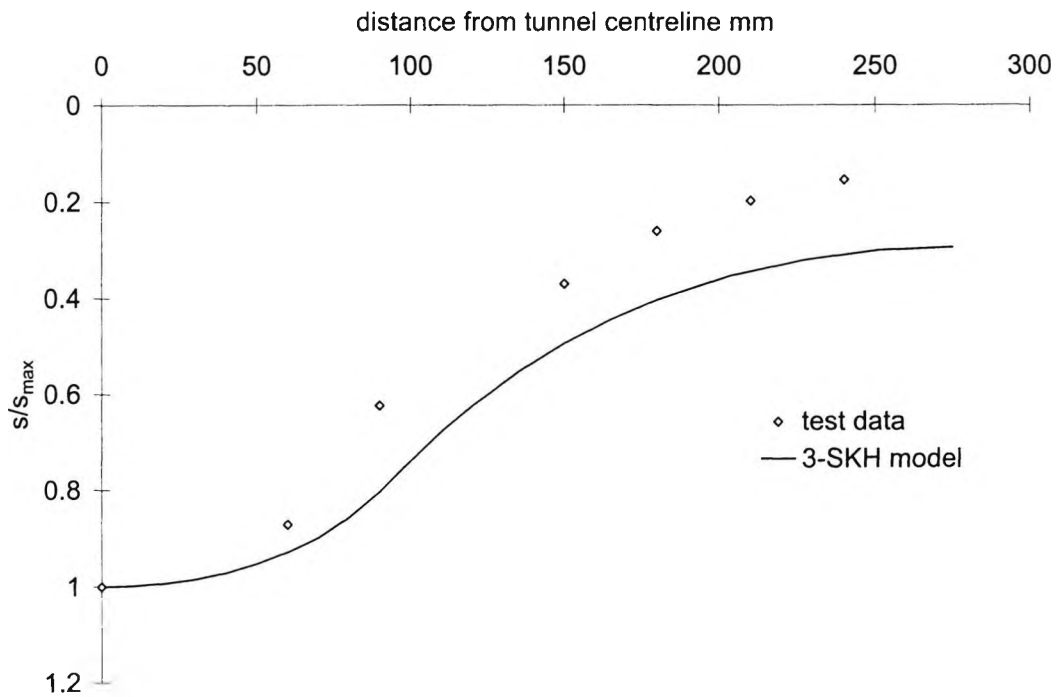


Figure 6.18 Normalised tunnel settlement profiles at ground surface for a 20% volume loss for centrifuge tunnel test

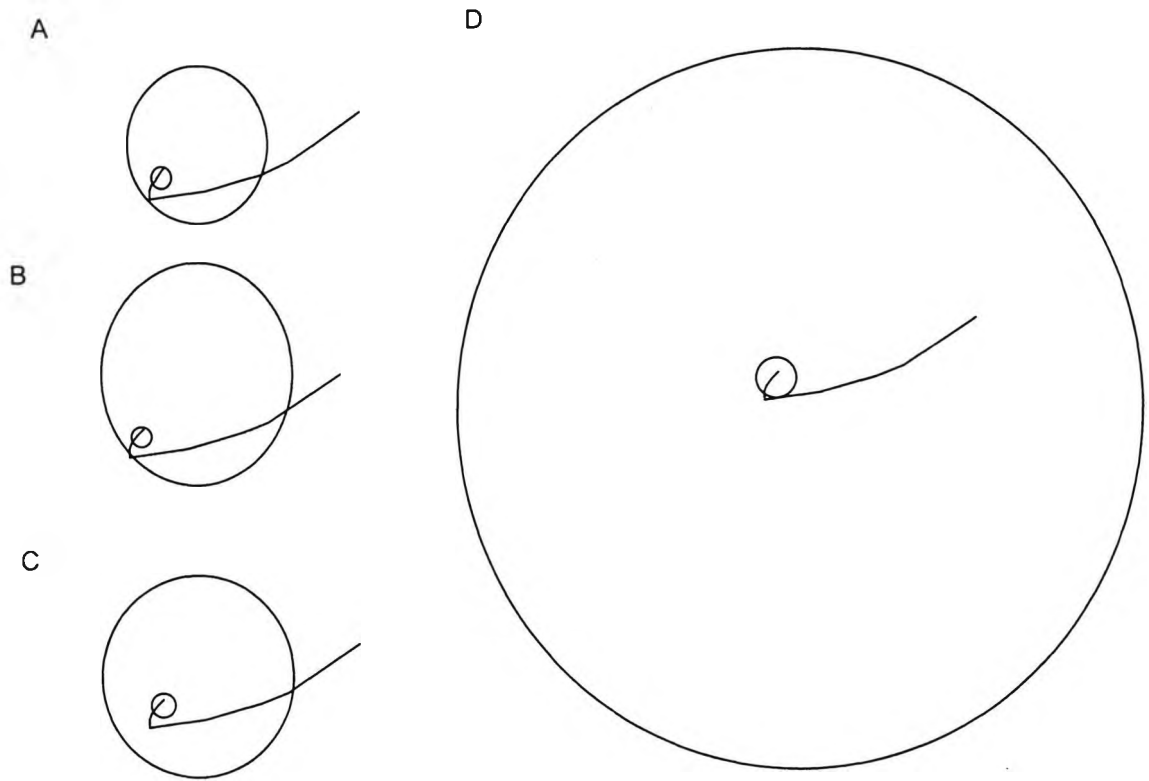


Figure 7.1 Approximate size and location of the kinematic surfaces of the 3-SKH model prior to the modelling of the geotechnical events for an element of soil at the top of the clay layer

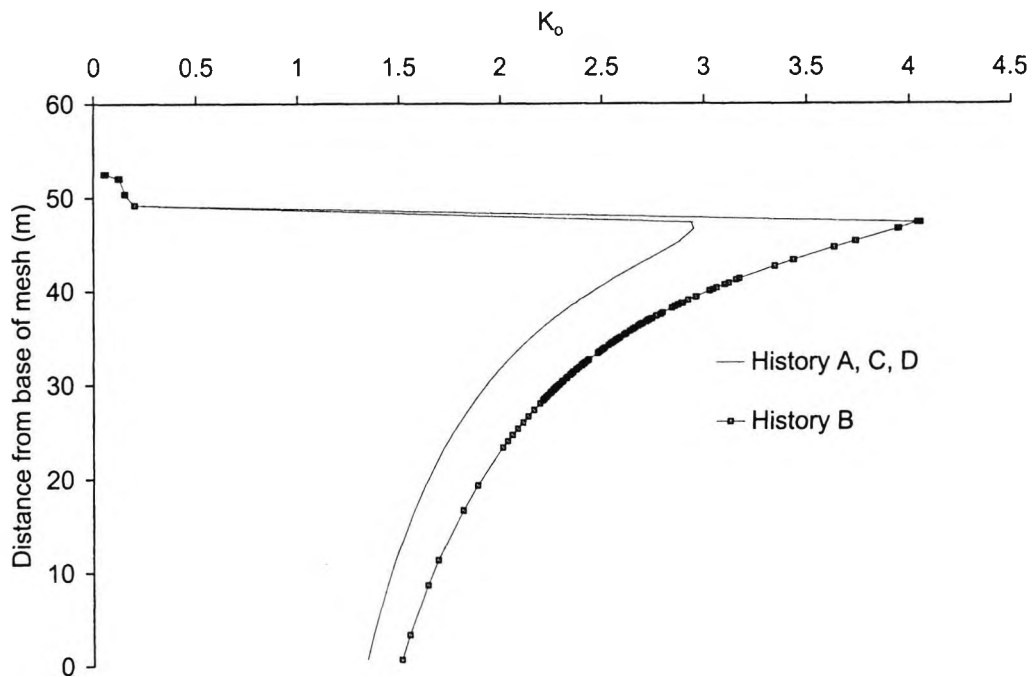


Figure 7.2  $K_0$  profiles predicted by the finite element analyses prior to reduction of tunnel pressures

123.0m  
Terrace gravel and made ground  
118.0m  
London clay

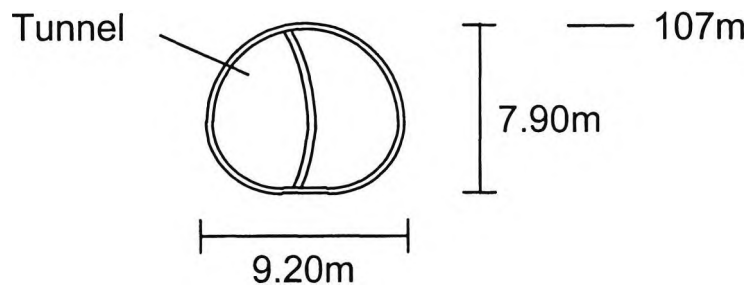


Figure 7.3 The geometry of the tunnel problem

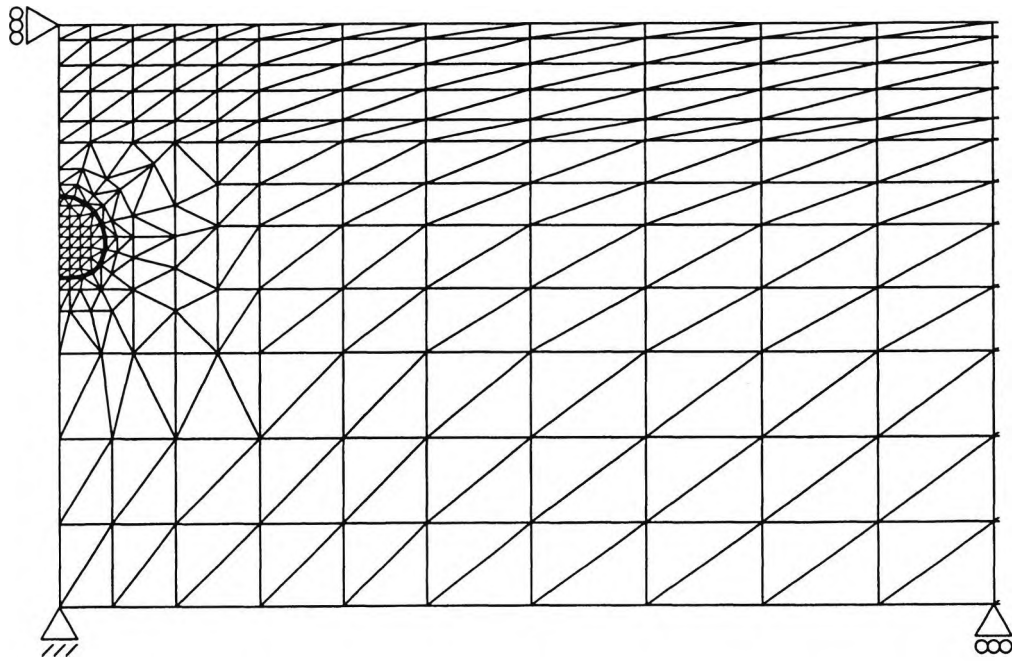


Figure 7.4 Finite element mesh used for the tunnel problem

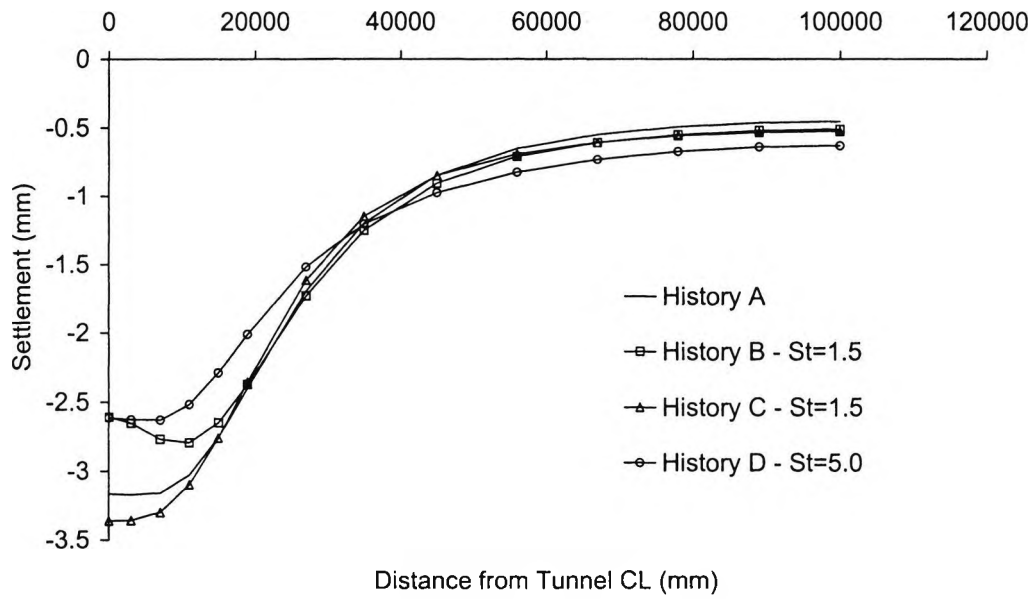


Figure 7.5 Clay/gravel interface settlement profiles at 0.5% volume loss

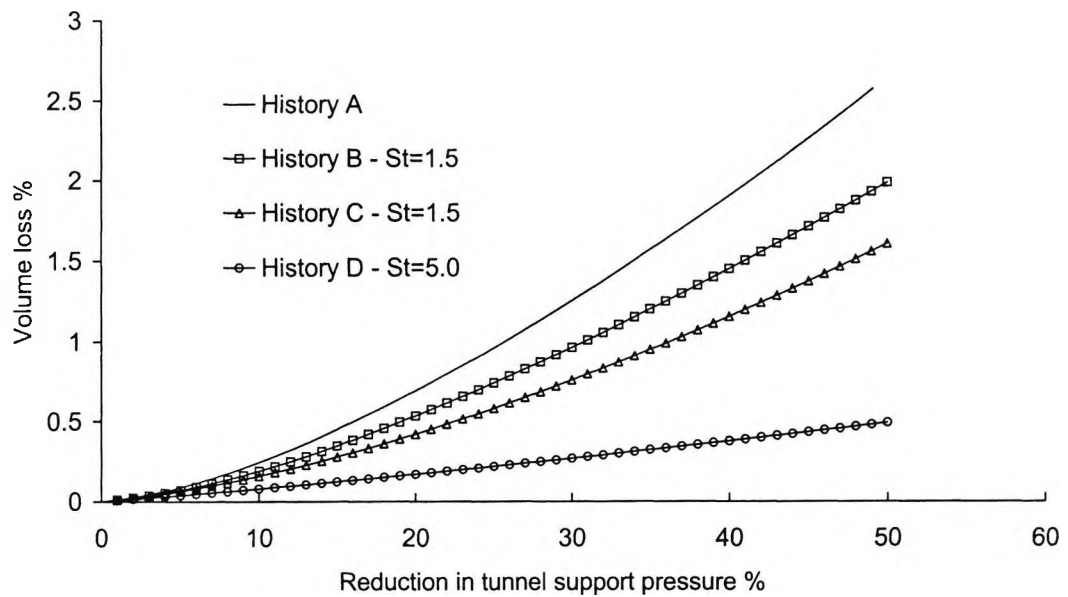


Figure 7.6 Percentage reduction in tunnel support pressure against percentage volume loss

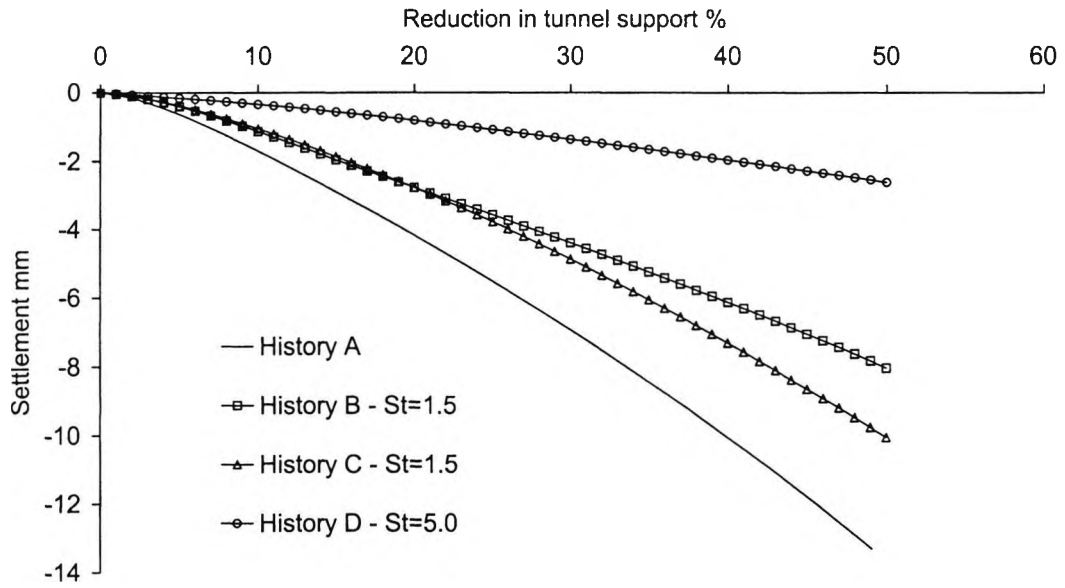


Figure 7.7 Surface settlement above tunnel centreline against percentage reduction in tunnel support pressure

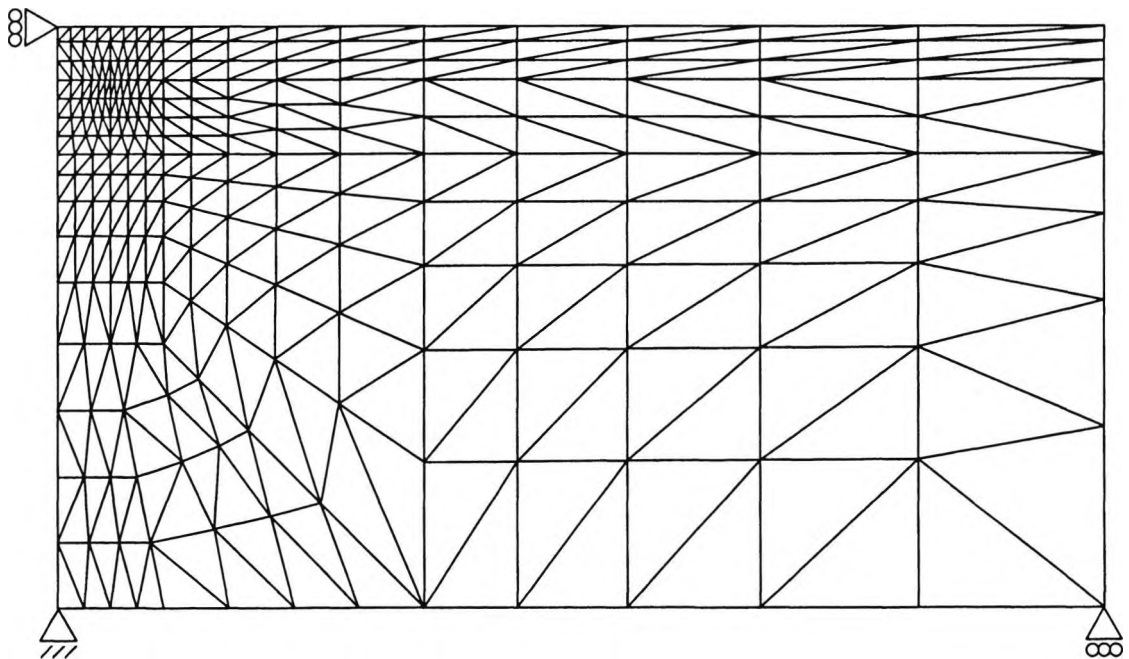


Figure 7.8 Finite element mesh for the foundation problem

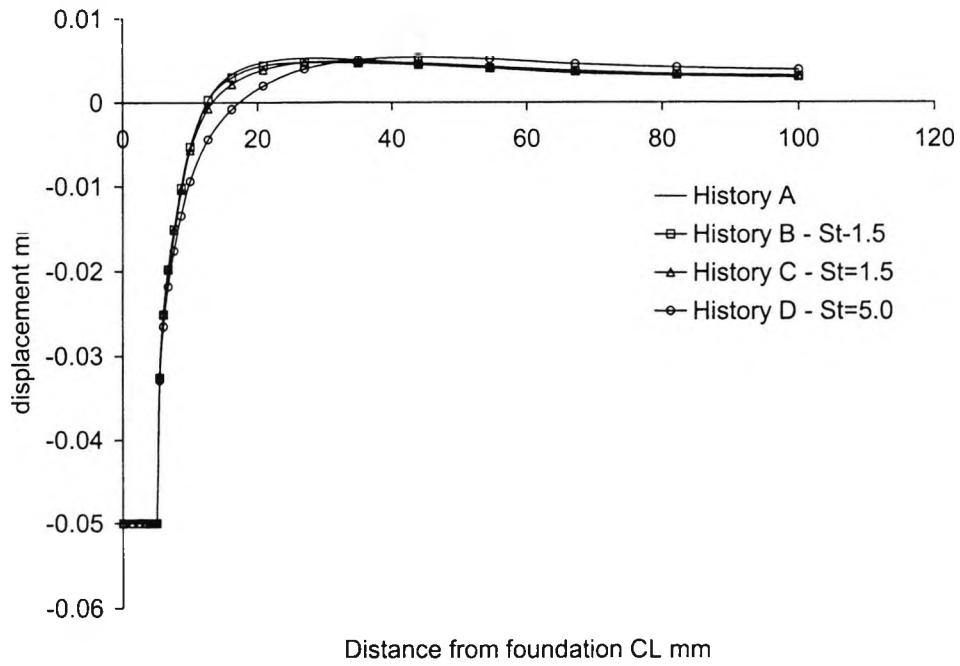


Figure 7.9 Settlement profiles predicted at the clay/gravel interface for a foundation displacement of 5mm

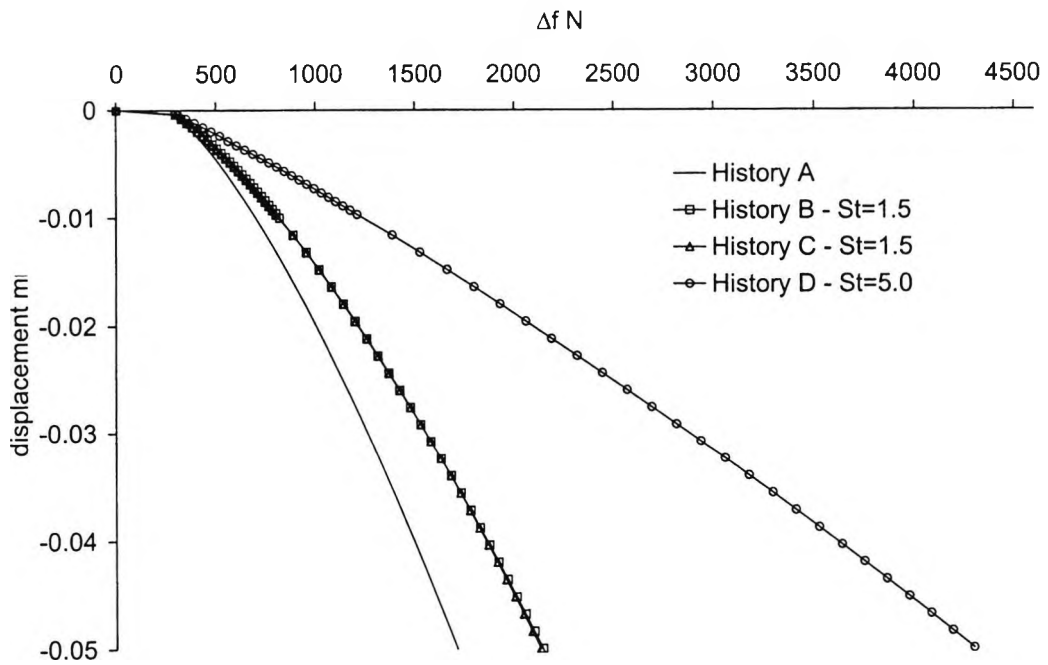


Figure 7.10 Change in vertical force applied to foundation against displacement at centreline

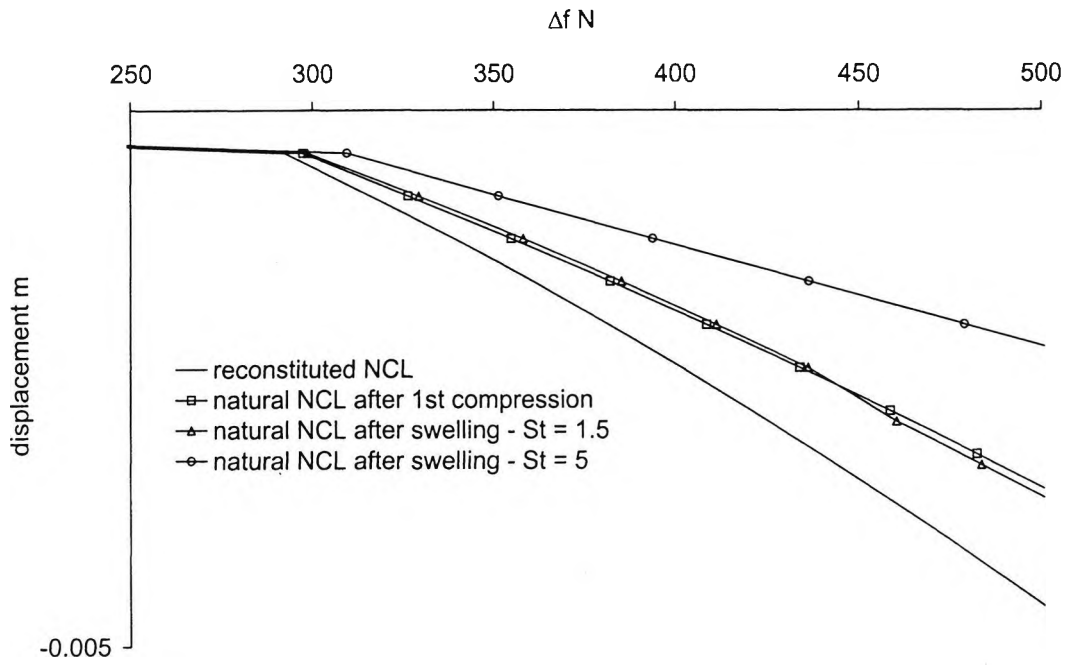


Figure 7.11 Detail of initial portion of Change in vertical force applied to foundation against displacement at centreline curve

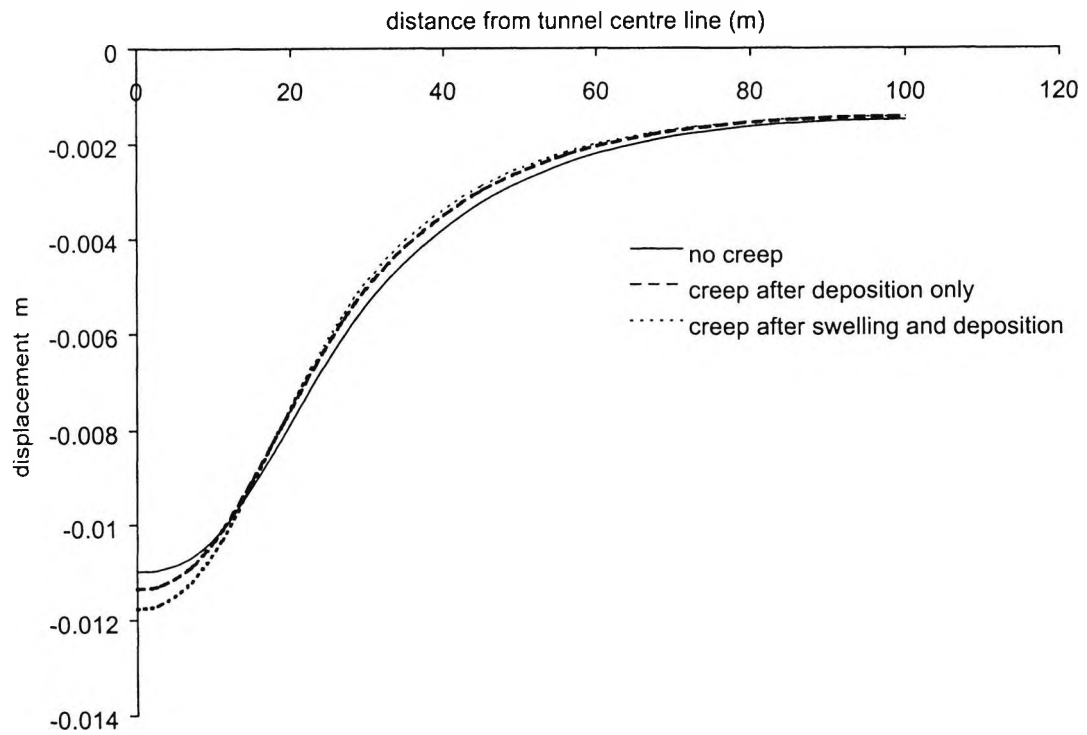


Figure 7.12 Settlement troughs at ground surface for 1.5% volume loss.

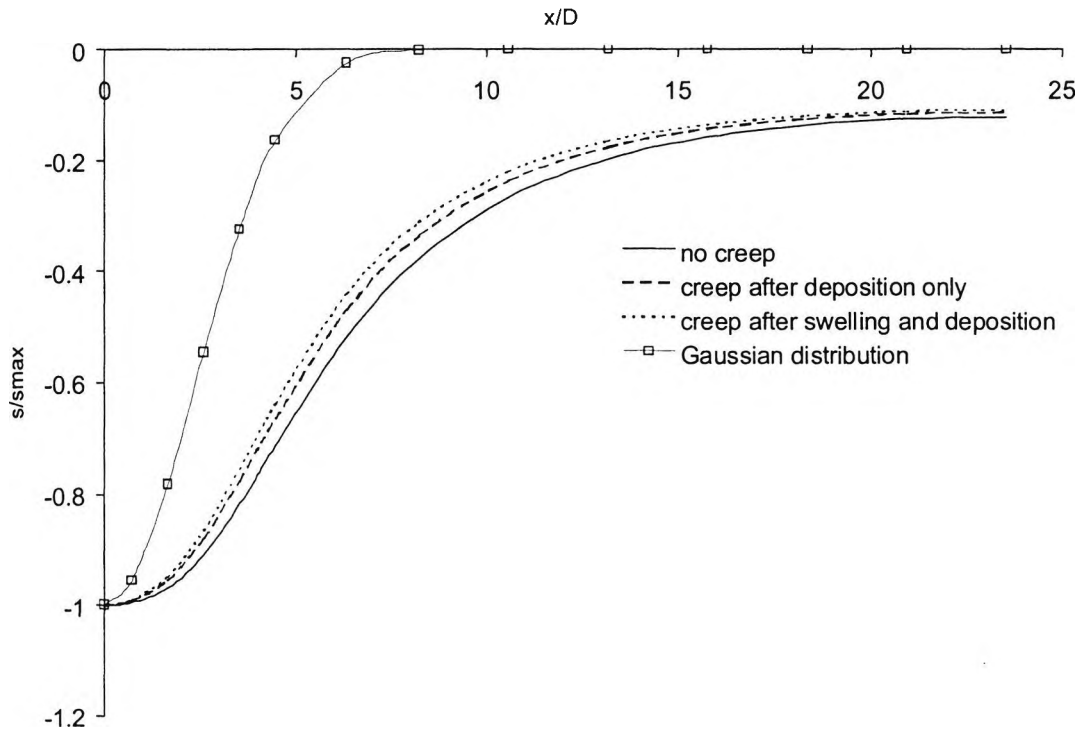


Figure 7.13 Normalised settlement profiles at ground surface, showing Gaussian distribution.

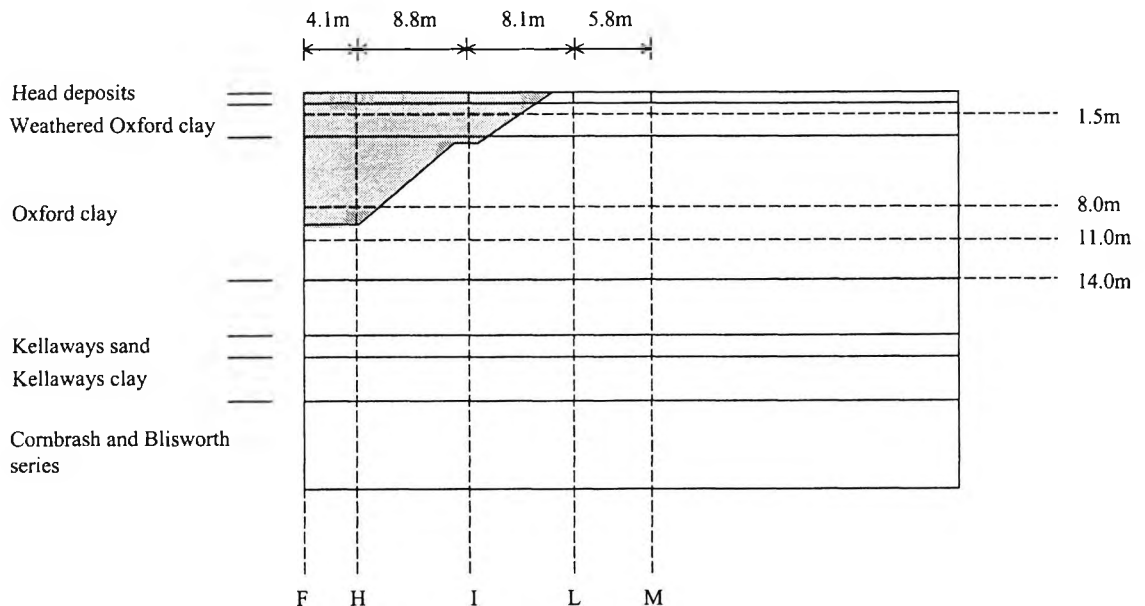


Figure 7.14 Schematic showing location of monitoring sections and soil strata

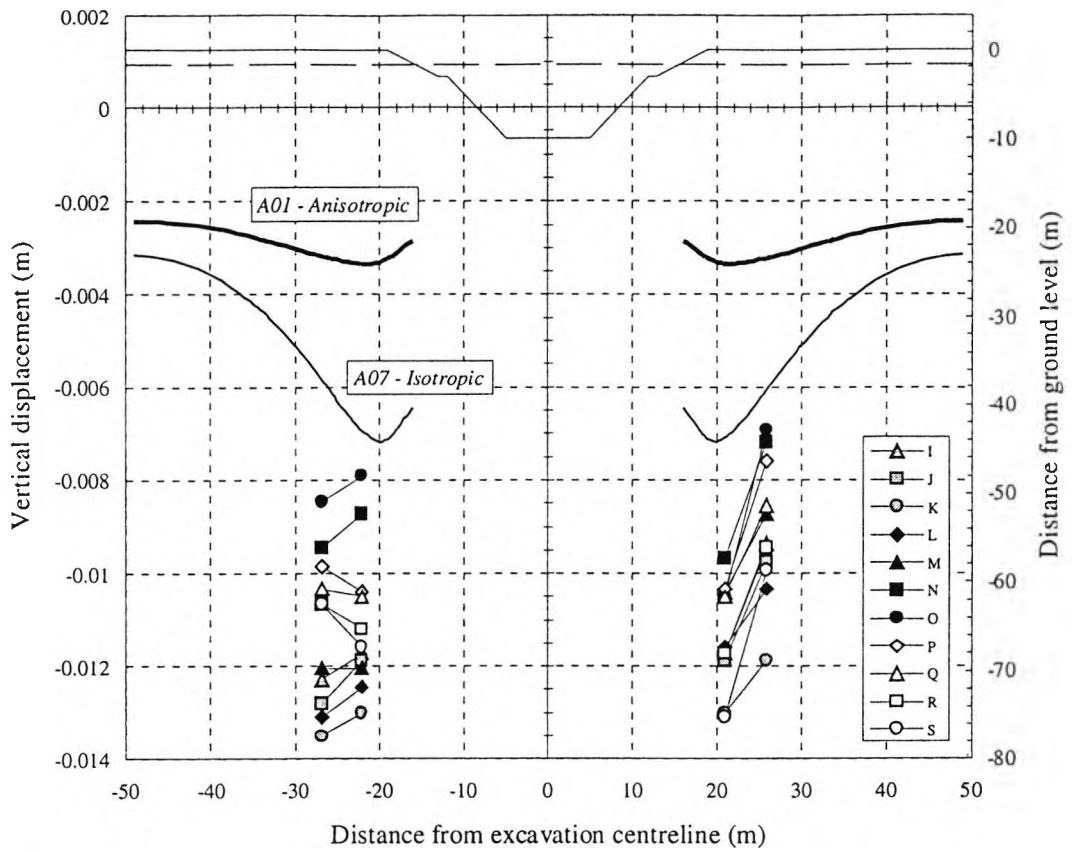


Figure 7.15 Prediction of vertical displacement at 1.5m depth for model O.C. (after Pierpoint, 1996)

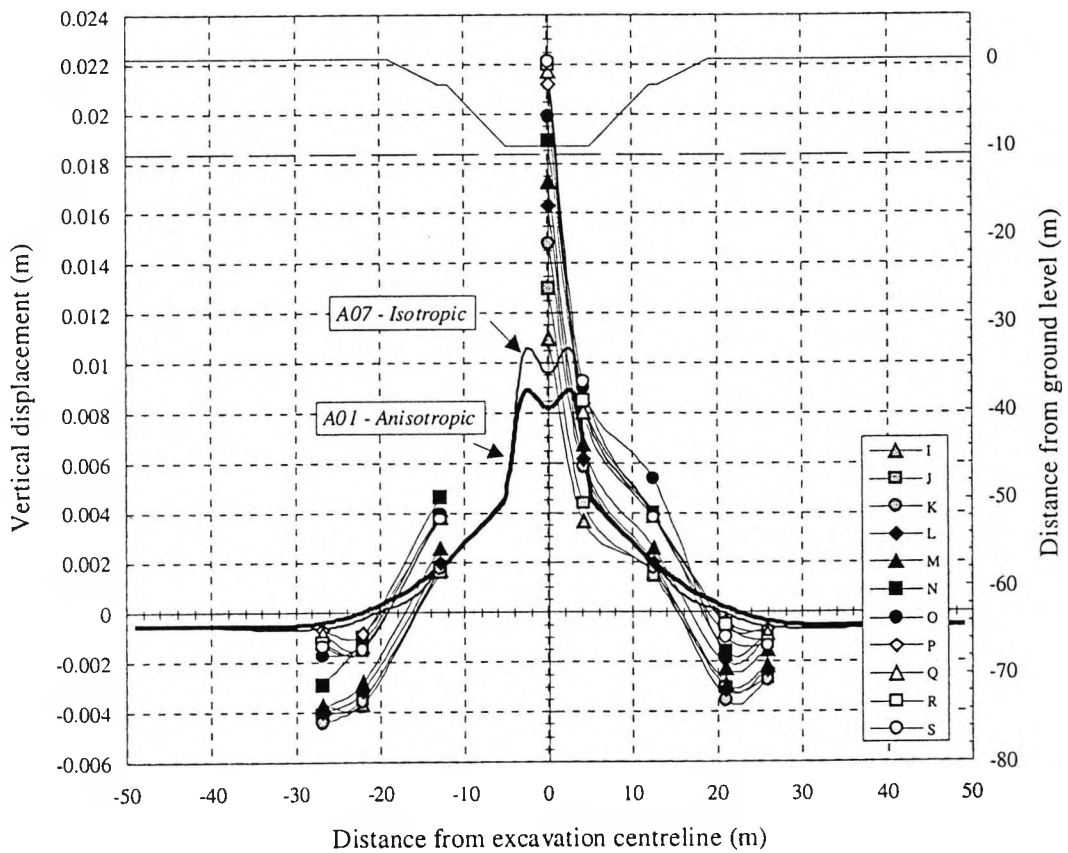


Figure 7.16 Prediction of vertical displacement at 11m depth for model O.C. (after Pierpoint, 1996)

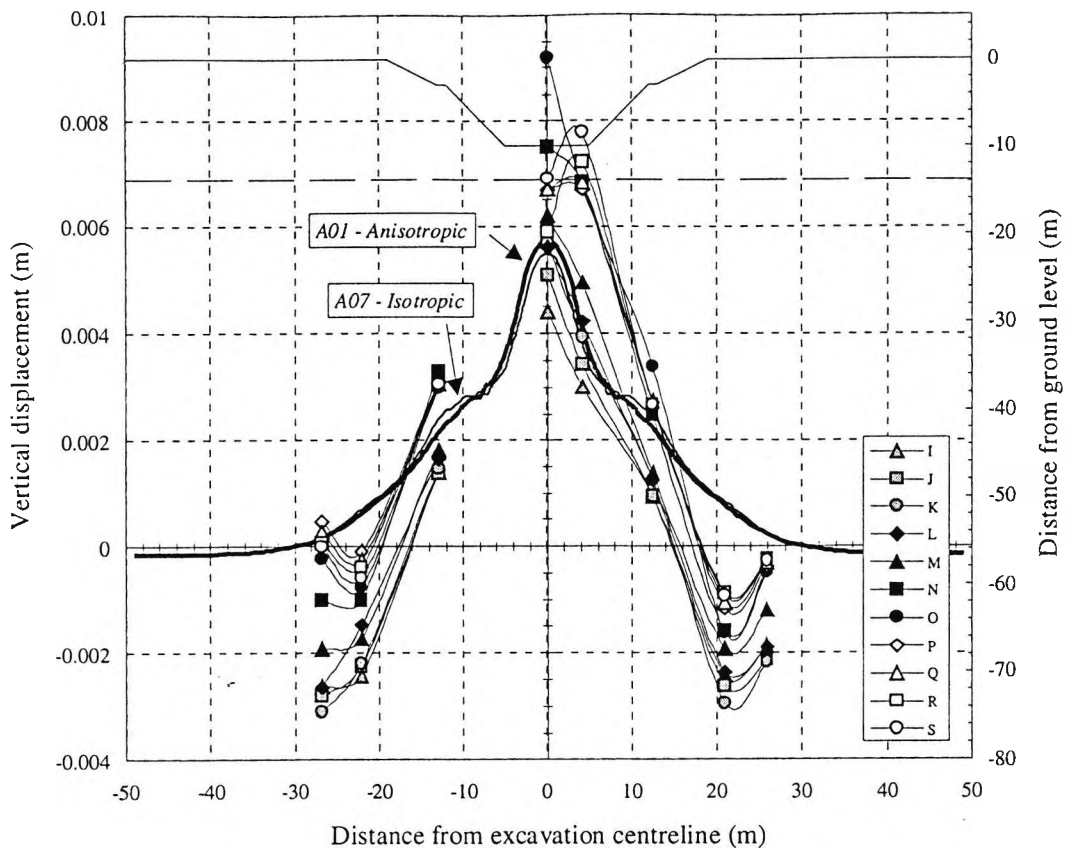


Figure 7.17 Prediction of vertical displacement at 14m depth for model O.C. (after Pierpoint, 1996)

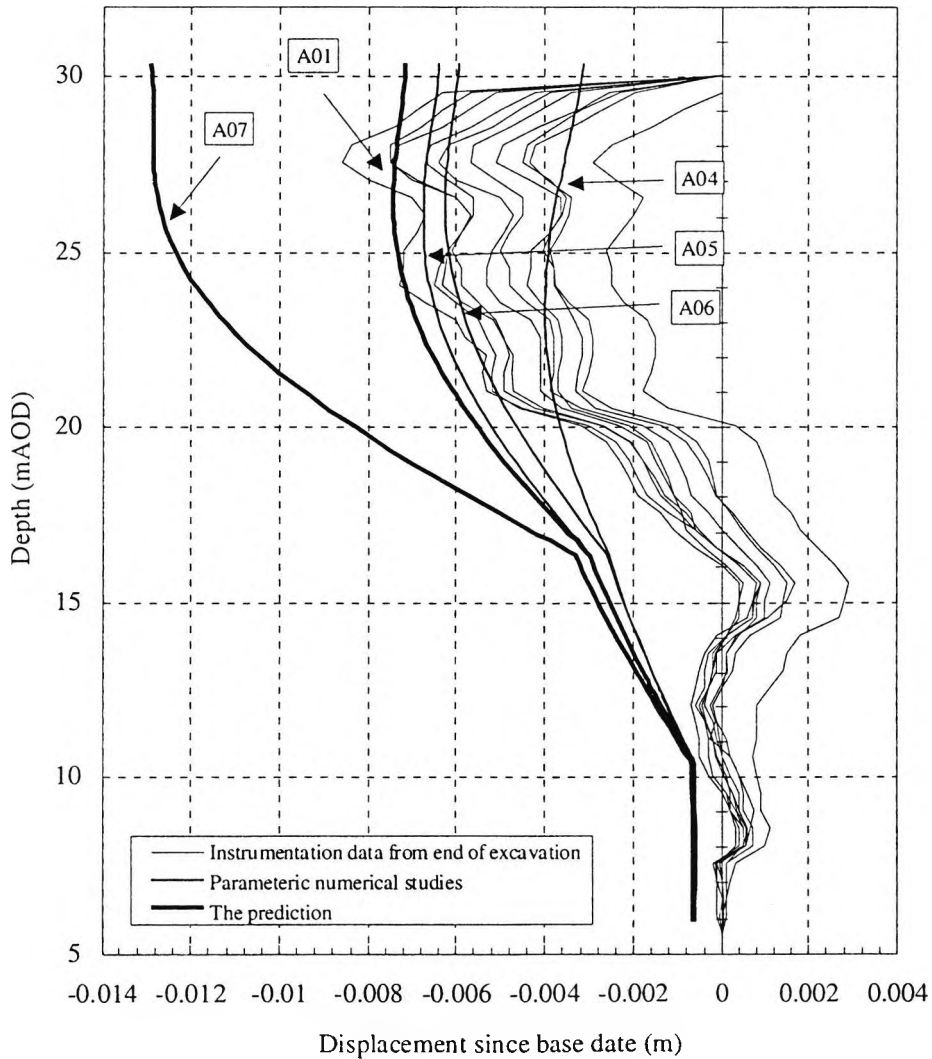


Figure 7.18 Prediction of horizontal displacement at section L for model O.C. (after Pierpoint, 1996)

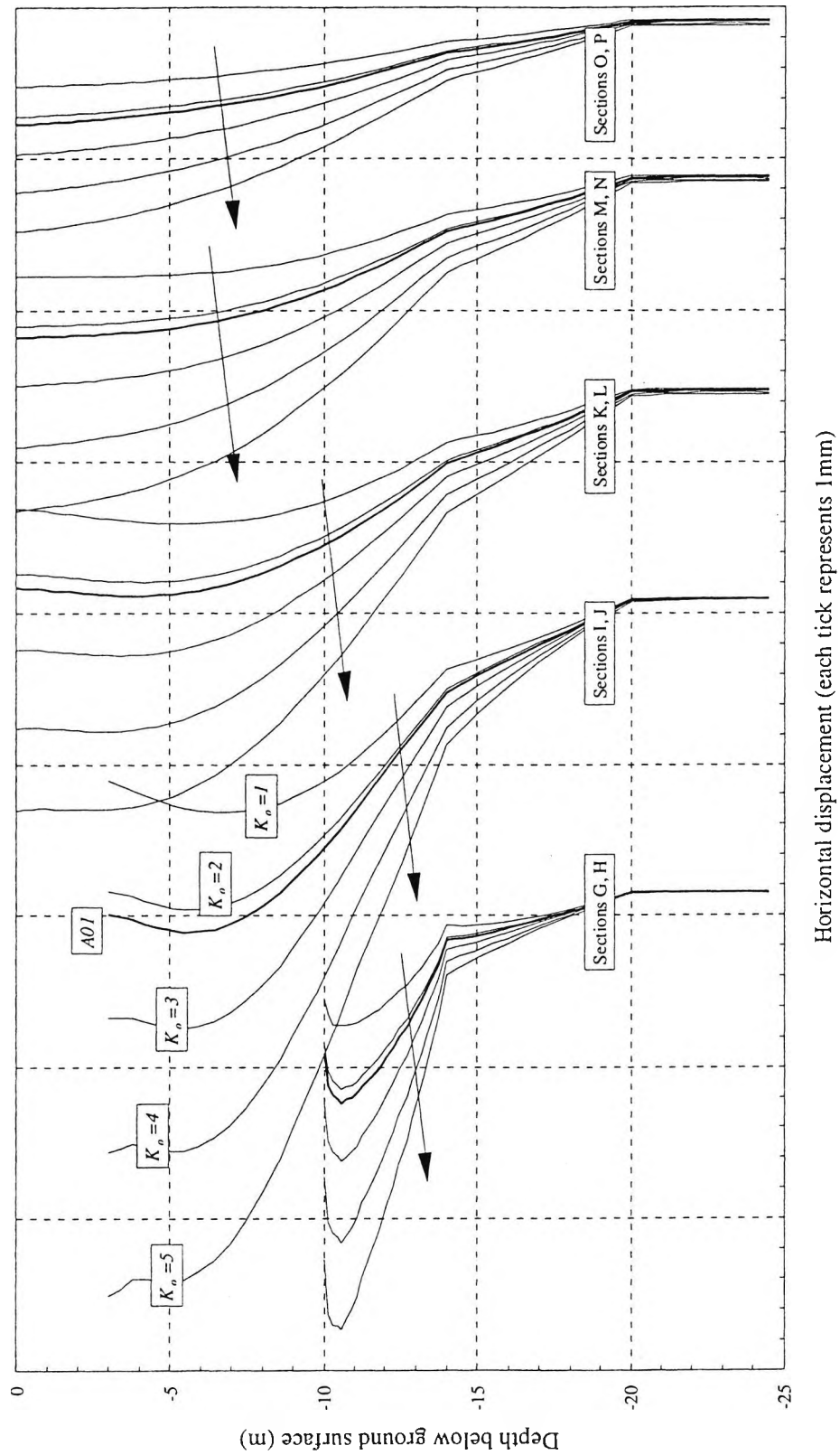


Figure 7.19 Prediction of horizontal displacement with varying  $K_0$  at various distances from the excavation centreline for model O.C. (after Pierpoint, 1996)

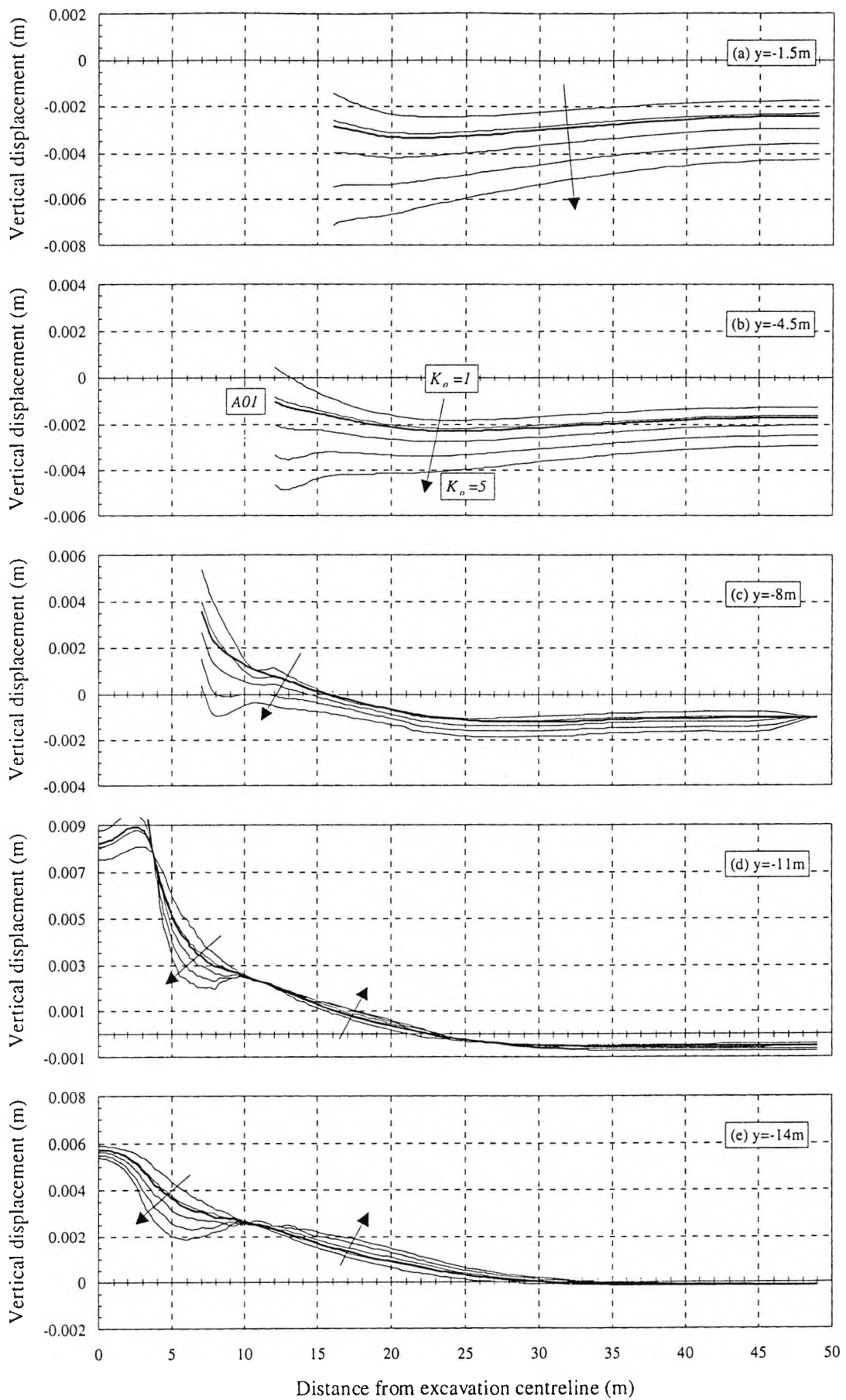


Figure 7.20 Prediction of vertical displacement with varying  $K_0$  at various depths for model O.C. (after Pierpoint, 1996)

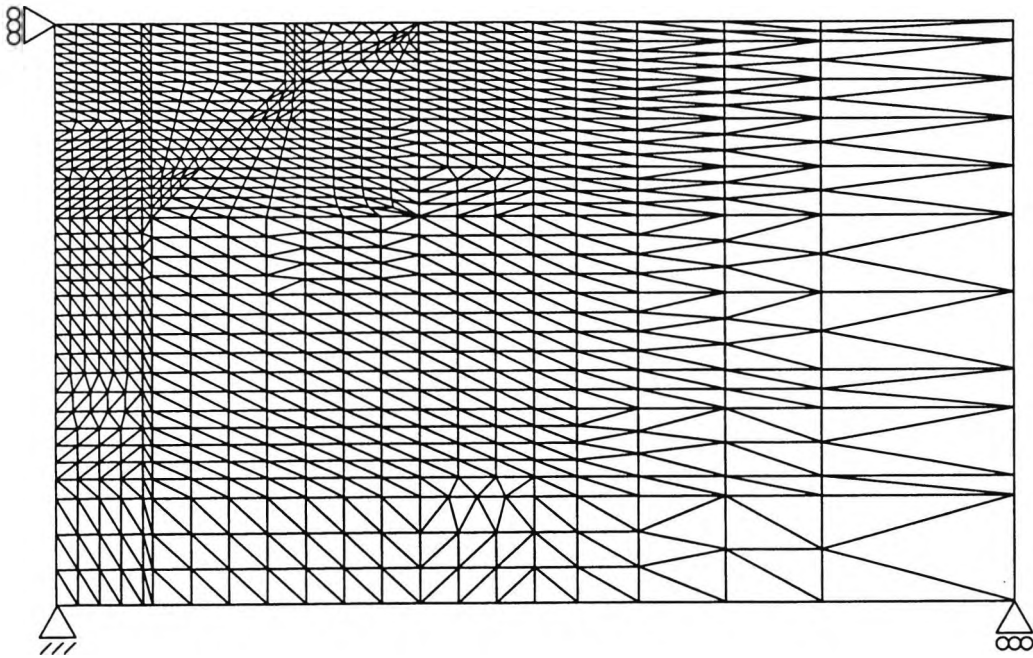


Figure 7.21 Finite element mesh for the Elstow excavation analyses

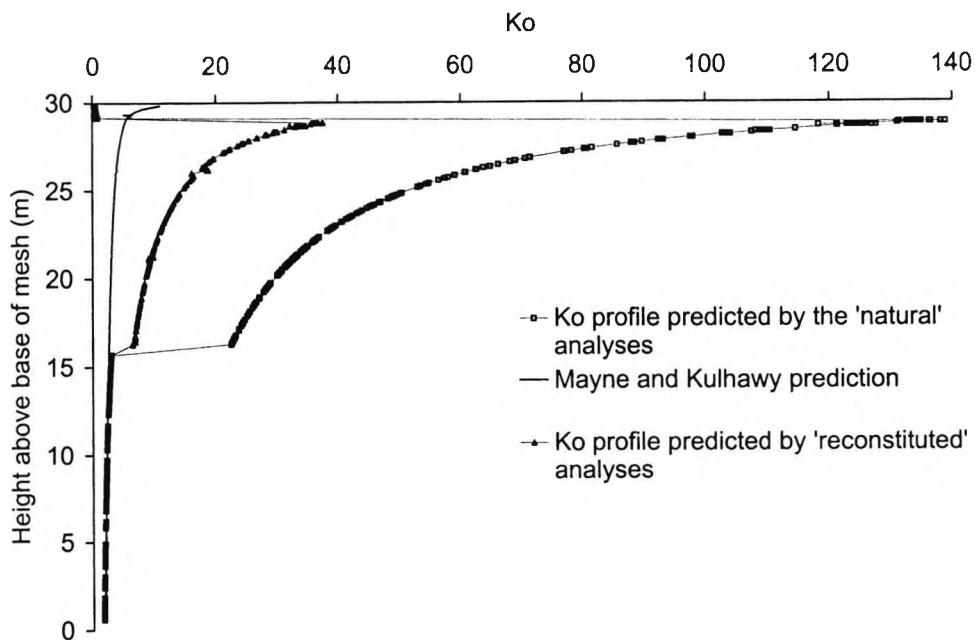


Figure 7.22  $K_0$  profiles predicted by the finite element analyses prior to excavation

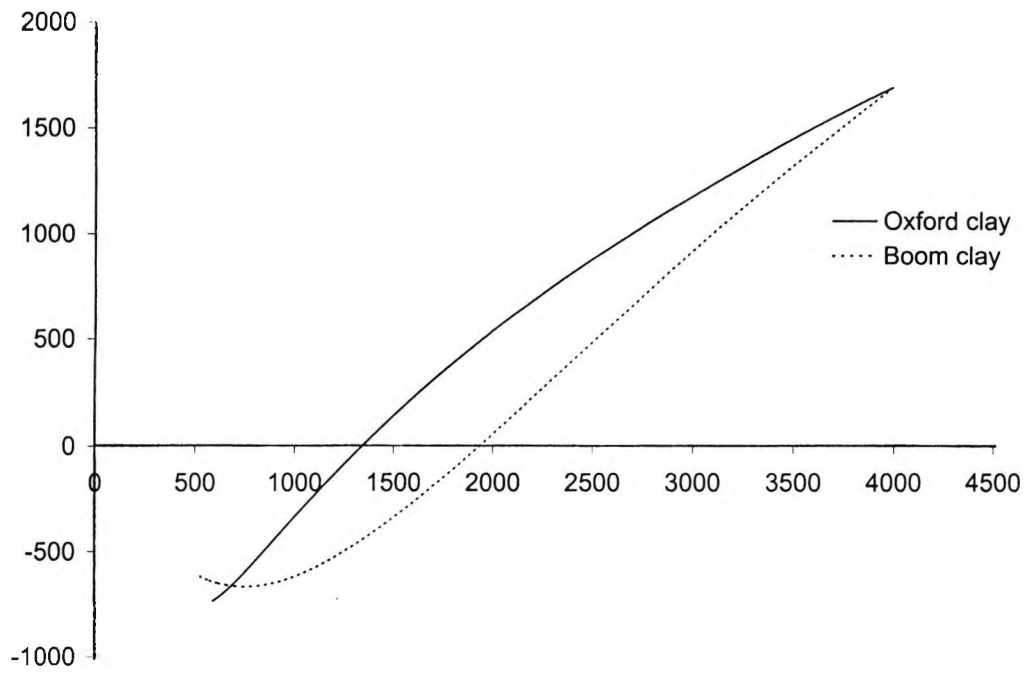


Figure 7.23 Predicted unloading curve for the Oxford clay analyses

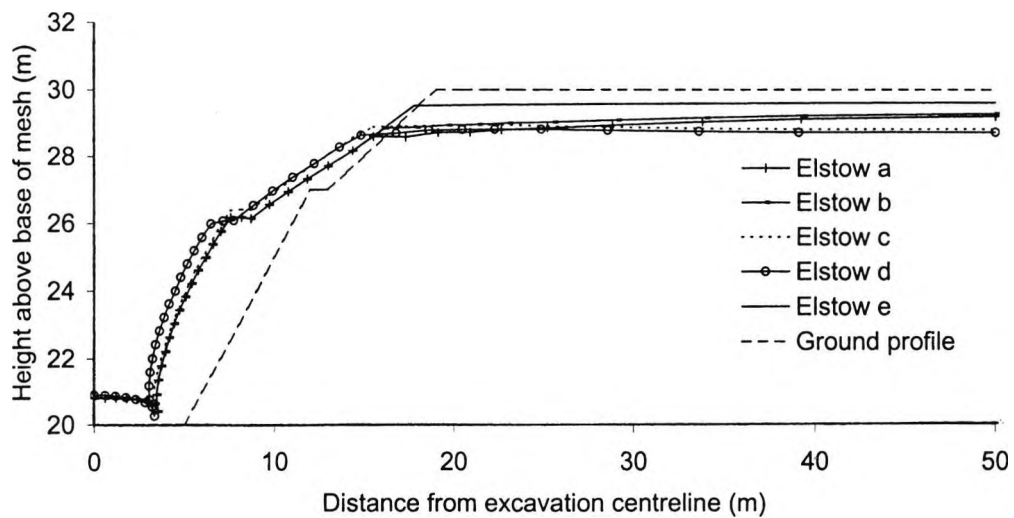


Figure 7.24 Amplified displacements (x100) along excavation profile

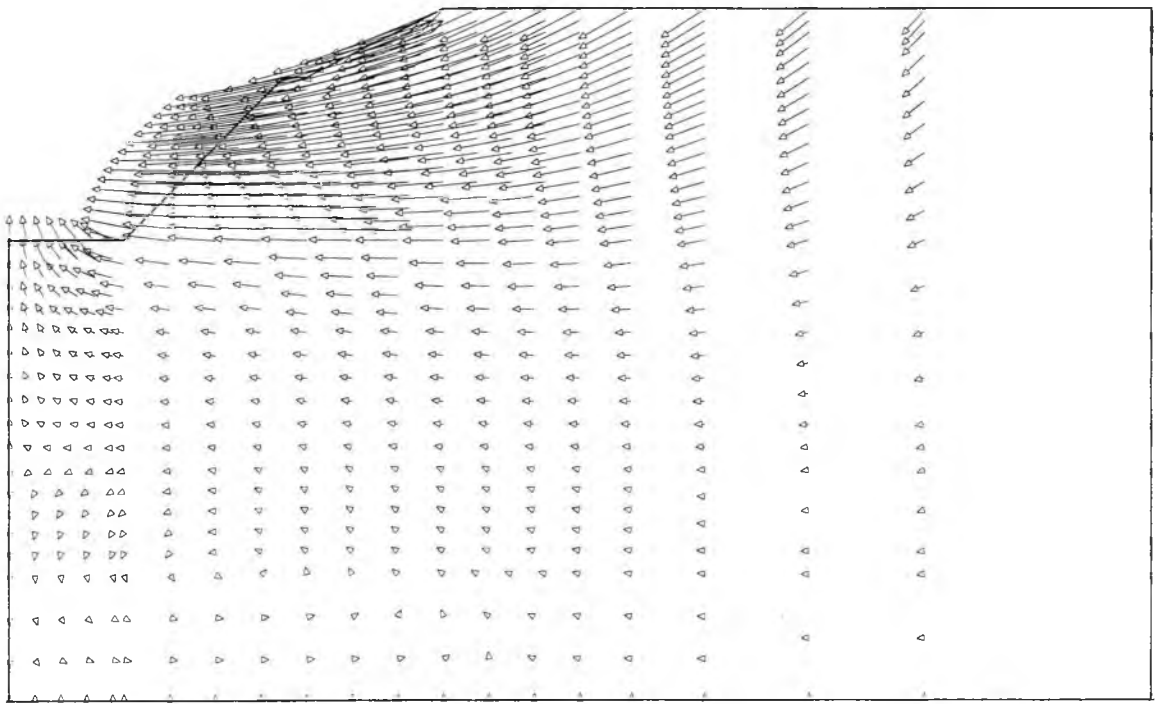


Figure 7.25 Displacement vectors for the Elstow excavation analysis Elstow a (magnified by 100)

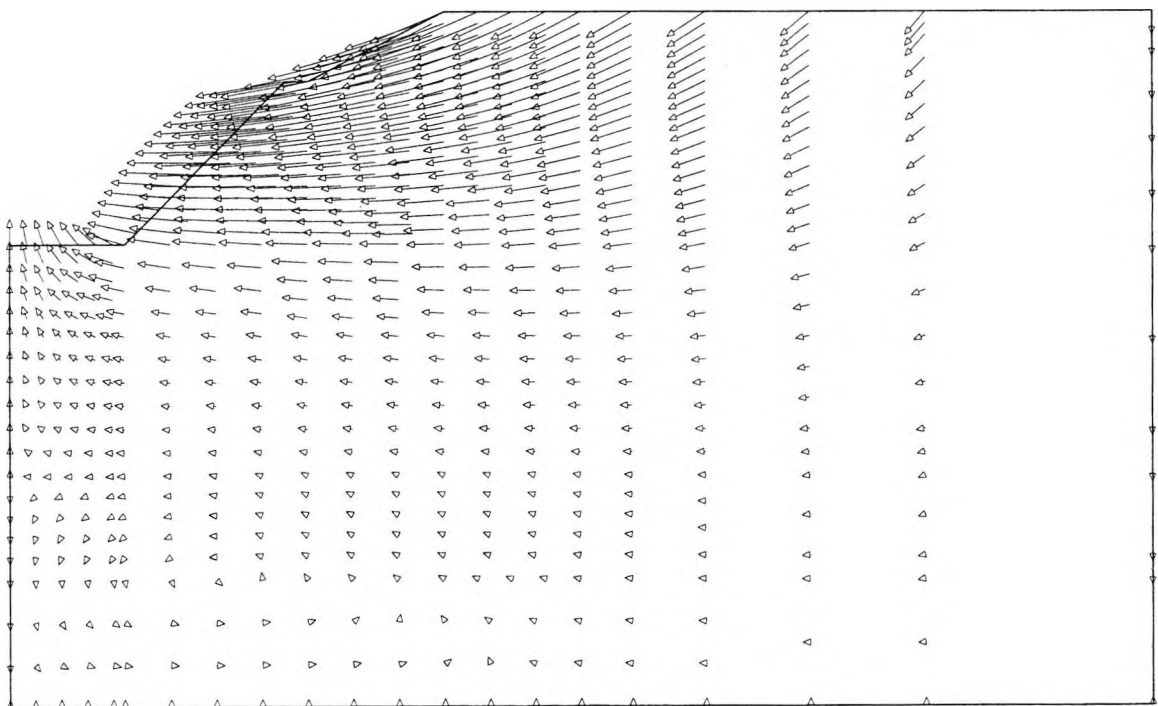


Figure 7.26 Displacement vectors for the Elstow excavation analysis Elstow b (magnified by 100)

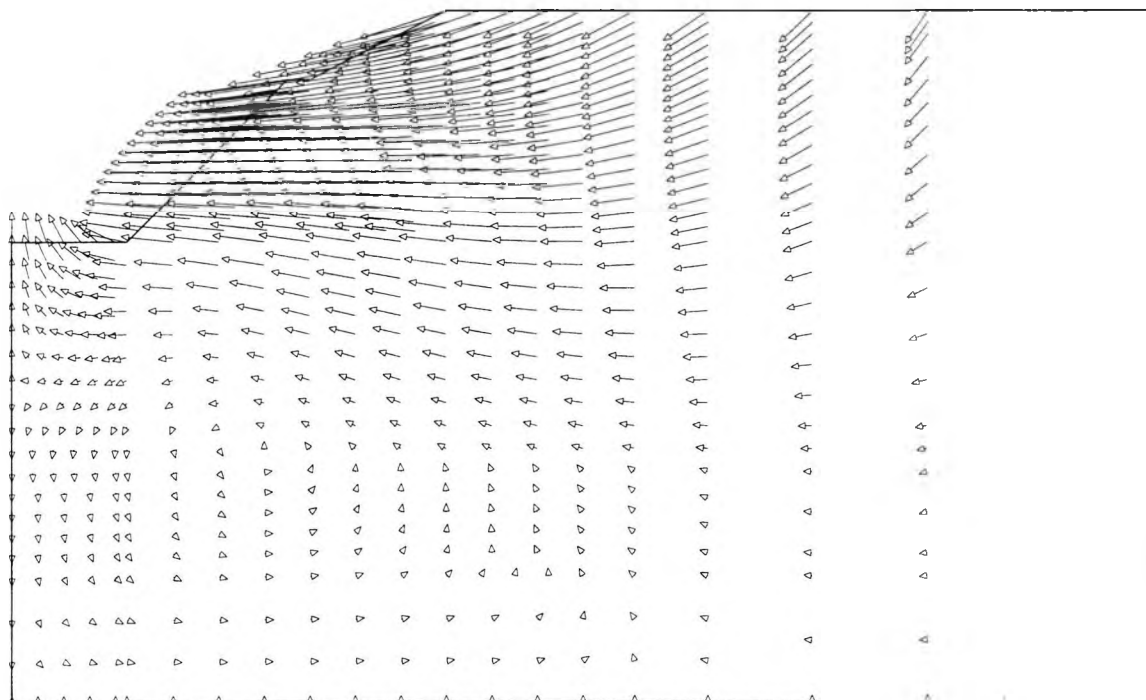


Figure 7.27 Displacement vectors for the Elstow excavation analysis Elstow c (magnified by 100)

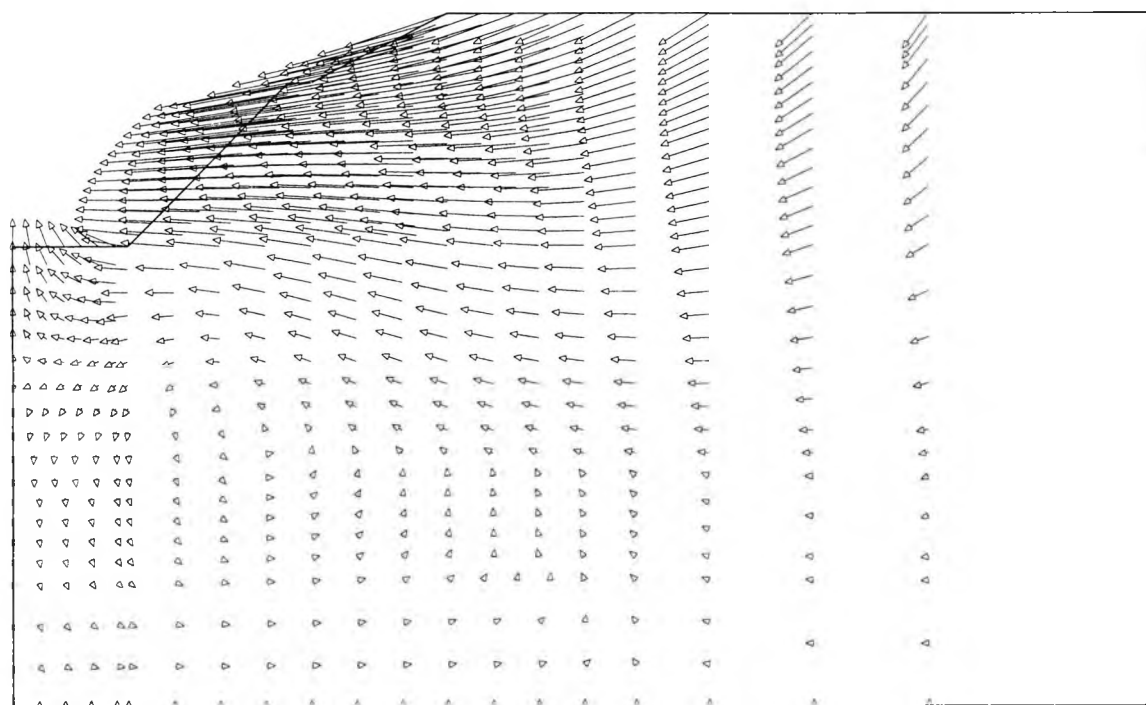


Figure 7.28 Displacement vectors for the Elstow excavation analysis Elstow d (magnified by 100)

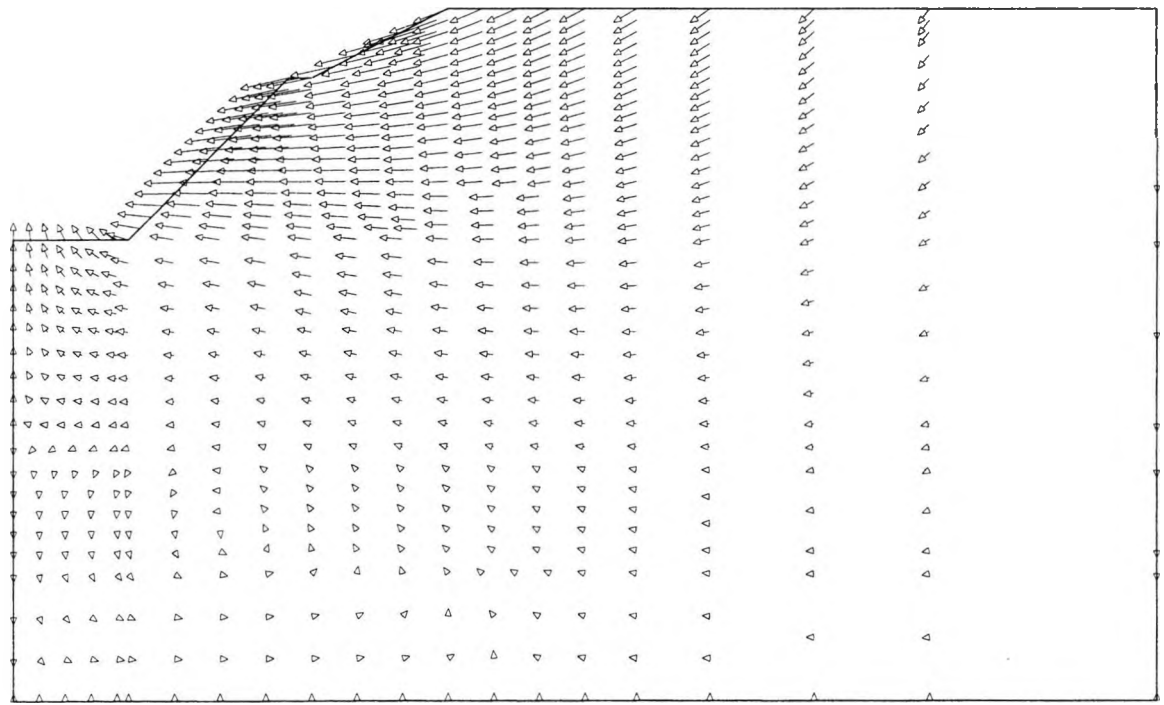
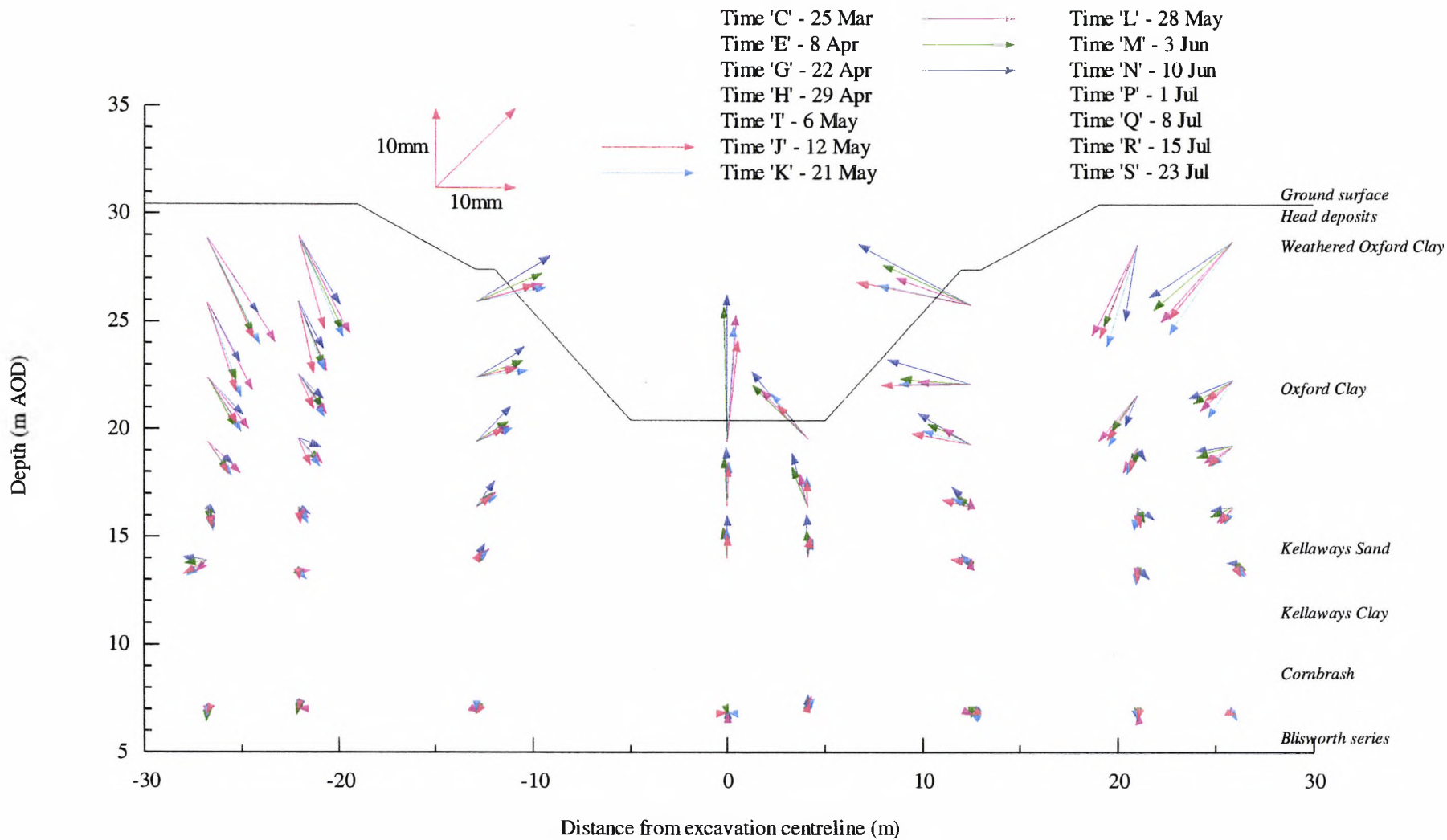


Figure 7.29 Displacement vectors for the Elstow excavation analysis Elstow e (magnified by 100)

Figure 7.30 Observed vectors of displacement around the Elstow excavation (after Pierpoint, 1996)



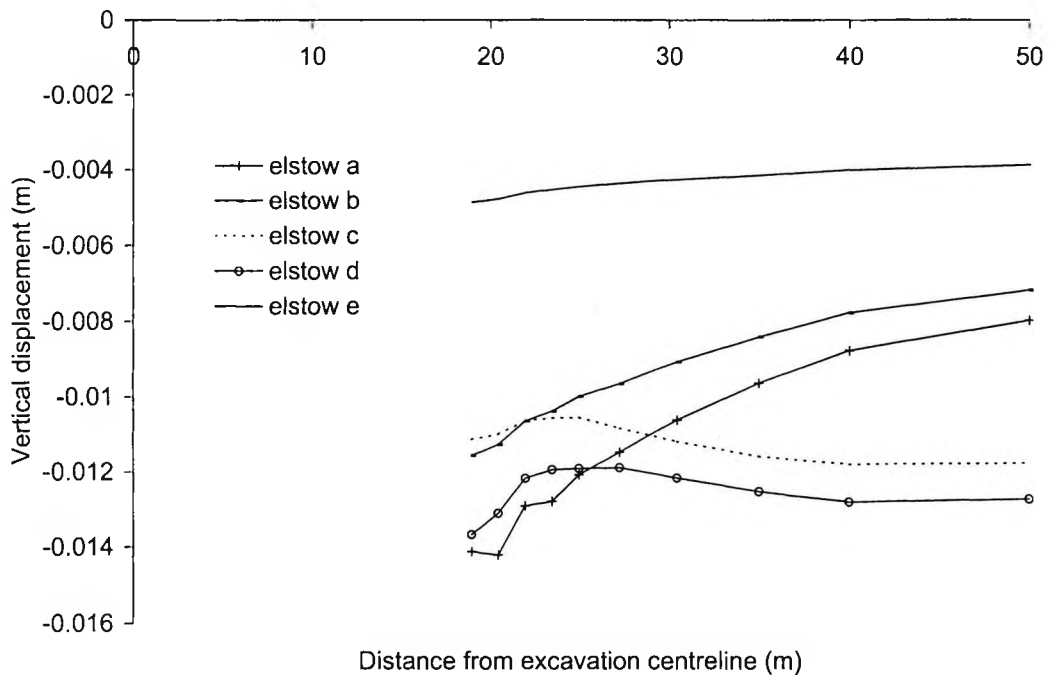


Figure 7.31 Settlement profiles at ground surface

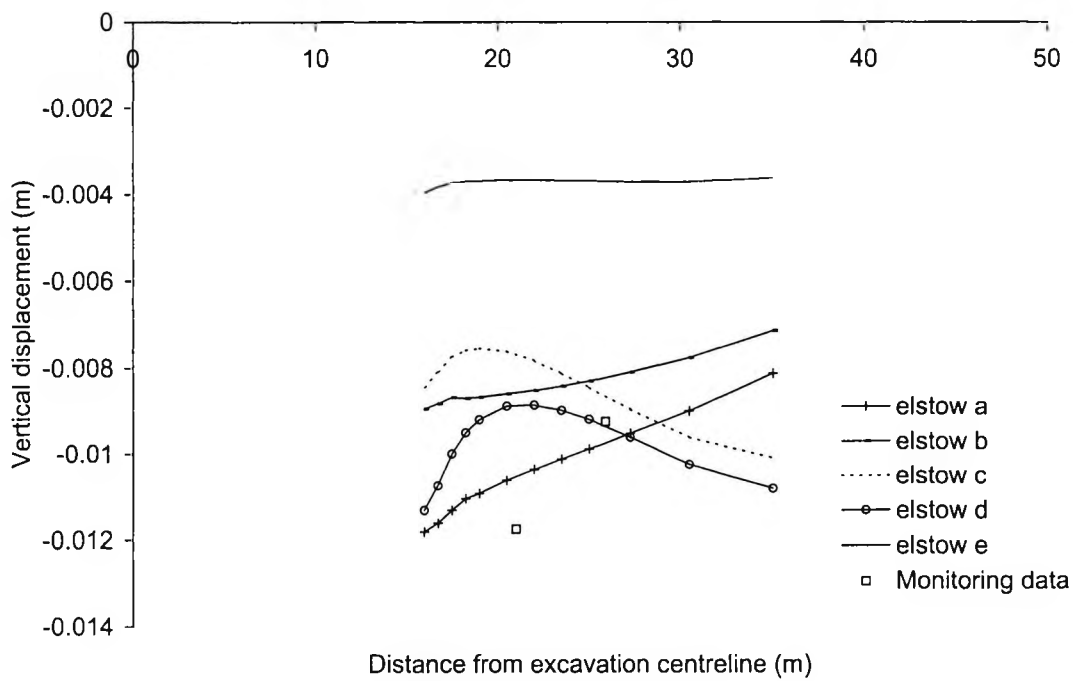


Figure 7.32 Vertical displacement at 1.5m below ground surface

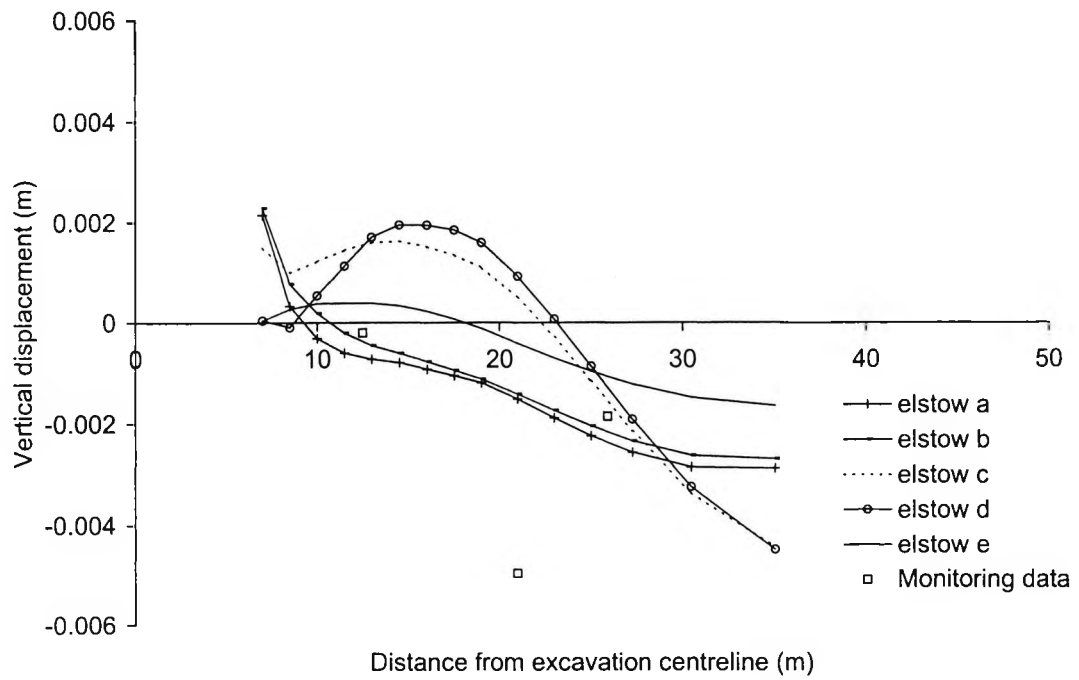


Figure 7.33 Vertical displacement at 8m below ground surface

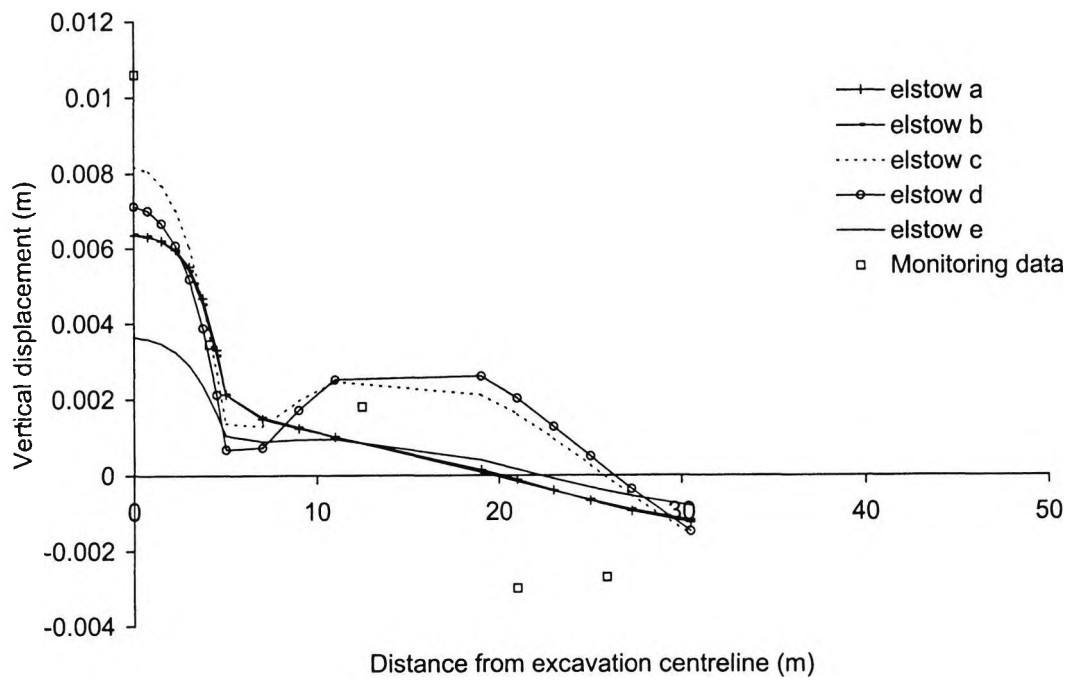


Figure 7.34 Vertical displacement at 11m below ground surface

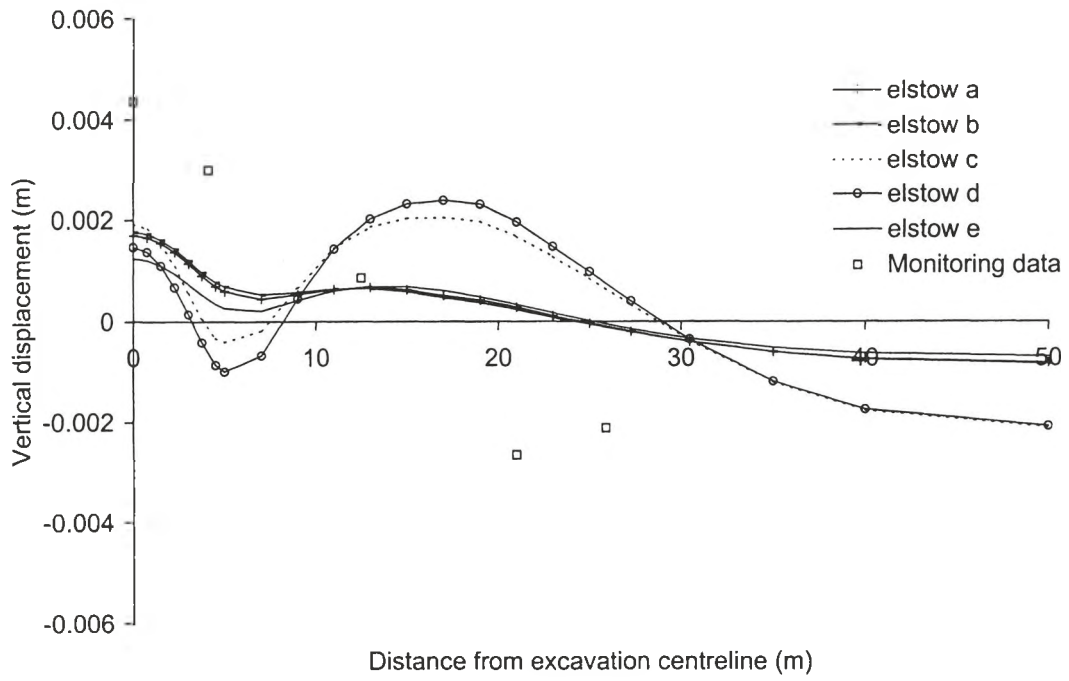


Figure 7.35 Vertical displacement at 14m below ground surface

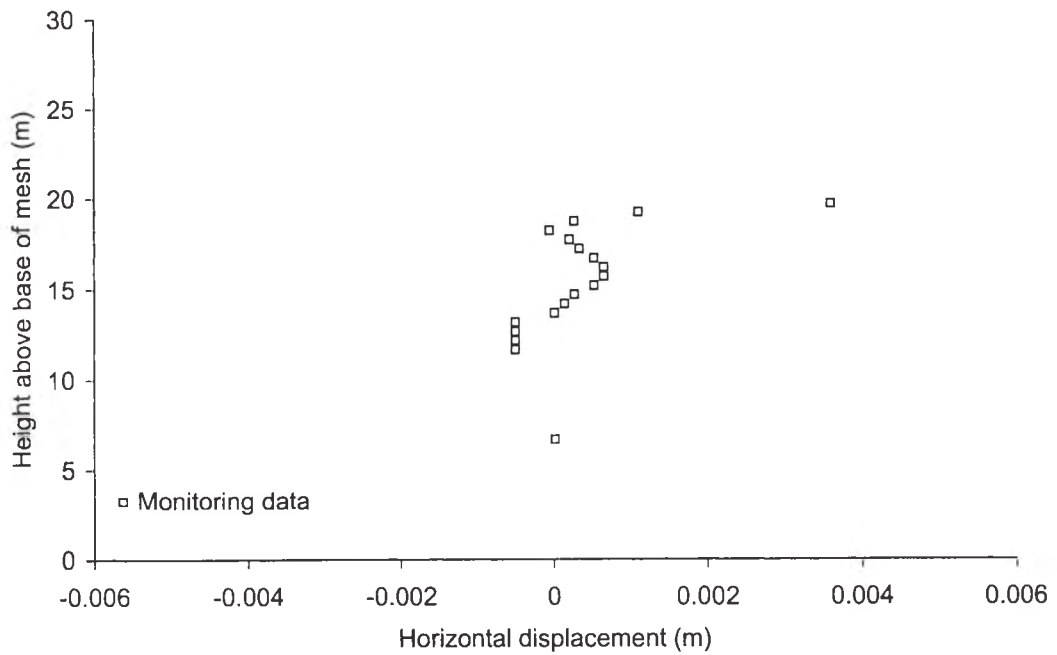


Figure 7.36 Horizontal displacement at excavation centreline (section F)

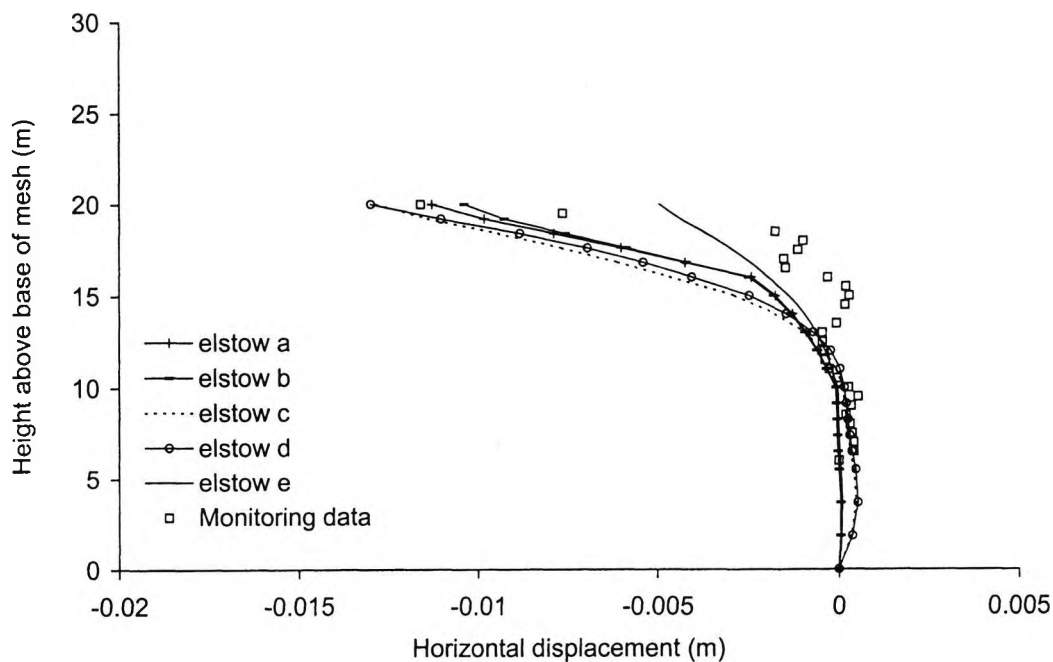


Figure 7.37 Horizontal displacement at section H

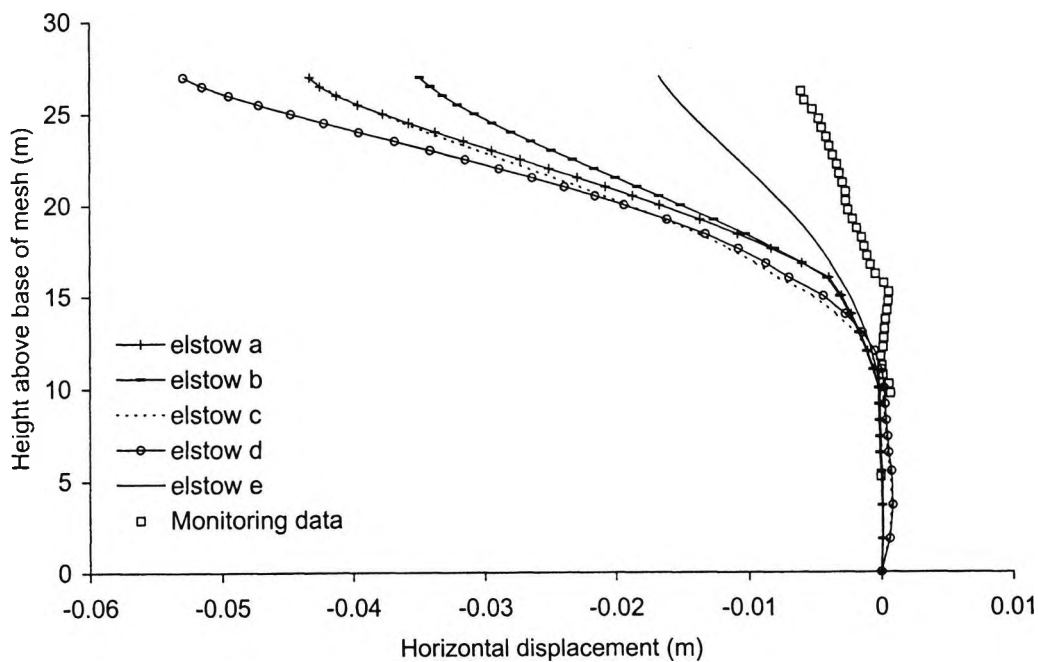


Figure 7.38 Horizontal displacement at section I

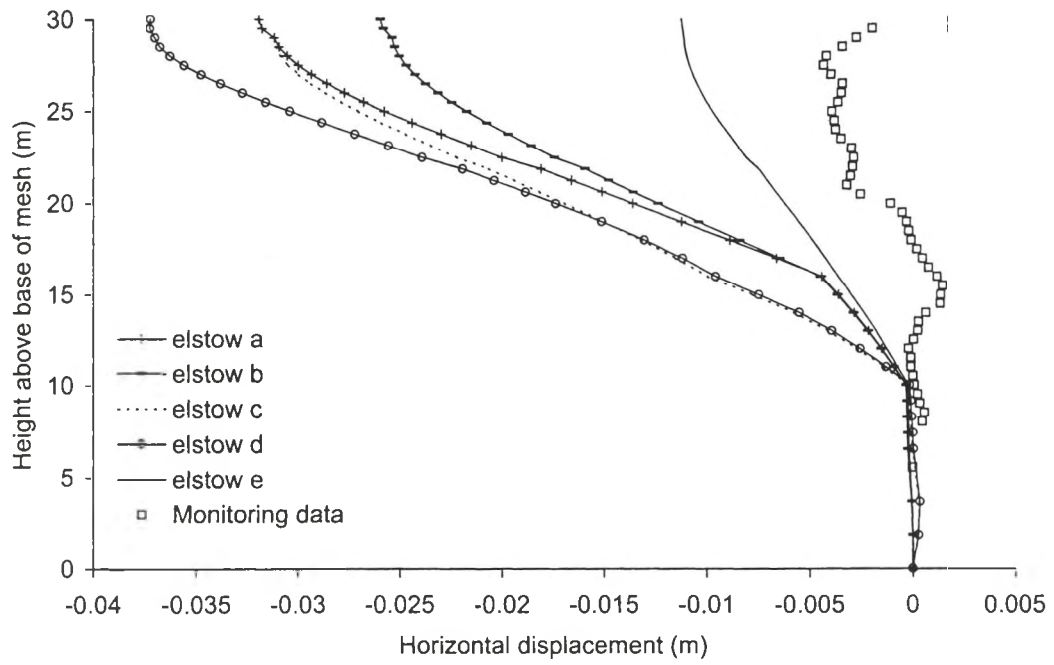


Figure 7.39 Horizontal displacement at section L

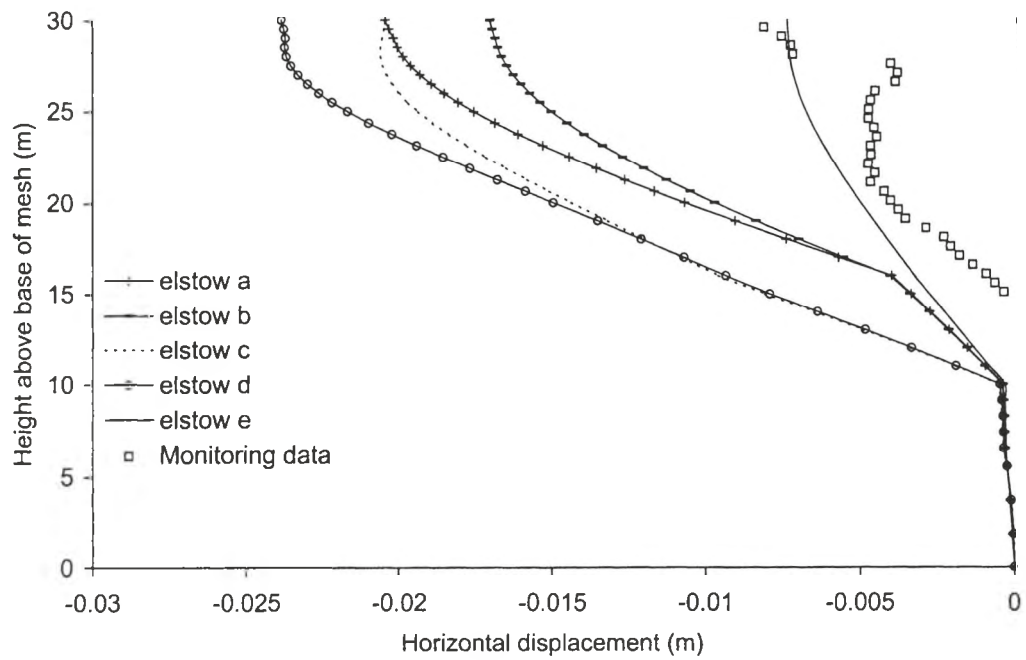


Figure 7.40 Horizontal displacement at section M